Surface-subsurface Transport Cycle of Chloride Induced by Wetland-focused Groundwater Recharge

by

Masaki Hayashi

A thesis
presented to the University of Waterloo
in fulfillment of the
thesis requirement for the degree of
Doctor of Philosophy
in
Earth Sciences

Waterloo, Ontario, Canada, 1996

The University of Waterloo requires that the signature of all persons using or photocopying this thesis. Please sign below, and give address and date.

ABSTRACT

Surface-subsurface transport cycle of chloride induced by wetland-focused groundwater recharge

The glacial plain in the northern prairie region has numerous wetlands. These wetlands provide wildlife habitat, and particularly those located at relatively high elevation are the major source of groundwater recharge. Our field site in southern Saskatchewan is located in a typical northern prairie landscape. One of the main hydrologic connections between the recharge wetland and the surrounding farm land is the large snowmelt runoff resulting from low infiltration capacity of the frozen soil. In the spring time, a large volume of water is transferred from the slope to the wetland, and infiltrates to form a groundwater mound below the wetland. This, in turn, induces the subsurface flow from the wetland to the slope. Most of the infiltration in the wetland is consumed by evapotranspiration in the surrounding slope; however, a small portion recharges the 25-m deep aquifer. Little net infiltration occurs into the slope because the average flow direction in the vadose zone is upward; therefore, groundwater recharge is focused below the wetland. The large infiltration leaches chloride from the sediments below the wetland. Most of the chloride is transported to the slope by subsurface flow, and accumulates in the root zone during evapotranspiration. The accumulated chloride is leached again by snowmelt runoff and is transported to the wetland via overland flow; therefore, chloride is cycled between the wetland and the slope. A small portion of chloride leached under the wetland is transported down to the aquifer and eventually leaves the catchment. A numerical model that incorporates both surface and subsurface transport processes observed in the field shows that the output of chloride to the aquifer becomes balanced with the atmospheric input on the order of 10^3 years. The model also shows that the average chloride concentration in the groundwater entering the aquifer is roughly equal to that in shallow groundwater under the wetland. The product of this concentration and groundwater recharge must be equal to the atmospheric input which is monitored at many locations in North America. Therefore, we can estimate groundwater recharge from the concentration of chloride in shallow groundwater under recharge wetlands. This method is best suited to estimate the average recharge over an entire catchment, which is difficult to estimate from sparse measurements of the hydraulic gradient and hydraulic conductivity. The water and mass transfer characteristics of a wetland will be dramatically altered, if an artificial stress is applied to the system. For example, the drainage of the wetland will stop the divergent subsurface flow. As a result, the dissolved species will accumulate in the wetland, and the groundwater recharge will be reduced. Therefore, the impact of drainage and other land-use practices must be carefully evaluated before implementation.

ACKNOWLEDGMENT

I would like to thank Dr. Garth van der Kamp for being an excellent mentor for me. I would also like to thank Dr. Dave Rudolph for doing a great job of co-supervising my thesis. Other thesis committee members, Dr. John Cherry, Dr. Emil Frind, and Dr. Ron Nicholson; and the external examiners, Dr. Neil Thomson of the Civil Engineering Department and Dr. Mike English of Wilfrid Laurier University, are acknowledged for their advice. I would like to thank Randy Schmidt of the National Hydrology Research Institute (NHRI) for helping me with his superb field skills. I would also like to thank many people from NHRI who helped me in various phases of the research; Vijay Tumber, Brad Fahlman, Jim Banner, Tom Maxin, John Mollison, Ken Supeene, Connie Neiser, Randy George, Darren Schill, and Dan Matthews. The Canadian Wildlife Service (CWS) is acknowledged for giving us the access to the St. Denis National Wildlife Area. I would like to thank Bob Clark of CWS for the use of unpublished field data. I would like to thank Warren Eilers of the Saskatchewan Institute of Pedology for the use of unpublished field data and his advice. Dr. E. de Jong of the Saskatchewan Institute of Pedology and Harm Maathuis of the Saskatchewan Research Council are acknowledged for the use of field instruments. I would like to thank Dr. Mike Celia of Princeton University is for the use of his computer code, Dave Redman of the University of Waterloo (UW) for his assistance in time domain reflectometory, Jim Warren of UW for his assistance on clay mineral analysis and useful discussions, and Steve Shikaze and Gary Parkin of UW for reading earlier drafts of my thesis. Many thanks are also extended to my friends at NHRI and UW. Part of my research was supported by the Government of Canada Awards Scholarship. Funding for the project was provided by NHRI and by a Natural Sciences and Engineering Research Council of Canada (NSERC) operating grant to Dave Rudolph.

TABLE OF CONTENTS

LIST OF TABLES

LIST OF FIGURES

Chapter 2

Chapter 3

Chapter 1

Introduction

This thesis is about a wetland in the northern prairie region of Canada where countless similar wetlands occupy the depressions in the undulating terrain created by the last glaciation. The wetlands are important to this region, because they support a diverse community of wildlife, and recharge the groundwater in underlying aquifers. However, the destruction of a large number of wetlands in the last several decades to increase the crop production raised public concerns about the future of the wildlife and water resources in the region (Batt et al., 1989; Winter, 1989).

The prediction about the future of the wetlands and its inhabitants can only be based on sound scientific studies. The Wetland Ecosystem Vulnerability Studies (WEVS) was started by the Environment Canada to understand the effects of land-use and climate change on the hydrology and ecosystem of the wetlands. As one of many participants of WEVS, I undertook a small project to investigate the transfer of water and dissolved chemicals between wetlands and the surrounding farm lands.

There have been many studies on the hydrology of the northern prairie wetlands. Many of them focused on quantifing the amount of water transferred between the wetlands and the surrounding area (Meyboom, 1966; Sloan, 1972; Zebarth et al., 1989; Woo and Rowsell, 1993; and others). However, it is difficult to represent the heterogeneous surface and subsurface environment of the wetland by a small number of hydrologic measurements. Therefore, the extrapolation of the hydrologic data needs to be examined carefully by some independent measurements.

Distribution of dissolved mass in both the surface and subsurface environments of the wetlands and the surrounding area reflects the flow of water averaged over a long time period. Previous studies have shown that the concentration of dissolved species in the wetland is an effective indicator of groundwater recharge or discharge condition (Rozkowski, 1967; Lissey, 1968; Miller et al., 1985; LaBaugh et al., 1987; and others). However, those studies were mostly descriptive, and the dissolved species were not used to quantify the water and mass transfer between the wetlands and the surrounding area.

In this thesis, the hydrologic measurements and the analysis of dissolved mass distribution are combined to improve the accuracy of the estimate of water and mass transfer flux between the wetland and the surrounding slope. Using the improved estimate, a numerical model of the hydrology and solute transport in a system of a wetland and its catchment is constructed, which can be used to answer questions regarding the response of the system to changes in hydrologic conditions.

The thesis consists of three separate papers, each of which has more detailed introduction to the respective subjects than this short chapter. The first paper (Chapter 2) describes the hydrologic interaction between the wetland and the surrounding slope using the hydrologic measurements. Chapter 3 uses chloride as a tracer to confirm the findings in Chapter 2, as well as to understand the processes of solute transport. Chapter 4 presents the numerical model of the wetland-slope system which is based on the detailed field studies presented in earlier chapters. Detailed information on the field instruments and uninterpreted data are attached as the appendices.

References

Batt, B.D.J, Anderson, M.G., Anderson, C.D. and Caswell, F.D., 1989. The use of prairie potholes by North American ducks. In: Northern prairie wetlands, van der Valk, A., ed., 204-227, Iowa St. Univ. Press, Ames, Iowa.

LaBaugh, J.W., Winter, T.C., Adomaitis, V.A. and Swanson, G.A., 1987. Hydrology and chemistry of selected Prairie wetlands in the Cottonwood Lake area, Stutsman County, North Dakota, 1979-1982. U.S.G.S. Prof. Pap., 1431. 26pp.

Lissey, A., 1968. Surficial mapping of gronndwater flow systems with application to the Oak River Basin, Manitoba. Ph.D. thesis, Univ. of Saskatchewan, Saskatoon, Saskatchewan.

Meyboom, P., 1966. Unsteady groundwater flow near a willow ring in hummocky moraine. J. Hydrol., 4, 38-62.

Miller, J.J., Acton, D.F. and St. Arnaud, R.J., 1985. The effect of groundwater on soil formation in a morainal landscape in Saskatchewan. Can. J. Soil Sci., 65, 293-307.

Rozkowski, A., 1967. The origin of hydrochemical patterns in hummocky moraine. Can. J. Earth Sci., 4, 1065-1092.

Sloan, C.E., 1972. Ground-water hydrology of prairie potholes in North Dakota. U.S. Geol. Survey Prof. Paper 585-C, 28pp.

Winter, T.C., 1989. Hydrologic studies of wetlands in the norhtern prairies. In: Northern prairie wetlands, ed. van der Valk, A., 17-54. Iowa Univ. Press.

Woo, M.-K. and Rowsell, R.D., 1993. Hydrology of a prairie slough. J. Hydrol., 146, 175-207.

Zebarth, B.J., de Jong, E. and Henry, J.L., 1989. Water flow in hummocky landscape in central Saskatchewan, Canada, II, Saturated flow and groundwater recharge. J. Hydrol., 110, 181-198.

Chapter 2

Hydrologic cycle and focused groundwater recharge in a northern prairie wetland

Introduction

The landscape of the northern prairie region of North America is characterized by undulating terrain with a large number of seasonal and semipermanent wetlands which support a diverse community of wildlife species. These wetlands are called sloughs in Canada and prairie potholes in the United States. The number of wetlands has decreased dramatically in the last several decades due to drainage by farmers (Leitch, 1989). This has raised some concern about the future of the wildlife that depend on the wetlands (Batt et al., 1989). In addition to being the habitat of wildlife, the wetlands are also important as water resources (Winter, 1989), because groundwater recharge in the northern prairie region occurs primarily from the wetlands (Zebarth et al., 1989).

A hydrological study of a wetland, i.e. a study of quality and quantity of water, requires evaluation of the transfer of water and dissolved mass between the wetland and the underlying geological material. The interaction between the surface and subsurface water is particularly important for the northern prairie wetlands that do not usually have inflow and outflow streams. The average direction of water transfer between the northern prairie wetlands and the underlying material reflects the landscape setting. Wetlands that have net infiltration of water are usually located in the elevated areas of the undulating terrain, and are commonly called "recharge wetlands" (Lissey, 1968). Wetlands in the low area generally have net exfiltration, and are called "discharge wetlands". One can usually, though not always, distinguish the former from the latter based on vegetation and salinity of water in the wetlands. The recharge wetlands supply groundwater to aquifers in the region, as well as to the discharge wetlands that are hydraulically connected through local groundwater systems. Therefore, we will focus on the recharge wetlands in this study.

Large amount of infiltration in the recharge wetlands drives the subsurface flow system under the wetlands and the surrounding slopes. The downward flow is "focused" in the wetland, while the divergent flow distributes the water from the wetland to the surrounding slopes (Meyboom, 1966b; Lissey, 1968; Sloan, 1972; Miller et al., 1985; Mills and Zwarich, 1986; LaBaugh et al., 1987; Trudell, 1994).

Infiltration in the recharge wetlands occurs because the wetlands receive a large amount of snowmelt runoff from the surrounding slope. The soil frost in the cold winter in the northern

prairie region reduces the infiltration capacity during the snowmelt period and generates snowmelt runoff into wetlands in the spring (Woo and Winter, 1993). Major overland flow generally occurs only in the snowmelt period (Woo and Rowsell, 1993; Winter and Rosenberry, 1995), and the water level in the wetlands after the spring snowmelt is essentially controlled by precipitation, evapotranspiration, and infiltration.

Traditionally, the subsurface flow has been evaluated by measuring water levels in piezometers under the wetlands and the slopes (e.g. Zebarth et al., 1989). Such methods are prone to error due to the small number of measurements used to represent the heterogeneous subsurface environment. On the other hand, the fluctuation of water level in the wetland indicates the combined rate of precipitation, evapotranspiration, infiltration, and hence "integrates" the heterogeneous hydrology of the wetland and the slope (Winter and Rosenberry, 1995). To separate each process controlling the wetland water level, some researchers assumed without clear field evidence that the infiltration rate was constant over a time period of days to weeks (Eisenlohr, 1966; Shjeflo, 1968; Woo and Rowsell; 1993). However, Meyboom (1967) recorded a large change in the infiltration rate (3.5 mm d^{-1}) between the day and night. This controversy over the infiltration rate needs to be resolved.

The function of recharge wetlands can be more fully understood when all major components of hydrologic cycle in both wetlands and surrounding slopes are described. This paper is a part of a broader study which aims to describe the hydrologic and solute transport cycle in a wetland-slope system, and then to model those processes in a geological time scale. The results of a four-year long hydrologic study of a wetland in Saskatchewan, Canada is presented. The objective of the study is to describe each component of hydrologic cycle, and to estimate the rate of water transfer among the components, which will be required in modelling of the wetland-slope system.

Field site

The study site is located in the St. Denis National Wildlife Area (106°06'W, 52°02'N), 50 km east of Saskatoon, Saskatchewan, Canada (Fig. 2.1). The elevation of the St. Denis area ranges between 545 and 560 m above mean sea level. The topography of the area is described as moderately rolling knob-and-kettle moraine with slopes varying from 10 to 15 % (Miller et al., 1985). Relatively large wetlands (up to 50000 m^2) occur in lowlands with native vegetation (indicated as untilled grassland and shrubs in Fig. 2.1). The wetlands in the lowlands typically have water with high (>1500 μS/cm) electrical conductivity throughout the year. The high electrical conductivity is an indication of groundwater discharge conditions, because it reflects high concentration of dissolved solid transported by groundwater into the wetlands (Sloan, 1972; LaBaugh et al., 1987). Surrounded by the lowlands are cultivated and tame grass uplands

that have a number of small wetlands. These wetlands have seasonal bodies of water that are low in electrical conductivity (<500 μS/cm) indicating groundwater recharge conditions.

We selected a recharge wetland, identified as S109 by the Canadian Wildlife Service, for a detailed field study. It has an average size (1000-5000 m^2) of recharge wetlands in the northern prairie region, and is situated in a typical prairie setting; undulating terrain underlain by glacial till. Therefore, it serves as a representative of the groundwater recharge wetlands in this region. S109 and other wetlands along the transect AB (Fig. 2.1) were previously studied (Miller, 1983; Miller et al., 1985), and part of their field facilities were available for our work. The vegetation in the wetland is characterized by sedge, spike rush, and other aquatic species, while silver willow, trembling aspen, and balsam poplar grow along the wetland margin. Similar wetland margin vegetation was called a "willow ring" by Meyboom (1966a, b). The willow ring and the adjacent grassland mark the transition from the wetland to the cultivated field, which was cropped to spring wheat in 1993 and 1994, summer fallowed in 1995, and cropped to oil seeds in 1996.

In this study, the term "wetland" refers to a topographic depression characterized by aquatic vegetation, while the term "pond" refers to the inundated portion of the wetland (Fig. 2.2). The term "slope" is used to denote the area surrounding the wetland, which includes both the cultivated field and the willow ring. Accordingly, the wetland of S109 is defined as the region enclosed by the 552.5 m elevation contour (Fig. 2.3), and has an area of 2400 m^2. The catchment of S109 cannot be uniquely defined because the runoff water may overflow from adjacent small depressions in years of large snowmelt, hence two catchment boundaries are shown in Figure 2.3. The boundary of the smaller catchment is based on elevation contours, while the larger catchment includes the adjacent small depressions. The ambiguity of the catchment area is a common characteristic of undulating terrain in the northern prairie region. In this study the area of the smaller catchment (24000 m^2) is used in water balance calculations. This choice is justified considering a large uncertainty in the actual size of the effective catchment.

According to Miller (1983), the area is underlain by glacial till of the Battleford and Floral Formations (Fig. 2.4). This was confirmed by the drilling program associated with the current study. However, the boundary between the two formations was not clear, hence is not indicated in Figure 2.4. In some areas the glacial till is overlain by up to 2 m of stratified silty sediments. The average texture of the till is 45% sand, 30% silt, and 25% clay (Miller et al., 1985). The till is oxidized to a depth of 5-6 m (oxidation front) and is olive brown and well-fractured. The fracture spacing in a typical oxidized till in this region is 0.3-0.8 m (Keller et al., 1988). The unoxidized till below the oxidation front is dark gray and less fractured. Thin (0.1-1.0 m) sand lenses occur frequently in the till, but they appear to be discontinuous. A thin (0.3 m) but extensive layer of dense clay occurs below S109 at a depth of 8-9 m. A thicker (> 1.5 m) sand layer is found at a depth of 25 m in two deep bore holes near S109 and another wetland S125S

(Fig. 2.4). A sand layer at a similar depth and thickness is also found in a bore hole located 1500 m west of the site, hence it is regarded as an aquifer that connects groundwater flow systems under all wetlands in the area.

The 30-year annual mean air temperature at Saskatoon Airport is 1.7 °C, with a range of 50 °C which peaks in late July and reaches a minimum in January (Woo and Rowsell, 1993). The area becomes covered by snow in November; therefore, we define a hydrologic year to start on November 1 of the preceding calendar year and end on October 31. A hydrologic year consists of a winter (November - March) and a summer (April - October); for example the winter of 1994 starts in November 1993. The 90-year mean annual precipitation in Saskatoon is 360 mm, of which 84 mm occurs in winter mostly as snow (Atmospheric Environment Service, 1996). The annual lake evaporation in this area is 690-710 mm (Morton, 1983), based on the data from the Last Mountain Lake, located 100 km south-east of the study site.

A part of the wetland S109 becomes inundated in the spring of most years. The Canadian Wildlife Service (CWS) has been recording the presence or absence of surface water in the center of S109 on a two-week interval since 1980 (Woo et al., 1993; Bob Clark, personal communication). The length of inundation of S109 is defined as the number of months for which water is present in the center. It varied between 0 and 8 months in the period 1980-1996 with an average of 3.6 months. The precipitation during this period had considerable variation (Fig. 2.5). The correlation between the summer precipitation and the length of inundation is insignificant (the square of the correlation coefficient $r^2 = 0.06$), while the correlation between the snowmelt and the length of inundation will be described later.

Field and laboratory methods

Survey methods

The site was level surveyed on 5-10 m grid using a total station (Wild, T2000), and a topographic map was produced (Fig. 2.3). The relationships between the volume of water in the pond and the depth of water in the pond (volume-depth function), and between the area of pond and the depth (area-depth function) for S109 were obtained from the survey data.

Precipitation, evaporation, and pond water level

Summer precipitation in the hydrologic years 1994-1996 was measured by a tipping bucket rain gauge installed near the willow ring (indicated as WRG in Fig. 2.3). The rain gauge was located at large enough distance from the willow ring to avoid the influence of the trees. Summer precipitation in 1993 and winter precipitation in 1993-1996 were obtained from the Saskatoon Airport, 50 km west of the site (Atmospheric Environment Service, 1996). Snow depth was measured along a north-south transect (CD in Fig. 2.3) using a 61 mm diameter

aluminum snow survey tube. Snow water equivalent was calculated by measuring the volume of each snow sample upon melting.

The water level in the pond in 1994 was monitored using a Stevens F-type chart recorder. The water level in 1995 and 1996 was monitored using a pressure transducer (Geokon, 4500ALV-5) placed in the bottom of a 3.8 cm diameter stilling well, drilled 1.8 m into sediments to avoid temperature fluctuation. A transducer reading was taken every two minutes and averaged over a 30-minute interval using a data logger (Campbell Scientific, CR10). Hydrographs on Stevens recorder charts were digitized. Each hydrograph was traced ten times on a digitizer tablet, and the average was used to estimate the water level at 30 minute intervals. This procedure was used to eliminate the errors due to irregular movement of the cursor on the tablet.

Evaporation from the pond water surface was measured with a partially submerged Class-A pan in the center of the pond. Only the top 5-10 cm of 25 cm deep pan was kept above the pond water level, and the pan water temperature and pond water temperature were monitored by thermisters (Campbell Scientific, 107) and a data logger (Campbell Scientific, CR21X) to confirm that thermal equilibrium was maintained. The pan water level was monitored using a Stevens F-type chart recorder.

The evapotranspiration in the pond was measured using the Bowen ratio-energy balance method with a Campbell Scientific Bowen Ratio System (Malek and Bingham, 1993) in the center of the pond. In this method the terms on the left hand side of the energy balance equation are measured or estimated:

$$R_n + G_{sed} + \Delta Q_w + \Delta Q_{sed} = H + LE \qquad (2.1)$$

where R_n (J m^{-2}) is the net radiation in a given time period, G_{sed} (J m^{-2}) is the heat conduction through the top 0.4 m of the pond bottom sediments, ΔQ_w (J m^{-2}) is the heat storage change in the water, ΔQ_{sed} is the heat storage change in the top 0.4 m of the sediments, H (J m^{-2}) is the sensible heat transfer into the atmosphere, LE (J m^{-2}) is the latent heat transfer into the atmosphere. The terms on the right hand side are unknown, but the ratio H/LE can be estimated from the measurements of humidity and temperature gradient in the boundary layer, hence we can calculate each term.

The energy balance was applied on a daily basis to minimize the error in estimating ΔQ_w, as well as to avoid unfavorable conditions that may occur if shorter intervals are used (Ohmura, 1982). The R_n was measured with a net radiometer (Radiation & Energy Balance Systems, Q*7). The temperature gradient was measured with chromel-constantan thermocouples (Campbell Scientific). The humidity gradient was measured by a cooled mirror system (Campbell Scientific). The detail of these measurements can be found in Malek and Bingham (1993). The ΔQ_w was estimated from temperature difference and the average depth of water, while ΔQ_{sed} was assumed to be negligible because temperature difference between days was

small. The G_{sed} was estimated from the average thermal gradient measured by thermisters at depths of 0.1m and 0.4m into the sediments. The thermal diffusivity of the pond sediments (2.7×10^{-7} m^2 s^{-1}) was estimated by analyzing the amplitude and phase lag of the diurnal temperature fluctuation at the two depths (Hillel, 1980, p.304). The heat capacity per unit volume of the sediments (3.7×10^6 J m^{-3} K^{-1}) was estimated from the measured water, mineral, and organic matter content of sediment samples and the specific heat of the three components listed by Hillel (1980, p.161).

Groundwater

Miller (1983) installed 20 piezometers and water table monitoring wells in 1980 (numbered from 1 to 20 in Fig. 2.3). In addition, we installed 14 piezometers in October, 1993, and four other piezometers and wells at various times between 1993 and 1994. Miller's piezometers were made of 3.2 cm inside diameter PVC pipes and installed in 15 cm diameter holes. Sand packs, 0.7-1.9 m in length, were installed around screens and were sealed by bentonite pellets and clay to the surface. Most of the new piezometers were made of 1.3 cm inside diameter polyethylene tubes, while some were made of 2.4 to 5.2 cm inside diameter PVC pipes to house pressure transducers. The new piezometers were installed in 15 cm diameter holes drilled by a solid-stem auger. Sand packs, 0.7-3.6 m in length, were installed around screens and the bore holes were sealed by bentonite pellets and chips to the surface. Up to three piezometers were installed in a single hole. The new water table monitoring wells were made of 4 cm inside diameter PVC pipe, and were installed in the bore holes drilled by smaller size (5 to 10 cm diameter) augers. The holes for the wells were filled with sand to the surface.

The length of piezometer screens varied between 0.2 and 0.4 m. In glacial tills that have low hydraulic conductivity, the length of screens is not important. It is the length and the diameter of sand packs that determines the response of piezometers. Longer sand packs were used in deeper piezometers to ensure reasonably quick response. The basic time lag (Hvorslev, 1951) for most piezometers was within 50 hours, with exception of a few of Miller's piezometers installed in low hydraulic conductivity zones. The detailed information related to the individual piezometers, such as elevation, depth, sand pack length, and basic time lag is found in Appendix B.

All piezometers were monitored manually at one week to one month intervals. A few piezometers were continuously monitored by vibrating wire pressure transducers and a data logger. Saturated hydraulic conductivity was calculated from the basic time lag, measured by standard slug tests performed on the piezometers.

Vadose zone

Tensiometers were constructed from 23 mm diameter standard porous cups (Soil Measurement Systems, SP-031), PVC pipes, and acrylic tubes (Martheler et al., 1983; Cassel

and Klute, 1986). They were installed by creating access holes, slightly larger in diameter than the porous cups, with a soil sampler and inserting them into a slurry made of in-situ materials. They were filled with deaerated water and measured with a hand-held pressure transducer (Soil Measurement Systems, SW-030). Twenty tensiometers were installed in three nests (indicated as TOP, MID, and WRG in Fig. 2.3) at depths ranging from 0.2 m to 2.0 m. In addition to measuring the soil matric potential, the tensiometers were also used to measure unsaturated hydraulic conductivity (Gardner, 1960; Appendix A).

Soil moisture content was monitored using time domain reflectometry (TDR). TDR probes were made of a pair of stainless steel rods (diameter 6.4 mm, spacing 50 mm). Probes longer than 50 cm were covered with PVC pipes (outside diameter 13 mm) leaving only the bottom 20 cm exposed to the soil to avoid conductive loss of the signal in saline soil. The idea of using PVC to cover the rods is similar to the method proposed by Topp and Davis (1985). The PVC-cased probes were inserted into access holes having the same diameter as the probes to the depth just above the proposed monitoring zone. Once the sharp tips of the probes reached the bottom of the access holes, they were pounded 20 cm into the undisturbed soil to ensure direct contact between the exposed part of the probes and the soil. Three nests of seven TDR probes were installed within 1 m of the tensiometer nests (TOP, MID, and WRG in Fig. 2.3) at depths ranging from 0.1 m to 2.1 m. The apparent dielectric constant, K_{app}, of the soil was determined by analyzing the wave forms obtained by a portable reading unit (Soil Moisture Equipment Corp., 6050X1) using a computer program developed by Redman (1996). Soil moisture content was calculated from K_{app} using the formula of Topp et al. (1980).

Two arrays of seven copper-constantan thermocouples were installed near tensiometer nests TOP and WRG at depths ranging from 0.2 m to 2.0 m. The temperature was measured by a portable read out device (Cole-Parmer, 8528-20).

Results

Survey results

The area-depth and volume-depth functions for the wetland S109 are given by;

$$A = 2sd \qquad V = sd^2 \tag{2.2}$$

where A (m^2) is the area of the pond, V (m^3) is the volume of water in the pond, d (m) is the depth of the pond, and s (m) is a scaling factor. For S109, s = 1500 m. The matching between the field data and the functions is good (Fig. 2.6).

Precipitation

Total and winter precipitation in the hydrologic years 1993-1996 are listed in Table 2.1. As mentioned earlier, a hydrologic year starts in November. The total precipitation in 1994, for example, is the precipitation occurred between November 1993 and October 1994.

Snow accumulation

Snow pack thickness and water equivalent were measured at 20 locations along the transect CD (Fig. 2.3) just before the snow melt period (March 3, 1994 and March 13, 1996). The snow survey was not conducted in 1995. Due to the snow drift during the winter, the snow was almost absent near the top of the slope in both 1994 and 1996. In contrast, a thick snow pack developed in the wetland, particularly along the willow ring (Fig. 2.7). Woo and Rowsell (1993) reported similar snow accumulation patterns in a wetland located 1500 m west of the site. The total snow water equivalent in the catchment is estimated as follows. We assume that the catchment has a circular shape and the snow has radially symmetric distribution in the north and south halves of the catchment (Fig. 2.7). By integrating the snow water equivalent shown in the graph, we estimate the total snow water equivalent of 1600 m^3 in both 1994 and 1996. This volume, divided by the actual catchment area 24000 m^2, gives the average snow water equivalent of 66 mm.

The soil temperature near the willow ring never went below 0 °C at all depths throughout the winters of 1994 and 1996 (Fig. 2.8d, only 0.4m and 1.0 m data are shown), indicating the effect of thermal insulation by the thick snow pack. The snow depth at WRG site was only about 25 cm in 1995, compared to 100 cm in 1994 (Fig. 2.7), and the shallow soil temperature went below 0 °C (Fig. 2.8d). The soil temperature near the top of the slope went below 0 °C in all three winters, suggesting frozen conditions, and did not completely thaw until May (Fig. 2.8e).

Snowmelt runoff

The snowmelt runoff occurred in several phases and lasted for 25-30 days as indicated by water level change in the pond in early spring (Fig. 2.8b). Between the early phases of snowmelt, the shallow water in the pond completely froze up with the sediments. The pond sediment did not thaw when the pond water melted in the later snowmelt phases. The similar phenomena is common in the northern prairie region (Woo and Winter, 1993).

At the end of the snowmelt period the volume of water in the pond, estimated from the water level, was 1100 m^3 in 1994, 500 m^3 in 1995, and 1100 m^3 in 1996. This volume is defined as the volume of effective snowmelt runoff. The effective snowmelt runoff is significantly smaller than the amount of snow in the catchment before the snowmelt started (1600 m^3 in 1994 and 1996), presumably due to infiltration and evaporation in the slope. The effective snowmelt runoff for each year (Table 2.1) is calculated by dividing the volume of snowmelt runoff by the area of the catchment.

Because the snowmelt runoff is highly variable from one year to another, the values obtained in 1994-1996 may not represent the average over many years. The pond water level was monitored by Saskatchewan Institute of Pedology between 1981 and 1985 (Warren Eilers,

personal communication), therefore we can estimate the effective snowmelt runoff for this period. In the time periods 1981-1985 and 1994-1996, a positive correlation ($r^2 = 0.84$) exists between the effective snowmelt runoff plus summer precipitation and the length of inundation of the wetland (Fig. 2.9). Note that the effective snowmelt runoff is expressed as the average water depth in the wetland. The average length of inundation in the time period (1979-1996) is 3.6 months, hence the average of effective snowmelt runoff plus summer precipitation in 1979-1996 is estimated to be 480 mm (Fig. 2.9). The average summer precipitation in this period is 280 mm; therefore, the average of effective snowmelt runoff is 200 mm, or 20 mm averaged over the catchment. Therefore, it will be safe to assume 10-30 mm as the range of the effective snowmelt runoff, though it is impossible to estimate the statistical confidence interval.

Evapotranspiration and infiltration in the pond

The water level in the pond fluctuated during the summer in response to rainfall (Figs. 2.8a and 2.8b), but it gradually declined until the pond completely disappeared (October 1994, August 1995). We observed similar patterns in other groundwater-recharge wetlands in St. Denis area. The loss of water from the pond is due to two processes, evapotranspiration and infiltration.

Pond water level declined fast in the afternoon and slow in the morning and eveneing, resulting a step-like patterns of water level change (Fig. 2.10b). These patterns were previously interpreted as the result of fluctuation in evapotranspiration rate in the pond (Keller et al., 1986; Woo and Rowsell, 1993). They assumed that the evapotranspiration completely stops at night. Such an assumption is hard to justify because the water in the pond can store the radiation energy during the day and release it as the latent heat at night (Assouline and Mahrer, 1993). Our preliminary energy balance calculation showed that the diurnal fluctuation (Fig. 2.10b) was too large to be explained by the evaporation alone.

To directly measure the rate of evaporation, we installed a submerged pan in the pond during a two-week period in the summer of 1994, just a few weeks before the pond went dry (Fig. 2.8b). The slope in the pan water level curve indicates the rate of pan evaporation (Fig. 2.10c). The step-like patterns of the water level in the pan were weaker than that in the pond (Fig. 2.10b). When the pan water level change was subtracted from the water level change in the pond, the residual still showed step-like patterns (Fig. 2.10c). To remove the artificial noise, we took three segments (two to six days long) of the residual curve that did not have precipitation and subtracted the linear declining trend. The resulting water level functions were Fourier transformed to remove those frequency components that had more than eight peaks per day. This operation served as a low-pass filter to remove noises. The water level functions were then differentiated with respect to time. The derivative of the water level functions was added to the linear trend to estimate the infiltration rate (Fig. 2.10d). Even though the noise is still present, the distinct peak in mid afternoon is clearly identified, which indicates the high rate of

infiltration due to subsurface water uptake by roots of ; a) willow ring, b) vegetation in the non-inundated portion of the wetland, c) emergent vegetation within the pond.

The water level in a piezometer in the willow ring (9 in Fig. 2.3) had strong diurnal fluctuations, hence the difference (Δh) between the piezometer water level and the pond water level fluctuated, too (Fig. 2.10e). The depth of the piezometer is 1.4m, while the basic time lag of the piezometer is six minutes. Note that the pond water level was higher than the piezometer water level, hence the flow direction was from the pond to the willow ring. The shoreline of the pond was rapidly retreating during the experiment, and the distance between the shore and the piezometer increased from approximately 15 m to 20 m (i.e. 33 % increase). Assuming that the change in the distance is relatively small, the hydraulic gradient between the pond and the piezometer is roughly proportional to Δh. The peak in the diurnal fluctuation of hydraulic gradient occurs after the peak in the infiltration rate (Figs. 2.10d and 2.10e), suggesting that the high infiltration in mid afternoon is not induced by the hydraulic head drop in the willow ring. The average infiltration rate was nearly constant during the period of the experiment (Fig. 2.10d), while the hydraulic gradient increased significantly (Fig. 2.10e). Therefore the largest consumption of infiltrated water by transpiration was perhaps within the wetland.

Part of the pond in S109 had moderate growth of emergent vegetation, which made it impossible to separate the effects of the emergent vegetation on infiltration rate from those of the vegetation outside the pond. The pan measurement was also conducted in the pond in another wetland S120 (Fig. 2.1) that did not have emergent vegetation. The diurnal fluctuation in the residual curve in this experiment (Fig. 2.11b) was not caused by the emergent vegetation. Because S120 was similar to S109 except for the absence of the emergent vegetation, it is likely that fluctuation in the residual curve in S109 (Fig. 2.10c) was not caused by the emergent vegetation.

By elimination, the major consumption of infiltrated water occurs in the non-inundated portion of the wetland. This finding is significant because it indicates that only a part of the infiltration in the pond leaves the wetland, while the rest is evapotranspired within the wetland.

The average pan evaporation rate was 3.0 mm d^{-1} in S109, and 3.5 mm d^{-1} in S120 during the period of measurement, which was close to the evapotranspiration rate from the ponds obtained by the Bowen ratio-energy balance method (3.4 mm d^{-1} for S109 and 3.7 mm d^{-1} for S120). Note that these values are smaller than the evaporation rate in July (3.9-5.1 mm d^{-1}) reported at the Last Mountain Lake, 100 km south-east of the field site (Morton, 1983, p.98). Horizontal wind speed measurements during the pan experiments showed that the willow ring around the wetlands blocks the wind from the surrounding slopes. It is likely, therefore, that the rate of evapotranspiration from the wetlands is significantly smaller than the rate of evapotranspiration that would occur in an infinitely small wet surface in the adjacent dry land that has the same albedo and heat storage as the pond water surface.

The average infiltration rate during the period of measurement was 9.4 mm d^{-1} in S109 and 7.3 mm d^{-1} in S120, which were equal to 76 and 68 % of the total water loss from the respective wetland. These ratios represent only a few weeks in which the experiments were conducted. However, independent measurements by a chloride mass balance method showed that the average ratio of infiltration to total water loss over the entire summer and fall was also in the range of 70-80 % (Chapter 3).

Hydraulic property of glacial till

Saturated hydraulic conductivity measured by slug tests was on the order of 10^{-6} m s^{-1} near the surface, and decreased with depth in the oxidized till (Fig. 2.12), except in the piezometers that had the sand pack at the depth where sand lenses were found in drilling. In the unoxidized till, hydraulic conductivity was on the order of 10^{-9}-10^{-11} m s^{-1}. Similar contrast in hydraulic conductivity was reported in glacial till near Saskatoon (Keller et al., 1989). They concluded that the high hydraulic conductivity in the oxidized till was caused by a well-developed fracture network, and the low value represented the hydraulic conductivity of the till matrix. The lowest value at our site is approximately 10^{-11} m s^{-1} (shaded area in Fig. 2.12), which is consistent with the values reported by them. It should be noted that the unoxidized till still has the hydraulic conductivity higher than the matrix, therefore the fractures are likely present, though at a lower frequency, in the unoxidized till. Similar occurrence of fractures in the unoxidized till was reported by Keller et al. (1986).

Unsaturated hydraulic conductivity was measured for all 20 tensiometers in the fall of 1994, and for most of them in the summer of 1995 (Fig. 2.13). In general, conductivity decreased by orders of magnitude as matric potential head and moisture content decreased. The unsaturated conductivity of the deeper soil was lower than that of shallower soil at the same matric potential (Fig. 2.13). This difference is likely due to the reduction of saturated hydraulic conductivity with depth (Fig. 2.12).

Groundwater flow

The hydraulic head distribution in the spring of 1994 (Fig. 2.14a) indicates that the subsurface flow direction was outward, from the wetland to the slope. Dense contour lines at a depth of 8-9 m indicate that vertical flow was impeded by the clay layer (Fig. 2.4). The outward flow continued during the summer (Fig. 2.14b), but the pond became dry and horizontal gradients were negligible in the late fall (Fig. 2.14c). The contours in the vadose zone are only shown in Figure 2.14b, because tensiometer readings were only taken in the summer and fall of 1994. The field around the wetland was summer fallowed in 1995. The head distribution in the spring of 1995 was similar to that in 1994, however the water table in the slope area kept rising in the summer and the flow direction became inward in the fall (Fig. 2.14d).

The hydraulic head in the WRG piezometer (23 in Fig. 2.3, depth 1.9m) responded quickly to the water level rise in the pond in the spring, and remained lower than the pond water level in the summer (Fig. 2.8c). Note the curve labeled as "pond" in Figure 2.8c was measured in a water table monitoring well (5 in Fig. 2.3) located in the wetland, thus it indicates the groundwater table below the wetland. The water level in the TOP piezometer (26 in Fig. 2.3, depth 4.7 m) did not respond to snowmelt until mid-May (Fig. 2.8c). Comparison of Figures 2.8c and 2.8e shows that the water level rise in the slope started when soil thawing was complete. The delay in the WRG water level in 1995 is perhaps due to the freezing condition in the shallow soil under the willow ring that only occurred in 1995.

The vertical hydraulic gradient below the clay layer at the WRG and TOP sites was nearly constant and downward throughout the year (Fig. 2.15). At the WRG piezometer (25 in Fig. 2.3) the gradient between the depths of 14.6 m and 21.8 m was 0.17, while the harmonic mean hydraulic conductivity was 6.2×10^{-10} m s^{-1}. At the TOP piezometer (27 in Fig. 2.3) the gradient between 18.2 m and 21.9 m was 0.26, while the mean conductivity was 1.7×10^{-10} m s^{-1}. The estimated groundwater recharge rates at WRG and TOP sites are 3.3 and 1.4 mm yr^{-1}, respectively. This estimate is sensitive to the value of hydraulic conductivity, therefore the error in estimation is expected to be as large as 100-200 %.

Vadose zone

In response to storm events and subsequent periods of evapotranspiration the direction of hydraulic gradient changed frequently in the top one meter of the vadose zone in the slope, but the gradient was generally upward in the summer (Figs. 2.14b and 2.15). The gradient was consistently upward in the deeper vadose zone, while it was downward below the water table. An imaginary plane located at the transition point between the upward and downward gradient is called a divergent zero-flux plane (Wellings and Bell, 1980). The divergent zero-flux plane existed at the WRG and TOP sites throughout the summer, indicating that the infiltration from the surface never went below the root zone (depth of 1-2 m).

Soil moisture content measured at separate depth intervals (0-0.3, 0.3-0.5, 0.5-0.7, 0.7-0.9, 1.3-1.5, 1.9-2.1 m) was integrated to calculate total water storage between the surface and 2.1 m. The moisture content at missing interval, 0.9-1.3 and 1.5-1.9 m, was estimated by interpolation. The water storage in 1994 was maximum in spring and decreased during summer at all three TDR sites (Fig. 2.16). The steep increase of water storage at TOP site in spring indicates thawing, because the TDR method measures liquid water content. The water loss between JD 180 and JD 310 at WRG, MID, and TOP sites was 110, 120, and 110 mm, respectively.

The flow direction in the vadose zone under the slope is predominantly vertical, therefore the water balance in this zone is given by;

$$I - G - ET = \Delta S \tag{2.3}$$

where I is infiltration, G is drainage into the deeper zone, ET is evapotranspiration, and ΔS is the storage change. The water loss, $-\Delta S$, from the top 2.1m of till between JD 180 and JD 310 of 1994 was 110-120 mm. The rainfall in this 130-day period was 150 mm, most of which became infiltration (I = 150 mm) because overland flow did not occur during this period. The hydraulic gradient was mostly upward from the water table to the root zone (Fig. 2.15), hence the drainage flux was negative; $G < 0$. Therefore the evapotranspiration in this 130-day period was at least 260 mm ($ET = I - \Delta S - G > 150 + 110$) or 2 mm d^{-1} on average. From this observation, it is likely that the evapotranspiration on the slope is quite effective and capable of consuming all precipitation; therefore, very little net infiltration is expected in the slope. Zebarth and de Jong (1989) reported similar results in the slopes surrounding groundwater-recharge wetlands near Hafford, 100 km west of St. Denis.

Complexity of wetland-groundwater interaction

We have described the average patterns of subsurface flow; a large amount of infiltration in the wetland, divergent groundwater flow from the wetland to the slope, and upward flow from the water table to the root zone in the slope. The average patterns capture the essence of the flow system, but the wetland and groundwater interact in more complex ways.

For example the cultivated field on the south side of the wetland has a much steeper slope than the rest of the catchment (Fig. 2.3), which causes the hydraulic gradient in this side to become convergent when the water table under the wetland drops in late fall of dry years. The convergent hydraulic gradient was very weak in 1994 (Fig. 2.14c), but it was more pronounced in 1993. The similar reversal of hydraulic gradient was reported by Meyboom (1966b). We visited his site in 1995 to find that the piezometers used in his study to show the gradient reversal were also placed along the steepest slope in the catchment.

Another example of the complex wetland-groundwater interaction is the rises in the residual curve on JD 179 and JD 186 (Fig. 2.10c), which indicates that the pond was receiving water from the surrounding area. For the storm events in the period between April 1994 and August 1996 that had more than 10 mm of precipitation, the water level change caused by them was slightly higher than the amount of precipitation on average (Fig. 2.17). Only one storm during this period (not plotted in Fig. 2.17) caused the water level change significantly higher than the precipitation. The storm caused 210 mm of water level change (Fig. 2.18b) in the pond, even though the precipitation was only 54 mm (Fig. 2.18a). The hydraulic head in a piezometer (22 in Fig. 2.3, depth 1.9 m, basic time lag 1 minute) outside the willow ring became higher than the pond water level during the storm.

For normal storms (Fig. 2.17), the extra rise in water level in the pond (Fig. 2.10c) is likely to be caused by saturation overland flow in the proximity of the pond where the capillary fringe is close to the ground surface (Dunne, 1983; Gerla, 1992). The large water level change during

the unusually large storm (Fig. 2.18b) is likely to be caused by both saturation overland flow and subsurface storm flow.

Discussion

Divergent subsurface flow around S109

The flow field around S109 depicted by hydraulic head distribution was strongly divergent in the spring and summer (Fig. 2.14) of 1994. This pattern is a distinguishing feature of the groundwater-recharge wetlands (Meyboom, 1966b; Lissey, 1968; and others). The dense distribution of piezometers and tensiometers in this study made possible the detailed description of the stratified structure of the flow field reported in previous studies (Mills and Zwarich, 1986; Zebarth et al., 1989).

Due to the sharp contrast in saturated hydraulic conductivity between the strongly fractured and weakly fractured till (Fig. 2.12), and the presence of a clay layer, the flow direction is predominantly horizontal between the water table and the oxidation front in outward radial patterns, and vertically downward below the oxidation front, i.e. in the weakly fractured till (Fig. 2.19). Above the zone of horizontal flow, the flow direction is generally vertical upward. This trend was due to the contrast in the hydraulic conductivity, which decreases sharply once the soil becomes unsaturated (Fig. 2.13). To meet with the consumption of water in the slope, the horizontal flow zone acts like a conveyer belt that distributes water from the wetland to the root zone in the slope (Fig. 2.19).

The divergent flow is sustained by the infiltration in the wetland and the evapotranspiration in the slope. Evapotranspiration was greatly reduced in 1995, when the field in the slope was summer fallowed. Infiltration of precipitation in the slope caused continuous rise of water table at the TOP site in the summer (Fig. 2.8c), and the subsurface flow pattern became convergent in the fall (Fig. 2.14d). This observation indicates that the land use practice can have a large impact on the hydrology of the prairie wetlands.

Average water flux in the hydrologic cycle

From the detailed data of the hydrologic cycle in 1994, we can estimate the average flux of each component in the cycle in 1994 (Fig. 2.20). The annual precipitation for the hydrologic year 1994 is 376 mm (Table 2.1), of which 45 mm in the slope becomes effective snowmelt runoff (Table 2.1) and went into the wetland. Note that the area of the wetland is 1/9 of the area of the slope. The total input of water in the wetland, precipitation plus effective snowmelt runoff, is 781 mm.

Evapotranspiration rate in the pond in the wetland is assumed to be 25 % of the rate of water level drop based on the evaporation pan measurements. On this assumption we analyzed the hydrograph of the pond (Fig. 2.8b) and estimated the total evapotranspiration in the

summer and fall of 1994 to be 241 mm. The non-inundated part of the wetland has dense aquatic vegetation and the water table close to the ground surface. Due to the blockage of wind by the willow ring, the microclimate within the wetland is expected to be reasonably uniform. Therefore, we assume that the evapotranspiration in the non-inundated part is equal to that in the pond. Because the evapotranspiration in the winter and spring is expected to be small, we assume that the total evapotranspiration in the entire wetland is 300 mm.

Subtracting the evapotranspiration from the total input, the amount of water leaving the wetland is 481 mm, of which only 2 mm becomes groundwater recharge, and the rest is consumed by the evapotranspiration in the slope. Evapotranspiration in the slope consumed the water transferred from the wetland and the precipitation minus runoff and recharge, hence it is 389 mm. The estimated evapotranspiration in the slope is greater than that in the wetland, presumably because the willow ring blocks the wind and suppress the evapotranspiration in the wetland. Woo and Rowsell (1993), studying a wetland (S50) located 1500 m west of our field site, reported higher evapotranspiration in the wetland (213 mm) than in the slope (183 mm) in March-August 1990. The wetland S50 has trees only on its southern margin, therefore the wind speed is not significantly reduced in the wetland.

Even though the estimated flux in Figure 2.20 has a large degree of uncertainty, a few important points should be noted. First of all, the large infiltration occurs in the wetland, but only a small part of it becomes groundwater recharge to the underlying aquifer. Secondly a large amount of water is transferred from the wetland to the slope by horizontal subsurface flow. The magnitude of the divergent subsurface flow is approximately equal to that of effective snowmelt runoff from the slope to the wetland. Note that the magnitude of snowmelt runoff and the divergent flow in the average year will be considerably smaller, because the snowmelt runoff and summer precipitation in 1994 was much higher than the average value (Fig. 2.9).

Conclusions

The St. Denis National Wildlife Area, located in the undulating terrain of the northern prairies, has many wetlands. The wetlands at relatively high elevation recharge the groundwater system that supply water to the local aquifer and the wetlands at low elevation. Large infiltration in the recharge wetlands drives the divergent subsurface flow under the surrounding slopes. The subsurface flow from the wetlands to the slopes is particularly pronounced in the zone below the water table and above the oxidation front, because the saturated hydraulic conductivity in the oxidized glacial till in this zone is several orders of magnitude higher than the unoxidized till. Above the water table, the average flow direction is upward due to evapotranspiration. Below the oxidation front, the flow direction is downward throughout the year.

The infiltration in the wetland can be quantified by analyzing the water level fluctuation in the pond in the wetland, which is an integrated measure of precipitation, infiltration, and evapotranspiration. The infiltration accounts for 70-80 % of the water loss from the wetland in the summer. The evapotranspiration rate in the wetland is significantly smaller than the expected rate of evaporation from the wet surface in the surrounding slope, because the wind speed in the wetland is reduced by the willow ring that covers the perimeter of the wetland.

The cold winter in the northern prairie region freezes the top soil in the slope, and hence reduces the hydraulic conductivity of the soil. As a result, a large portion of snow in the slope becomes snowmelt runoff into the wetland. Therefore, the divergent subsurface flow is accompanied by the convergent surface flow. The amount of water transferred from the slope to the wetland as the surface flow each year is approximately equal to that of the subsurface water transfer from the wetland to the slope. This dual nature of the hydrologic cycle has a major influence on the transport cycle of dissolved chemical species, which will be investigated in the next chapter.

References

Assouline, S. and Mahrer, Y., 1993. Evaporation from Lake Kinneret. 1. Eddy correlation system measurements and energy budget estimates. Water Resour. Res., 29, 901-910.

Atmospheric Environment Service, 1996. Canadian daily climate data on CD-ROM, Western Canada. Atmospheric Environment Service, Environment Canada, Downsview, Ontario.

Batt, B.D.J, Anderson, M.G., Anderson, C.D. and Caswell, F.D., 1989. The use of prairie potholes by North American ducks. In: Northern prairie wetlands, van der Valk, A., ed., 204-227, Iowa St. Univ. Press, Ames, Iowa.

Cassell, D.K. and Klute, A., 1986. Water potential: tensiometry. In: Methods of soil analysis, I. Physical and mineralogical methods - Agronomy Monograph no.9., 2nd ed., Soil Sci. Soc. Am., 563-596.

Dunne, T., 1983. Relation of field studies and modeling in the prediction of storm runoff. J. Hydrol., 65, 25-48.

Eisenlohr, Jr. Wm.S., 1966. Water loss from a natural pond through transpiration by hydrophytes. Water Resour. Res., 2, 443-453.

Gardner, W.R., 1960. Measurement of capillary conductivity and diffusivity with a tensiometer. Trans. 7th Intern. Congr. Soil Sci., Madison, Wisconsin, 300-305.

Gerla, P.J., 1992. The relationship of water-table changes to the capillary fringe, evapotranspiration, and precipitation in intermittent wetlands. Wetlands, 12, 91-98.

Hillel, D., 1981. Fundamentals of soil physics. Academic Press, New York, 413pp.

Hvorslev, M.J., 1951. Time lag and soil permeability in ground-water observations. Corps of Engineers, U.S. Army, Waterways Experiment Station, Bull. No.36. 50pp

Keller, C.K., van der Kamp, G. and Cherry, J.A., 1986. Fracture permeability and groundwater flow in clayey till near Saskatoon, Saskatchewan. Can. Geotech. J., 23, 229-240.

Keller, C.K., van der Kamp, G. and Cherry, J.A., 1988. Hydrogeology of two Saskatchewan tills, I. Fractures, bulk permeability, and spatial variability of downward flow. J. Hydrol., 101, 97-121.

Keller, C.K., van der Kamp, G. and Cherry, J.A., 1989. A multiscale study of the permeability of a thick clayey till. Water Resour. Res., 25, 2299-2317.

LaBaugh, J.W., Winter, T.C., Adomaitis, V.A. and Swanson, G.A., 1987. Hydrology and chemistry of selected Prairie wetlands in the Cottonwood Lake area, Stutsman County, North Dakota, 1979-1982. U.S.G.S. Prof. Pap., 1431. 26pp.

Leitch, J.A., 1989. Politicoeconomic overview of prairie potholes. In: Northern prairie wetlands, van der Valk, A., ed., 2-14, Iowa St. Univ. Press, Ames, Iowa.

Lissey, A., 1968. Surficial mapping of groundwater flow systems with application to the Oak River Basin, Manitoba. Ph.D. thesis, Univ. of Saskatchewan, Saskatoon, Saskatchewan.

Malek, E. and Bingham, G.E., 1993. Comparison of the Bowen ratio-energy balance and the water balance methods for the measurement of evapotranspiration. J. Hydrol., 146, 209-220.

Marthaler, H.P., Vogelsanger, W., Richard, F. and Wierenga, P.J., 1983. A pressure transducer for field tensiometers. Soil Sci. Soc. Am. J., 47, 624-627.

Meyboom, P., 1966a. Groundwater studies in the Assiniboine River drainage basin., Part I: The evaluation of a flow system in south-central Saskatchewan. Geol. Surv. Can. Bull., 139. 65pp.

Meyboom, P., 1966b. Unsteady groundwater flow near a willow ring in hummocky moraine. J. Hydrol., 4, 38-62.

Meyboom, P., 1967. Mass-transfer studies to determine the groundwater regime of permanent lakes in hummocky moraine of western Canada. J. Hydrol., 5, 117-142.

Miller, J.J., 1983. Hydrology of a morainic landscape near St. Denis, Saskatchewan, in relation to the genesis, classification and distribution of soils. M.Sc. thesis, Univ. of Saskatchewan, Saskatoon, Saskatchewan.

Miller, J.J., Acton, D.F. and St. Arnaud, R.J., 1985. The effect of groundwater on soil formation in a morainal landscape in Saskatchewan. Can. J. Soil Sci., 65, 293-307.

Mills, J.G. and Zwarich, M.A., 1986. Transient groundwater flow surrounding a recharge slough in a till plain. Can. J. Soil Sci., 66, 121-134.

Morton, F.I., 1983. Operational estimates of lake evaporation. J. Hydrol., 66, 77-100.

Ohmura, A., 1982. Objective criteria for rejecting data for Bowen ratio flux calculations. J. Appl. Meteorol., 21,595-598.

Redman, J.D., 1996. WATTDR user's guide. Internal report, Univ. of Waterloo, Waterloo, Ontario.

Shjeflo, J.B., 1968. Evapotranspiration and the water budget of prairie potholes in North Dakota. U.S. Geol. Survey Prof. Paper 585-B, 47pp.

Sloan, C.E., 1972. Ground-water hydrology of prairie potholes in North Dakota. U.S. Geol. Survey Prof. Paper 585-C, 28pp.

Topp, G.C. and Davis, J.L., 1985. Measurement of soil water content using time-domain-reflectometory (TDR): a field evaluation. Soil Sci. Soc. Am. J., 49, 19-24.

Topp, G.C., Davis, J.L. and Annan, A.P., 1980. Electromagnetic determination of soil water content: measurements in coaxial transmission lines. Water Resour. Res., 16, 574-582.

Trudell, M.R., 1994. Soil salinization associated with shallow groundwater flow systems in thin, fractured till moraine. Ph.D thesis, Univ. of Waterloo, Waterloo, Ontario.

Wellings, S.R. and Bell, J.P., 1980. Movement of water and nitrate in the unsaturated zone of Upper Chalk near Winchester, Hants, England. J. Hydrol., 48, 119-136.

Winter, T.C., 1989. Hydrologic studies of wetlands in the northern prairies. In: Northern prairie wetlands, ed. van der Valk, A., 17-54. Iowa Univ. Press.

Winter, T.C. and Rosenberry, D.O., 1995. The interaction of ground water with prairie pothole wetlands in the Cottonwood Lake area, east-central North Dakota, 1979-1990. Wetlands, 15, 193-211.

Woo, M.-K. and Rowsell, R.D., 1993. Hydrology of a prairie slough. J. Hydrol., 146, 175-207.

Woo, M.-K., Rowsell, R.D. and Clark, R.G., 1993. Hydrological classification of Canadian prairie wetlands and prediction of wetland inundation in response to climatic variability. Can. Wildlife Service, Occasional Pap., no. 79, 24pp.

Woo, M.-K. and Winter, T.C., 1993. The role of permafrost and seasonal frost in the hydrology of northern wetlands in North America. J. Hydrol., 141, 5-31.

Zebarth, B.J. and de Jong, E., 1989. Water flow in a hummocky landscape in central Saskatchewan, Canada, III. Unsaturated flow in relation to topography and land use. J. Hydrol., 110, 199-218.

Zebarth, B.J., de Jong, E. and Henry, J.L., 1989. Water flow in hummocky landscape in central Saskatchewan, Canada, II, Saturated flow and groundwater recharge. J. Hydrol., 110, 181-198.

Table 2.1 Summary of hydrologic parameters in 1993-1996; total annual precipitation, winter precipitation, snow water equivalent before the snowmelt period, effective snowmelt runoff, and the length of inundation of the wetland. Snow water equivalent and snowmelt are the value averaged over the catchment.

Year	Total pcp. (mm)	Winter pcp. (mm)	Snow water eqv. (mm)	Snowmelt (mm)	Inundation (months)
1993	367	60	no data	no data	5
1994	376	81	66	45	7
1995	393	77	no data	21	4
1996	390	75	66	45	8

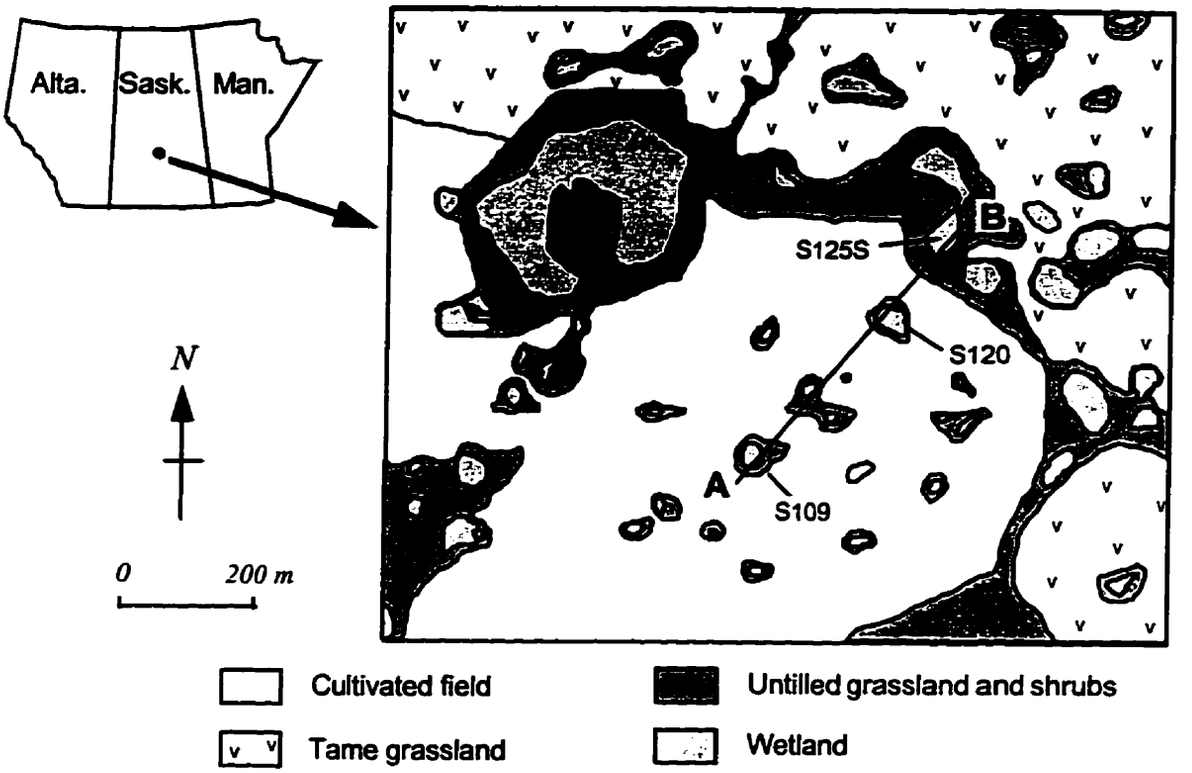

Fig. 2.1 Land classification map of the St. Denis National Wildlife Area. The original map was prepared by the Canadian Wildlife Service.

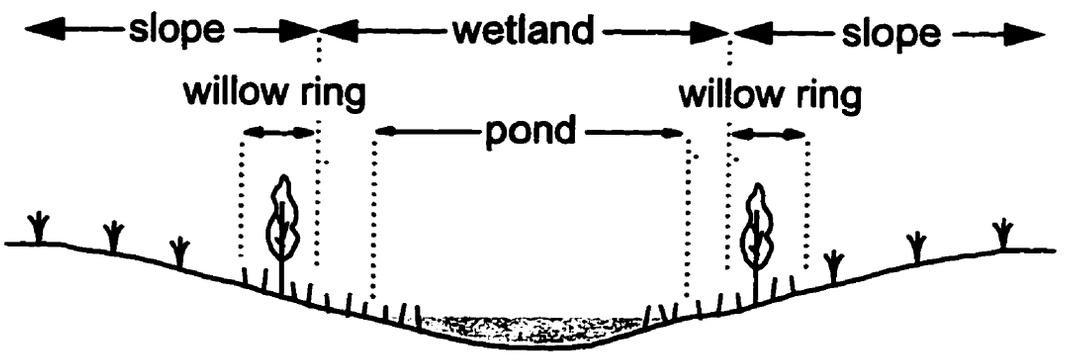

Fig. 2.2 Definition of the pond, wetland, willow ring, and the slope.

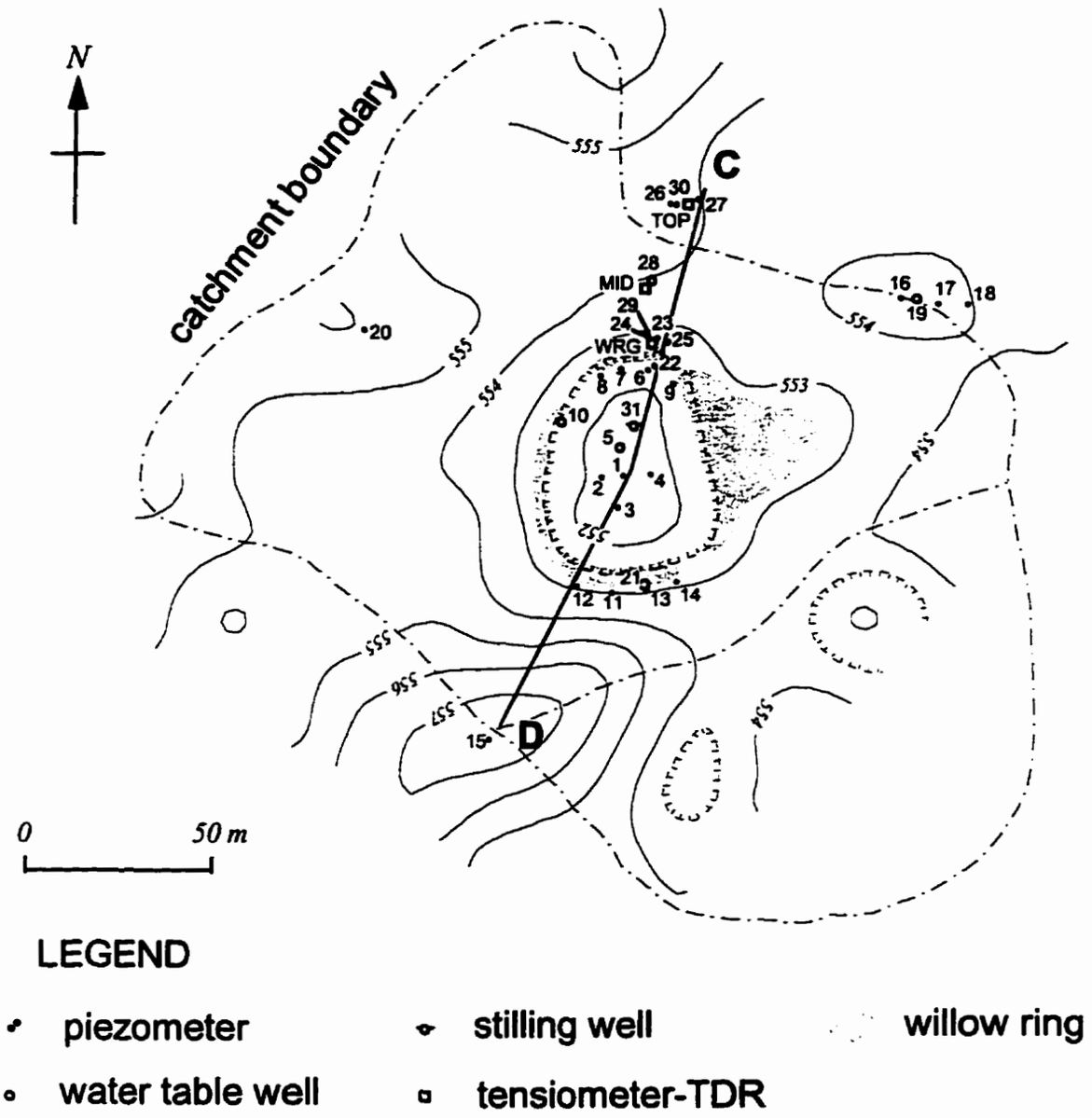

Fig. 2.3 Topographic map of the study site. The location of field instruments is indicated in the map. The elevation is in meters above sea level.

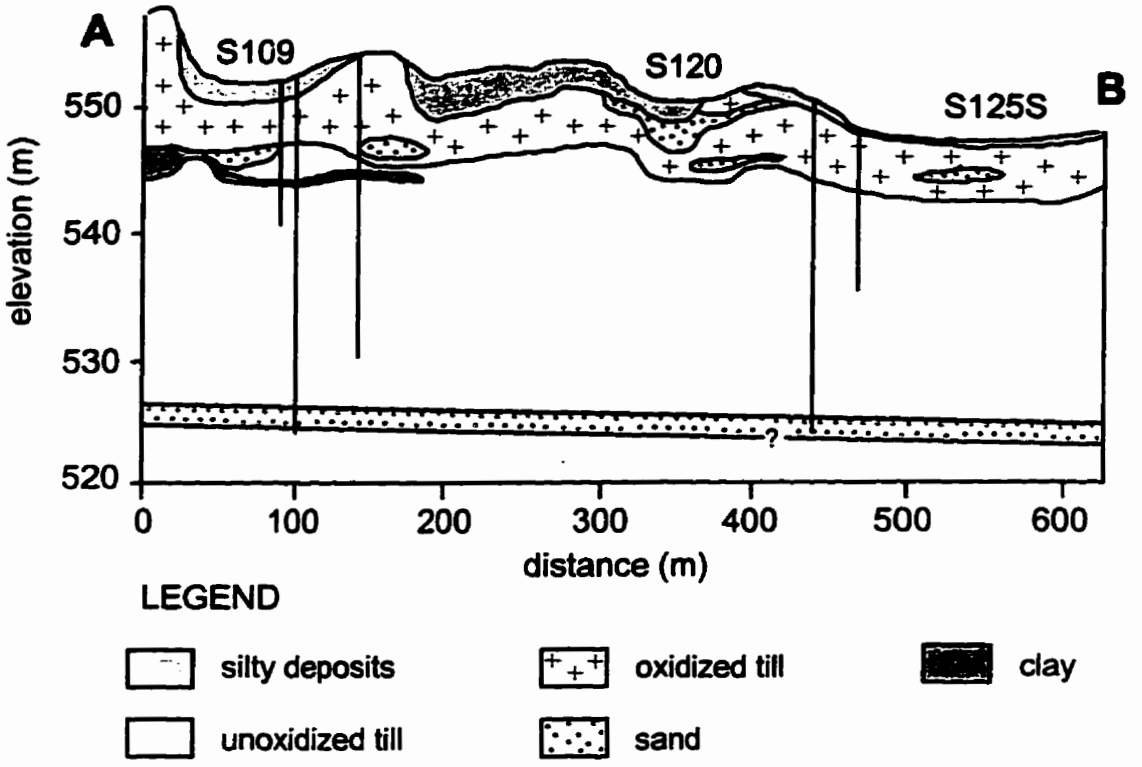

Fig. 2.4 Geological cross section of the transect AB in Figure 2.1 (modified from Miller, 1983). The location of new bore holes are shown by vertical lines.

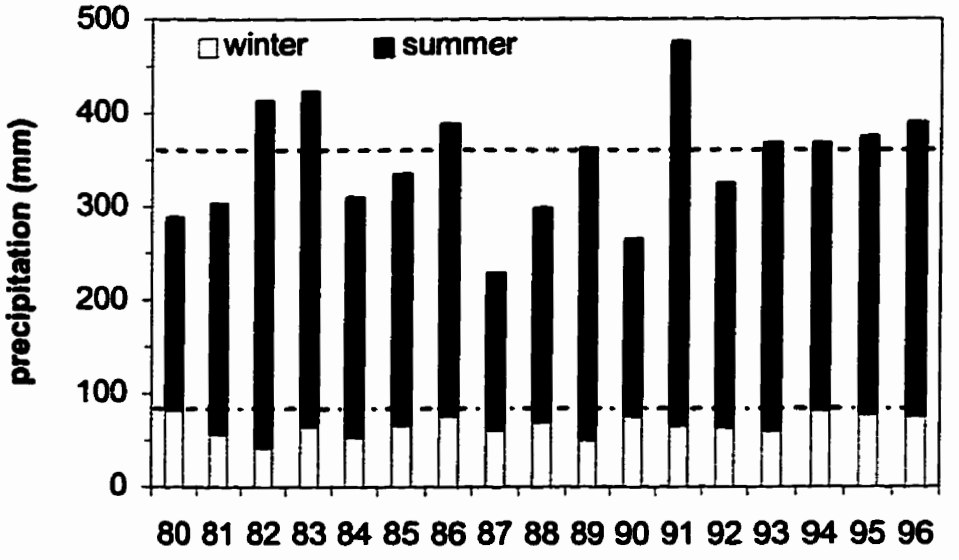

Fig. 2.5 Annual precipitation in hydrologic years 1980-1996. The dashed line and the broken line indicate 90-year mean annual and winter precipitation, respectively.

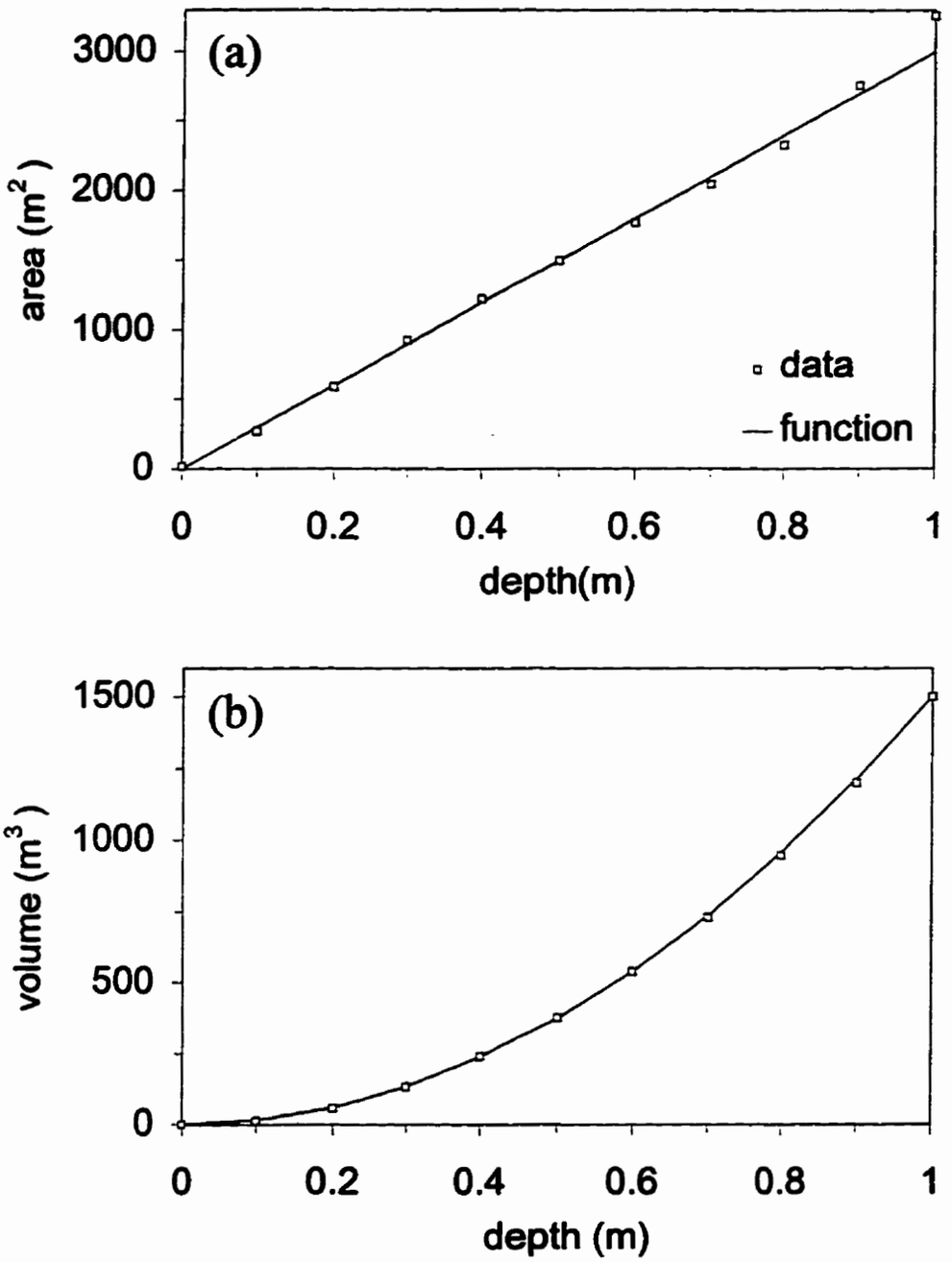

Fig. 2.6 The area-depth and volume-depth functions. (a) area-depth function. (b) volume-depth function.

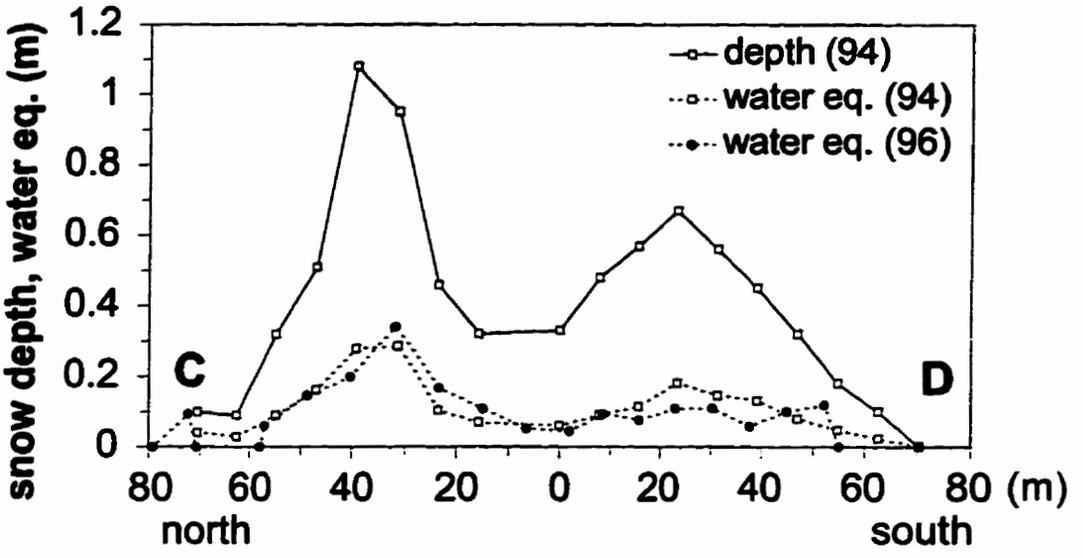

Fig. 2.7 Distribution of snow depth and water equivalent along the transect CD in Figure 2.3. The willow ring is located at 30 m from the center.

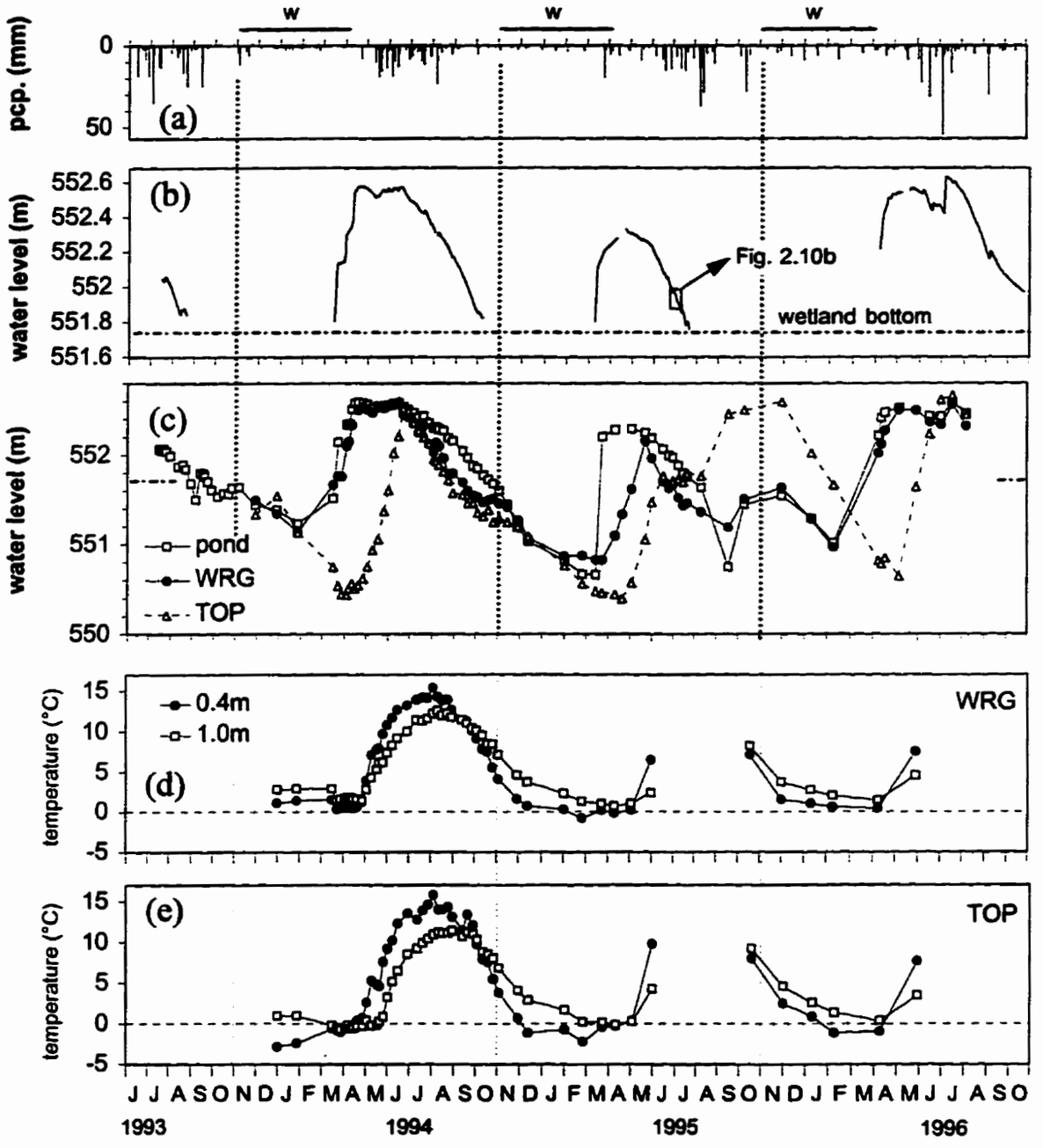

Fig. 2.8 Daily precipitation, water level, and soil temperature. Dotted lines indicate the division between hydrologic years. The winter months are indicated by bars on top of the graphs. (a) precipitation. (b) pond water level. (c) water levels in piezometers and a water table well. (d) soil temperature at WRG site. (e) soil temperature at TOP site.

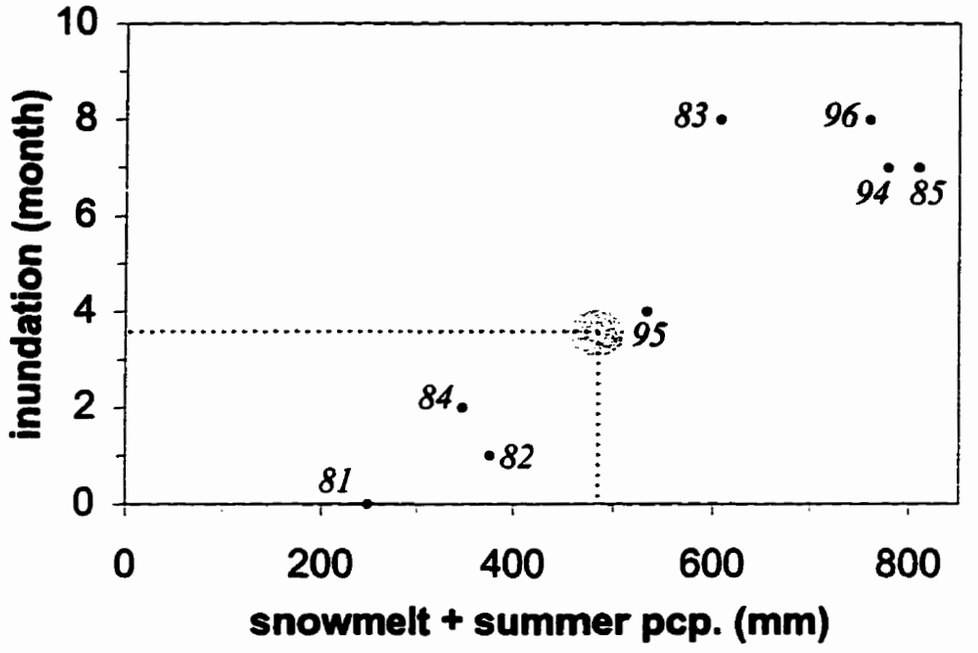

Fig. 2.9 Relationship between effective snowmelt runoff plus summer precipitation and the length of inundation. The numbers on points indicate the hydrologic year. The shaded area indicates the average length of inundation (3.6 months) in 1980-1996.

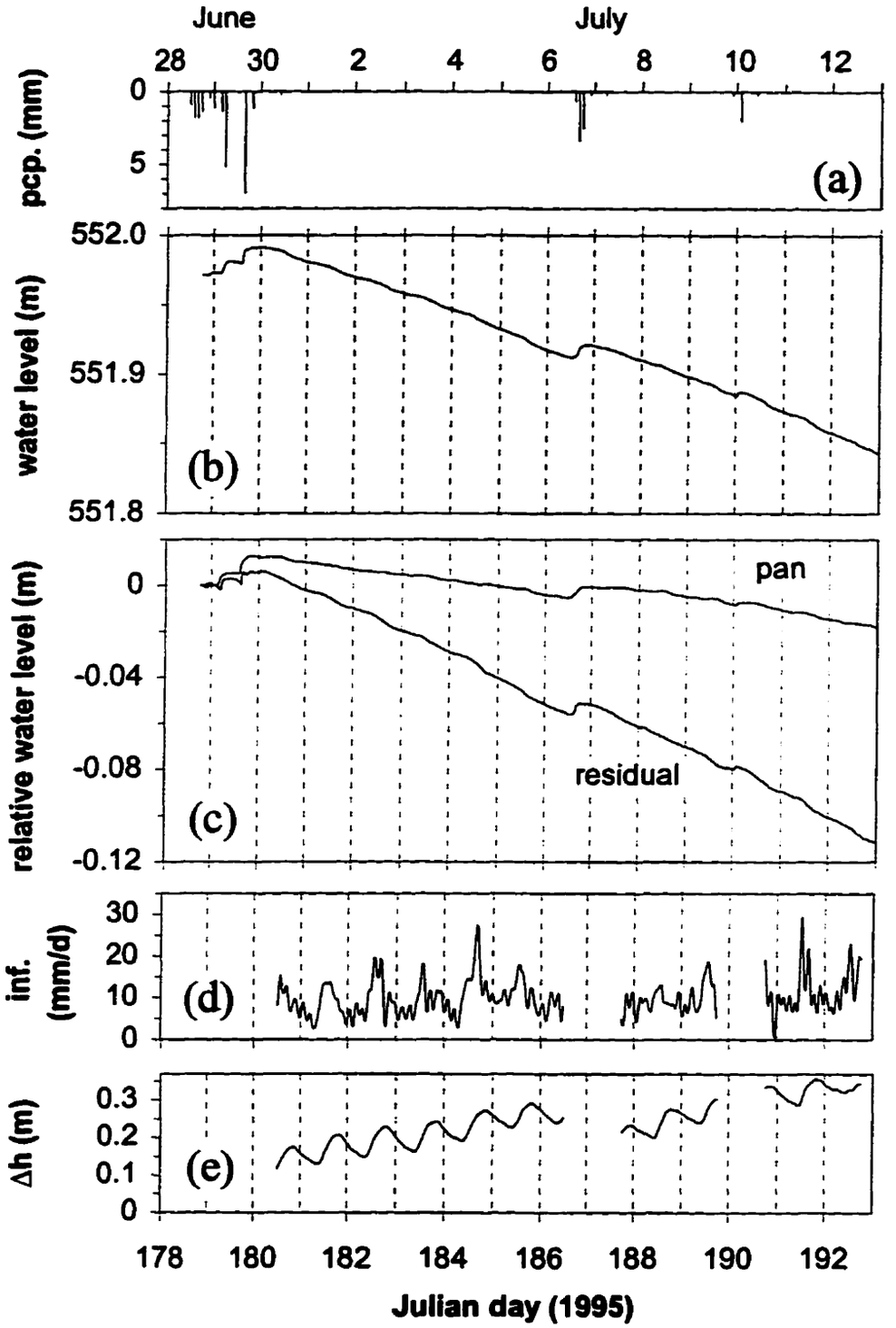

Fig. 2.10 Water level fluctuation in the pond in S109 during the period of evaporation measurement. The grid lines indicate the beginning of each day, 0:00. (a) two-hour precipitation. (b) water level in the pond. (c) water level in the pan and the residual water level, both relative to the initial level. (d) infiltration rate. (e) water level difference between the pond and a piezometer in the willow ring.

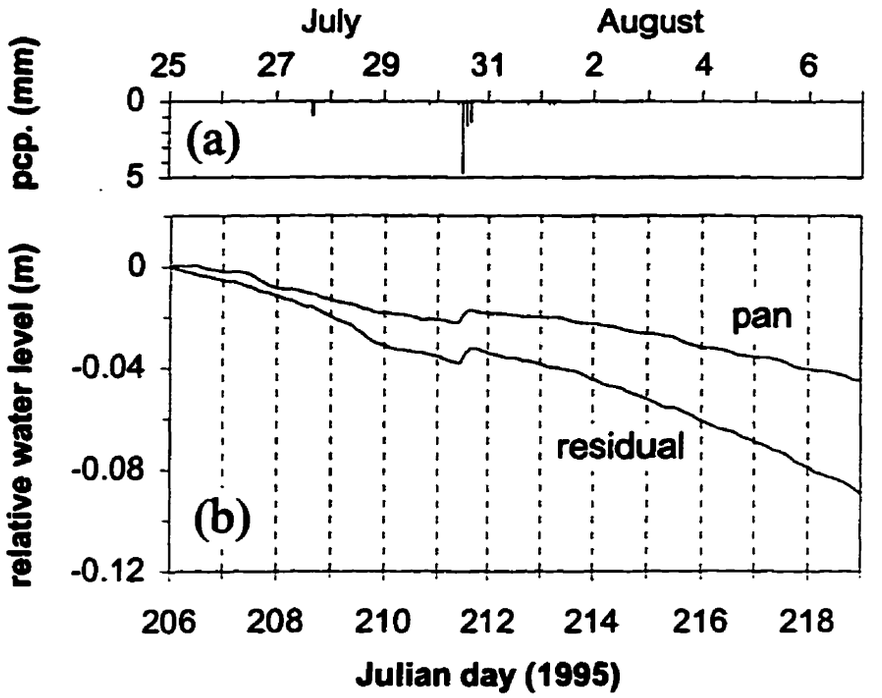

Fig. 2.11 Water level fluctuation in the pond in S120 during the period of evaporation measurement. The grid lines indicate the beginning of each day, 0:00. (a) two-hour precipitation. (b) water level in the pan and the residual water level, relative to the initial level.

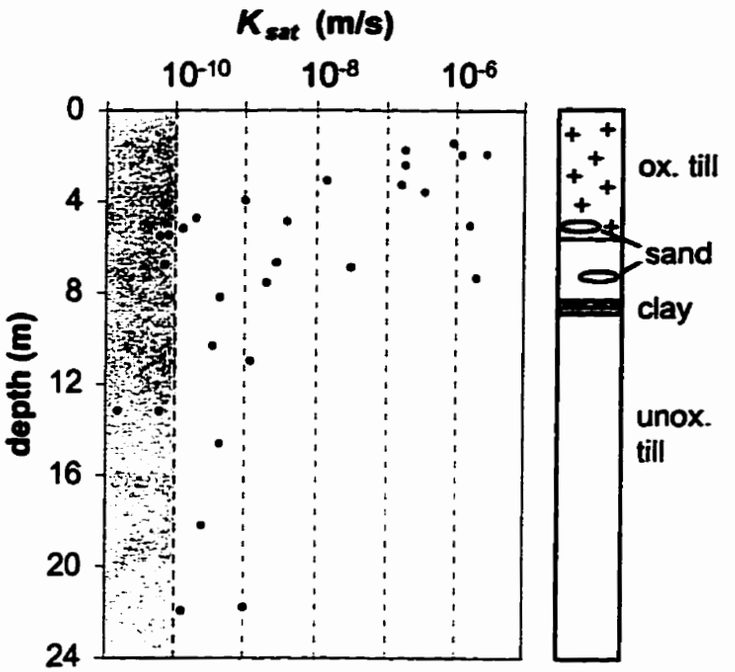

Fig. 2.12 Distribution of saturated hydraulic conductivity. Shaded area indicates the till matrix conductivity. Stratigraphy of the area is schematically shown beside the graph.

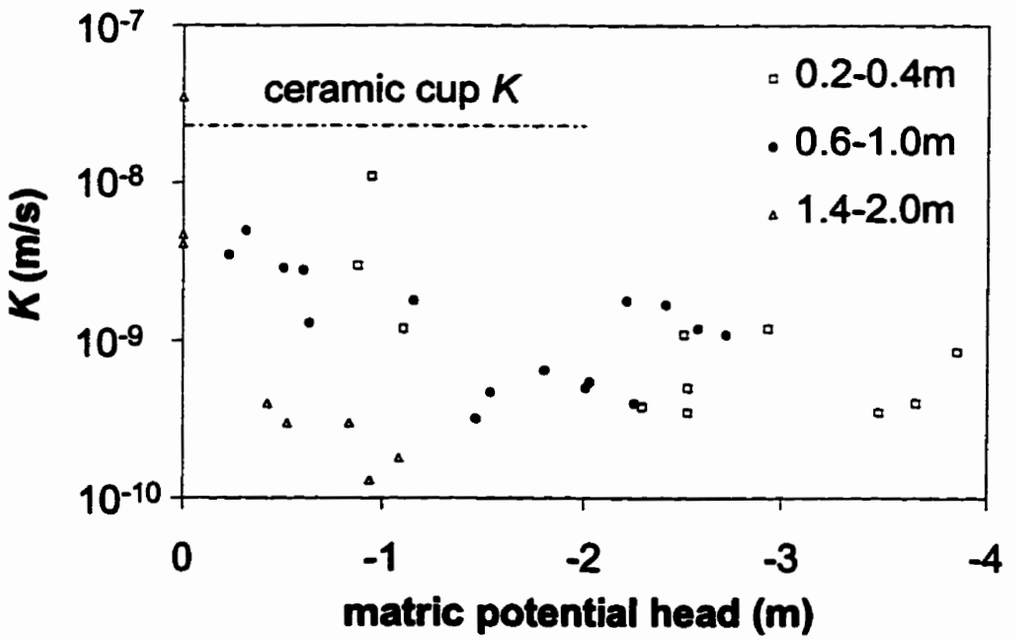

Fig. 2.13 Unsaturated hydraulic conductivity measured by the tensiometer response tests. Points are classified by the depth of porous cup. The measurement is not reliable above porous ceramic cup conductivity.

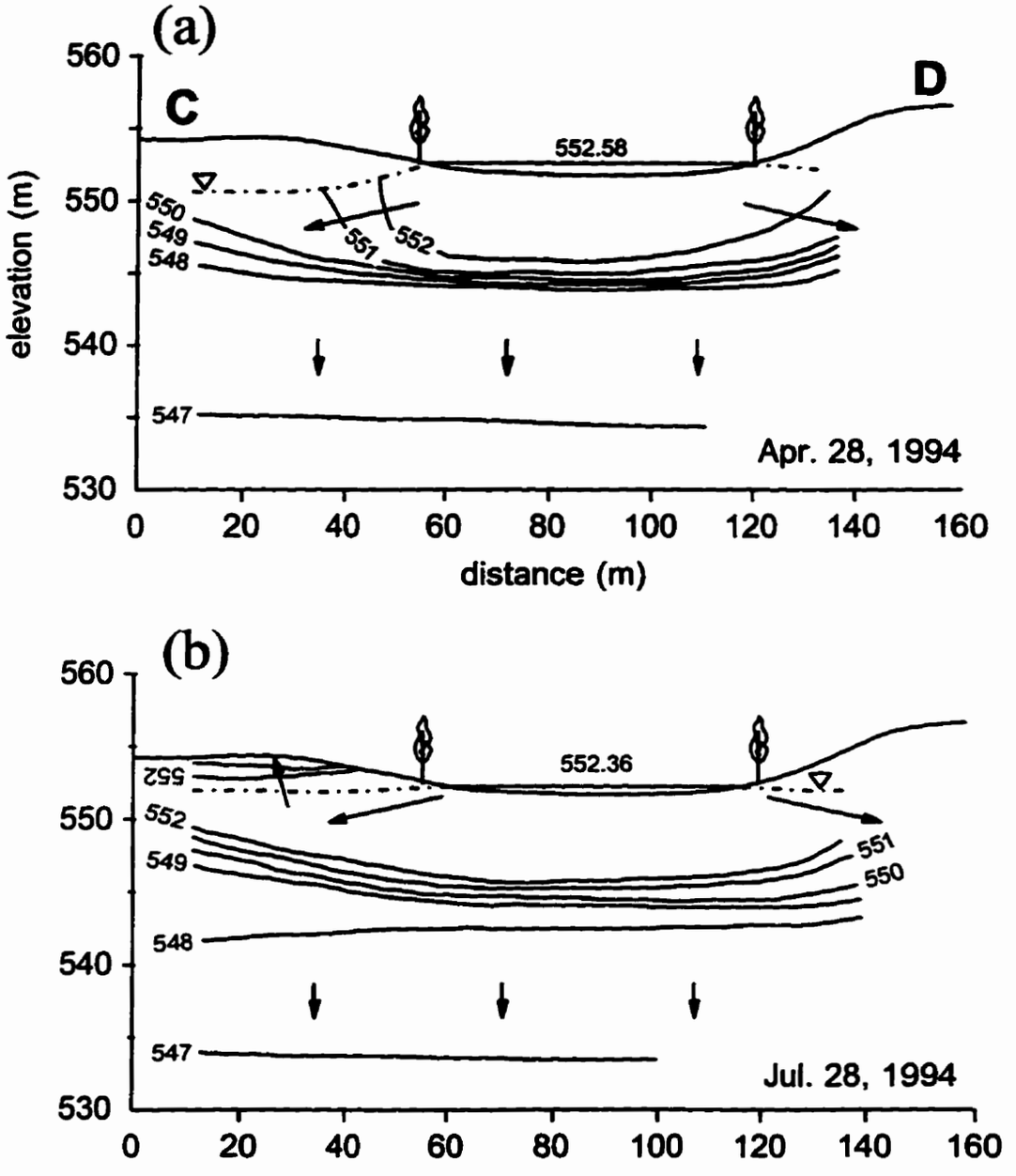

Fig. 2.14 Hydraulic head distribution along the transect CD. Arrows indicate general flow direction. (a) April 28, 1994. (b) July 28, 1994. (c) December 13, 1994. (d) September 18, 1995.

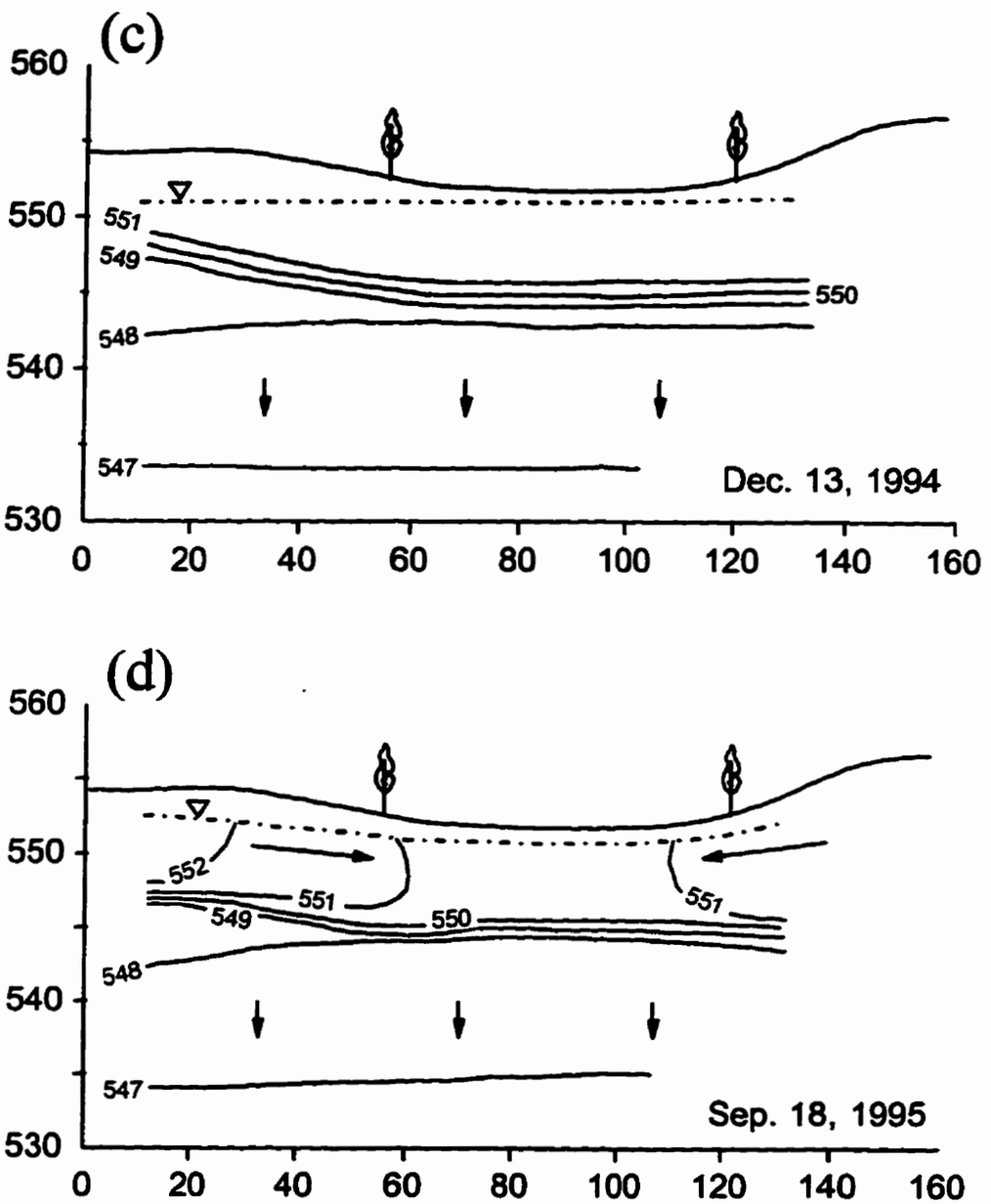

Fig. 2.14 Continued.

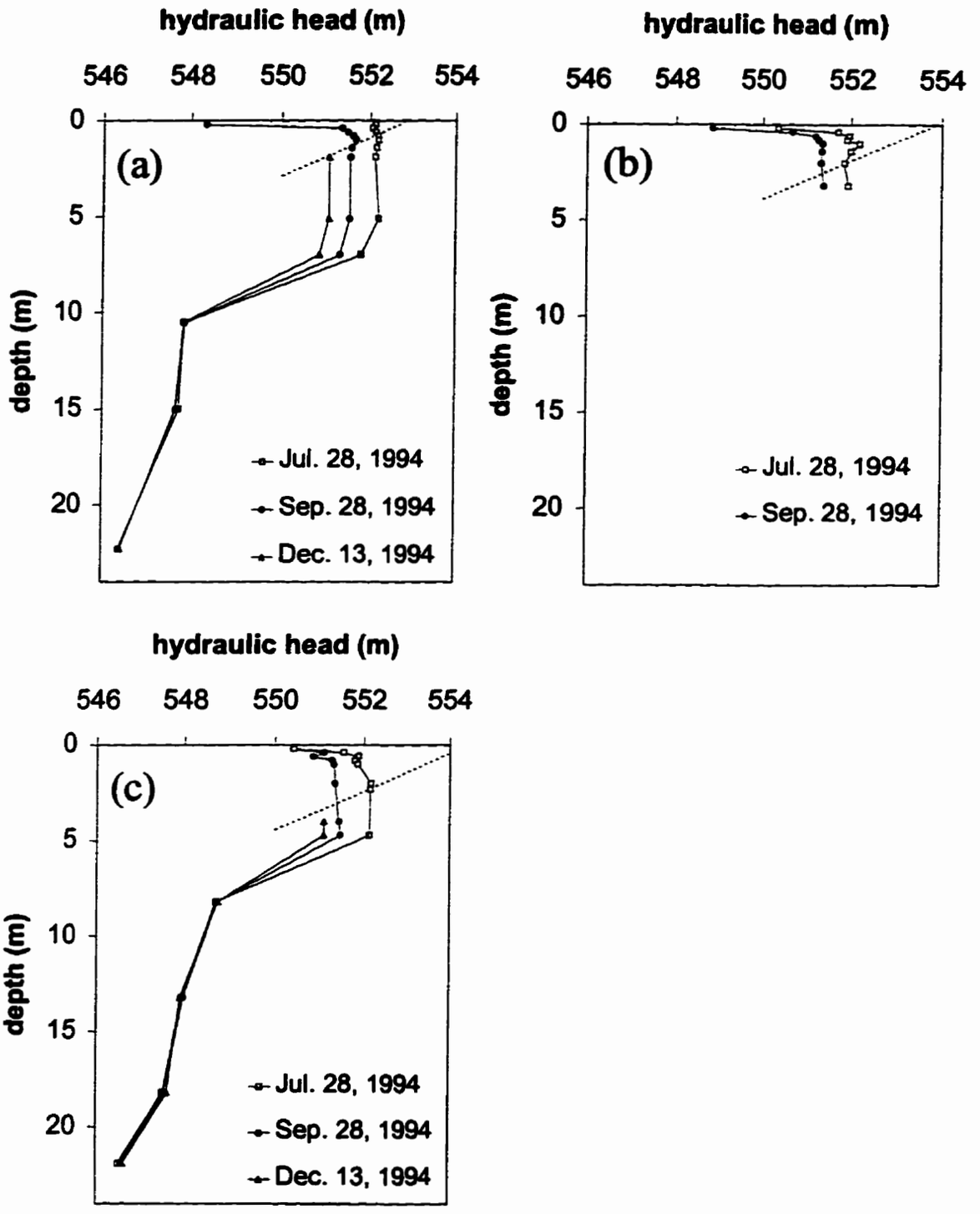

Fig. 2.15 Vertical hydraulic head distribution at three tensiometer-piezometer nests. Intersection between a profile and the dotted line (WT) indicates the position of water table. (a) WRG site. (b) MID site. (c) TOP site.

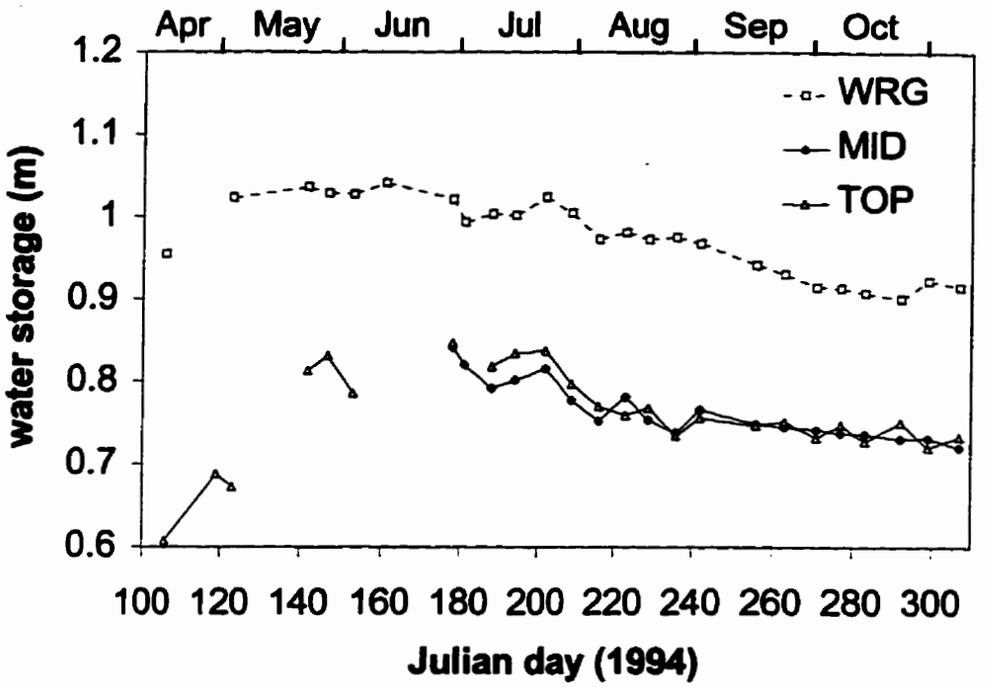

Fig. 2.16 Change in water storage in the top 2.1 m of soil at three TDR nests.

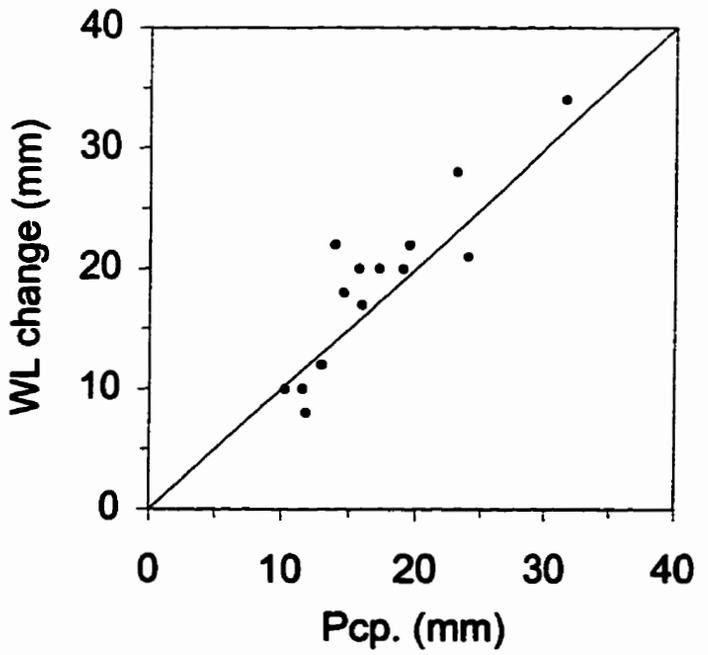

Fig. 2.17 Precipitation versus pond water level change. The straight line shows the slope of one.

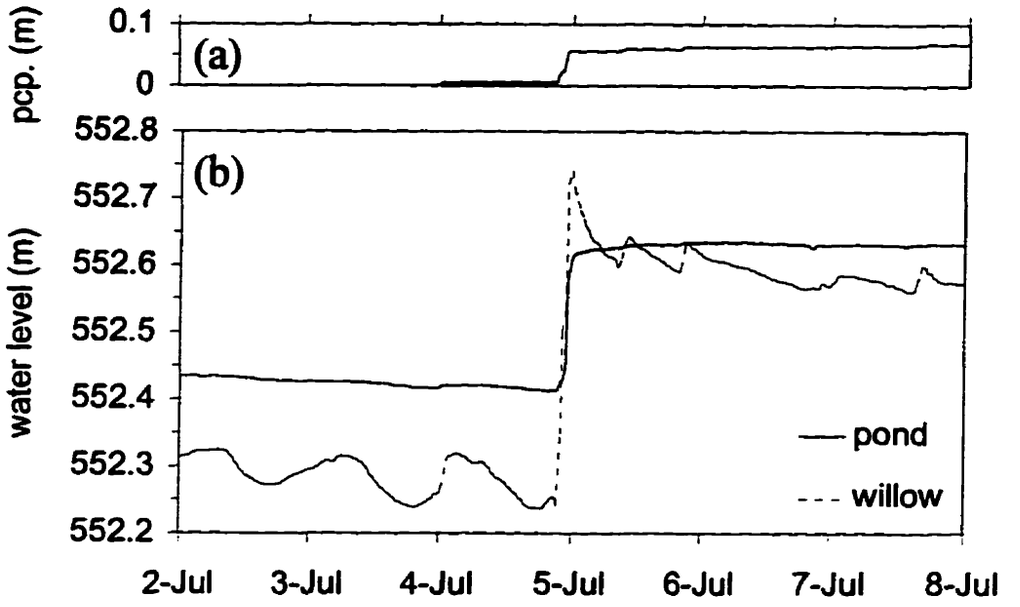

Fig. 2.18 Response of water levels to a storm on July 4, 1996. (a) Cumulative precipitation. (b) Water level in the pond and a piezometer just outside the willow ring.

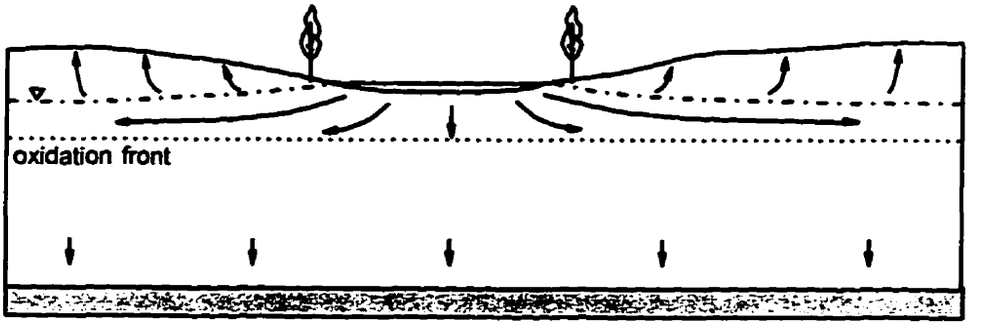

Fig. 2.19 The average subsurface flow patterns.

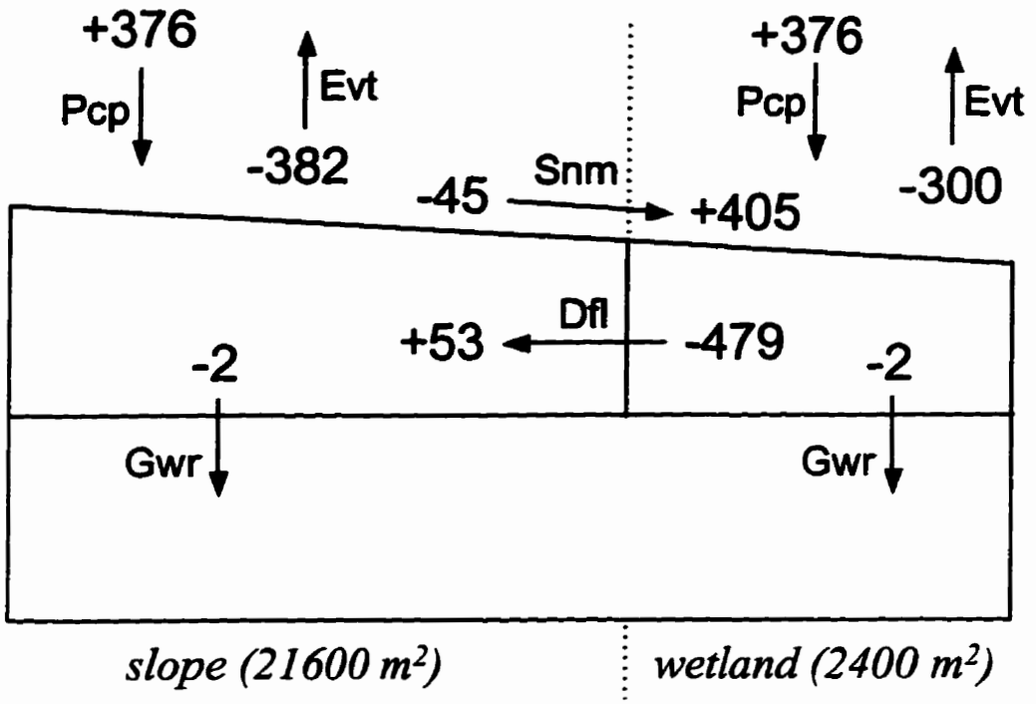

Fig. 2.20 Estimation of annual average water flux (mm) in 1994. Pcp (precipitation), Evt (evapotranspiration), Snm (snowmelt runoff), Dfl (divergent subsurface flow), Gwr (groundwater recharge).

Chapter 3

Chloride balance and surface-subsurface transport cycle in a northern prairie wetland

Introduction

The northern prairie region of North America is characterized by numerous wetlands of glacial origin commonly called sloughs or prairie potholes, which are important wildlife habitats (Batt et al. ,1989). Many prairie wetlands are located in cultivated fields, hence they are susceptible to loading of farm chemicals and excessive amounts of nutrients, which may endanger the wetland ecosystem. To understand how those dissolved chemical species move from the cultivated catchment to the wetland, it is necessary to evaluate the transport processes in each part of the surface and subsurface hydrologic systems.

The undulating terrain of the northern prairie region does not have integrated drainage systems, and each wetland serves as a focus of hydrologic processes in a closed catchment (Meyboom, 1966; Lissey, 1968). Previous researchers were mainly interested in the effects of this unique hydrologic setting on soil genesis and salt accumulation (Miller et al., 1985; Knuteson et al., 1989; Steinwand and Richardson, 1989; Keller et al., 1991; Arndt and Richardson, 1993) or chemistry of water in the wetlands (Rozkowski, 1967; LaBaugh et al., 1987). As a result, the primary focus of those studies was the subsurface transport of sulfates and carbonates. Sulfates and carbonates, however, participate in oxidation-reduction and acid-base reactions, and hence it is difficult to understand the basic transport processes of these species.

Chloride does not participate in chemical reactions in most terrestrial environments, and can be used as a tracer to study surface and subsurface transport processes. It has been successfully used as an indicator of water balance components, such as evapotranspiration in a forested catchment (Juang and Johnson, 1967; Claassen and Halm, 1996) and regional groundwater recharge (Allison and Hughes, 1983). It is also a common practice to use a conservative species such as chloride to estimate water balance of a lake (Nir, 1973; Stauffer, 1985; Krabbenhoft and Webster, 1995).

This chapter is a part of the broader study which aims to understand hydrology and hydrochemistry of the northern prairie wetlands that recharge groundwater. In Chapter 2, the hydrologic interaction between a recharge wetland and the surrounding slope in Saskatchewan, Canada was described. In this chapter, chloride is used as a tracer to confirm the findings of Chapter 2, as well as to understand how the wetland-focused flow field influences the

subsurface distribution of dissolved species. The conceptual model of flow and transport in the recharge wetland and the surrounding slope based on previous studies including Chapter 2 is presented in the next section, which is followed by the field results that support the model.

Conceptual model of chloride transport cycle

The northern prairie region experiences cold winter, which causes deep soil frost in the surrounding slope in early spring, and hence causes large snowmelt runoff into the wetlands (Woo and Winter, 1993; Woo and Rowsell, 1993). The snowmelt water infiltrates and forms a mound of groundwater under the recharge wetlands, and hence causes divergent subsurface flow (Meyboom, 1966; Lissey, 1968; and others). Chapter 2 showed that the majority of divergent flow occurs in the oxidized zone of saturated glacial till (zone II in Fig. 3.1) that has high saturated hydraulic conductivity due to well-developed fractures. Above zone II, the unsaturated hydraulic conductivity significantly decreases, and the flow direction is mostly upward due to evapotranspiration (zone I). Below zone II, the saturated hydraulic conductivity decreases by several orders of magnitude, and flow direction is mostly downward recharging the underlying aquifer (zone III).

Soluble salts are nearly absent under recharge wetlands (Miller et al., 1985; Keller et al., 1991), because the large infiltration of snowmelt water removes the salts from under the wetlands (Fig. 3.1). A portion of the salt is transported to the slope surrounding the wetland by divergent flow in zone II and accumulates in the top soil (Mills and Zwarich, 1986; Stolte et al., 1992), while the rest is transported down to the aquifer by groundwater recharge.

The divergent subsurface transport of salts from the wetland to the slope is accompanied by the convergent surface transport of salts from the slope to the wetland by snowmelt runoff (Fig. 3.1). For example, Knuteson et al. (1989) reported that runoff water transported dissolved carbonates to microdepressions in North Dakota, USA. Chapter 2 showed that the average flux of surface and subsurface flow is similar in magnitude. Therefore, it is likely that the surface and subsurface transport flux of chloride have similar magnitude, too.

When a system of a recharge wetland and the surrounding slope is considered, the input of chloride to the system is supplied by atmospheric deposition, and the output leaves the system as groundwater recharge, while chloride is cycled within the system by surface and subsurface transport paths (Fig. 3.1). The distribution of chloride in different parts of the system and the flux between them will be examined in the following sections.

Study site

A recharge wetland, located in St. Denis National Wildlife Area (106°06'W, 52°02'N), 50 km east of Saskatoon, Saskatchewan was selected as the study site (Fig. 3.2). The wetland,

identified as S109 by Canadian Wildlife Service, had been originally studied by Miller (1983), and was recently studied extensively for the interaction of surface water and groundwater (Chapter 2).

The geomorphology of the site is described as moderately rolling knob and kettle moraine (Miller, 1983). The area is underlain by glacial till and silty stratified sediments (Fig. 3.3). The tills are of Floral and Battleford Formation (Miller, 1983), which are Middle to Late Wisconsin in age (Christiansen, 1992). The boundary between the two formations is not clear, thus not indicated in Figure 3.3. Discontinuous sand lenses occur commonly in the till, while an extensive sand layer at the depth of 25-30 m is an aquifer that connects groundwater flow systems under all wetlands in the area. The glacial till is oxidized to the depth of 5-6 m and is olive brown, while the unoxidized till below that depth (oxidation front) is dark gray. The oxidized till has well-fractured structure and high saturated hydraulic conductivity compared to the weakly fractured unoxidized till.

The subsurface flow shows seasonal fluctuation, but on average the flow field is divergent and stratified (Fig. 3.1). The average groundwater recharge rate to the aquifer, based on hydraulic gradient and conductivity measurements, is estimated to be in the range of 1-3 mm yr^{-1} (Chapter 2).

Prior to cultivation, perhaps in the middle of the century, this study area was covered with grassland-aspen grove vegetation (Miller, 1983). The present vegetation in the wetland is characterized by sedge, spike rush, and other aquatic species, while silver willow, trembling aspen, and balsam poplar grow along the wetland margin. Similar wetland margin vegetation was called a "willow ring" by Meyboom (1966). The willow ring and the adjacent grassland mark the transition from the wetland to the cultivated field, which was cropped to spring wheat in 1993 and 1994, summer fallowed in 1995, and cropped to oil seeds in 1996.

In this study the term "wetland" refers to the topographic depression characterized by aquatic vegetation, while the term "pond" refers to the inundated portion of the wetland (Fig. 3.4). The term "slope" is used to denote the area surrounding the wetland, which includes both cultivated field and willow ring. Accordingly the wetland of S109 is defined as the region enclosed by 552.5 m elevation contour (Fig. 3.2), which has the area of 2400 m^2. The boundary of the catchment is drawn based on elevation contours, but the effective catchment area cannot be uniquely defined because the runoff water may overflow from adjacent small depressions in years of large snowmelt (Fig. 3.2). With some degree of uncertainty in mind, we will use the area of the elevation-based catchment, 24000 m^2, in our water balance calculations.

The area becomes covered by snow in November; therefore, we define a hydrologic year to start on November 1 and end on October 31; for example the hydrologic year 1994 starts on November 1, 1993. The 90-year mean annual precipitation in Saskatoon is 360 mm, of which 84 mm occurs in winter (November - March) mostly as snow (Atmospheric Environment

Service, 1996). Precipitation-weighted wet deposition of chloride, estimated from the record of the three closest CAPMoN stations (Ro et al., 1995) in 1985-1994, is 0.041 mg l^{-1} (Fig. 3.5).

Field and laboratory methods

Precipitation and water level measurement

The summer precipitation in the hydrologic years 1994-1996 was measured by a tipping bucket rain gauge located outside the willow ring (near 23 in Fig. 3.2), while the summer precipitation in 1993 and the winter precipitation in 1993-1996 were obtained from the Saskatoon Airport, 50 km west of the site (Atmospheric Environment Service, 1996).

The pond water level was continuously monitored from July 1993 to October 1996 (Chapter 2). In addition to 20 piezometers and water table monitoring wells installed in 1980 by Miller (1983), we installed 17 new piezometers and wells in 1993 and 1994 (Fig. 3.2). The construction methods of piezometers are described in Chapter 2. Water level in most of piezometers and wells are measured manually, while some piezometers were continuously monitored by vibrating wire transducers (Geokon, ALV4500-5) and a data logger (Campbell Scientific, CR10).

Snow and water sampling

Snow samples were taken by first digging a pit down to the ground surface, and then scraping the wall of the pit with a clean plastic scoop from the snow surface to the depth 10 cm above ground surface.

Pond water samples were always taken from the center of the pond by submerging a clean plastic sample bottle 10-20 cm into the water. Groundwater samples were obtained from piezometers and water table monitoring wells using a peristaltic pump. Due to low hydraulic conductivity of the glacial tills, samples were taken without purging piezometers or wells. The samples were taken from the depth of the screen, which was usually at least several meters below the water level in the piezometer. Preliminary sampling with purging from a few fast-responding piezometers showed that chemistry of water did not change appreciably before and after purging. For the new piezometers constructed in 1993, periodical sampling from 1994 to 1995 showed that chloride in most new piezometers had reached stable concentration by July, 1995, hence the effect of contamination by bentonite (Remenda and van der Kamp, 1996) had become insignificant.

Water samples were passed through a 0.45 μm filter and kept at 4 °C for a few days to weeks prior to analysis. The major anions including Cl^- were analyzed by ion exchange chromatography, while the major cations were analyzed, after acidifying samples, by atomic absorption spectroscopy. Alkalinity was analyzed by sulfuric acid titration. Deuterium content was analyzed by a mass spectrometer using a standard zinc reduction technique.

Soil electrical conductivity

The soil electrical conductivity was surveyed with an electromagnetic terrain conductivity meter (Geonics, EM-31) on a 15 m grid. The penetration depth of the meter was 3-4m.

Pore water chloride extraction

Glacial till samples representing 0.4-1.5 m depth intervals were obtained by the auger-wrap technique (Keller and van der Kamp, 1988). A 15 cm diameter solid-stem auger was used to obtain the till samples from the maximum depth of 24 m. The bore holes were used to install piezometers after sampling. Shallow till samples from a few selected locations were also obtained by hand-augering at 0.2 m depth interval. The samples were sealed in plastic bags and kept at 4 °C for a few days before the soluble salts were extracted.

A representative sample consisting of many small (1 cm^3) pieces of till was transferred from each plastic bag to a 250 ml plastic bottle. Approximately 200 g of the till sample was mixed with 100 ml of deionized water in the bottle, vigorously shaken for four hours, and centrifuged at 900 times the gravitational acceleration for one hour. The supernatant was then passed through a 0.45 μm filter. The shaking time was selected based on the literature on standard methods (Rhoades, 1982).

Pore water chloride concentration in till was estimated from the concentration of supernatant and the dilution ratio based on the gravimetric moisture content of the till, which was determined by oven-drying 60-80 g of sample for 48 hours at 105 °C. This method of calculation assumes that all pore water is accessible to extracting solution, which was confirmed for water molecules by using deuterium-tagged water as extractant for 22 representative samples. The assumption, however, may not be valid for chloride ions, as discussed later. The volumetric moisture content of the till was estimated from the gravimetric moisture content assuming that the density of till solid was 2700 kg m^{-3}.

Radial diffusion tests

The effective pore water volume that was accessible to chloride ion was determined by the radial diffusion method (van der Kamp et al., 1996). The intact till samples used in this method were obtained by advancing a solid-stem auger to the desired depth, cleaning the cuttings in the hole, and driving steel Shelby tubes into the till. The samples were wrapped immediately in plastic films and were stored at 4°C after sampling.

A cylinder-shaped intact till sample, 12 cm long and 7.2 cm in diameter, was allowed to equilibrate with deionized water in a small (25-30 cm^3) reservoir placed in the center of the sample through molecular diffusion process. Deionized water was injected in the reservoir, the sample was sealed to prevent evaporation, left for 50-130 days to ensure equilibrium, and water was sampled through 0.45 μm filter for analysis. The procedure was repeated four times,

resulting in the dilution of pore water in the till at each step according the volume ratio between the central reservoir and the pore space accessible to chloride.

Time series extraction

The radial diffusion tests indicated an extra source of chloride that was not dissolved in pore water, as described later. The time series extraction was conducted to determine if shaking samples more than four hours will extract the extra chloride. A set of till-water mixtures was packed in bottles, shaken for one hour, stirred by a spatula to completely disperse the mixture, and poured into a large glass beaker and homogenized, and re-distributed into bottles. The bottles were shaken again for a specified length of time up to 72 hours and centrifuged. In some cases the till sample in the last bottle was mixed with deionized water for the second extraction with 96-hour shaking.

Till and clay analysis

Oven-dried till samples used for moisture content determination were crushed to pass a 2 mm screen, and homogenized using a mechanical sample splitter. The pulverized samples were then ground to powder size (< 75 μm). Carbonate content of till was estimated by acid digestion/atomic absorption method (Ross, 1986). Organic carbon content of till is represented by non-carbonate carbon content which was analyzed by Leco induction furnace equipped with Horiba IR detector after removing carbonate with HCl.

Clay from 20 g of air-dried till was extracted by gravity sedimentation technique, saturated with $CaCl_2$ and KCl solutions, and oriented specimens for X-ray diffraction analysis were prepared on glass slides (Theisen and Harward, 1962). Seven diffractograms using different pretreatments and temperature conditions were obtained using the method described by Dudas and Pawluk (1982).

Results

Chloride in snow and snowmelt water

The snow samples were taken from three locations; center of the wetland, outside the willow ring, and middle of the slope in March, 1994 just before the snowmelt began. The snow thickness in the three locations were 0.49, 0.62, and 0.34 m, respectively. The snow samples appeared clean without dust or soil particles. The concentration of chloride in the samples was 0.1-0.2 mg l^{-1}, which represented the concentration in snow that had not been in contact with the soil.

The snow samples were taken from similar locations in March, 1996. The field around the wetland was summer fallowed in 1995, and the top soil was exposed to the snow without stubble and a layer of hay that cover the soil surface in normal years. The snow was noticeably

more "dirty" in 1996 than in previous years, presumably because more soil particles were incorporated in the snowdrifts. The chloride concentration in the dirty snow ranged from 0.3 to 3.3 mg l^{-1}.

Near the end of the snowmelt period (April 8) in 1996 the ground surface was completely wet, and shallow (0-10 cm) puddles were abundant on the slope. The snowmelt water slowly cascaded down the slope from one puddle to another. It is likely that the snowmelt runoff occurs as a combination of overland flow and subsurface flow in a top few centimeters of the soil. Water samples were taken from two of the puddles, which had chloride concentration of 1.3 and 3.0 mg l^{-1}. Snowmelt water, which originally had little chloride (0.1-0.2 mg l^{-1}) when it was clean, dissolved a significant amount of chloride as it came in contact with the top soil.

Chloride in pond water

The water level in the pond rose rapidly during the snowmelt period (Fig. 3.6b). The snowmelt started on March 12 in 1994, March 10 in 1995, and March 15 in 1996. It occurred in several events and lasted until April 13 in 1994, April 15 in 1995, and April 8 in 1996. The chloride concentration in the snowmelt water in the pond varied from year to year (2-5 mg l^{-1}). In 1996, it was in the order of 2-3 mg l^{-1} (Fig. 3.6c), similar to the value found in snowmelt water in the puddles on the slope.

The concentration in the pond fluctuated during the summer and fall (Fig. 3.6c), but the variation was in the order of only a few milligrams per liter. The chloride mass in the pond was calculated by taking the product of concentration and the volume of water in the pond estimated from the volume-depth function (Chapter 2, Eq. 2.2). The chloride mass rapidly increased in the snowmelt period, and decreased as the water level declined in summer (Fig. 3.6d). The maximum mass was reached within several weeks after the snowmelt period, of which a large portion was likely transported from the slope.

Estimation of infiltration and evapotranspiration

The chloride concentration and mass change in the pond reflects the water balance, therefore, can be used as a practical method to estimate evapotranspiration and infiltration in the pond. Evapotranspiration in the pond includes open water evaporation and transpiration by the emergent vegetation. From a physical point of view the two phenomena are different. However, they are indistinguishable when chloride mass balance in the pond is considered, because the chloride accumulating along the shallow root system, or precipitating on the leaves, of the aquatic vegetation is easily mixed with the pond water.

Assuming no groundwater input and negligible chloride in precipitation, the mass of chloride in the pond is approximated by (see the end of the chapter);

$$C(t_1) = \frac{M_0}{V(t_1)} \exp\left\{ -f \int_0^{t_1} \frac{A(t)P(t) - \frac{dV}{dt}}{V(t)} dt \right\} \tag{3.1}$$

where $C(t_1)$ is the chloride mass in pond water at time t_1, M_0 is the initial mass, $V(t)$ is the volume of water in pond, $A(t)$ is the area of pond, and $P(t)$ (m s^{-1}) is the precipitation rate. The ratio of infiltration to total water loss, f, is defined by;

$$f = I / (I + E) \tag{3.2}$$

where E (m s^{-1}) is the evapotranspiration rate, and I (m s^{-1}) is the infiltration rate. The terms under integral are all measurable in the field.

Chloride concentration in the pond is calculated from (3.1) using three different values of f (Fig. 3.7). The initial dates are set at May 27 (JD 147) in 1994 and May 3 (JD 123) in 1995. It was impossible to use (3.1) to analyze the data for 1996, because a large storm on July 5 caused a major subsurface storm flow into the pond (Chapter 2, Fig. 2.18). Therefore, the assumption of negligible groundwater input was violated.

Calculated chloride concentration was sensitive to the variation of f only in the late part of the curves shown in Figure 3.7. This is because the sensitivity of pond water chloride concentration increases as the volume of water in the pond decreases. Comparison of measured and calculated concentration suggests $f = 0.7$-0.8 on average. This value is in agreement with the value, $f = 0.76$, obtained from physically measured evaporation and infiltration rate in a two weeks period (JD 180-193) in 1995 (Chapter 2).

The pond existed until late fall in 1994 and 1996, which gave us unique opportunities to use the pond itself as a large pan to measure the evapotranspiration from the wetland. The pond evapotranspiration rate, given by

$$E(t) = f\left[P(t) - \frac{1}{A(t)} \frac{dV}{dt} \right] \tag{3.3}$$

was integrated over the summer and fall to estimate the total pond evapotranspiration (Table 3.1). The value of $f = 0.75$ was used in the calculation. The total pond evapotranspiration in the summer and fall was close to the total precipitation during this period (Table 3.1). This makes sense because the chloride concentration in the pond water did not change appreciably in summer and fall (Fig. 3.6c); precipitation and evapotranspiration was balanced.

Chloride in groundwater

The groundwater under the wetland was sampled from Miller's old piezometers in 1993 and 1994, of which 1994 data are shown in Figure 3.8. The chloride concentration was in the range of 4-9 mg l^{-1}. This is similar to the concentration range in pond water, as we expect because the large portion ($f = 0.75$) of the water in the pond infiltrates without evaporitic

enrichment. The concentration in 1993 was 0.3-1.3 mg l^{-1} lower than the 1994 value for each corresponding piezometer. The difference is not considered significant.

The groundwater under the slope was sampled from the new piezometers in 1995. The chloride concentration under the middle to lower slope was in the similar range as under the wetland, but it was in the higher range under the upper slope (Fig. 3.8).

The glacial till samples obtained from five bore holes along the transect BC (Fig. 3.2) were used to determine the pore water chloride concentration by the extraction method. The pore water concentration was reasonably uniform (4-10 mg l^{-1}) in the wetland and the lower slope, and it was significantly higher in the upper slope (Fig. 3.9). This pattern is consistent with the groundwater chloride concentration (Fig. 3.8).

The occurrence of high chloride concentration in the upper slope is commonly observed in prairie wetlands (Mills and Zwarich, 1986; Zebarth et al., 1989). The high chloride concentration is associated with high salinity, hence high soil electrical conductivity. As a result, the area of high chloride concentration can be delineated by a soil electrical conductivity survey using a EM-31 (Fig. 3.10). Band-like areas of the high salinity develop roughly along the catchment boundary. A similar band of salinity around a prairie wetland, referred to as a saline ring, was reported by Mills and Zwarich (1986). Note that the major constituent of high salinity detected by EM-31 was sulfate, as groundwater samples obtained from the zone of high salinity were saturated with respect to gypsum, though high concentrations of chloride and sulfate occurred together.

Shallow till samples were obtained from three locations (23, 26, and 28 in Fig. 3.2) along the transect BC by hand-augering. At each location the samples were taken at three different times (July 1994, November 1994, and June 1996) from the area within several meters of the corresponding piezometers, and pore water chloride concentration was estimated by the extraction method to examine the seasonal variation. At the middle and upper slope locations, the chloride concentration in the top soil (< 0.2 m) was low in early summer, and increased in late fall (Fig. 3.11), while the trend was opposite at the location near the willow ring. Note that each point in the graphs represents an analysis of one sample, while a large spatial variation in the concentration is expected. Therefore, the data should be interpreted qualitatively. The low concentration in the top soil in early summer at the middle and upper slope was likely due to leaching caused by snowmelt runoff, while the high concentration in early summer at the lower slope may indicate some unknown subsurface transport mechanism.

Chloride cycling

The high chloride concentration in the upper slope (Fig. 3.9) indicates accumulation of chloride. A portion of the accumulated chloride on the slope is transported to the wetland by snowmelt runoff each year. Annual chloride load to the wetland is perhaps 4-5 kg (Fig. 3.6d). Due to the high infiltration rate, most of the chloride mass in the pond is transported to the

underlying groundwater. Part of this groundwater recharges the local aquifer, allowing chloride to leave the system. However, most of the groundwater flows horizontally, transporting chloride from the wetland to the slope. This chloride, along with the atmospheric deposition, accumulates on the slope (Fig. 3.1). Therefore, the chloride is cycled between the wetland and the slope by surface and subsurface transport processes.

The influence of chloride cycling is limited in the shallow subsurface (zones I and II in Fig. 3.1), and the chloride in the deeper zone is no longer part of the cycle. The downward flow of groundwater is focused under the wetland (Fig. 3.1), therefore the majority of groundwater leaving the cycle has the concentration range of 4-9 mg l^{-1} (Fig. 3.8). This range is 100-200 times greater than the average concentration of precipitation (0.04 mg l^{-1}). Chapter 2 estimated the groundwater recharge rate of 1-3 mm yr^{-1}, averaged over the catchment. The annual precipitation, 360 mm yr^{-1}, is 100-300 times greater than the groundwater recharge rate. It appears, therefore, that atmospheric input of chloride to the cycle is roughly balanced by the groundwater output. This situation is analogous to a forested catchment in mountains in which chloride is cycled between soil and plants, and atmospheric input is balanced by output through a discharging stream (Juang and Johnson, 1967; Claassen and Halm, 1996).

Discussion

Inconsistency of the chloride extraction technique

The subsurface distributions of chloride concentration directly measured for piezometer samples (Fig. 3.8) and that estimated from extraction (Fig. 3.9) are qualitatively similar. However, a close examination of the concentration profiles in the lower and upper slope locations (23 and 26 in Fig. 3.2) shows that the pore water concentration estimated by the extraction do not always represent the groundwater concentration (Fig. 3.12).

The inconsistency in concentration is likely due to problems in the chloride extraction technique, particularly in the method used to estimate the dilution ratio based on the gravimetric moisture content. The gravimetric moisture content represents the total pore volume, V_p, in a saturated till sample, however the effective pore volume, V_{pe}, that is accessible to chloride may be smaller than V_p; i.e. underestimation of the concentration. On the other hand, if there are extra sources of chloride in the till such as adsorption sites, the concentration based on the moisture content will overestimate actual pore water concentration.

The radial diffusion method (van der Kamp, et al., 1996) was used to determine if the difference between V_p and V_{pe}, or extra sources of chloride, existed for two intact glacial till samples taken from a bore hole near the willow ring (23 in Fig. 3.2, depths 3.3 m and 6.4m). In this method, a central reservoir in the sample is emptied and filled with deionized water at each step. When the concentration in the central reservoir at each successive dilution is plotted against the net mass removed (Fig. 3.13), the reciprocal of the slope of the curve is equal to the

product of V_{pe} and the retardation factor, R, that indicates the effects of extra sources of chloride, while the intercept of the curve is equal to the original pore water concentration (van der Kamp. et al., 1996, Eq. 7). Regression analyses gave the straight lines shown in Figure 3.13, for which the values of $V_{pe}R$ for 23-3.3 m and 23-6.4 m were 145 ml and 162 ml, respectively. The total pore volume of the two samples were 113 ml and 103 ml, respectively. Because V_{pe} can not exceed V_p, the values of R for the two samples must be at least 1.3 and 1.6, respectively. This indicates the presence of extra sources of chloride in the two till samples.

The two samples were removed from the diffusion cell after the last measurement, and subjected to the time series extraction to determine how long shaking time is needed to extract the extra chloride. The pore water concentration shown in Figure 3.14a was estimated from the concentration in the extractant and the dilution ratio based on V_p. After four hours of shaking the estimated pore water concentration was almost identical to the concentration in the central reservoir in the last point of the radial diffusion tests (Fig. 3.13). At least for these two samples, four-hour shaking extracted only the chloride that was dissolved in pore water.

The estimated pore water concentration increased with the shaking time; the extra chloride was released into the solution as samples were shaken longer. After 70 hours the second extraction was started by decanting the supernatant in the bottles and adding deionized water. The samples were shaken for 96 hours, and more chloride was extracted (Fig. 3.14a).

The radial diffusion method was applied to only two samples. To determine if the presence of the extra chloride was the general property of the glacial till in the site, four other till samples were subjected to the time series extraction. Characteristics of the six samples used in the time series extraction are listed in Table 3.2. Only one out of four samples showed the increase in concentration (Fig. 3.14b), and therefore, it is likely that the extra chloride only occurs in some locations and depths. In all samples, the extra chloride was not extracted in the four-hour shaking used to construct Figure 3.9, therefore, the major part of the inconsistency shown in Fig. 3.12 was likely caused by the spatial heterogeneity rather than the extra chloride.

Extra chloride in tills

Although we do not have convincing data to explain how the extra chloride exists in the till, several observations are stated here. The dissolution of trace chloride contained in silicate minerals (Peters, 1991) can not explain the curves in Figure 3.14, because such process is extremely slow under room temperature and the neutral pH condition buffered by abundant carbonate. The dissolution of chloride contained in carbonate minerals can not explain the curves, either, because the samples that did and did not release extra chloride both had similar carbonate content (Table 3.2). In addition, the amount of chloride in carbonate minerals is generally in order of several hundreds $\mu g\ g^{-1}$ (Hem, 1985, p. 5; Remenda, 1993, p. 75), which is not large enough to account for the amount of the extra chloride in Figure 3.14.

The X-ray diffractograms of four till samples taken under the willow ring (23 and 25 in Fig. 3.2) showed clear peaks corresponding to montmorillonite, kaolinite, muscovite, and chlorite in order of decreasing abundance. This assemblage of minerals is typical for the clay fraction of prairie soils (Kodama, 1979). Amorphous aluminosilicates that may have large number of pH-dependent ion exchange sites (Wada, 1989) was not detected. Therefore, non-specifically adsorbed chloride on pH-dependent exchange site (Stumm, 1992, p.19) is unlikely the cause of increased concentration. Organic carbon content and the oxidation state of the till did not appear to affect the presence of extra chloride (Table 3.2).

The mechanism of chloride retention in the glacial till will have significant consequence in transport processes of other negatively charged chemical species, for example pesticides and nutrients, of great ecological importance. Therefore it warrants further research.

Non-ideal behavior of chloride as a tracer

It became clear that chloride was somehow trapped and released from the till material at some locations and depths, and as such, showed non-ideal behavior as a tracer. The time scale of trap and release is expected to be in the order of 10^1-10^2 days, because the phenomena were observed in the radial diffusion tests that were conducted in similar time scale.

Suppose that one is planning a year-long experiment using chloride to trace the movement of groundwater. The transfer of chloride mass between pore water and till solid will certainly affect the results of the experiment. Therefore, the mass transfer process has to be explicitly dealt with as a time-dependent process (van Genuchten and Wierenga, 1976; Rao et al., 1980) in the interpretation of the data.

The analysis of divergent flow patterns and groundwater recharge rate presented earlier in this chapter deals with the time scale of 10^2-10^3 years. Therefore, the mass transfer between pore water and till solid can be treated as an instantaneous process; retardation. The results of the radial diffusion tests and time series extraction suggests that the retardation occurs only at some locations, and that the retardation factor is unlikely to exceed two. The mild retardation will not affect the patterns of chloride distribution (Figs. 3.8 and 3.9), though it may stabilize the distribution against changes in subsurface flow regime. The mass flux of chloride leaving the system with groundwater recharge (Fig. 3.1) only takes place in the dissolved phase. Once the balance between the atmospheric input and the subsurface output is established in the system, the chloride mass balance is not affected by retardation. Therefore, the chloride method to estimate groundwater recharge needs not take into account the retardation over long time periods.

Conclusions

Distribution of chloride in a groundwater recharge wetland and the surrounding slope delineates the key hydrologic processes in the system. Low chloride concentration in groundwater under the wetland indicates large infiltration of snowmelt water. High concentration in the soils in the upper slope indicates the divergent flow of groundwater that transports dissolved salts from the wetland to the slope, and the accumulation of the salts in the slope caused by evapotranspiration. The analysis of snowmelt and the pond water in early spring indicates that the chloride in the upper slope soil is transported to the wetland by snowmelt runoff. The surface flow and subsurface flow of water transport chloride in the opposite directions, and hence drive the chloride cycle in the system.

The chloride concentration in the pond water does not change appreciably in the summer and fall, indicating that infiltration accounts for the majority of water loss in the pond. This is in agreement with the results of the hydrologic study which showed that evaporation rate from the wetland is considerably smaller than the potential rate of wet surface evaporation in the surrounding slope. The large infiltration, however, does not contribute to groundwater recharge. Most of the infiltrated water is evapotranspired within the wetland or in the slope.

The chloride cycle in the wetland-slope system receives a steady input by atmospheric deposition, while the groundwater recharge to the local aquifer carries chloride away from the system. In geological time scale, the input and output likely become balanced, and the chloride concentration in the groundwater leaving the system can be used as an indicator of the recharge rate. The recharge rate estimated based on the chloride mass balance in the system is 0.5-1 % of the precipitation rate, which is in agreement with the estimation based on the measurements of hydraulic gradient and conductivity.

Chloride is trapped in and released from the glacial till in some locations and depths in the study area. The mechanism of the trap and release is unknown, and warrants further research. The non-ideal behavior of chloride due to the trap and release will affect the short term observation of the transport processes, but it should not affect the transport processes in geological time scale that controls the distribution of the concentration in the chloride cycle.

Appendix

The water balance and chloride mass balance in a pond without groundwater input is described by;

$$\frac{dV}{dt} = A(P - E - I) \tag{3.A1}$$

$$V\frac{dC}{dt} + C\frac{dV}{dt} = A(C_p P - CI) \tag{3.A2}$$

where V is the volume of water in pond, A is the area of pond, P is the precipitation rate, E is the evaporation rate, I is the infiltration rate, C is the average chloride concentration in pond water, and C_p is the chloride concentration in precipitation. The above set of equations are reduced to (Nir, 1973; Eq. 14a):

$$\frac{dC}{dt} = -\frac{A(P-E)}{V}C + \frac{AP}{V}C_p \tag{3.A3}$$

Re-arranging (A1) we get;

$$AE = (1-f)(AP - \frac{dV}{dt}) \tag{3.A4}$$

where $f = I/(I+E)$ is a ratio of infiltration to total water loss, assumed constant. Using (3.A4) and noting that C_p is negligible for short term mass balance, the solution to (3.A3) is given by;

$$C(t_1) = \frac{M_0}{V(t_1)}\exp\left\{-f\int_0^{t_1}\frac{A(t)P(t) - \frac{dV}{dt}}{V(t)}dt\right\} \tag{3.1}$$

where $C(t_1)$ is the chloride mass in pond water at time t_1, and $M_0 = C_0V_0$ is the initial mass.

References

Allison, G.B. and Hughes, M.W., 1983. The use of natural tracers as indicators of soil-water movement in a temperate semi-arid region. J. Hydrol., 60, 157-173.

Arndt, J.L. and Richardson, J.L., 1993. Temporal variations in the salinity of shallow ground water from the periphery of some North Dakota wetlands. J. Hydrol., 141, 75-105.

Atmospheric Environment Service, 1996. Canadian daily climate data on CD-ROM, Western Canada. Atmospheric Environment Service, Environment Canada, Downsview, Ontario.

Batt, B.D.J, Anderson, M.G., Anderson, C.D. and Caswell, F.D., 1989. The use of prairie potholes by North American ducks. In: Northern prairie wetlands, van der Valk, A., ed., 204-227, Iowa St. Univ. Press, Ames, Iowa.

Christiansen, E.A., 1992. Pleistocene stratigraphy of the Saskatoon area, Saskatchewan, Canada: an update. Can. J. Earth Sci., 29, 1767-1778.

Claassen, H.C. and Halm, D.R., 1996. Estimates of evapotranspiration or effective moisture in Rocky Mountain watersheds from chloride ion concentrations in stream baseflow. Water Resour. Res., 32, 363-372.

Dudas, M.J. and Pawluk, S., 1982. Reevaluation of the occurrence of interstratified clays and other phylosilicates in Southern Alberta soils. Can. J. Soil Sci., 62, 61-69.

Hem, J.D., 1985. Study and interpretation of the chemical characteristics of natural water. U. S. Geol. Surv. Water-Supply Pap. 2254.

Juang, F.H.T. and Johnson, N.M., 1967. Cycling of chlorine through a forested watershed in New England. J. Geophys. Res., 72, 5641-5647.

Keller, C.K. and van der Kamp, G., 1988. Hydrogeology of two Saskatchewan tills, II. Occurrence of sulfate and implications for soil salinity. J. Hydrol., 101, 123-144.

Keller, C.K., van der Kamp, G. and Cherry, J.A., 1991. Hydrogeochemistry of a clayey till, 1. Spatial variability. Water Resour. Res., 27, 2543-2554.

Knuteson, J.A., Richardson, J.L., Patterson, D.D. and Prunty, L., 1989. Pedogenic carbonates in a calciaquoll associated with a recharge wetland. Soil Sci. Soc. Am. J., 53, 495-499.

Kodama, H., 1979. Clay minerals in Canadian soils: Their origin, distribution and alteration. Can. J. Soil. Sci., 59, 37-58.

Krabbenhoft, D.P. and Webster, K.E., 1995. Transient hydrogeological controls on the chemistry of a seepage lake. Water Resour. Res., 31, 2295-2305.

LaBaugh, J.W., Winter, T.C., Adomaitis, V.A. and Swanson, G.A., 1987. Hydrology and chemistry of selected Prairie wetlands in the Cottonwood Lake area, Stutsman County, North Dakota, 1979-1982. U.S.G.S. Prof. Pap., 1431. 26pp.

Lissey, A., 1968. Surficial mapping of groundwater flow systems with application to the Oak River Basin, Manitoba. Ph.D. thesis, Univ. of Saskatchewan, Saskatoon, Saskatchewan.

Meyboom, P., 1966. Unsteady groundwater flow near a willow ring in hummocky moraine. J. Hydrol., 4, 38-62.

Miller, J.J., 1983. Hydrology of a morainic landscape near St. Denis, Saskatchewan, in relation to the genesis, classification and distribution of soils. M.Sc. thesis, Univ. of Saskatchewan, Saskatoon, Saskatchewan.

Miller, J.J., Acton, D.F. and St. Arnaud, R.J., 1985. The effect of groundwater on soil formation in a morainal landscape in Saskatchewan. Can. J. Soil Sci., 65, 293-307.

Mills, J.G. and Zwarich, M.A., 1986. Transient groundwater flow surrounding a recharge slough in a till plain. Can. J. Soil Sci., 66, 121-134.

Nir, A., 1973. Tracer relations in mixed lakes in non-steady state. J. Hydrol., 19, 33-41.

Peters, N.E., 1991. Chloride cycling in two forested lake watersheds in the west-central Adirondack Mountains, New York, U.S.A. Water, Air and Soil Pollution, 59, 201-215.

Rao, P.S.C., Rolston, D.E., Jessup, R.E. and Davidson, J.M., 1980. Solute transport in aggregated porous media: Theoretical and experimental evaluation. Soil Sci. Soc. Am. J., 44, 1139-1146.

Remenda, V.H., 1993. Origin and migration of natural groundwater tracers in thick clay tills of Saskatchewan and Lake Agassiz clay plain. Ph. D thesis, Univ. of Waterloo, Waterloo, Ontario.

Remenda, V.H. and van der Kamp, G., 1996. Contamination from sand-bentonite seal in monitoring wells installed in tight porous media. Groundwater (in press).

Rhoades, J.D., 1982. Soluble salts. In: Methods of soil analysis, 2. Chemical and microbiological properties. Agronomy, 9, 167-179.

Ro, C.U., Vet, R.J., Ord, D., and Holloway, A., 1995. Canadian Air and Precipitation Monitoring Network (CAPMoN) Annual Summary Reports (1983-1994). Atmospheric Environment Service, Environment Canada, Downsview, Ontario.

Ross, W.C., 1986. Atomic absorption method for quantitative determination of carbonates in tills. Tech. Rep., 214. Sask. Res. Council, Saskatoon, Saskatchewan.

Rozkowski, A., 1967. The origin of hydrochemical patterns in hummocky moraine. Can. J. Earth Sci., 4, 1065-1092.

Stauffer ,R.E., 1985. Use of solute tracers released by weathering to estimate groundwater inflow to seepage lakes. Environ. Sci. Technol., 19, 405-411.

Steinwand, A.L. and Richardson, J.L., 1989. Gypsum occurrence in soils on the margin of semipermanent prairie pothole wetlands. Soil Sci. Soc. Am. J., 53, 836-842.

Stolte, W.J., Barbour, S.L. and Eilers, R.G., 1992. A study of the mechanisms influencing salinity development around Prairie sloughs. Trans. Am. Soc. Agric. Eng., 35, 795-800.

Stumm, W., 1992. Chemistry of the solid-water interface. John Wiley, New York, 428pp.

Theisen, A.A. and Harward, M.E., 1962. A paste method for preparation of slides for clay mineral identification by X-ray diffraction. Soil Sci. Soc. Am. Proc., 26, 90-91.

van der Kamp, G., Van Stempvoort, D.R. and Wassenaar, L. I., 1996. The radial diffusion method. 1. Using intact cores to determine isotopic composition, chemistry, and effective porosities for groundwater in aquitards. Water Resour. Res., 32, 1815-1822.

van Genuchten, M. Th. and Wierenga, P.J., 1976. Mass transfer studies in sorbing porous media: I. Analytical solutions. Soil Sci. Soc. Am. J., 473-480.

Wada, K., 1989. Allophane and imogolite. In: Minerals in soil environments (2nd ed.), 1051-1087. Soil Sci. Soc. Am., Madison, Wisconsin

Woo, M.-K. and Rowsell, R.D., 1993. Hydrology of a prairie slough. J. Hydrol., 146, 175-207.

Woo, M.-K. and Winter, T.C., 1993. The role of permafrost and seasonal frost in the hydrology of northern wetlands in North America. J. Hydrol., 141, 5-31.

Zebarth, B.J., de Jong, E. and Henry, J.L., 1988. Water flow in hummocky landscape in central Saskatchewan, Canada, II, Saturated flow and groundwater recharge. J. Hydrol., 110, 181-198.

Table 3.1 Estimated evapotranspiration (ET) from the pond and precipitation.

Year	Period	ET (mm)	Precip. (mm)
1994	May 27 - Oct. 7	241	227
1996	May 29 - Oct. 24	213	198

Table 3.2 Data summary of the till samples used in the time series extraction; sample location, depth, presence of extra chloride, volumetric moisture content, organic carbon content, carbonate content, and the oxidation state (oxidized/unoxidized) of the till based on color.

Location	Depth (m)	Extra Cl	Moist. content	Org. C (wt %)	CO_3 (wt %)	Oxidation state
22	6.4		0.24	0.4	21	Unox.
23	2.1		0.36	0.3	22	Ox.
23	3.3	x	0.26	0.1	19	Ox.
23	6.4	x	0.26	0.4	31	Unox.
23	9.5		0.29	0.6	22	Unox.
26	6.4	x	0.24	0.4	19	Unox.

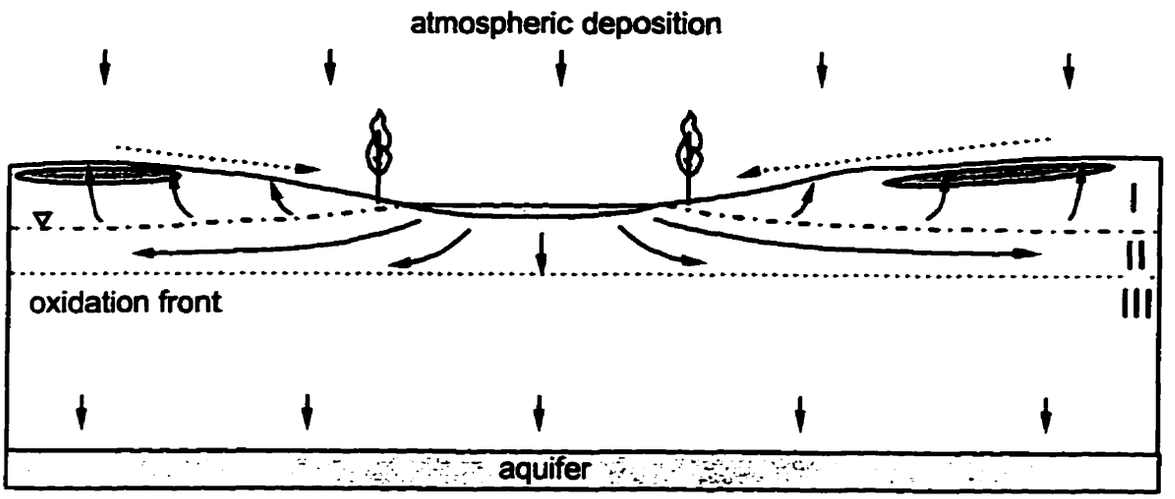

Fig. 3.1 Chloride transport by subsurface flow (solid line with arrow) and snowmelt runoff (dotted line with arrow). Dark shaded area near the ground surface indicates accumulation of chloride.

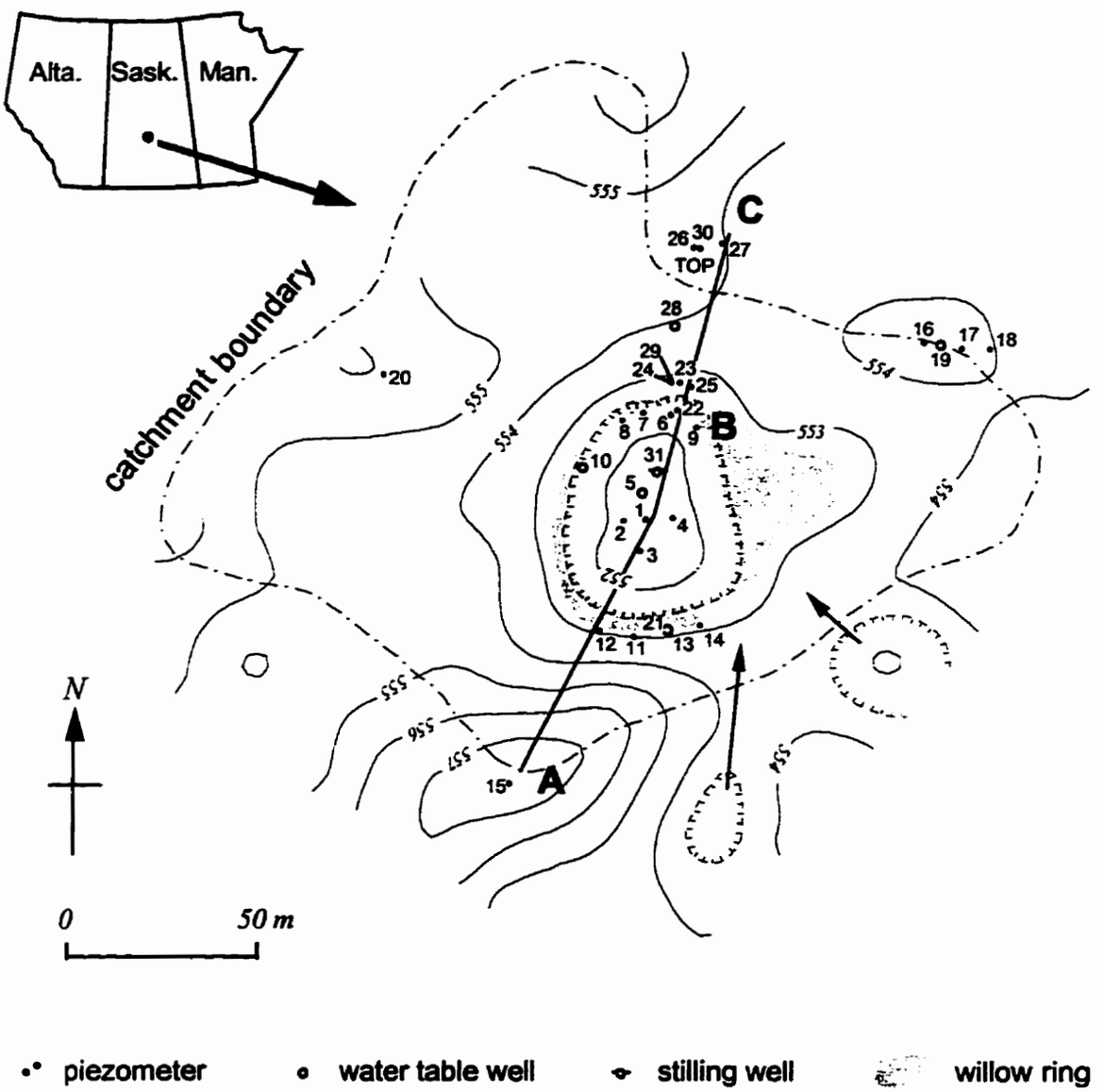

Fig. 3.2 Topographic map of the study area. The location of field instruments is indicated in the map. The elevation is in meters above sea level. Arrows show the direction of overflow from small depressions.

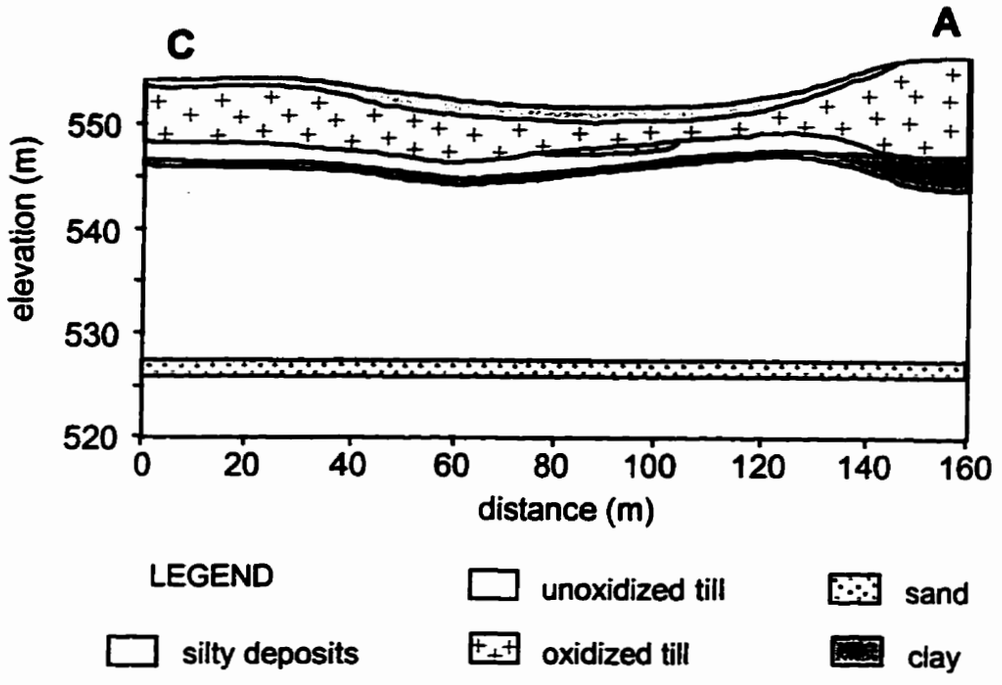

Fig. 3.3 Geological cross section along the transect AC in Figure 3.2 (modified from Miller, 1983).

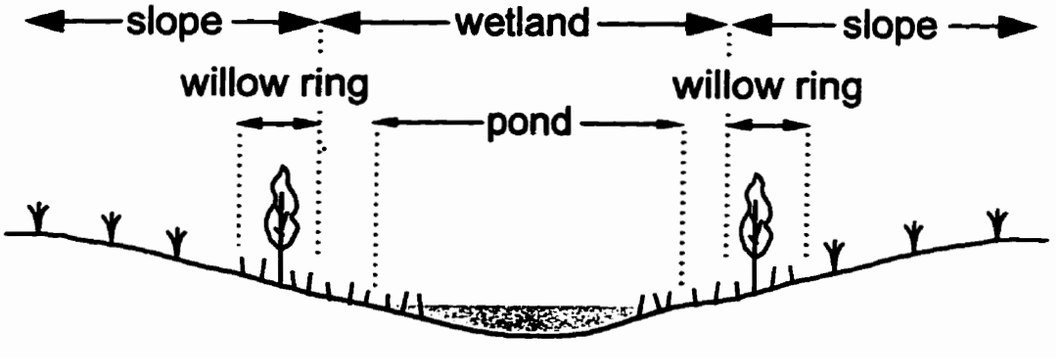

Fig. 3.4 Definition of the pond, wetland, willow ring, and slope.

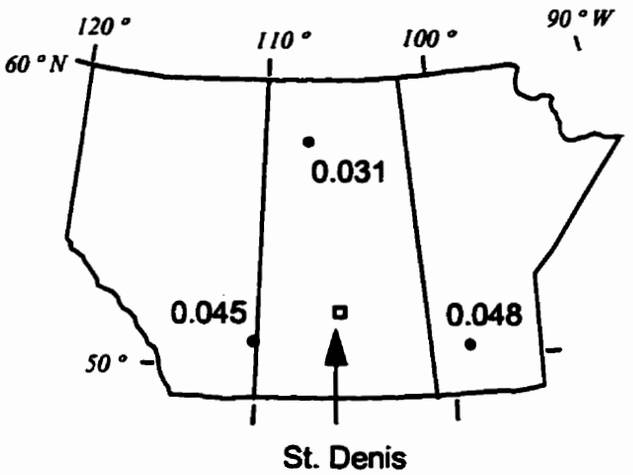

Fig. 3.5 Location of the CAPMoN sites and the precipitation-weighted wet chloride deposition (mg/l) in 1985-1994.

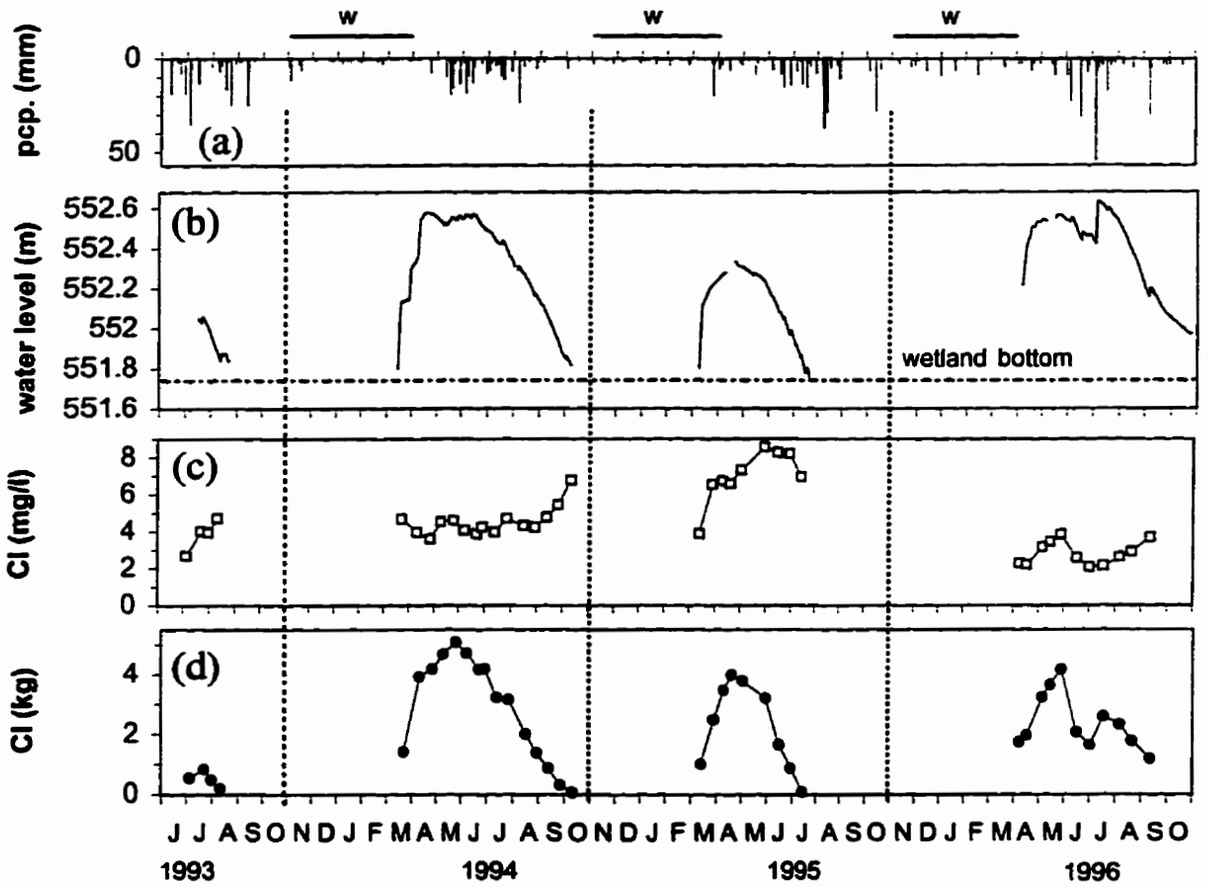

Fig. 3.6 Precipitation, water level, and chloride in S109. Dotted line indicate the division between hydrologic years. (a) daily precipitation. (b) pond water level. (c) chloride concentration in the pond water. (d) chloride mass in the pond.

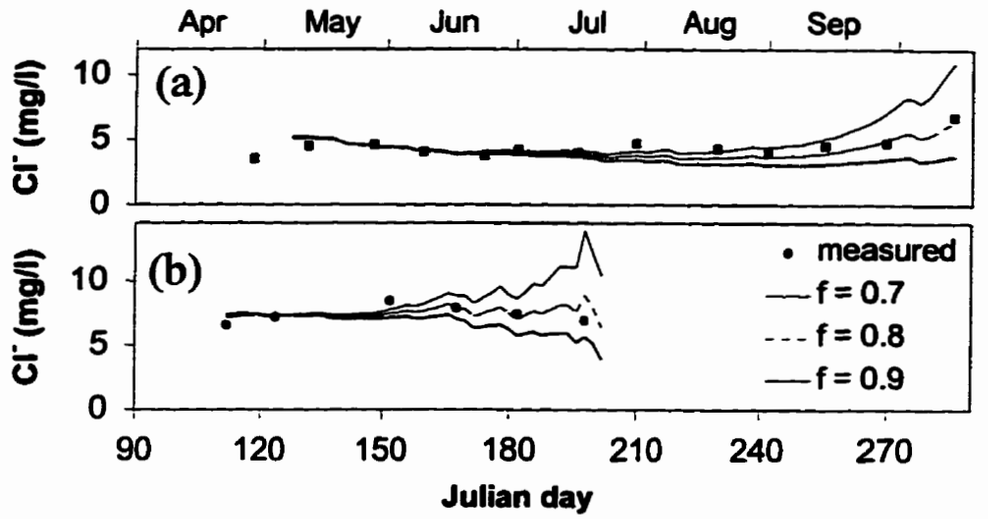

Fig. 3.7 Measured and calculated chloride concentration in the pond. The calculation is based on the mass balance equation. (a) 1994. (b) 1995.

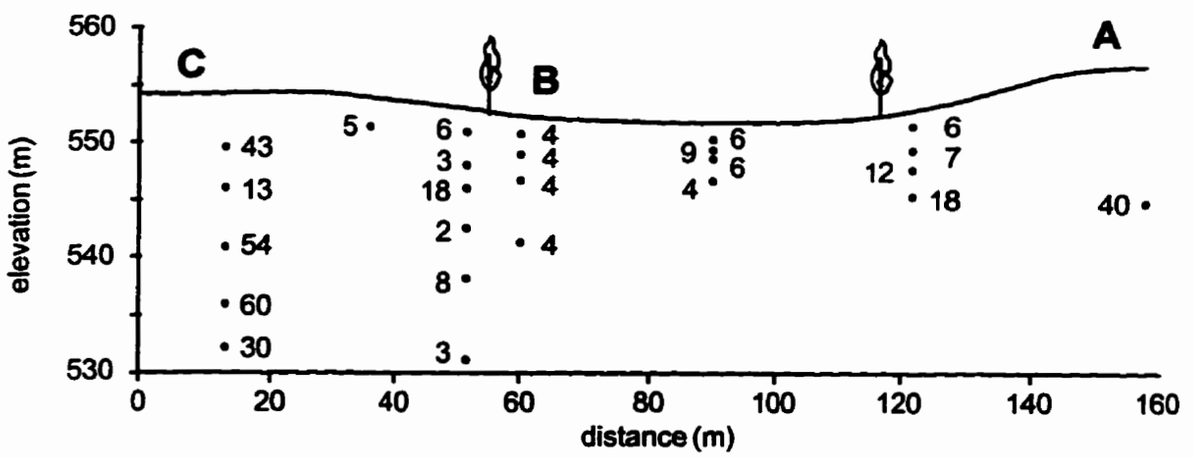

Fig. 3.8 Chloride concentration (mg/l) in groundwater.

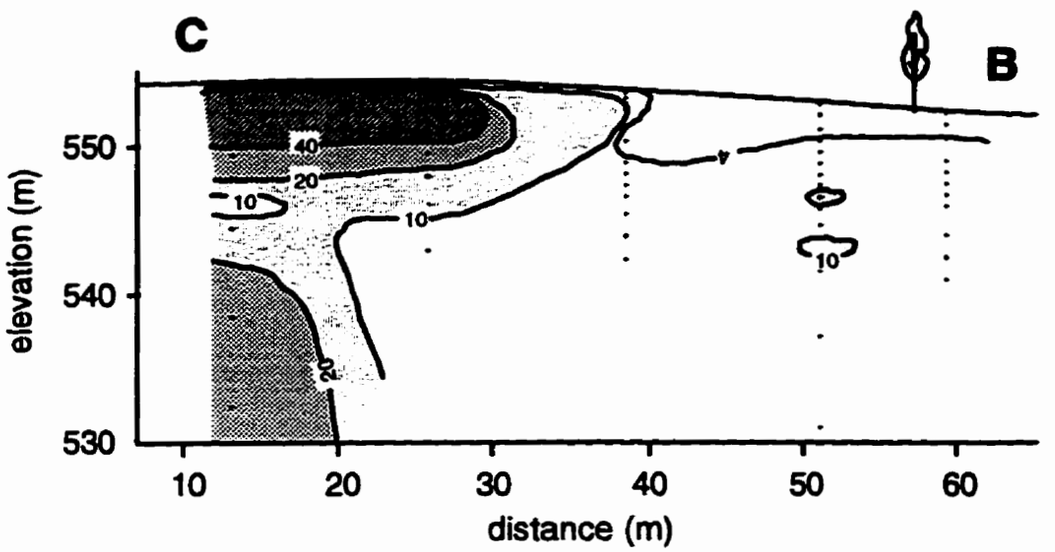

Fig. 3.9 Pore water chloride concentration (mg/l) estimated by the extraction. The dots show the sample points.

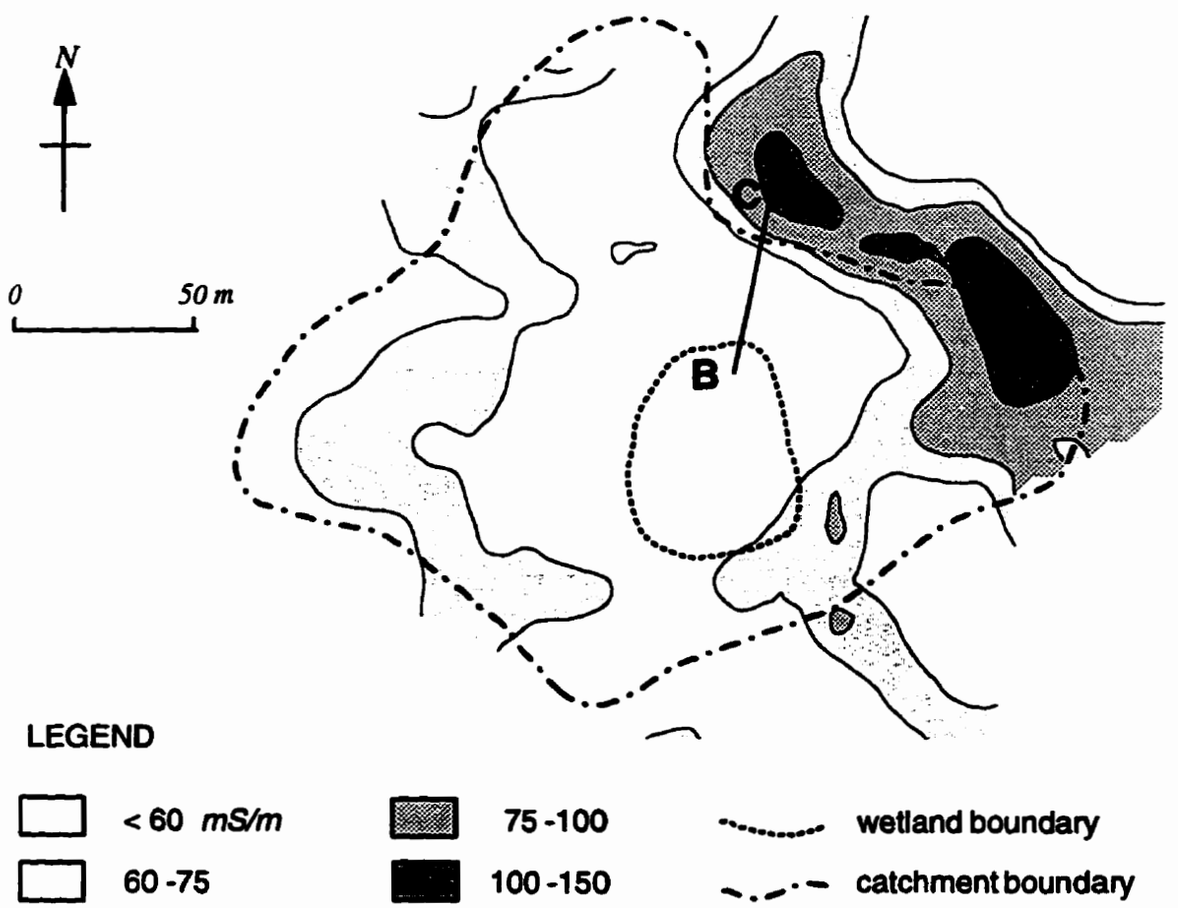

Fig. 3.10 Distribution of the soil electrical conductivity measured by EM-31.

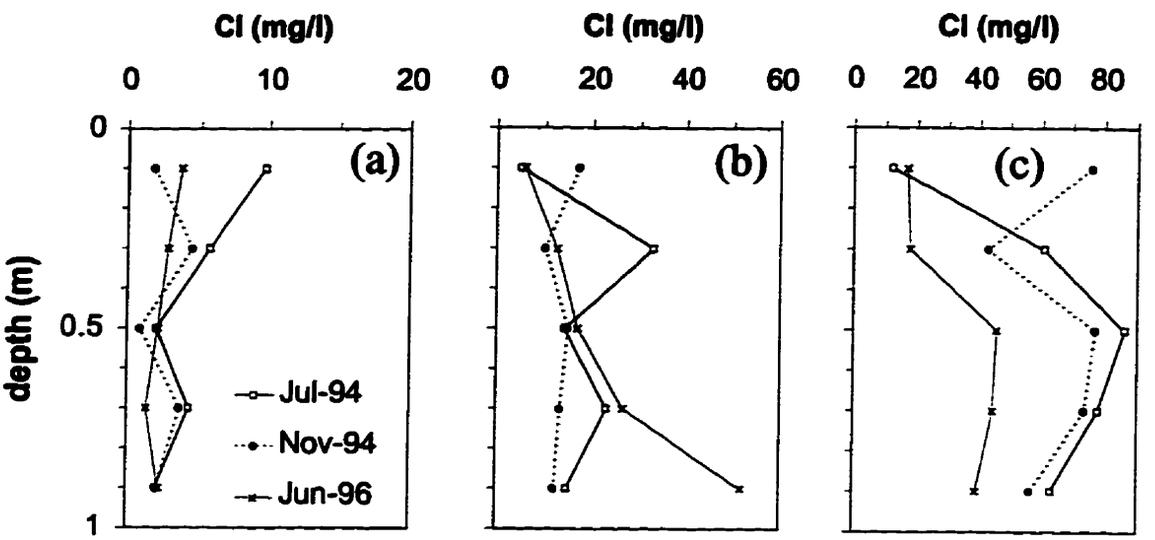

Fig. 3.11 Pore water chloride concentration in the near-surface soil estimated by extraction. Samples were taken at three different times. (a) lower slope. (b) middle slope. (c) upper slope.

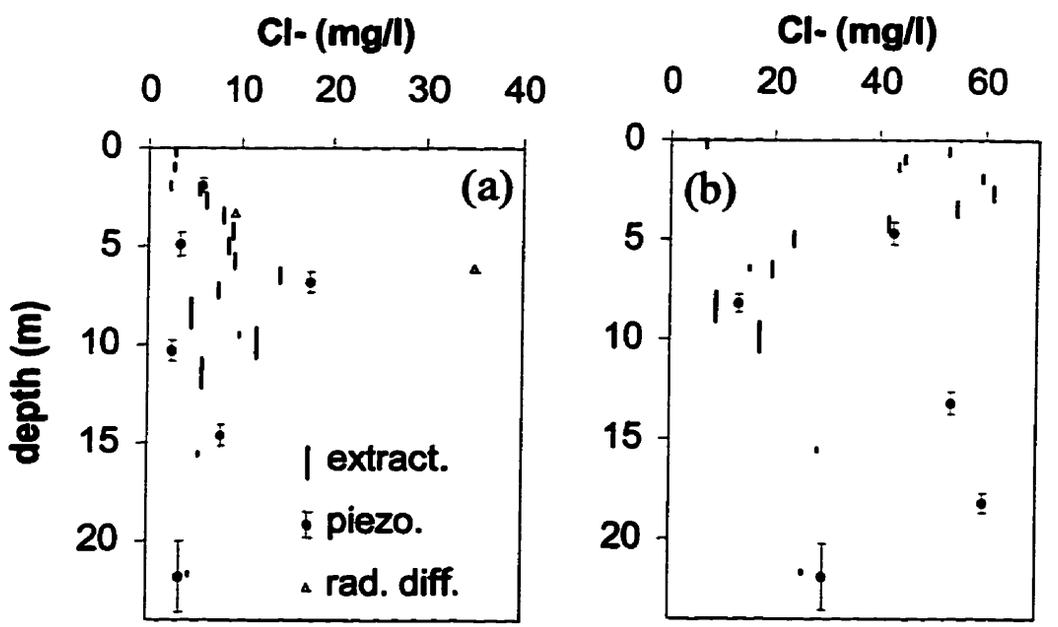

Fig. 3.12 Comparison of pore water chloride concentration; estimated by the extraction, piezometer samples, and the radial diffusion method. The length of markers indicate sampled intervals and piezometer sand packs. (a) lower slope. (b) upper slope.

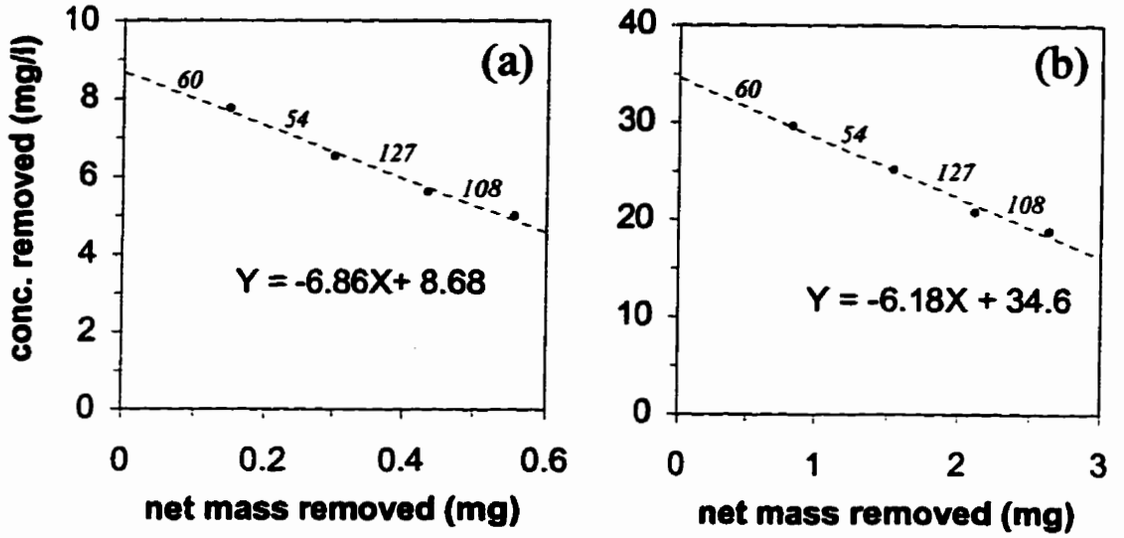

Fig. 3.13 Results of the radial diffusion tests. The concentration in the central reservoir is plotted against the net mass removed from the till. Linear regression lines and corresponding equations are shown in the graphs. The numbers between each point indicates equilibration time in days. (a) 23-3.3 m. (b) 23-6.4 m.

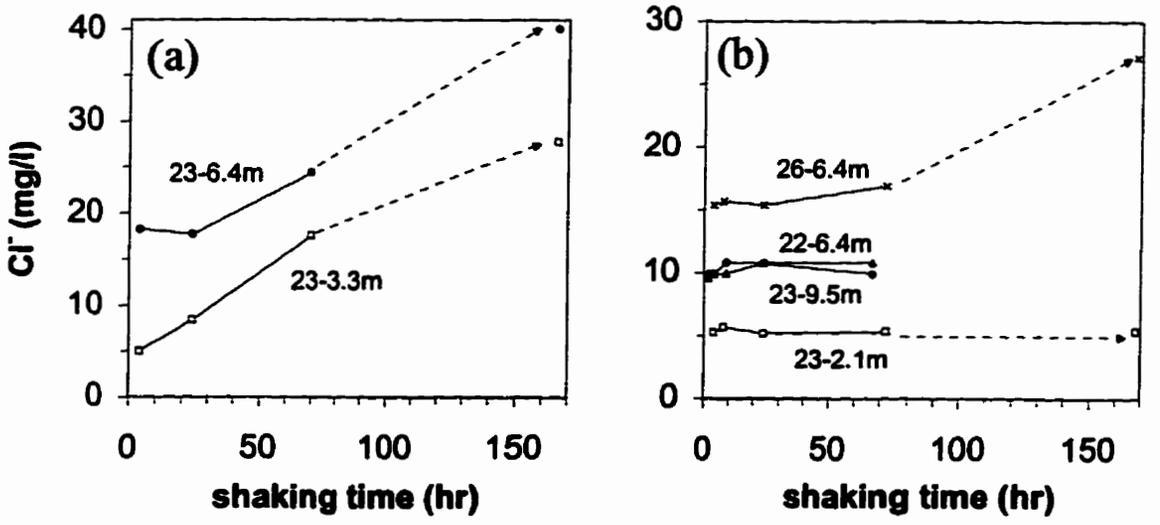

Fig. 3.14 Estimated pore water chloride concentration by the time series extraction. Dashed lines with arrows indicate the second extraction. (a) samples used in the radial diffusion tests. (b) other samples.

Chapter 4

Simulation of surface-subsurface chloride cycle induced by wetland-focused groundwater recharge

Introduction

The northern prairie region of North America is characterized by undulating terrain with numerous wetlands, called sloughs or prairie potholes. The wetlands are important to this region, because they support a diverse community of wildlife, and recharge the groundwater in underlying aquifers. However, the destruction of a large number of wetlands in the last several decades to increase the crop production raised public concerns about the future of the wildlife and water resources in the region (Batt et al., 1989; Winter, 1989). The evaluation of the impact of the destruction on water resources requires an estimation of wetland-focused recharge.

Groundwater recharge is conventionally estimated by measuring the hydraulic gradient and conductivity, or by analyzing the fluctuation of water table (Meyboom, 1966; Rehm et al. 1982; Zebarth et al., 1989). However, it is difficult to represent the recharge rate in a given area by a few hydraulic measurements. Therefore, it is desirable to have an independent estimate of recharge to evaluate the representativeness of hydraulic measurements. The mass balance of dissolved species may be used to obtain such an independent estimate, because the concentration of dissolved species in the wetland has shown to be an effective indicator of groundwater recharge or discharge condition (Rozkowski, 1967; Lissey, 1968; Miller et al., 1985; LaBaugh, 1991).

Atmospheric chloride is commonly used as a tracer to estimate groundwater recharge (Eriksson, 1955: Allison and Hughes, 1983). However, the application of the chloride method is generally limited in the cases where subsurface flow is dominantly vertical. The wetland-focused groundwater recharge induces strong horizontal subsurface flow from the wetland to the surrounding slope, hence the chloride method is not applicable in its commonly used form (Meyboom, 1966, Lissey, 1968; Zebarth et al., 1989; Trudell, 1994).

The subsurface distribution of chloride in the recharge wetlands and surrounding slopes is characterized by the low concentration under the wetlands indicating large infiltration of snowmelt water, and high concentration in the middle to upper slopes indicating enrichment by evapotranspiration (Miller et al., 1985; Mills and Zwarich, 1986). Chapter 3 showed that chloride is cycled between a recharge wetland and the surrounding slope, and that the ratio of the concentration in shallow groundwater under the wetland to that in precipitation is

approximately equal to the ratio of annual precipitation to groundwater recharge. To examine if such a relationship is generally applicable to other wetlands, we will develop a mathematical model to represent flow and transport processes in a recharge wetland and its catchment, based on detailed field studies of a recharge wetland located in a typical undulating terrain of the northern prairie region (Chapters 2 and 3).

Because the accumulation of chloride occurs in the vadose zone, it is critical to incorporate unsaturated flow and transport processes in the model. Numerical analysis of interaction between wetlands and the vadose zone was presented by Winter (1983) for flow, and by Stolte et al. (1992) for flow and solute transport. They emphasized the importance of seasonal and shorter-term change in flow boundary conditions at the ground surface. However, it is impossible to measure such boundary conditions in field sites at fine temporal and spatial resolution required in transient simulations. Therefore, we do not attempt to develop a model that represents the full complexity of field sites. The intent of our analysis is to clarify and illustrate the most essential processes governing the distribution of chloride in a long time scale (10^3-10^4 years).

The model will emphasize the coupling of surface and subsurface transport processes, hence the effects of chloride cycling. Though the motivation for developing such a model comes from the study of the specific type of prairie wetlands, the mathematical concepts and numerical schemes described in this paper will be applicable to general solute transport problems involving surface-subsurface cycling.

Conceptual model

The conceptual model is based on the field studies of a wetland located in the St. Denis National Wildlife Area, 50 km east of Saskatoon, Saskatchewan (Fig. 4.1), which was originally studied by Miller (1983) and Miller et al. (1985). The size of the wetland is the average of recharge wetlands in the northern prairie region, and the study area has cold and dry climate and glacial topography, typical of the region. The wetland has aquatic vegetation characterized by sedge and spike rush in the central part, and a dense ring-like bush of willow and aspen in the marginal area; a "willow ring" (Meyboom, 1966). In this study the term "wetland" refers to the area inside the willow ring, while the term "pond" refers to the inundated portion of the wetland (Fig. 4.2). Note that the pond dries up by the end of summer in most years. The term "slope" is used to denote the area surrounding the wetland, which includes both cultivated field and willow ring. The area of the wetland is 2400 m^2, while the area of the catchment is 24000 m^2.

Deep soil frost (1-2 m) in the slope in early spring reduces the infiltration capacity, and hence causes large snowmelt runoff into the wetlands (Woo and Winter, 1993; Woo and Rowsell, 1993). The snowmelt water infiltrates and forms a mound of groundwater under the

wetlands, and hence causes divergent subsurface flow (Fig. 4.3). The majority of the divergent flow occurs in the zone between the water table and the oxidation front, in which the oxidized glacial till has high hydraulic conductivity due to well-developed fracture network (Keller et al., 1989). The unsaturated hydraulic conductivity is orders of magnitude smaller than the saturated value, and the flow direction is mostly upward in the vadose zone due to evapotranspiration. The saturated hydraulic conductivity decreases by several orders of magnitude in the unoxidized till, and the flow direction is mostly downward recharging the underlying aquifer. In this paper, the groundwater recharge is defined as the flux of water that enters the aquifer and eventually leaves the catchment. The downward flux of water across the water table is not considered groundwater recharge, because the water can be transferred horizontally and consumed by evapotranspiration elsewhere within the catchment.

Soluble salts are nearly absent under recharge wetlands, because the large infiltration of snowmelt and rain water removes the salts from under the wetlands (Fig. 4.3). A portion of the salts is transported to the slope by divergent flow, and accumulates in the top soil (Mills and Zwarich, 1986; Stolte et al., 1992), while the rest is transported down to the aquifer by groundwater recharge. The accumulation of the salts in the middle to top slope is delineated by the soil electrical conductivity (Fig. 4.4). The snowmelt runoff leaches a portion of the accumulated salts from the slope, and transport it to the wetland (Knuteson et al., 1989). Therefore, the salts are cycled between the wetland and the slope.

Chloride is reasonably conservative in the glacial tills, and the atmospheric deposition is the only source of chloride in the catchment that is capable of sustaining steady input in geological time scale (Fig. 4.3). Chloride leaves the system at the bottom boundary with the groundwater recharge. Because the groundwater recharge is reasonably steady, the chloride input and output becomes balanced in long time scale. This situation is similar to a completely mixed reservoir at the steady-state concentration, except that the mixing is incomplete and chloride is unevenly distributed in the system (Fig. 4.3). Noting that the groundwater recharge is the only mechanism of chloride output, and that we can estimate chloride input with reasonable accuracy; we can estimate groundwater recharge, if we know the average concentration of chloride in the groundwater entering the aquifer. A similar principle is commonly used to estimate evapotranspiration in forested catchments in which atmospheric chloride is cycled between soil and plants, and discharged eventually into a single stream that leaves the catchment (Juang and Johnson, 1967; Peck and Hurle, 1973; Peters, 1991; Classen and Halm, 1996).

To estimate the concentration in the output flux, suppose there is an imaginary steel plate along a part of the oxidation front that is under the top slope in Figure 4.3, and hence the water that leaves the system at the bottom boundary is completely separated from the region of chloride accumulation. Clearly, the average concentration in the output flux is equal to the concentration in shallow groundwater under the wetland. When the steel plate is removed, the

groundwater under the top slope interacts with the region of chloride accumulation; therefore the average concentration in the output flux is no longer equal to the concentration under the wetland. The objective of the modelling is to examine how the concentration under the wetland is effected by changes in flow and transport parameters.

Site characteristics

The following is a summary of the site characteristics presented in Chapters 2 and 3. Mean annual precipitation is 360 mm, of which 84 mm occurs in winter as snow. The historical record (1979-1996) of the spring water level in the wetland indicates that the effective snowmelt runoff that reaches the wetland in the average year is 10-30 mm. The distribution of snow water equivalent immediately before the snowmelt period in 1994 was roughly symmetrical about the center of the wetland (Fig. 4.5). Assuming the radial flow of snowmelt runoff, the amount of water that flows over a given point in the entire snowmelt period is calculated from the snow water equivalent, and defined as the cumulative snowmelt runoff (Fig. 4.5). Surface runoff is rarely caused by summer storm events.

The saturated hydraulic conductivity, K_{sat}, estimated from the basic time lag (Hvorslev, 1951) of piezometers shows distinct zoning due to fractures (Fig. 4.6). Discontinuous sand lenses have high K_{sat}. A thin (0.3 m) but continuous clay layer at the depth of 8 m must have a lower K_{sat} than the glacial till because the hydraulic gradient observed in the field dramatically increases within this clay layer.

Unsaturated flow parameters have large spatial variation. For example the relationship between the moisture content and the matric potential head measured at a nest of tensiometers and time domain reflectometry (TDR) probes in the middle of the transect BC showed that variation of unsaturated flow parameters with depth existed even at a single site (Fig. 4.7). Nevertheless the relationship is assumed to be represented by a simple moisture retention function (van Genuchten, 1980), which has five fitting parameters; the saturated moisture content (θ_{sat}), the residual moisture content (θ_{res}), a parameter related to the height of capillary fringe (α), and two dimensionless parameters (n and m). The two dimensionless parameters are related by $m = 1 - 1/n$ (van Genuchten, 1980, Eq.22). The θ_{sat} decreases with depth as the till becomes more consolidated. The θ_{sat} estimated from the gravimetric moisture content of till samples is in the range of 0.42-0.48 near the surface and decreases to 0.26-0.30 at depths greater than 10 m. Based on Figure 4.7 and other field data, we assume that θ_{res} (= 0.06) and α (= 2 m^{-1}) are constant, and that n = 1.25 in the shallow soil (<0.6 m), and n =1.15 in the till.

The average subsurface flow field is expected to be similar to the flow field observed in the summer of 1994 (Fig. 4.8). The dense contours at the depth of 8 m reflect the low hydraulic conductivity of the clay layer. The vertical hydraulic gradient below the clay layer is nearly constant throughout the year. The groundwater recharge estimated from the hydraulic gradient

and conductivity is 1-3 mm yr^{-1}. The net infiltration in the wetland in 1994 was estimated to be 479 mm. Chapter 2 showed that the summer precipitation and evapotranspiration in the wetland have similar magnitude, and hence the net infiltration is controlled by the amount of effective snowmelt runoff. Considering the relative magnitude of the snowmelt runoff in 1994 (45 mm) and the average year (10-30 mm), the net infiltration in the average year is expected to be 110-320 mm. It should be noted that the seasonal fluctuation of the flow velocity and direction is neglected in the average flow field, but it has important effects in the dispersion of chloride.

Precipitation-weighted wet deposition of chloride estimated from the CAPMoN data base (Ro et al., 1995) is 0.041 mg l^{-1}. The studies in the interior North America indicate that the dry deposition is insignificant (Vet, et al., 1988; Classen and Halm, 1996), or only a small fraction of the wet deposition (Shepard et al., 1989), as long as the site is away from salt lakes. Therefore, we assume that the total atmospheric input of chloride is equal to the wet deposition.

Pore water chloride concentration along the transect BC is shown in Figure 4.9; the model must produce the concentration patterns similar to this. Remenda (1993, p.68) showed that the glacial till that had not been affected by post glaciation water had 20-40 mg l^{-1} of pore water chloride for all four of her study sites across the northern prairie region. Her sites were located on relatively flat landscape, not on undulating terrain. However, it is reasonable to expect that glacial tills under the continental ice sheet had similar pore water chloride concentration. Therefore, we assume that the pore water concentration in the glacial till in the study site was 30 mg l^{-1} when the last glaciers retreated (10,000 years ago).

Mathematical model

Basic idea

We will formulate a mathematical model of a recharge wetland that incorporates the essential characteristics of transport processes to answer two specific questions; (1) what is the relationship between the groundwater recharge and the chloride concentration under the wetland ? (2) how is this relationship affected by changes in hydrologic conditions ?

Examining the conceptual model of chloride transport (Fig. 4.3), the spatial variation of the subsurface flow velocity vector is critically important, and this point will be stressed in the mathematical model. In contrast, seasonal and year-to-year variation in the subsurface flow is averaged out and steady-state condition is assumed, because the problem is formulated in geological time scale to examine chloride distribution in the field that has been slowly formed over many years. The effects of small time scale variation in hydrologic condition should appear as dispersion of chloride in large time scale, in the same way as the effects of micro scale variation in flow velocity appear as dispersion in macro scale (Scotter and Raats, 1968; Goode and Konikow, 1990).

Model domain and governing equations

Topography and chloride distribution is roughly symmetrical about the center of the wetland (Fig. 4.4); therefore, a radial cross section represents the catchment (Fig. 4.10). The left side of the domain is the axis of symmetry, the right side is the catchment boundary, and the bottom is the aquifer. The domain has a layered structure reflecting the variation in K_{sat} (Fig. 4.6).

The subsurface and surface transport of chloride are the essential processes to be modelled. The subsurface transport is described by a standard advection-dispersion equation;

$$\theta \frac{\partial C}{\partial t} = \nabla \cdot (\theta \mathbf{D}_e \nabla C - \theta \mathbf{v}_e C) \tag{4.1}$$

where θ (**x**) is the moisture content, $C(\mathbf{x},t)$ (kg m^{-3}) is the concentration, ∇ is the differential operator in cylindrical coordinates, $\mathbf{D}_e(\mathbf{x})$ (m^2 s^{-1}) is the dispersion coefficient tensor, and $\mathbf{v}_e(\mathbf{x})$ (m s^{-1}) is the flow velocity vector. The transport equation is written for the equivalent porous media (Berkowitz, et al., 1988; McKay et al., 1993), because the scales of our problem (10^1-10^2 m) is much larger than the fracture spacing (10^{-1} m) common in this region, and also because the time scale is large.

The surface transport process involves transfer of chloride mass from the soil near ground surface to runoff water. Laboratory studies (Ahuja and Lehman, 1983) of short duration (60 min) storms showed that the mass transfer occurred from a thin (< 2 cm) mixing layer in the top soil to the overlying sheet of water (Fig. 4.11), and the mass transfer flux was approximated by (Ahuja, 1990, Eq. 4b)

$$J = R(C_s - C_{roff}) \cong RC_s \tag{4.2}$$

where $J(\mathbf{x}, t)$ (kg m^{-2} s^{-1}) is the mass flux density, $R(\mathbf{x})$ (m s^{-1}) is the runoff rate, $C_s(\mathbf{x}, t)$ (kg m^{-3}) is the concentration at the soil surface, C_{roff} is the concentration in the runoff water that is assumed to be negligible. This assumption, $C_{roff} = 0$, is introduced to reduce the complexity of the model dramatically, even though C_{roff} increases toward the center of the catchment in reality. We propose that Eq. (4.2) describes mass transfer by snowmelt runoff. However, the time scale of the modelling is different from that of the laboratory experiments. To stress this point, (4.2) is re-written with a generic mass transfer coefficient k (m s^{-1}), rather than the runoff rate.

$$J = kC_s \tag{4.3}$$

Equation (4.3) is applied to the slope portion, ∂W_2, of the top boundary (Fig. 4.10) to calculate the mass flux from subsurface to surface. The total mass, M_T (kg s^{-1}), leaving the slope is given by

$$M_T(t) = \int_{\partial W_2} k(\mathbf{x}) C_s(\mathbf{x},t) dA \tag{4.4}$$

which is transferred to the wetland portion, ∂W_1, of the top boundary (Fig. 4.10). Therefore the mass flux density in the wetland, J_w (kg m^{-2} s^{-1}), from surface to subsurface is given by

$$J_w = M_T / A_w \tag{4.5}$$

where A_w (m^2) is the area of the wetland.

The surface-subsurface transport cycle of chloride is completely described by a set of Eqs. (4.1)-(4.5), once the coefficients and the initial and boundary conditions are specified.

Estimation of the coefficients: subsurface transport

To specify the flow velocity vector and moisture content in Eq. (4.1), the steady-state flow equation in variably saturated porous media

$$\frac{1}{r}\frac{\partial}{\partial r}\left[rK(h)\frac{\partial h}{\partial r}\right] + \frac{\partial}{\partial z}\left\{K(h)\left[\frac{\partial h}{\partial z} + 1\right]\right\} = \frac{\partial \theta}{\partial t} = 0 \tag{4.6}$$

is solved with appropriate boundary conditions, where h (m) is the matric potential head, and $K(h)$ (m s^{-1}) is the hydraulic conductivity. The functional form of $K(h)$ is given by the equation developed by van Genuchten (1980). The solution of Eq. (4.6) gives hydraulic head and moisture content in the simulation domain. The flow velocity vectors are calculated by multiplying the hydraulic gradient by the hydraulic conductivity and moisture content. Majority of flow in saturated glacial till likely occurs in fractures (Keller, at al., 1988), however the explicit treatment of discrete fractures is out of the scope of our study. The flow velocity calculated from Eq. (4.6) represents the velocity in the equivalent porous media, which is the product of the fracture velocity and the fracture porosity divided by the total porosity (van Genuchten and Dalton, 1986).

The effective longitudinal dispersion coefficient in the equivalent porous media is estimated from the fracture spacing and the average flow velocity using a simplified form of van Genuchten and Dalton's (1986, Eq. 49) equation;

$$D_e = L^2 v_e^{\,2} / 3D_a \tag{4.7}$$

where D_e (m^2 s^{-1}) is the effective dispersion coefficient, L is the half distance between parallel fractures, v_e is the average flow velocity, and D_a (m^2 s^{-1}) is the matrix diffusion coefficient. Equation (4.7) suggests the longitudinal dispersivity, α_L (m) for the equivalent porous media:

$$\alpha_L = L^2 v_e / 3D_a \tag{4.8}$$

Keller et al. (1988) reported fracture spacing, $2L$, in a similar glacial till to be 0.3-0.8 m, therefore we assume $2L$ = 0.5 m. Remenda et al. (1996) estimated $D_a = 1.7 \times 10^{-10}$ m^2 s^{-1} for $H_2{}^{18}O$, and we use this value for chloride. The longitudinal dispersivity is evaluated in each finite element (described later) using the velocity calculated from (4.6). Equation (4.7) is derived for plane fractures parallel to the direction of flow. The fracture network in the till is much more complex, and Eq. (4.7) should be regarded as a crude approximation of the natural

system. For the same reason it is impossible to accurately predict the transverse dispersivity, hence it is arbitrarily assumed to be one-tenth of α_L, based on a review of studies in sand and gravel aquifers (Gelhar et al., 1992).

The dispersivity given by Eq. (4.7) assumes the steady-sate flow without short-term oscillations. Scotter and Raats (1968, Fig. 2) showed that the magnitude of the macroscale dispersion in periodically oscillating flow field increased with the amplitude of oscillation. Our field observation showed that the oscillation was almost absent in the vertical flow zone below the oxidation front, while it was significant in the horizontal flow zone and in the vadose zone. Therefore, the dispersivity estimated by Eq. (4.8) is multiplied by a factor, β, greater than one to account for the enhanced dispersion in the zone above the oxidation front.

The magnitude of β is difficult to estimate. For an ideal sinusoidal oscillation, extending Scotter and Raats' (1968, Eq. 10) analysis, it can be shown that;

$$\beta = 1 + 2a_0 / \pi v_e \tag{4.9}$$

where a_0 (m s^{-1}) is the amplitude of flow velocity oscillation. The rate of summer evapotranspiration in the wetland is in the order of several millimeters per day (Chapter 2), hence several hundreds to thousands millimeters per year, which is several to ten times larger than the annual average infiltration rate. Therefore, a_0 / v_e is in the order of 1-10, and we assume β to be in the order of 1-10.

Estimation of the coefficients: surface transport

Equation (4.2) describes the mass transfer process, when it is used in the actual time scale of the experiments (Ahuja, 1990). Our mathematical model averages out the seasonal fluctuation of hydrologic condition, hence is not formulated in the actual time scale. To examine the effects of averaging, each term in Eq. (4.2) is separated into the average and fluctuation parts; e.g. $J(t) = \bar{J} + J'(t)$. Taking the mathematical expectation of both sides of Eq. (4.2),

$$\bar{J} = \bar{R}\,\bar{C}_s + \overline{R'C_s'} \tag{4.10}$$

where the last term is the correlation between R and C_s. Clearly, the runoff rate is highest in the snowmelt period ($R' > 0$), while the concentration in the soil surface is lowest in the same period ($C_s' < 0$). Therefore, the correlation is negative, and we can write

$$\bar{J} = \gamma\,\bar{R}\,\bar{C}_s = k\bar{C}_s \qquad 0 \le \gamma \le 1 \tag{4.11}$$

where γ is a dimensionless variable representing the time scaling effect. Equation (4.11) shows that the magnitude of k is generally smaller than the average runoff rate.

In a loose sense, γ represents the mass transfer efficiency of runoff. It must be close to 1, if the runoff is constant throughout the year. In the northern prairie region, however, the efficiency is low because the chloride in the surface soil is washed away in the beginning of the snowmelt period, and runoff in the rest of the snowmelt period does not contribute to mass

transfer. Note that γ is a function of r in general, because the cumulative runoff rate increases toward the center of the wetland (Fig. 4.5). However, we assume γ is uniform over the solution domain, and will test the validity of this assumption in the sensitivity analysis.

Flow boundary conditions

The boundary conditions for the flow equation are listed in Table 4.1. Two side boundaries have no flow, while the bottom boundary has constant hydraulic head, h_T = -5.2 m, based on field observation. The datum of the head is at ground surface in the center of the wetland, or the top left corner of the model domain. The specified flux boundary condition at the top of the domain requires a detailed explanation.

Because it is impossible to accurately measure the boundary flux in the field site, we guess the top boundary flux functions (FBC1-3 in Fig. 4.12) using the water balance of the catchment. We admit the arbitrariness of the functions, and will show later in the sensitivity analysis that changing spatial distribution of boundary flux does not a make significant difference in chloride concentration under the wetland. Based on the site characteristics, the net infiltration in the wetland is assumed to be 167 mm yr^{-1} for FBC1 and FBC2, and 104 mm yr^{-1} for FBC3. Note that the net infiltration is smaller than the actual infiltration due to high evapotranspiration in the summer. Part of the infiltration contributes to the groundwater recharge, assumed to be 2 mm yr^{-1}, while the rest is consumed by the evapotranspiration in the slope. Therefore, the total boundary flux in the slope has to be upward with the magnitude equal to the difference between the total net infiltration in the wetland and the total groundwater recharge.

The upward flux is high in the bottom slope, decreases outward, and becomes slightly downward in the top slope (Fig. 4.12). The hydraulic head distribution, particularly the location of the water table, is sensitive to the distribution of the upward flux. Therefore it is possible to estimate reasonable flux distributions by matching the simulated water table to the observed water table, as described later. To reflect the plant root uptake, which is the majority of evapotranspiration, the top boundary flux is uniformly distributed in a 0.8 m thick root zone as internal source and sink.

Transport boundary conditions

The transport boundary conditions are listed in Table 4.1. Two side boundaries have no flux, while the bottom boundary condition has a zero-gradient of concentration. Frind (1988) pointed out that the zero-gradient boundary may cause erroneous behavior of the solution when the solute plume reached the boundary. Results of test simulations using a deeper domain (50 m) for which the chloride plume did not reach the bottom boundary were essentially same as the ones using the regular domain (Fig. 4.10) for which the plume did reach the boundary. Therefore the zero-gradient boundary condition was considered appropriate for our model.

The top boundary receives the atmospheric input of chloride, which is uniform and assumed to be the product of the precipitation-weighted wet deposition (0.041 g m^{-3}) and precipitation (0.36 m yr^{-1}). In reality, the atmospheric chloride is transported by infiltration to a certain depth in each storm event, and gradually transported back to the surface by evaporation or enriched in the root zone. To account for these processes, which is ignored in the steady-state flow model, the atmospheric input is uniformly distributed in the root zone as internal sources. The boundary flux due to the mass transfer (Eqs. 4.3 and 4.4), is superimposed on the atmospheric boundary flux.

Transport initial condition : separation of solutions

Noting that the transport boundary conditions are homogeneous except for the top boundary, the solution can be separated into two parts using Duhamel's principle (Guenther and Lee, 1988, p.110).

$$C = C_1 + C_2 \tag{4.12}$$

The first part, C_1, is the evolution of the initial distribution, and the second part, C_2, is the transient response of the system to the atmospheric forcing.

The first part of the solution is obtained by solving Eqs. (4.1)-(4.5) without atmospheric input of chloride, using the initial condition; $C_1(\mathbf{x},0) = C_0$. The second part is obtained by solving the same equations with the atmospheric input, using the initial condition $C_2(\mathbf{x},0) = 0$. The combined solution, $C(\mathbf{x},t)$, satisfies Eqs. (4.1)-(4.5) and all boundary conditions listed in Table 4.1, as well as the initial condition; $C(\mathbf{x},0) = C_0$.

We now define dimensionless concentrations

$$C_1^* = C_1 / C_0 \qquad C_2^* = qC_2 / PC_p \tag{4.13}$$

where q (m s^{-1}) is groundwater recharge rate, C_p (kg m^{-3}) is the precipitation-weighted wet deposition, and P (m s^{-1}) is the precipitation rate. The concentration C_2^* roughly indicates the mass leaving the system from the bottom boundary divided by the mass entering the system from the top boundary, while the meaning of C_1^* is obvious. Once the equations are solved for C_1^* and C_2^*, solutions for any arbitrary combination of C_0 and PC_p/q can be immediately obtained from Eqs. (4.12) and (4.13).

Numerical methods

The equations are solved by finite element methods using a FORTRAN program based on Princeton UNSAT-2D developed by Celia et al. (1990). The vertical spacing (Δz) of triangle finite elements is 0.1 m at the top of the domain, and gradually increases to 2 m at the bottom. The horizontal spacing (Δr) is 4 m at the left end of the domain, decreases to 1 m in the transition zone from the wetland to the slope, increases to 2 m in the middle slope, and increases to 5 m in the top slope.

Equation (4.6) is solved first to generate velocity vectors and dispersion tensors used in Eq. (4.1). Equations (4.1)-(4.5) are solved separately for C_1 and C_2. The grid Peclet numbers (Daus et al., 1985) are mostly less than 2, but become as large as 8 in part of the domain. The time step $\Delta t = 100$ days was used in several transport solutions to ensure the grid Courant number (Daus et al., 1985) was less than 1. The solutions with $\Delta t = 100$ days and the same solutions with $\Delta t = 10000$ days, however, showed no difference in long term (t > 500 yr) behavior. Therefore, the solutions used for the sensitivity analysis are obtained with $\Delta t = 10000$ days.

The formulation to couple surface and subsurface transport equations is developed specifically for our model, hence special numerical algorithms are required to incorporate them to the standard Galerkin method used in UNSAT-2D. The special schemes essentially make long range connections between the slope nodes and the wetland nodes (Fig. 4.10), details of which are described in the end of this chapter. The application of the new method for surface-subsurface coupling is not limited to the case that involves only one wetland and catchment. The method simply extends to the cases that involve many wetlands in a given region in three-dimensional setting.

The concentration of chloride in the shallow (< 0.5m) wetland sediments is expected to be reasonably uniform because the pond water easily mixes with water in the soft and organic-rich sediments. To represent this process, line elements with several orders of magnitude higher dispersion coefficients than the triangular elements are placed on the surface (∂W_1) and in the top 0.5 m of the wetland part of the domain (Fig. 4.10). The numerical algorithms to install line elements were presented by Sudicky et al. (1995) and VanderKwaak and Sudicky (1995).

Results

Subsurface flow velocity vectors

Solutions for Eq. (4.6) with three top boundary flux functions (FBC1, 2 , and 3) indicated divergent flow fields with strong horizontal flow in the zone between the oxidation front and the water table. Figure 4.13 shows the solution with the function FBC1. The position and slope of the water table obtained with FBC1 was reasonably close to the water table observed in the field (Fig. 4.8). The function FBC3 gave similar water table location, but FBC2 gave the steeply declining water table that was considerably different from the field observation.

The difference between FBC1 and FBC2 is the relative distribution of upward flux (Fig. 4.12). Noting that the catchment has radial flow patterns, increasingly steep hydraulic gradient is required to maintain the flow of water from the wetland to the top slope. At the same time the thickness of the high conductivity zone, between the water table and the oxidation front, decreases as the water table becomes deep, which increases the gradient even more. From this observation, we choose FBC1 for the base case setting and compare them to the simulations

using FBC2 and FBC3. This procedure is necessary, because the average boundary flux functions are based on qualitative field data, thus have a large degree of uncertainty.

A large uncertainty also exits in the choice of parameters for moisture retention functions. A flow velocity field similar to Figure 4.13 can be obtained by solving Eq. (4.6) with different combinations of boundary conditions and moisture retention functions. However, for the analysis of chloride transport in the time scale of 10^3 years, it is enough to have a simulated flow velocity field similar to the average flow velocity field observed in the study site. Therefore, it is not necessary to uniquely determine the boundary conditions and moisture retention functions.

Validity of steady-state flow assumption

The steady-state flow velocity field (Fig. 4.13) will be used to determine the coefficients in Eq. (4.1) in the following sections. We assumed earlier that the effects of short-term variation in the flow field appear as dispersion, thus do not change overall subsurface distribution of chloride. To justify our assumption, we solve the flow and transport equations simultaneously with seasonally changing top boundary flux, and compare the results to the solution obtained by assuming the steady-state flow. For the seasonally changing flow case, the value of enhanced dispersion factor is set at $\beta = 1$, while several values of $\beta > 1$ is used for the steady-state flow cases to examine the sensitivity of the solution to β.

Simultaneous solutions of transient flow and transport equations, similar to our model, was also presented by Stolte et al. (1992) to simulate short-term transport of salts in the recharge wetland studied by Mills and Zwarich (1986).

The seasonally changing boundary flux is generated by multiplying the boundary flux function FBC1 by the factors listed in Table 4.2. For example at the center of the wetland the flux is zero in winter (November - February), +340 mm yr^{-1} in spring (March - May), +500 mm yr^{-1} in summer (July - September), and -60 mm yr^{-1} in fall (October - November), while the average flux is +200 mm yr^{-1}. Different sets of factors are used for the wetland and the slope portion of the boundary (Table 4.2). To avoid numerical instability arising from having singular points (sources and sinks) in the root zone, the boundary flux for the flow simulations in this section is applied to the boundary surface for both seasonally changing and steady-state cases.

When the first part of the solution, C_1^*, is examined, the best match between the solution with seasonally changing flow field (Fig. 4.14a) and with the average flow field (Fig. 4.14b) at $t =$ 20 yr is obtained when $\beta = 2$ is used in the latter. This value is consistent with the theoretical prediction using Eq. (4.9) and the relative magnitude of maximum flux to the average flux (Table 4.2). The simulation with seasonally changing flow that used the adaptive time steps required approximately 700-800 times longer computation time than the one with the average flow that used the constant time steps of $\Delta t = 10$ day.

The actual amplitude of oscillation in the field is expected to be larger than the values listed in Table 4.2, which is used to demonstrate the effects of seasonal variation without causing numerical instability. Therefore $\beta = 5$ is used in the base case setting, and other values are used to examine the sensitivity of chloride distribution to the flow oscillation.

Fate of initial mass

The solution for C_1^* with the base case setting (Table 4.3) shows that chloride accumulates in the slope in early stage ($t = 20$ yr) of the transport process (Fig. 4.14b). Similar results were reported by Stolte et al. (1992). The accumulation in the slope, however, is a temporary phenomena, and chloride is eventually ($t = 4000$ yr) transported downward by slow advection (Fig. 4.14c). The same results are obtained for many different combinations of parameters and functions (Table 4.3). This indicates that the chloride we observe in near surface soil (Fig. 4.9) is not the relict of the mass that was in the area in the beginning of the post glacial period (10,000 years ago).

Atmospheric input of chloride

The solution for C_2^* with the base case setting at $t = 4000$ yr shows a patch of high concentration in the middle to upper slope (Fig. 4.14d). The similar pattern is obtained when γ is increased to 2, but the intensity of chloride accumulation is much weaker (Fig. 4.14e). The ratio of the concentration in the wetland to that in the slope is similar to the field value in the former case, but not in the latter. The simulated chloride distribution that is consistent with the field data (Fig. 4.9) is obtained for the range of γ between 0.05 and 0.5. The change in other parameters and functions only has minor effects in the patterns of chloride distribution. Changing the values of γ with r also has only minor effects; therefore the assumption of uniform γ over the domain is justified.

The values of γ is smaller than 1 as predicted by theoretical analysis. However, it is difficult to attach a physical meaning to the range of γ, 0.05-0.5. The simple mass transfer equation (4.2) is a highly idealized description of complex physical processes such as overland flow and interflow during the snowmelt period, plowing in the spring, infiltration and evapotranspiration in the summer, activity of animals, and numerous other processes. Understanding of the mass transfer processes will require detailed field investigations of each specific process, which is out of the scope of the current study.

The evolution of chloride distribution is characterized by the change in concentration under the wetland (Fig. 4.15). Regardless of the choice of the parameters and functions, near stable concentration is reached in 2000-3000 years. Chapter 3 showed that chloride may be affected by mild retardation (retardation coefficient less than 2). The retardation will increase the time to reach stable concentration, but it will not affect the final value of concentration. Similarly,

the concentration patterns that develops in geological time scale will not be altered by the mild retardation.

Using the base case parameters, hence using the solutions shown in Figs. 4.14c and 4.14d, the simulated concentration (Fig. 4.14f) is matched to the field data by setting $C_0 = 30$ mg l^{-1}, $C_p = 0.04$ mg l^{-1}, and $P = 360$ mm yr^{-1} in Eqs. (4.12) and (4.13). The chloride mass near the ground surface in the middle to upper slope is of atmospheric origin, while part of chloride mass near the right bottom corner of the solution domain is the relict of the initial mass.

Concentration under the wetland

The flow boundary flux functions and the enhanced dispersion (β) due to flow oscillation are the major unknowns in our model. When the value of β is fixed at 5, the choice of flow boundary flux functions has minor effects on the relationship between γ and C_2^* under the wetland (Fig. 4.16a). Similarly, when the boundary flux function FBC1 is used, the relationship between γ and C_2^* is only weakly affected by change in β for $\gamma > 0.01$ (Fig. 4.16b). Therefore, the sensitivity of the chloride concentration under the wetland to the parameters with the largest uncertainty is low, and the results of the numerical analysis may be valid under reasonably general hydrologic conditions.

Discussion

Chloride concentration under wetlands

In the range of γ (= 0.05-0.5) that gives the simulated chloride distribution consistent with the field results, C_2^* under the wetland takes the value 0.5-0.8 (Fig. 4.16). The value will approach one, if γ becomes large enough. For $C_2^* = 1$, recalling Eq. (4.13), we have

$$C_2 = C_p P / q \tag{4.14}$$

which describes the enrichment of chloride in precipitation by evapotranspiration in a completely mixed system (Eriksson, 1955, Eq. 1). As stated in the conceptual model, Eq. (4.14) will also hold in the incompletely mixed system of the wetland and slope, if the groundwater recharge flux does not interact with the region of chloride accumulation, and hence the average chloride concentration in the recharge is equal to the concentration under the wetland.

In our simulations, the recharge flux does pick up chloride under the top slope, and hence the concentration under the wetland is lower than the average concentration in the output flux. The deviation of C_2^* from the ideal value of one becomes more significant, when the intensity of chloride accumulation increases due to low efficiency (γ) of the mass transfer by snowmelt runoff (Fig. 4.16). Because the flow direction is upward in the region of high chloride concentration, dispersion must be responsible for transferring chloride from the high

concentration region to the underlying downward flow zone. However, dispersion also spreads the chloride in the top zone horizontally, thus weakens the intensity of chloride accumulation. Therefore, the deviation of C_2^* from one is smaller for larger value of β in Figure 4.16b.

Chloride as an indicator of groundwater recharge

The mass transfer efficiency γ is related to the seasonal distribution of runoff flux. In the northern prairie region, where most of the surface runoff occurs in snowmelt period, the value of γ is expected to be in the similar range (0.05-0.5). Therefore, we suppose that C_2^* under recharge wetlands in this region is in the range of 0.5-0.8, and the groundwater recharge in a catchment containing a wetland is estimated from

$$0.5PC_p / C_2 < q < 0.8PC_p / C_2 \qquad (4.15)$$

where C_2 in this inequality is the shallow groundwater concentration under the wetland. The estimated groundwater recharge should represent the average over last 1000-2000 years. The concentration of chloride under the presently studied wetland is approximately 5 mg l^{-1}. Assuming C_p = 0.04 mg l^{-1} and P = 360 mm yr^{-1}, the estimated groundwater recharge is 1.4-2.3 mm yr^{-1}, consistent with the value estimated from the hydraulic gradient and conductivity (1-3 mm yr^{-1}).

A survey of previously studied recharge wetlands across the northern prairie region (Fig. 4.1) shows that chloride concentration in shallow groundwater under the wetlands falls in a narrow range with the average of 5.8 mg l^{-1} (Table 4.4). The annual precipitation in these sites is in the range of 360-450 mm, hence the wetland-focused groundwater recharge estimated from (4.15) is in the range of 1-5 mm yr^{-1}. The estimation of wetland-focused groundwater recharge in these studies (Table 4.4) were mostly based on the analysis of hydraulic gradient and conductivity measured in a small number of piezometers, or the response of water table in a small number of water table monitoring wells to recharge events. It is difficult, however, to represent hydrologic parameters of a large catchment by a small number of data points. Therefore part of the large variation in recharge rate is likely due to the error in estimation.

The strikingly similar chloride concentration in groundwater under many prairie wetlands may indicate that the groundwater recharge rate is not as variable as previously thought. Under similar climatic condition across the prairies, the soils and vegetation perhaps adjust the evapotranspiration rate to result in the groundwater recharge in order of 1-5 mm yr^{-1} regardless of other conditions such as hydraulic conductivity of tills or the depth to local aquifers.

Conclusions

The hydrologic interaction between a recharge wetland and the surrounding slope is reasonably well approximated by the solution of the steady-state flow equation. The flow

velocity vectors generated by the flow equation are used in the advection-dispersion equation, which is coupled with an equation to describe mass transfer of chloride from the surface soil to snowmelt runoff. The coupled transport equations have solutions similar to the field data, when the mass transfer coefficient is 0.05-0.5 of the average snowmelt runoff. Therefore, the mathematical model represents well the transport processes induced by the wetland-focused groundwater recharge.

The system of a recharge wetland and its catchment receives the input of atmospheric chloride, which is enriched by evapotranspiration while cycled in the system by subsurface flow and snowmelt runoff, and eventually transported to the underlying aquifer. The input and output becomes balanced in geological time scale (10^3 years), and the subsurface chloride achieves stable distribution. At this stage, the concentration in shallow groundwater under the wetland is slightly smaller than the average concentration of the groundwater recharging the aquifer. The ratio of the concentration under the wetland to the average concentration in the groundwater recharge is 0.5-0.8, when the mass transfer coefficient is in the reasonable range. Therefore, we can estimate groundwater recharge by dividing the atmospheric input by the concentration under the wetland times 0.5-0.8.

The chloride method is an attractive alternative to water balance or hydraulic gradient methods, because it is not influenced by spatial heterogeneity within the catchment or the errors in measurement of evapotranspiration, in addition to its simplicity. When the chloride method is applied to previously published case studies across the northern prairie region, the estimated values of groundwater recharge fall in a surprisingly small range (1-5 mm yr^{-1}). While the method needs more field testing, these preliminary results suggest that the groundwater recharge in the northern prairie region may not be as variable as previously thought.

Appendix

The solution of Eq. (4.1) is approximated by a trial function

$$C(t,\mathbf{x}) \cong \sum_{J=1}^{n} c_J(t) N_J(\mathbf{x})$$

using the finite element method (Huyakorn and Pinder, 1983, Eq. 2.4.1.2; hereafter HP83), where c_J is the nodal concentration at Jth node, and N_J is the basis function. Applying the Galerkin method to Eq. (4.1), we get a set of ordinary differential equation in a matrix form (HP83, Eqs. 5.6.2.8a-d)

$$[Q]\{dc/dt\} + [S]\{c\} + \{f\} + [F]\{c\} = 0 \qquad (4.A1)$$

The last term on the left hand side of Eq. (4.A1) is a new term that represents the transport of chloride by snowmelt runoff, which operates independently from the externally given boundary

condition $\{f\}$. For example $\{f\}$ may represent the atmospheric input of chloride, while $[F]$ represents the surface path of chloride cycling. The entry of matrices and vectors are given by

$$Q_{IJ} = \sum_e \int_{W^e} \theta_J N_I N_J dV \tag{4.A2}$$

$$S_{IJ} = \sum_e \int_{W^e} \left\{ \bar{\theta} v_i \frac{\partial N_I}{\partial x_i} N_J - \bar{\theta} D_{ij} \frac{\partial N_I}{\partial x_i} \frac{\partial N_J}{\partial x_j} \right\} dV \tag{4.A3}$$

$$f_I = \sum_e \int_{W^e} G N_I dV + \sum_e \int_{\partial W} \left\{ \bar{\theta} D_{ij} \frac{\partial N_J}{\partial x_j} - \bar{\theta} v_i \frac{\partial N_J}{\partial x_i} \right\} n_i N_I dA \tag{4.A4}$$

where summation is applied to elements (e), and volume (dV) and area (dA) integration is applied to each element (W^e). The θ_J is the volumetric moisture content at Jth node, $\bar{\theta}$ is the elemental average moisture content, G is the strength of source (negative) or sink (positive), and n_i is the ith component of the outward unit normal vector. Note that Eqs. (4.A3) and (4.A4) are slightly different from the equations in HP83, because Green's theorem is applied to both advection and dispersion terms in our formulation.

The new matrix $[F]$ is evaluated differently in the wetland (∂W_1) and slope (∂W_2) part of the top boundary (Fig. 4.10). For those rows representing the nodes in the slope, Eq. (4.3) is used with the Galerkin method to give

$$F_{IJ} = \sum_e \int_{\partial W^e_2} k N_J N_I dA \tag{4.A5}$$

where ∂W^e_2 denotes the boundary of each element which is also a part of the slope. Note that Ith row of the matrix resulting from Eq. (4.A5) has non-zero entries in only those columns representing the nodes that share a face (or side in two-dimensional case) of an element with Ith node; short range connection.

The total mass flux from the slope is given by Eq. (4.4); therefore, in the Galerkin method

$$M_T = \sum_e \int_{\partial W^e_2} k c_J N_J dA \tag{4.A6}$$

The total flux is distributed over the wetland area as an input flux (Eq. 4.5), therefore for those rows representing the wetland part of the boundary

$$F_{IJ} = -\sum_e \frac{1}{A_w} \int_{\partial W^e_1} N_I dA \sum_e \int_{\partial W^e_2} k N_J dA \tag{4.A7}$$

Note that the Ith row of matrix resulting from Eq. (4.A7) has non-zero entries in columns representing the nodes in the slope that are many elements away from the Ith node; long range connection (Fig. 4.10). The equations are derived in Cartesian coordinates for the clarity of presentation, but it is straight-forward to formulate the problem in cylindrical coordinates (HP83, p.113).

References

Ahuja, L.R., 1990. Modeling soluble chemical transfer to runoff with rainfall impact as a diffusion process. Soil Sci. Soc. Am. J., 54, 312-321.

Ahuja, L.R. and Lehman, O.R., 1983. The extent and nature of rainfall-soil interaction in the release of soluble chemicals to runoff. J. Environ. Qual., 12, 34-40.

Allison, G.B. and Hughes, M.W., 1983. The use of natural tracers as indicators of soil-water movement in a temperate semi-arid region. J. Hydrol., 60, 157-173.

Al-Taweel, B.H., 1983. Soil genesis in relation to groundwater regimes in a hummocky ground moraine area near Hamiota, Manitoba. Ph.D. thesis, Univ. of Manitoba, Winnipeg, Manitoba.

Batt, B.D.J, Anderson, M.G., Anderson, C.D. and Caswell, F.D., 1989. The use of prairie potholes by North American ducks. In: Northern prairie wetlands, van der Valk, A., ed., 204-227, Iowa St. Univ. Press, Ames, Iowa.

Berkowitz, B., Bear, J. and Braester, C., 1988. Continuum models for contaminant transport in fractured porous formations. Water Resour. Res., 24, 1225-1236.

Celia, M.A., Bouloutas, E.T. and Zarba, R.L., 1990. A general mass-conservative numerical solution for the unsaturated flow equation. Water Resour. Res., 26, 1483-1496.

Claassen, H.C. and Halm, D.R., 1996. Estimates of evapotranspiration or effective moisture in Rocky Mountain watersheds from chloride ion concentrations in stream baseflow. Water Resour. Res., 32, 363-372.

Daus, A.D., Frind, E.O. and Sudicky, E.A., 1985. Comparative error analysis in finite element formulation of the advection-dispersion equation. Adv. Water Resour., 8, 86-95.

Eriksson, E., 1955. Air borne salts and the chemical composition of river waters. Tellus, 7, 243-250.

Frind, E. O., 1988. Solution of the advection-dispersion equation with free exit boundary. Numer. Meth. Partial Diff. Eqs., 4, 301-313.

Gelhar, L.W., Welty, C. and Rehfeldt, K.R., 1992. A critical review of data on field-scale dispersion in aquifers. Water Resour. Res., 28, 1955-1974.

Goode, D.J. and Konikow, L.F., 1990. Apparent dispersion in transient groundwater flow. Water Resour. Res., 26, 2339-2351.

Guenther, R.B. and Lee, J.W., 1988. Partial differential equations of mathematical physics and integral equations. Prentice-Hall, Englewood Cliffs, New Jersey, 562pp.

Huyakorn, P.S. and Pinder, G.F., 1983. Computational methods in subsurface flow. Academic Press, San Diego, California. 473pp.

Juang, F.H.T. and Johnson, N.M., 1967. Cycling of chlorine through a forested watershed in New England. J. Geophys. Res., 72, 5641-5647.

Keller, C.K., van der Kamp, G. and Cherry, J.A., 1988. Hydrogeology of two Saskatchewan tills, I. Fractures, bulk permeability, and spatial variability of downward flow. J. Hydrol., 101, 97-121.

Keller, C.K., van der Kamp, G. and Cherry, J.A., 1989. A multiscale study of the permeability of a thick clayey till. Water Resour. Res., 25, 2299-2317.

Knuteson, J.A., Richardson, J.L., Patterson, D.D. and Prunty, L., 1989. Pedogenic carbonates in a calciaquoll associated with a recharge wetland. Soil Sci. Soc. Am. J., 53, 495-499.

LaBaugh, J.W., 1991. Spatial and temporal variation in chemical characteristics of ground water adjacent to selected lakes and wetlands in the North Central United States. Verh. Internat. Verein. Limnol., 24, 1588-1594.

LaBaugh, J.W., Winter, T.C., Adomaitis, V.A. and Swanson, G.A., 1987. Hydrology and chemistry of selected Prairie wetlands in the Cottonwood Lake area, Stutsman County, North Dakota, 1979-1982. U.S.G.S. Prof. Pap., 1431. 26pp.

Lissey, A., 1968. Surficial mapping of groundwater flow systems with application to the Oak River Basin, Manitoba. Ph.D. thesis, Univ. of Saskatchewan, Saskatoon, Saskatchewan.

Mckay, L.D., Gillham, R.W. and Cherry, J.A., 1993. Field experiments in a fractured clay till. 2. Solute and collid transport. Water Resour. Res., 29, 3879-3890.

Meyboom, P., 1966. Unsteady groundwater flow near a willow ring in hummocky moraine. J. Hydrol., 4, 38-62.

Miller, J.J., 1983. Hydrology of a morainic landscape near St. Denis, Saskatchewan, in relation to the genesis, classification and distribution of soils. M.Sc. thesis, Univ. of Saskatchewan, Saskatoon, Saskatchewan.

Miller, J.J., Acton, D.F. and St. Arnaud, R.J., 1985. The effect of groundwater on soil formation in a morainal landscape in Saskatchewan. Can. J. Soil Sci., 65, 293-307.

Mills, J.G. and Zwarich, M.A., 1986. Transient groundwater flow surrounding a recharge slough in a till plain. Can. J. Soil Sci., 66, 121-134.

Peck, A.J. and Hurle, D.H., 1973. Chloride balance of some farmed and forested catchments in southern Australia. Water Resour. Res., 9, 648-657.

Peters, N.E., 1991. Chloride cycling in two forested lake watersheds in the west-central Adirondack Mountains, New York, U.S.A. Water, Air and Soil Pollution, 59, 201-215.

Rehm, B.W., Moran, S.R. and Groenewold, G.H., 1982. Natural groundwater recharge in an upland area of central North Dakota, U.S.A. J. Hydrol., 59, 293-314.

Remenda, V.H., 1993. Origin and migration of natural groundwater tracers in thick clay tills of Saskatchewan and the Lake Agassiz clay plain. Ph.D. thesis, Univ. of Waterloo, Waterloo, Ontario.

Remenda, V.H., van der Kamp, G and Cherry, J.A., 1996. Use of vertical profiles of $\delta^{18}O$ to constrain estimates of hydraulic conductivity in a thick unfractured aquitard. Water Resour. Res., 32, 2979-2987.

Ro, C.U., Vet, R.J., Ord, D., and Holloway, A., 1995. Canadian Air and Precipitation Monitoring Network (CAPMoN) Annual Summary Reports (1983-1994). Atmospheric Environment Service, Environment Canada, Downsview, Ontario.

Rozkowski, A., 1967. The origin of hydrochemical patterns in hummocky moraine. Can. J. Earth Sci., 4, 1065-1092.

Scotter, D.R. and Raats, P.A.C., 1968. Dispersion in porous mediums due to oscillating flow. Water Resour. Res., 4, 1201-1206.

Shepard, J.P., Mitchell, M.J., Scott, T.J., Zhang, Y.M. and Raynal, D.J., 1989. Measurements of wet and dry deposition in a northern hardwood forest. Water Air Soil Pollut., 48, 225-238.

Stolte, W.J., Barbour, S.L. and Eilers, R.G., 1992. A study of the mechanisms influencing salinity development around Prairie sloughs. Trans. Am. Soc. Agric. Eng., 35, 795-800.

Sudicky, E.A., Unger, A.J.A. and Lacombe, S., 1995. A noniterative technique for the direct implementation of well bore boundary conditions in three-dimensional heterogeneous formations. Water Resour. Res., 31, 411-415.

Trudell, M.R., 1994. Soil salinization associated with shallow groundwater flow systems in thin, fractured till moraine. Ph.D thesis, Univ. of Waterloo, Waterloo, Ontario.

VanderKwaak, J.E. and Sudicky, E.A., 1995. Natural coupling of groundwater-surface water interactions in numeric models. EOS, Trans. Am. Geophys. Union, vol. 76, no. 46, F219.

van Genuchten, M.Th., 1980. A closed-form equation for predicting the hydraulic conductivity of unsaturated soils. Soil Sci. Soc. Am. J., 44, 892-898.

van Genuchten, M.Th. and Dalton, F.N., 1986. Models for simulating salt movement in aggregated field soils. Geoderma, 38, 165-183.

Vet, R.J., Sirois, A., Jeffries, D.S., Semkin, R.G., Foster, N.W., Hazlett, P. and Chan, C.H., 1988. Comparison of bulk, wet-only, and wet-plus-dry deposition measurements at the Turkey Lakes Watershed. Can. J. Fish. Aquat. Sci., 45S, 26-37.

Winter, T,C, 1983. The interaction of lakes with variably saturated porous media. Water Resour. Res., 19, 1203-1218.

Winter, T.C., 1989. Hydrologic studies of wetlands in the northern prairies. In: Northern prairie wetlands, ed. van der Valk, A., 17-54. Iowa Univ. Press.

Woo, M.-K. and Rowsell, R.D., 1993. Hydrology of a prairie slough. J. Hydrol., 146, 175-207.

Woo, M.-K. and Winter, T.C., 1993. The role of permafrost and seasonal frost in the hydrology of northern wetlands in North America. J. Hydrol., 141, 5-31.

Zebarth, B.J., de Jong, E. and Henry, J.L., 1989. Water flow in hummocky landscape in central Saskatchewan, Canada, II, Saturated flow and groundwater recharge. J. Hydrol., 110, 181-198.

Table 4.1 External boundary conditions for numerical simulations. Internal boundary condition that represents surface mass flux is also used for the transport simulation.

	Flow simulation	Transport simulation
Top	Specified flux (Fig. 4.10) average recharge = 0.002 m yr^{-1}	Specified flux flux = 0.015 g m^{-2} yr^{-1}
Sides	No flux	No flux
Bottom	Specified head (uniform) h = -5.2 m	Zero-gradient

Table 4.2 Seasonal variation of the top boundary flux for the flow equation. The values listed in the table are the relative magnitude. The boundary flux is determined by multiplying the flux functions in Figure 4.12 by the relative magnitude.

Period	Wetland	Slope
Nov. - Feb.	0.0	0.0
Mar. - May	1.7	-0.2
Jun. - Aug.	2.5	3.0
Sep. - Oct.	-0.3	1.8

Table 4.3 The base case setting and the range of variation of hydrologic parameters and functions. Top boundary flux function, enhanced dispersion factor β, and the mass transfer efficiency γ.

	Boundary flux	β	γ
Base case	FBC1	5	0.1
Variation	FBC2, FBC3	2,10	0.001-2

Table 4.4 Data summary of previously studied recharge wetlands; source article, specific site, depth of groundwater sample, area of the wetland, area of the catchment, average groundwater recharge, and groundwater chloride concentration under the wetland. The location of the sites is shown in Figure 4.1.

	Source	Site	Depth (m)	Wetland (m^2)	Catchment (m^2)	Recharge (mm yr^{-1})	Cl (mg l^{-1})
1	Meyboom	Slough center	1.5	1000	8100	11	4.9†
2	Al-Taweel	Site 2 (W5)	2	1300			6.0
3	Miller	Site 3	1.7	2400	24000	1 - 3	5.9†
3	Miller	Site 11	1.3	2100	38000		5.4†
4	LaBaugh	T3 (well 12)	2	1900			7
4	LaBaugh	T8 (well 4)	3	6400			7
5	Zebarth	F site, MSL	2.5	1000	14000	21	6.2†
5	Zebarth	S site, MSL	2.5	3300	18000	45	6.3†
6	Trudell	155	3.0	4100	44000	8 - 13	5.4
6	Trudell	157	2.5	2500	28000	8 - 13	5.9
6	Trudell	173	7.8	500	4700	3 - 7	3.0
6	Trudell	197	2.8	3700	23000	17 - 25	6.0
Average				2500	22000		5.8

†Water samples were analyzed in the present study using ion exchange chromatography.

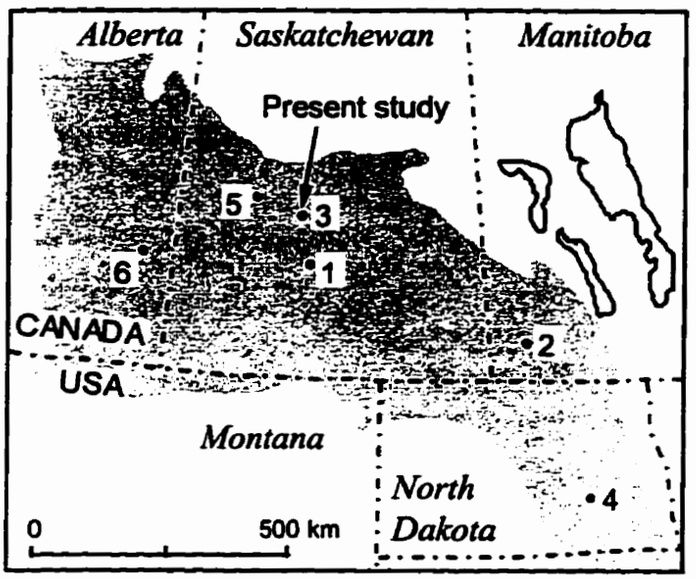

Fig. 4.1 Location of the present and previous study sites. 1. Meyboom (1966), 2. Al-Taweel (1983), 3. Miller et al. (1985), 4. LaBaugh et al. (1987), 5. Zebarth et al. (1989), 6. Trudell (1994). Stippled area indicates the extent of northern prairie wetlands (Winter, 1989).

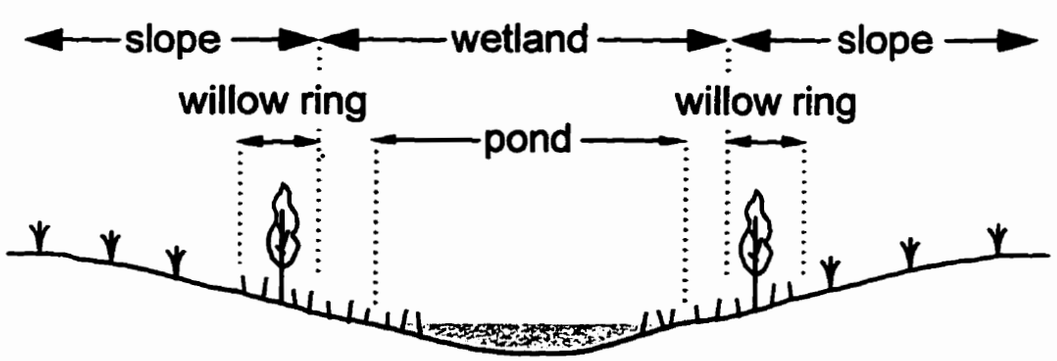

Fig. 4.2 Definition of the pond, wetland, willow ring, and slope.

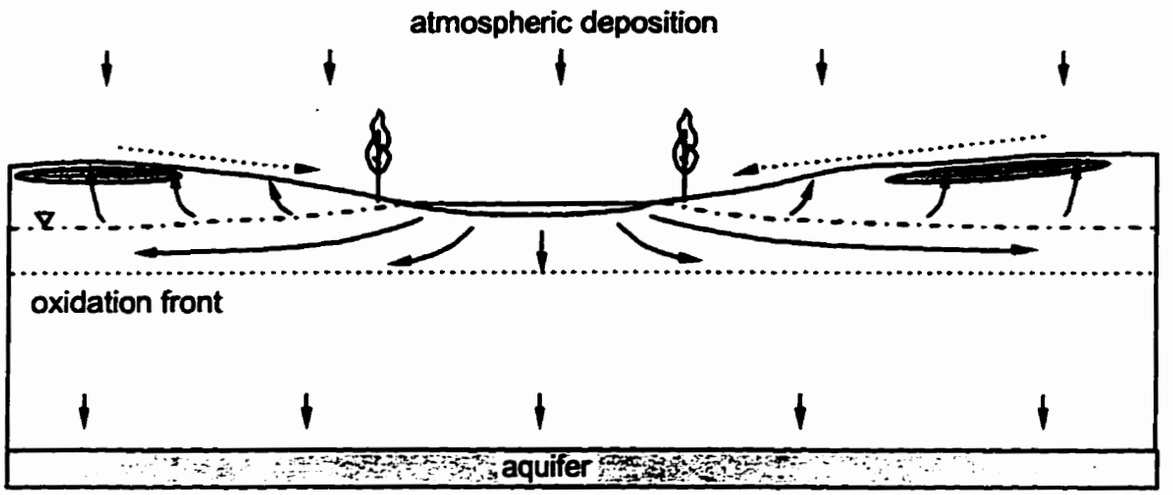

Fig. 4.3 Conceptual model of chloride transport. Arrows indicate the direction of subsurface flow (solid line) and snowmelt runoff (dotted line). Dark shaded area near the ground surface indicates accumulation of chloride. Modified from Chapter 3.

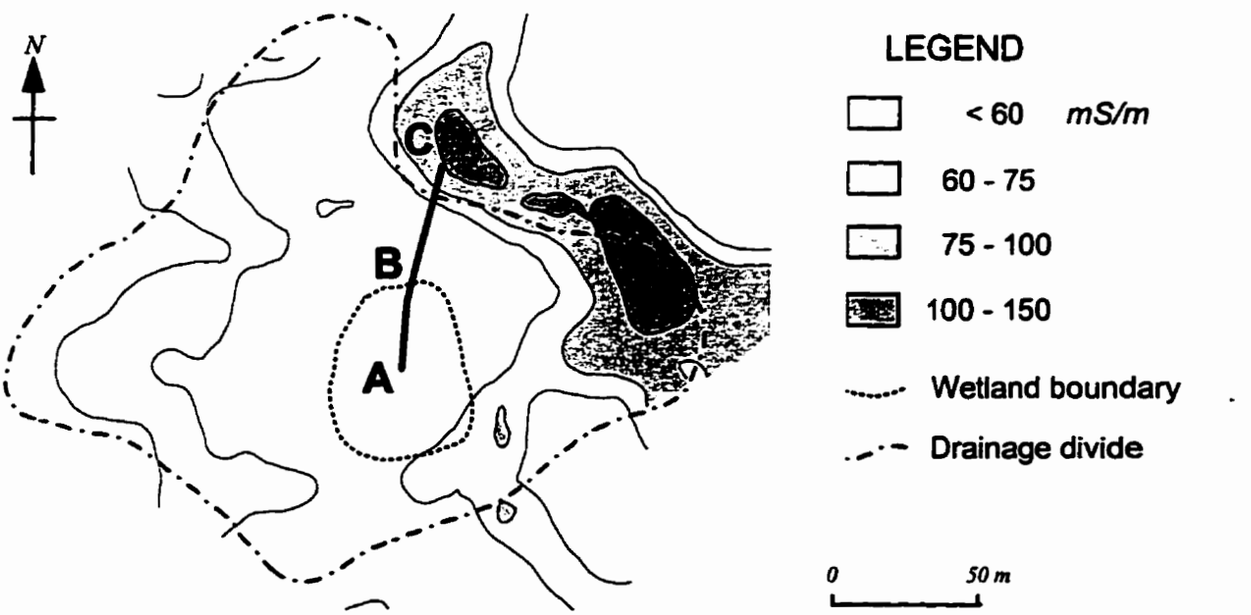

Fig. 4.4 Distribution of the soil electrical conductivity. Cross sections for the hydraulic head (Fig. 4.8) and the subsurface chloride distribution (Fig. 4.9) are taken along the transect ABC. Modified from Chapter 3.

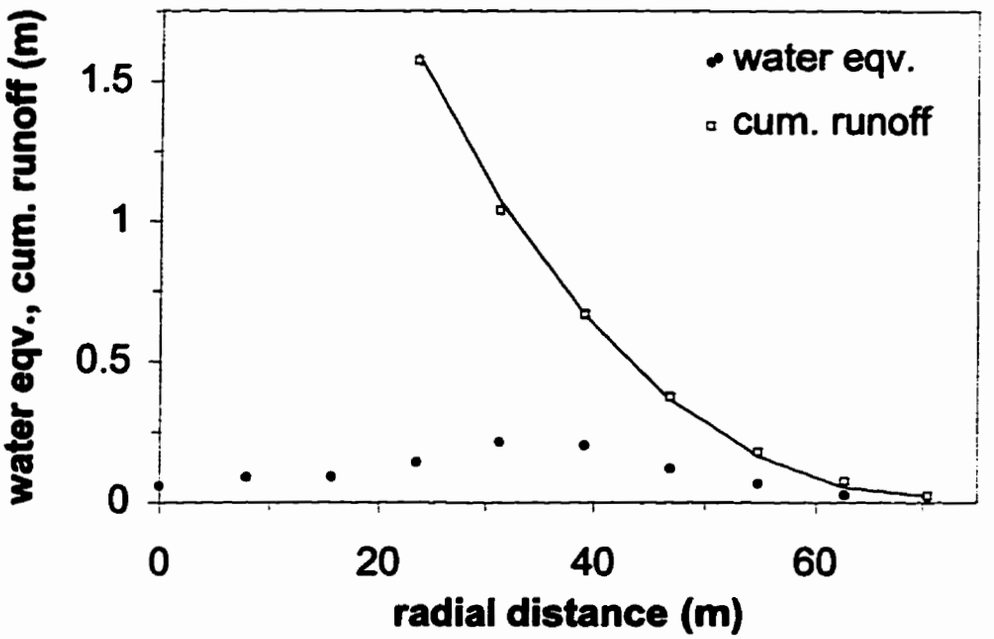

Fig. 4.5 Radial distribution of snow water equivalent and cumulative snowmelt runoff.

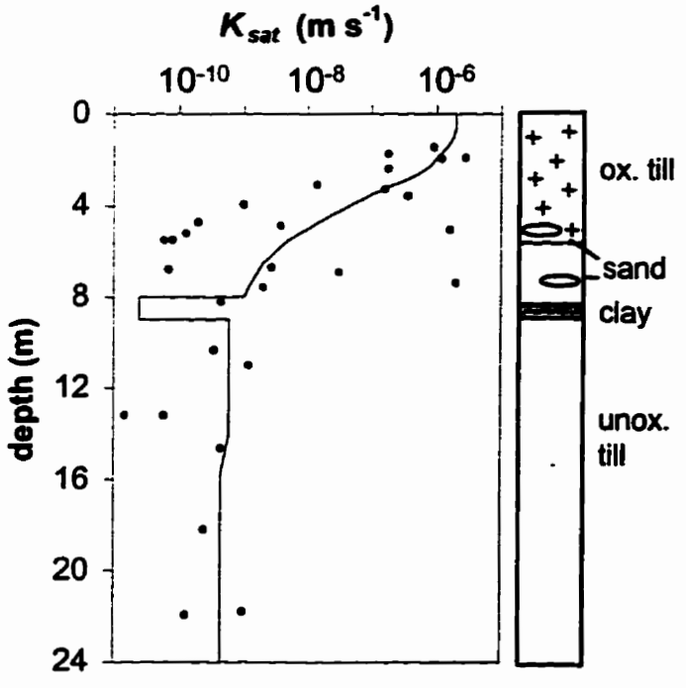

Fig. 4.6 Saturated hydraulic conductivity and the stratigraphy of the site. The solid curve is the values used in the flow simulations.

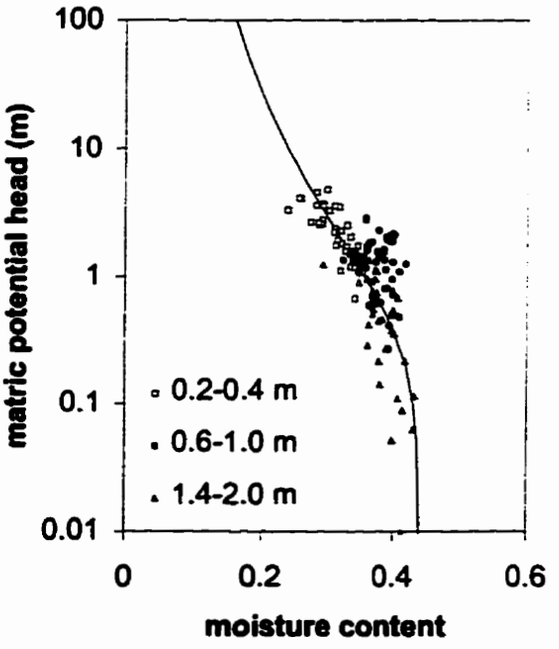

Fig. 4.7 Moisture-matric potential relationship. Points are classified by the depth. The solid curve is the van Genuchten function with θ_{sat} = 0.44 and α = 1.25 m^{-1}.

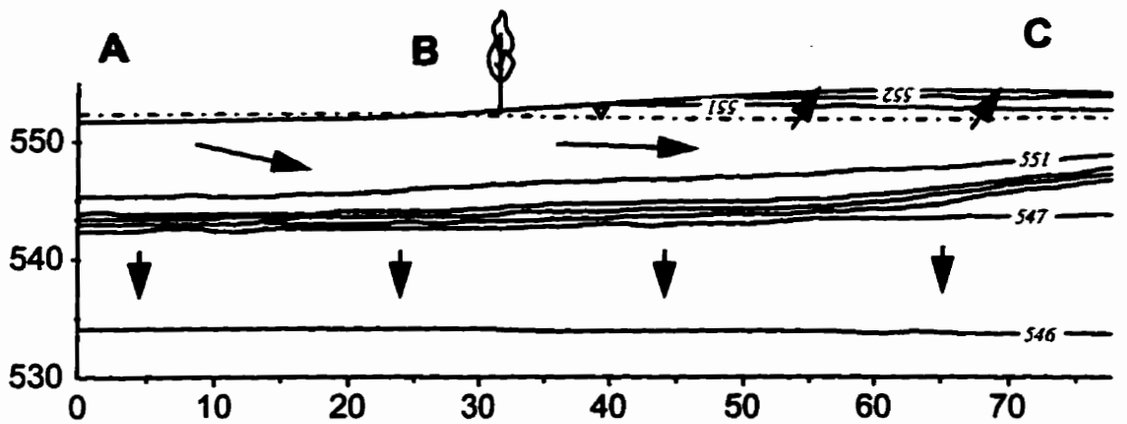

Fig. 4.8 Hydraulic head distribution in July 1994. The head is referenced to the mean sea level. Contour interval is one meter. Arrows indicate subsurface flow direction. Modified from Chapter 2.

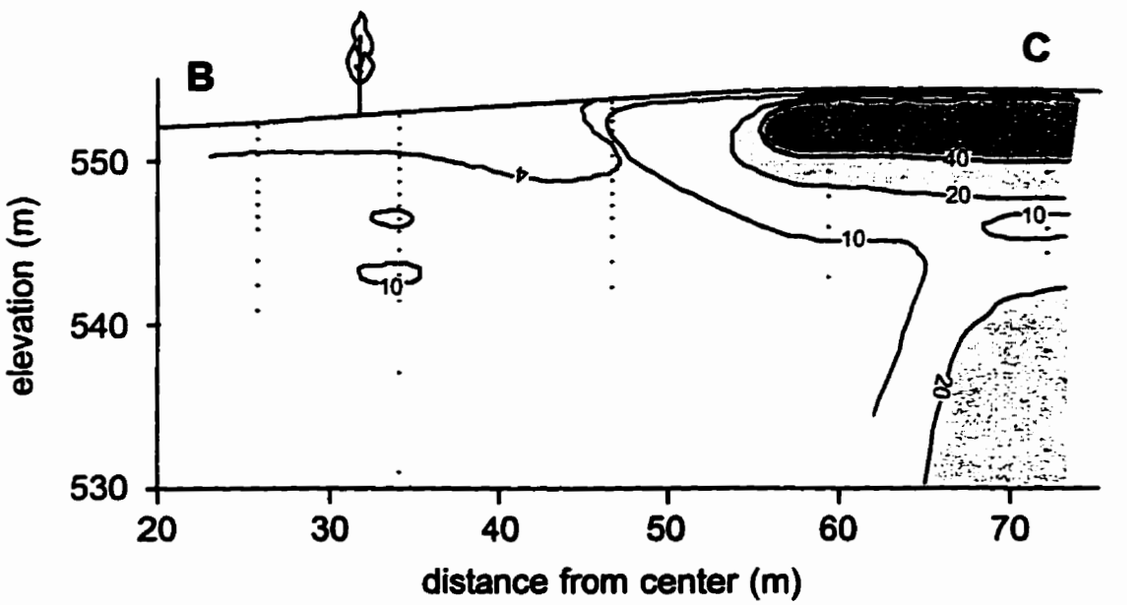

Fig. 4.9 Pore water chloride concentration (mg l^{-1}). Modified from Chapter 3.

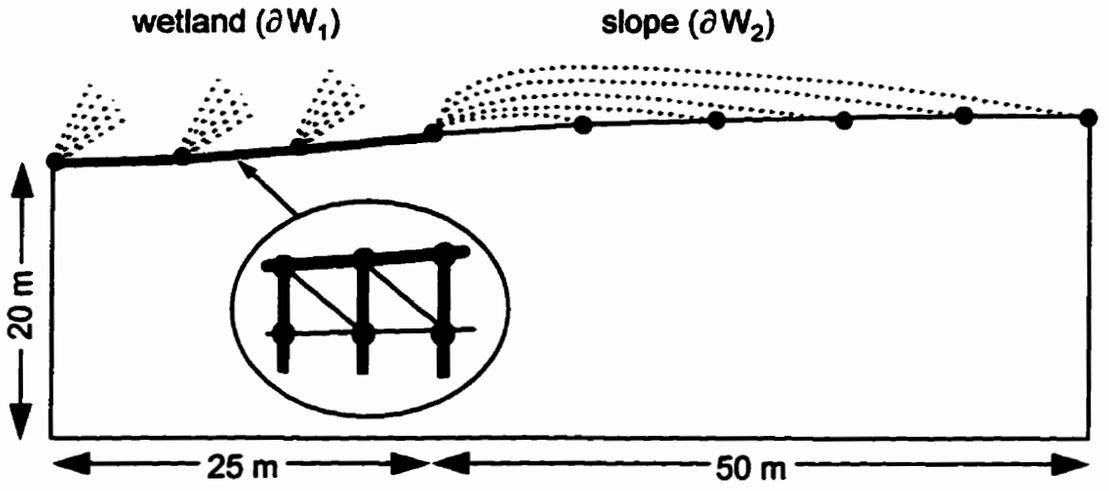

Fig. 4.10 A cross section of an axisymmetric model domain. Nodes and elements are shown schematically, hence not to scale. The long range connection between the slope nodes and the wetland nodes are indicated by the dashed curves.

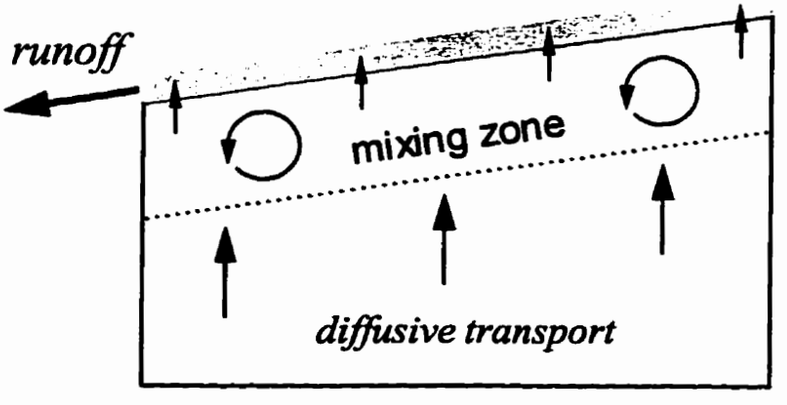

Fig. 4.11 Schematic diagram of the mass transfer mechanism by surface runoff.

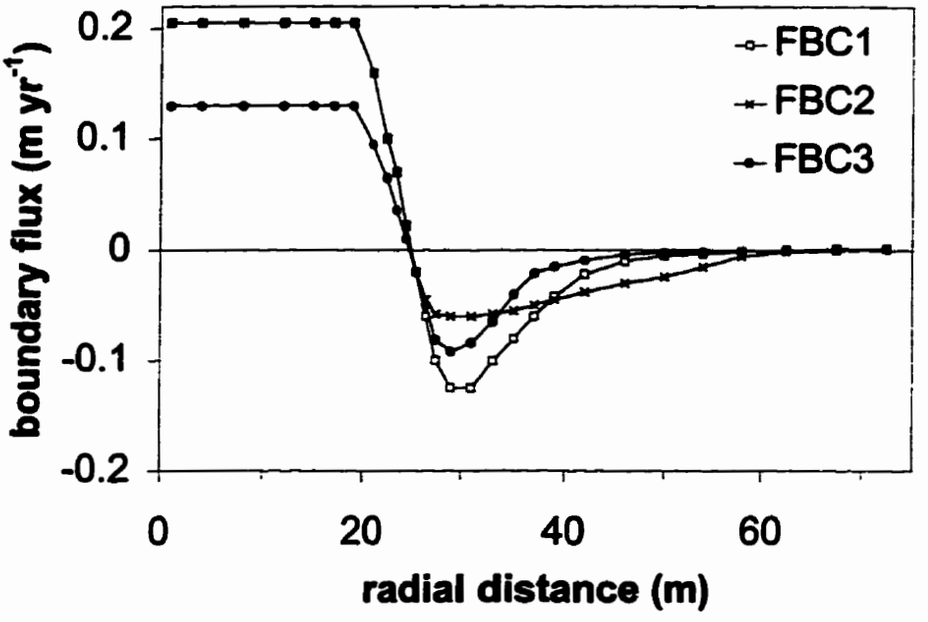

Fig. 4.12 Top boundary flux functions used in flow simulations. Positive flux indicates downward flow.

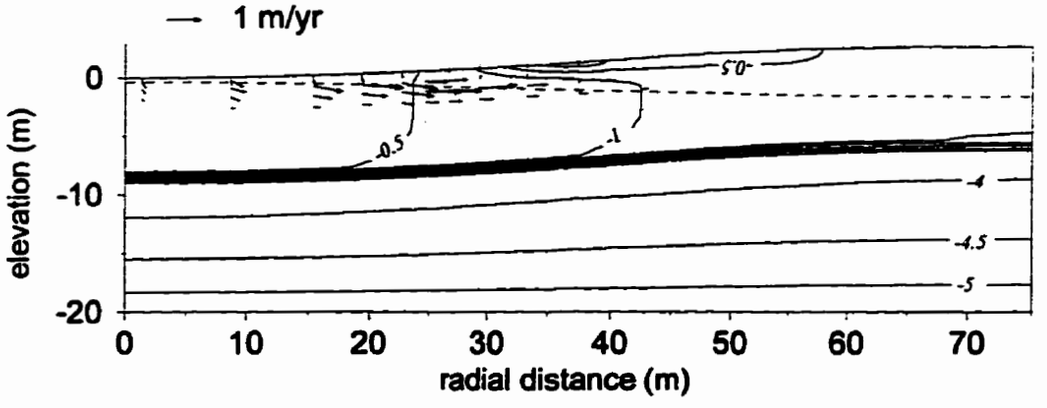

Fig. 4.13 Distribution of hydraulic head and Darcy flux vectors. They were generated by numerical solution of the flow equation with boundary flux function FBC1. The potential contours are in 0.5 m interval. Note that arrow is not shown for every element.

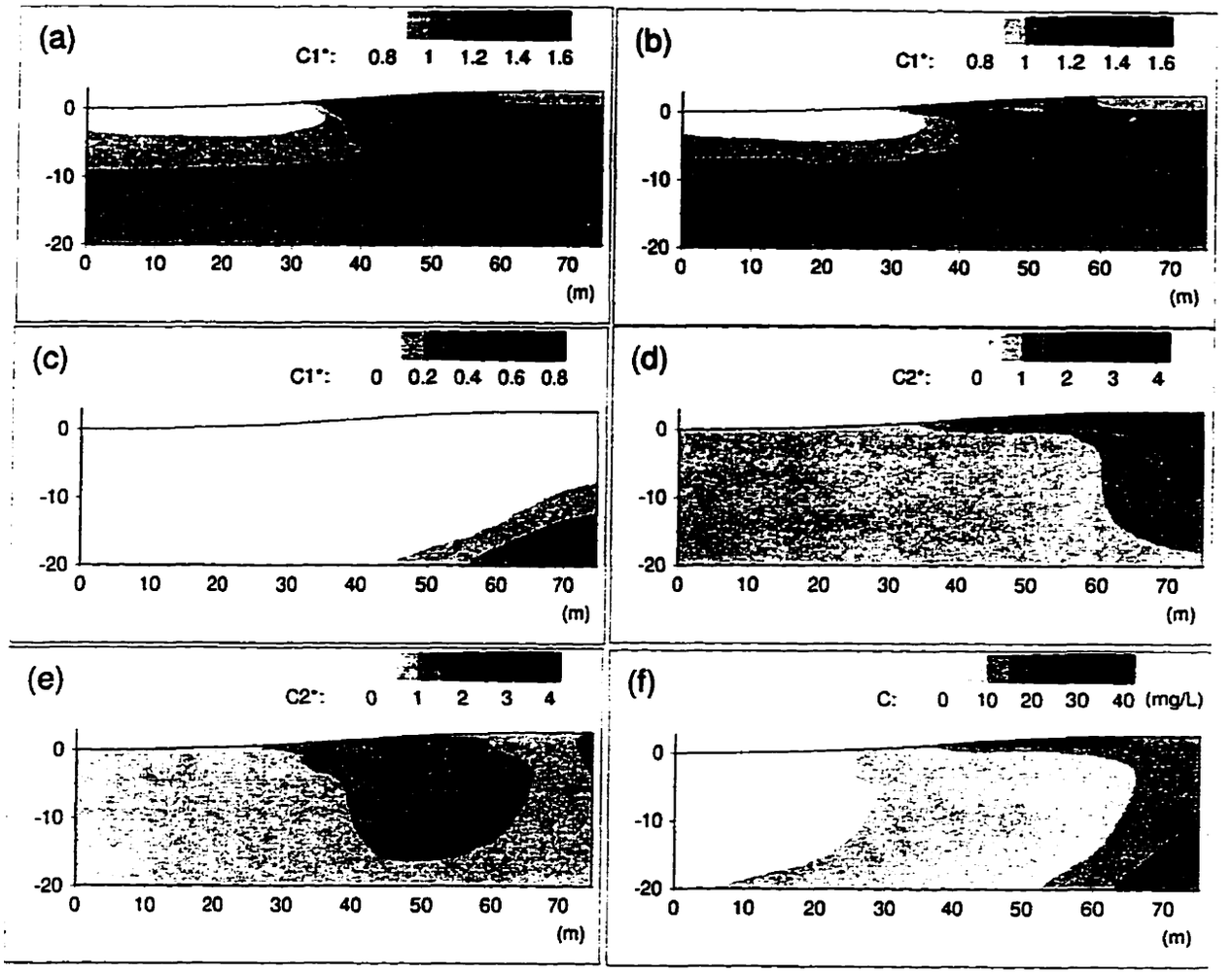

Fig. 4.14 Simulated distributions of chloride concentration. (a) C_1^* at $t = 20$ yr, with seasonally changing flow boundary flux applied to the top surface. (b) C_1^* at t = 20 yr, with the average flow boundary flux applied to the surface. (c) C_1^* at $t = 4000$ yr. (d) C_2^* at $t = 4000$ yr. (e) C_2^* at $t = 4000$ yr, with $\gamma = 2$. (f) Concentration distribution that matches with field data (Fig. 4.9). The base case setting is used for all simulations unless otherwise stated. The flow boundary flux is distributed in the root zone unless otherwise stated. Concentrations are dimensionless except in (f).

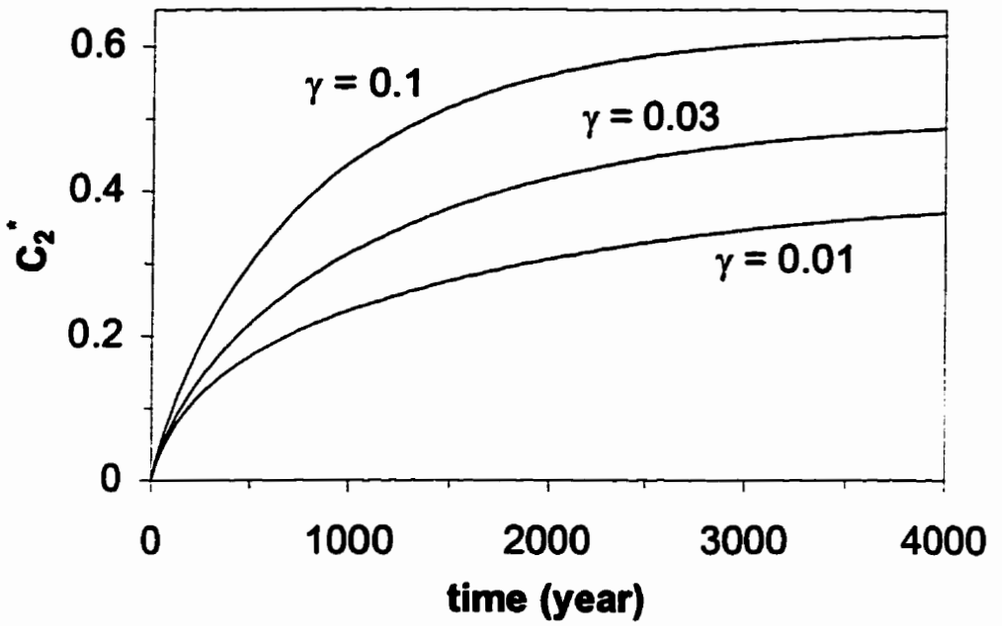

Fig. 4.15 Evolution of chloride concentration under the wetland. The base case setting is used except for γ.

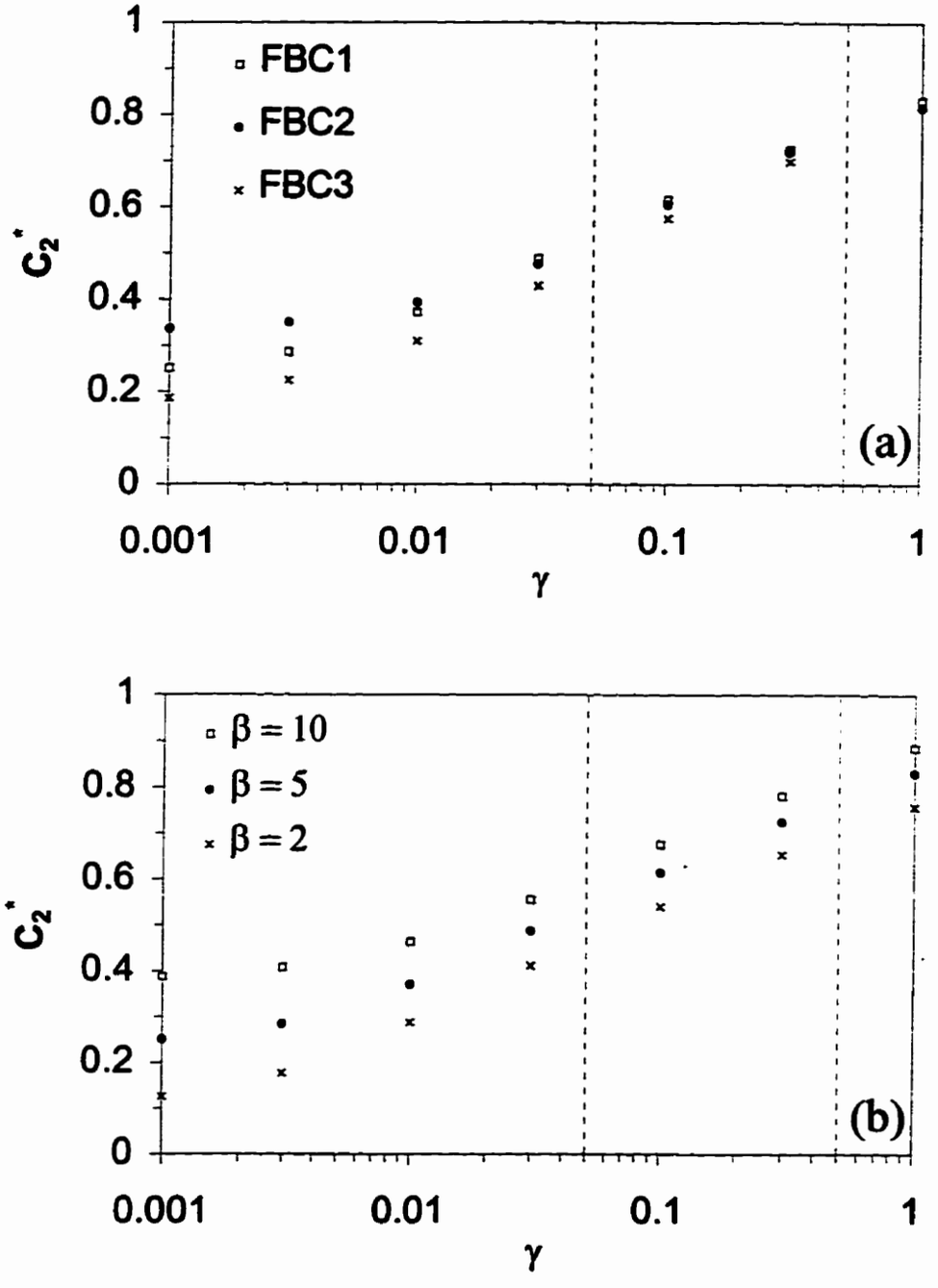

Fig. 4.16 Concentration under the wetland at $t = 4000$ yr. (a) effects of changing the top boundary flux functions. (b) effects of changing the enhanced dispersion factor.

Chapter 5

Conclusions and implications

The wetlands located in the elevated area of undulating terrain in the northern prairie region recharge the underlying groundwater. The recharge wetland selected for the field study represents countless other recharge wetlands in the region.

Soil frost in the winter reduces the hydraulic conductivity of the top soil, and hence causes a large snowmelt runoff from the surrounding slope to the wetland. The snowmelt water forms a pond in the wetland that usually dries up in the summer. The convergent surface flow in the snowmelt period is an important characteristic of the hydrology of the northern prairie wetlands.

A large portion (70-80%) of the snowmelt and summer precipitation infiltrates, and drives the divergent subsurface flow from the wetland to the slope. The majority of the divergent subsurface flow occurs in the saturated zone above the oxidation front, because the hydraulic conductivity of the strongly fractured glacial till in this zone is several orders of magnitude higher than the weakly fractured till in the zone below.

High rate of evapotranspiration in the slope keeps the average flow direction in the vadose zone upward, and little net infiltration occurs in the slope. Therefore, infiltration is focused in the wetland. Most of the infiltration in the wetland, however, is used by evapotranspiration in the slope, and only a small portion becomes groundwater recharge (1-3 mm yr^{-1} over the catchment).

Evapotranspiration in the wetland (300 mm yr^{-1}) is lower than the evaporation from a large lake in the region (700 mm yr^{-1}), perhaps due to the reduced wind speed by the willow ring in the perimeter of the wetland. The wetland evapotranspiration is approximately equal to the summer precipitation; therefore, the net infiltration in the wetland is determined by the snowmelt runoff, i.e. the divergent subsurface flow is driven by the convergent surface flow.

The average flow patterns describe the essence of the hydrologic interaction between the wetland and the slope. It should be noted, however, that the flow field around the wetland is not perfectly symmetric due to complex topography, and that the temporary reversals in subsurface flow direction may be caused by heavy storms. The flow reversal is also caused by summer fallowing the slope, thus reducing the evapotranspiration in the slope.

Subsurface distribution of chloride concentration reflects the average flow regime. The concentration under the wetland is close to the concentration in the pond water due to high infiltration. The concentration under the bottom and middle slope is similar to the concentration under the wetland, but the concentration under the top slope is much higher indicating accumulation of chloride by evapotranspiration. The accumulated chloride in the top

soil is leached by the snowmelt runoff each year, and transferred to the wetland; chloride is cycled between the slope and the wetland.

The input of chloride to the wetland-slope system is atmospheric deposition, which is considered constant over many years. Chloride is cycled within the shallow part of the system by the convergent surface flow and the divergent subsurface flow. Chloride is transferred from the shallow part to the deep part of the system by the wetland-focused groundwater recharge that eventually carries chloride out of the system. In geological time scale, the atmospheric input and the groundwater output becomes balanced, and the chloride cycle reaches the steady state. The chloride concentration, C_g, in shallow groundwater under the wetland indicates the mass balance state of the system, because it represents the concentration in the wetland-focused groundwater recharge, i.e. output flux.

The numerical model of the wetland-slope system based on the field observations shows that the subsurface chloride distribution is only mildly sensitive to the details of boundary conditions, and that the ratio of the average concentration in the precipitation to that in the shallow groundwater under the wetland, C_p/C_g, is proportional to the ratio of the groundwater recharge to the precipitation with a proportionality constant 1.3-2. A survey of published data on 11 recharge wetlands in the northern prairie region shows that the ratio C_p/C_g for those wetlands falls in remarkably narrow range (0.006-0.013), which may indicate the recharge rate of several millimeters per year, while the annual precipitation in the region is 300-400 mm.

The convergent-divergent hydrologic system in the recharge wetlands implies that exporting snowmelt water from the system by artificial drainage will stop the divergent subsurface flow and groundwater recharge. It will also stop the transport of dissolved chemical species from the wetland to the slope, hence causing a major change in the subsurface distribution of dissolved chemicals in the catchment. The environmental impacts of these changes must be evaluated carefully before drainage projects are undertaken.

If the ratio C_p/C_g is a true indicator of groundwater recharge, then strikingly similar values of the ratio observed in the northern prairie region will suggest that the spatial variation of groundwater recharge in the region is reasonably small. It will be interesting to conduct a systematic survey of C_p/C_g in many wetlands in the region to find a regional trend in the value, which may reveal the relation between the recharge and climatic conditions or land use practice.

Appendix A

Reevaluation of the tensiometer response method to measure unsaturated soil hydraulic conductivity

INTRODUCTION

The flux of water in the unsaturated zone was first expressed as the product of hydraulic gradient and hydraulic conductivity by Buckingham (1907). It is now a routine practice to estimate the hydraulic gradient using tensiometers, but there is no universally applicable method to measure hydraulic conductivity of unsaturated field soils under a wide range of soil moisture conditions. Standard methods were reviewed by Green et al. (1986), but they all have limitations, particularly in clay-rich soil in which the drainage flux of water is slow.

Gardner (1960) proposed a method to estimate unsaturated soil hydraulic conductivity based on the response of a tensiometer after the pressure in the tensiometer was artificially perturbed from equilibrium. Though promising in principle, the method has several potential shortcomings, as pointed out in the original discussion by Gardner. First of all, the soil hydraulic conductivity in unsaturated soil is a function of matric potential. Perturbing the equilibrium of pressure in the tensiometer disturbs matric potential in the soil, and alters the conductivity from its equilibrium value. It may be difficult, therefore, to know which matric potential value corresponds to the estimated conductivity. Similarly, the effect of soil water hysteresis on tensiometer response is not well understood. The second problem is that the method measures the average hydraulic conductivity weighted heavily on the soil in the close vicinity of the porous cup. It is practically impossible to avoid disturbing the soil around a porous cup during the installation of a tensiometer; therefore, the estimated conductivity may not be representative of the undisturbed soil (d'Astous et al., 1989).

Gardner's method has not been commonly used to measure conductivity, perhaps due to the problems listed above (Tokunaga, 1992). However the method is attractive in many field sites with clay-rich, low permeability soil, for which other methods are not applicable or too expensive and time consuming. Recent development of a sophisticated parameter estimation technique (Gribb, 1996) has a potential to overcome the first problem mentioned in the preceding paragraph, but its algorithm is still too complicated for routine field applications. We will develop a simple theory to interpret the field data of tensiometer response tests, based on well known theory of piezometer slug tests. The validity of the theory will be examined by numerical simulations and laboratory experiments. The second problem, the disturbance effects, cannot be solved by theoretical studies. We will estimate the expected degree of error

due to such effects by laboratory experiments. The practicality of the method will be evaluated in a field site.

THEORY

In the tensiometer response test the pressure in the air pocket of a tensiometer is instantaneously increased by, for example, connecting a syringe that contains a small volume of air at atmospheric pressure (Fig. A1). The excess pressure dissipates as water in the porous cup moves into the soil causing the air in the tensiometer to expand. When the porous cup conductance is sufficiently high, the response of tensiometer is controlled by the gauge sensitivity and the soil hydraulic conductivity. Thus it is possible to estimate the soil hydraulic conductivity from the pressure dissipation data (Richards et al., 1937; Gardner, 1960). A similar method to determine hydraulic conductivity in saturated porous media from piezometer response is commonly called slug test (Bouwer and Rice, 1976). In the following, we will assume that the soil hydraulic parameters do not depend on matric potential, and develop a linear theory of the tensiometer response test. It will be shown later by numerical analysis and laboratory experiments that the assumption of linearity is acceptable.

Linear theory without soil water storage

In the first step of the theoretical development, we assume that the soil has no capacity to store water, and that the flow rate, $Q(t)$ ($m^3\ s^{-1}$), from the porous cup to the soil is given by

$$Q = FK\Delta h_T \qquad [1]$$

where F (m) is a shape factor representing porous cup geometry, and K ($m\ s^{-1}$) is the soil hydraulic conductivity, and $\Delta h_T(t)$ (m) is the difference in the total soil water potential head between the porous cup and the boundary of the system. Because the soil water storage is neglected in Eq. [1], the potential distribution in the soil at any instance during a response test is identical to that of the steady-state flow that would result if Δh_T was kept constant. Using Eq. [1], the linear slug test equation to describe the rate of pressure change in a tensiometer is (Hvorslev, 1951)

$$S_g \frac{dh_T}{dt} = FK(h_T - h_{Teq}) \qquad [2]$$

where S_g (m^2) is the gauge storage, h_T (m) is the total soil water potential head in the porous cup, h_{Teq} is the equilibrium value of h_T. The gauge storage is defined as the volume of water that has to be removed from the tensiometer to cause a unit drop in the total potential head, which is the reciprocal of the gauge sensitivity (Richards et al., 1937). For a sufficiently small pressure change, the gauge storage does not change appreciably during the response test (Tokunaga, 1992), and it is given by

$$S_g = \frac{dV}{dh_T}\rho_w g \frac{dV}{dP} = \rho_w g \frac{V_l}{P_{eq}} \qquad [3]$$

where V_l (m^3) is the volume of air in the tensiometer, ρ_w (kg m^{-3}) is the density of water, g (m s^{-2}) is the gravitational acceleration, and P_{eq} (kg m^{-1} s^{-2}) is the equilibrium pressure of air in the tensiometer. The air volume (V_l) consists of the volume of the air pocket, the air chamber in the tensiometer, and the air bubbles (Fig. A1). The gauge storage in Eq. [3] does not account for the dissolution of air, and hence overestimates actual gauge storage. The effects of dissolution become significant as the ratio of the area of the air-water interface to the air volume increases; such as in small air bubbles. The volume of air bubbles in tensiometer-transducer systems, however, rarely exceeds 10-20 % of the total air volume. Therefore the dissolution effects can be neglected in the tensiometer response tests.

The shape factor for any type of porous cup can be determined from Eq. [1] by solving the steady-state flow equation with suitable boundary conditions to calculate Q. Assuming a homogeneous and isotropic soil of infinite extent, a porous cup is approximated by a spheroid of the same aspect ratio, $N = L/D$, and the surface area (Fig. A2). The shape factor for a spheroid is given by (Maasland, 1957; Randolph and Booker, 1982)

$$F = 4\pi b \frac{(N^2-1)^{1/2}}{N \ln[N + (N^2-1)^{1/2}]} \qquad [4]$$

where the half length of the spheroid, b (m), is related to the surface area, A (m^2) , and the aspect ratio of the spheroid by:

$$A = 2\pi b^2 \left\{ \frac{1}{N^2} + \frac{1}{(N^2-1)^{1/2}} \sin^{-1}\left[\frac{(N^2-1)^{1/2}}{N}\right] \right\} \qquad [5]$$

For a given aspect ratio, it is clear from Eqs. [4] and [5] that F is proportional to $A^{1/2}$; therefore we define a dimensionless shape factor, $F^* = F / A^{1/2}$.

To check the accuracy of the spheroid formula, Eq. [4], the dimensionless shape factor for several types of commonly used porous cups (Fig. A2) were determined by solving the steady-state flow equation for each type of porous cup using a finite element program Princeton UNSAT-2D developed by Celia et al. (1990). The distance from the porous cup to the boundary of the domain was set at 500 times the radius of the cup to approximate infinity. Note that the hydraulic conductivity was held constant in these simulations, even though the program was capable of using variable hydraulic conductivity. The numerical solutions show that the spheroid formula approximates F^* within 10 % of accuracy (Fig. A3).

The tensiometer response is controlled by the soil hydraulic conductivity only when the porous cup has a higher hydraulic conductivity than the soil (Klute and Gardner, 1962; Towner, 1980). A low conductivity porous cup causes a large potential drop within the porous cup wall, reduces the flow rate for a given Δh_T, and introduces negative bias in the estimated soil hydraulic conductivity. The influence of porous cup conductivity on flow rate is evaluated

numerically by solving the steady-state flow equation for the standard round bottom porous cup of $N = 2.5$ and $d/D = 0.125$. The simulated flow rate, Q, is normalized to the flow rate for the case without a porous cup wall, Q_0. The reduction in flow rate is minor when the porous-cup conductivity, K_{pc}, is higher than the soil conductivity, K_{soil}, or $K_{pc}/K_{soil} > 1$ (Fig. A4).

Linear theory with soil water storage

Equation [1] assumes that the soil has no moisture storage, but this assumption needs justification. In general, the water flow in soil around a cavity is described by a set of equations written for the total potential head in the cavity, h_{Tc}, and in the soil, h_T, (Cooper et al., 1967)

$$S_g \frac{dh_{Tc}}{dt} = \iint_{\partial W} K \nabla h_T \cdot \mathbf{n} dA \qquad [6]$$

$$C_w \frac{\partial h_T}{\partial t} = K \nabla^2 h_T \qquad [7]$$

where ∂W denotes the outer surface of porous cup, $\mathbf{n}$ denotes the outward unit normal vector, and C_w (m^{-1}) is the water capacity of the soil. Noting that the characteristic length of a spheroidal cavity is b, we define dimensionless variables and an operator;

$$t^* = Kt / C_w b^2 \qquad h_T^* = (h_T - h_{Teq}) / (h_{T0} - h_{Teq})$$
$$x^* = x / b \qquad y^* = y / b \qquad z^* = z / b \qquad \nabla^* = b \nabla \qquad [8]$$

and we can write the dimensionless form of Eqs. [6] and [7].

$$\frac{dh_{Tc}^*}{dt^*} = \frac{C_w b^3}{S_g} \iint_{\partial W} \nabla^* h_T^* \cdot \mathbf{n} dA^* \qquad [9]$$

$$\frac{\partial h_T^*}{\partial t^*} = \nabla^{*2} h_T^* \qquad [10]$$

Note that for a given shape of the cavity, the behavior of the solution in dimensionless form is completely determined by a dimensionless constant $C_w b^3/S_g$. For a spheroidal cavity in Fig. A2, using the identities of spheroidal coordinates (Stratton, 1941, p.53), it can be shown that the behavior of the dimensionless solution is completely determined by a dimensionless constant

$$\gamma = 4\pi C_w b^3 (N^2 - 1)^{1/2} / S_g N^3 \qquad [11]$$

which indicates the relative size of the soil water storage to the gauge storage. A similar dimensionless parameter, α_C, was used by Cooper et al. (1967, Eq. 7) in their analysis of two dimensional radial flow around a cylindrical cavity. For a large aspect ratio (e.g. $N > 3$), it can be shown that $\gamma = 2\alpha_C$.

To see the effects of soil water storage on the response curve, Eqs. [6] and [7] with a standard porous cup ($N = 2.5$) were numerically solved for different values of γ. The method described by Sudicky et al. (1995) was incorporated into UNSAT-2D to simulate the coupling between a porous cup and soil. In this method, the gauge storage is represented by storage in

line elements superimposed on triangular finite element grids, which is similar in spirit to a method developed by Narasimhan and Dreiss (1986). For commonly used tensiometers that have the air pocket volume of 1-10 cm^3, the expected range of γ is 0.001-10. The effects of soil water storage becomes significant for large γ, and the response curve deviates from the straight line on a semi-log graph (Fig. A5). It is a routine practice in interpretation of piezometer slug tests to fit a straight line to the observed data and calculate the soil conductivity from the slope of the line. However, the fit is nonunique when the data has large curvature. Noting that all curves intersect the straight line at points near $h_T^* = 0.1$, the best estimate of conductivity is obtained by fitting a line to a portion of response curves between $h_T^* = 1.0$ and 0.1. With this procedure the error due to nonunique fit is less than 20-30 %. The numerical solutions also show, though not presented here, that the same method is applicable to porous cups that have $N = 10$.

The analysis presented in this section is applicable to both tensiometer response tests and conventional piezometer slug tests. For a piezometer with a stand pipe manometer to measure the total potential head, the dimensionless parameters are defined as

$$t^* = Kt / S_s b^2 \qquad \gamma = 4S_s b^3 (N^2 - 1)^{1/2} / r_c^2 N^3 \qquad [12]$$

where S_s (m^{-1}) is the specific storage of the saturated soil, and r_c (m) is the radius of the manometer.

Non-linear theory

The theory that has been presented so far assumes constant K, i.e. linear flow equations. Taking into account the dependence of hydraulic conductivity and water capacity on matric potential, the nonlinear flow equation is written as

$$C_w(h)\frac{\partial h_T}{\partial t} = K(h)\nabla^2 h_T \qquad [13]$$

where h (m) is the matric potential head; $h_T = h + z$, where z (m) is the elevation. To justify the linear flow assumption, Eqs. [6] and [13] were numerically solved and compared with the linear flow solution for which K and C_w were fixed at the equilibrium value.

In the numerical simulations, the soil water retention function of van Genuchten (1980) with the following parameters was used to represent a clay loam soil used in our laboratory experiments; $\theta_{sat} = 0.46$, $\theta_{res} = 0.03$, $\alpha = 0.6\ m^{-1}$, $n = 1.4$, $m = 1\text{-}1/n$. The size of the total potential head change was 0.5 m, while the equilibrium value of matric potential head was -1.5 m. The solution for the nonlinear equation was indistinguishable from the solution for linear equation in this setting (Fig. A6). Similar results were obtained for simulations with a wide range of matric potential head, as long as the pressure change was small. Therefore, the linear flow assumption is justified for a small pressure change.

MATERIALS AND METHODS

Tensiometer

Two types of tensiometers were used in this study. The first type is a commonly used design (Marthaler et al., 1983), made of a standard 1-bar porous ceramic cup, PVC pipe, acrylic tube, and a rubber septum stopper. The second one has a porous stainless steel cup. Specifications for porous cups are listed in Table A1. The saturated hydraulic conductivity of porous cups were measured by a standard falling head test. The range of applicability of the tensiometer response test is determined by the conductivity and bubbling pressure of porous cups. High-flow 1-bar porous ceramic cups are available from the manufacturers listed in Table A1, though were not used in this study.

Laboratory methods

The laboratory experiments were conducted using a clay-loam soil sampled from the St. Denis National Wildlife Area located 50 km east of Saskatoon, Saskatchewan, Canada. The Dark Brown Chernozemic soils in the area are mapped within the Weyburn Association, W2 map unit (Miller et al., 1985). The soil from A horizon was air dried and packed in a 20-L plastic pail to a bulk density of 1500 kg m^{-3}. The pail was perforated with 2-cm diameter holes on the side and the bottom to allow free evaporation of water. A tensiometer with a porous stainless steel cup (steel cup tensiometer) was installed near the center of the pail while the soil was being packed (Fig. A7). Soil was saturated with 0.005 M $CaSO_4$ solution by submerging the pail in a larger plastic tub. The soil was gravity drained once and a ceramic cup (A in Table A1) tensiometer was installed near the center by predrilling an access hole that had a slightly larger diameter than the porous cup and inserting it with slurry made from the soil; the method commonly used to install field tensiometers (Cassell and Klute, 1986). The soil was saturated again for several days before the experiment started. The soil moisture content was measured by weighing the entire apparatus.

The average saturated hydraulic conductivity of the soil was determined by applying a constant hydraulic head in one of the tensiometers (injection port), while keeping the pail submerged in the plastic tub with the water level slightly higher than the soil surface. The other tensiometer was used as the observation port. The conductivity was calculated from the flow rate at the injection port and the gradient between the observation port and the boundary of the pail assuming spherical symmetry of the flow around the injection port.

The soil was progressively dried to several different stages of moisture content. At each stage the pail was sealed by plastic wrap and left for several days to attain equilibrium and even distribution of moisture content and matric potential.

Additional set of experiments were conducted using a loam soil sampled from the campus of University of Guelph, Guelph, Ontario, Canada. In these experiments a porous ceramic cup

tensiometer, instead of a stainless cup tensiometer, was installed while soil was being packed, and another ceramic cup tensiometer was installed after soil was saturated and gravity drained by the access hole method. The former tensiometer is called "reference tensiometer", and the latter is called "installed tensiometer". The purpose of these additional experiments was to examine the effects of the soil damage caused during the installation of a standard tensiometer. However the porous ceramic cups used in these experiments (B in Table A1) had the saturated hydraulic conductivity considerably lower than those used in the main experiments (A in Table A1), and the unsaturated hydraulic conductivity of the soil became lower than the porous cup conductivity only in the low matric potential head range (h < -3.0 m). Therefore the quantitative interpretation of the data from these experiments was not possible, and the results will be mentioned only briefly.

Tensiometer response test

The pressure in the air pocket was measured continuously by a vibrating wire transducer (Geokon, 4500ALV-5) and data logger (Campbell Scientific, CR10) system. The pressure change, generally 3-5 kPa (0.3-0.5 m in head unit), was introduced by opening a valve that connected the tensiometer-transducer system to a plastic syringe (Fig. A1), and immediately closing it. The volume of air in the system (V_1) was calculated from the pressure (P_{syr}) and volume (V_{syr}) of air in the syringe, and the pressure in the air pocket before (P_{eq}) and after (P_0) the valve was open:

$$V_1 = V_{syr}(P_{syr} - P_0)/(P_0 - P_{eq}) \qquad [14]$$

The response time of the tensiometer is shorter for a smaller gauge storage, i.e. smaller V_1 (see Eq. [3]). Therefore, the membrane chamber in the transducer was filled with machine tool oil to reduce the chamber volume from 4 cm^3 to less than 1 cm^3. Knowing the volume of the air pocket and the membrane chamber in the transducer, the total volume of air bubbles in the tensiometer can be calculated from Eq. [14]. The calculated volume of the air bubbles was less than 10-20 % of V_1 for most field and laboratry tests.

The soil hydraulic conductivity was estimated by plotting the dimensionless total potential head versus time on a semi-log graph and fitting a straight line to the curve as described in the theory section. For the standard round-bottom porous ceramic cups used in these experiments, the shape factor is $F = 0.23$ m.

Field methods

Seven ceramic cup (A in Table A1) tensiometers, ranging in depths from 0.2 to 2.0 m, were installed in the St. Denis site by the access hole method in June 1994. A nest of time domain reflectometry (TDR) probes, each 20 cm long and ranging in depths from 0.1 to 2.1 m, were installed within one meter of the tensiometers to measure the soil moisture content (Topp et al.,

1980). The detailed description of installation is found in Chapter 2. The tensiometers and TDR probes were monitored throughout the summer and fall of 1994 at one-week interval. From this data the relationship between the soil moisture content and matric potential was obtained.

The response tests were conducted once in October 1994 for all seven of them, and once again in July 1995 for six of them that survived the freezing conditions over winter. The change in ambient temperature during the experiments affected the pressure in the tensiometer. Therefore, tensiometers and transducers were wrapped with a blanket and sheltered from the sun and wind by a cardboard box to minimize temperature changes. For slow-responding tensiometers, a hand-held pressure transducer (Soil Measurement Systems, SW-030), which had a chamber volume of less than 0.1 cm^3, was used to reduce the response time, and the reading was taken manually at suitable time intervals.

RESULTS AND DISCUSSION

Laboratory experiments

A pair of response tests were conducted at each matric potential using positive and negative pressure changes. The negative change was introduced to the system by setting P_{syr} below equilibrium pressure. The positive pressure change causes the flow from the porous cup to the soil (imbibition), while the negative pressure change causes the opposite flow (drainage). If nonlinear or hysteritic flow effects are significant, the tensiometer responses to the positive and negative pressure change will be significantly different.

Measured responses to the positive and negative pressure changes were almost linear on semi-log graph and indistinguishable from each other for all pairs of tests. An example is shown in Fig. A8 for the case of the positive (Δh_T = +0.34 m) and negative (Δh_T = -0.35 m) pressure changes when h = -1.55 m at the porous cup. Therefore, nonlinear or hysteretic flow effects were insignificant for a small pressure change, consistent with the results of numerical simulation. The straight line method to calculate hydraulic conductivity was easily applicable in the laboratory experiments, because all semi-log plots had little curvature.

The soil moisture content decreased with the soil matric potential head (Fig. A9). The van Genuchten (1980) equation was used to represent a water retention function, for which parameter values are shown on the graph. Soil hydraulic conductivity decreased exponentially with matric potential head (Fig. A10), similar to the trend predicted by the van Genuchten equation. In this set of experiments only the drainage curve was obtained. However, a imbibition curve can be obtained with the same ease if suitable instruments are used to allow monotonic increase of water content in the pail.

The hydraulic conductivity of the porous ceramic was much lower than the saturated conductivity of the soil (1.1×10^{-7} m s^{-1}); therefore, the conductivity estimated from the

ceramic tensiometer response tests should be lower than the actual soil conductivity in the high matric potential range.

In the intermediate matric potential range, the conductivity measured by the steel cup tensiometer was consistently lower than those measured by the ceramic cup tensiometer. As pointed out in the introduction to this paper, the measured conductivity is most sensitive to the soil directly in contact with the porous cup. If the soil is disturbed around a porous cup to a given thickness, the effect of such disturbance will be more pronounced for a small cup than for a large cup. Therefore, the stainless cup tensiometer that has small diameter is more susceptible to disturbance effects than the ceramic cup tensiometer. It is likely that the lower hydraulic conductivity measured by the steel cup tensiometer is due to such effects. The disturbance may have been caused mechanically during the installation or chemically during the measurement of saturated hydraulic conductivity when a large quantity (100 cm^3) of deionized water was injected.

In a separate set of experiments using the Guelph loam, the soil hydraulic conductivity measured with the installed ceramic cup tensiometer was 40-50 % lower than that measured with the reference tensiometer. The magnitude of errors in the tensiometer response tests due to the disturbance effects is expected to be less than 100 %.

In most of the laboratory tests, the semi-log plots of tensiometer response had smaller curvature (Fig. A8) compared to the results of numerical simulations using the hydraulic parameters for the tested soil (Fig. A6). The curvature is related to the ratio of the gauge storage (S_g) to the soil water capacity (C_w) by Eq. [11]. To investigate the influence of S_g on the curvature, a set of response tests with high (9.3×10^{-7} m^2) and low (1.1×10^{-7} m^2) values of S_g were conducted for the St. Denis soil using the ceramic cup tensiometer. The soil matric potential head was -2.8 m, at which the water retention function (Fig. A9) gave $C_w = 0.03$ m^{-1}. The size of pressure change in head unit was +0.76 m in the low S_g test, while positive (+0.34 m) and negative (-0.50 m) changes were applied in the high S_g tests. The linear flow equation in a numerical domain that had the same dimension and hydraulic conductivity (2.7×10^{-9} m s^{-1}) as the actual soil in the pail was solved to compare the observed response to the theoretical one.

The observed response had significantly smaller curvature compared to the simulated response with $C_w = 0.03$ m^{-1} (Fig. A11). The best match between the observed and simulated responses was obtained when $C_w = 0.0006$ m^{-1} was used; two orders of magnitude smaller than the value expected for the soil. This value was insensitive to the direction of flow and the gauge storage. Note that the "tail" of the response curves for the high S_g case became flat near the end of the test (Fig. A11b), because the pressure response reached the wall of the pail.

Hyder and Butler (1995, Fig. 8) reported the similar small curvature in numerically simulated piezometer response tests, which was caused by a layer of low conductivity around the screen with a large aspect ratio ($N = 25$). However, our numerical simulations that

incorporated a layer of low conductivity soil around the standard porous cup ($N = 2.5$) indicated that the large difference between predicted and observed C_w (Fig. A11) could not be explained by the effects of low conductivity soil alone. Therefore the water capacity under transient flow conditions may be different from the value based on measurement under static conditions. A similar observation was made by Rogers and Klute (1971) for one dimensional flow in repacked sand.

Field experiments

The relationship between matric potential head and moisture content at the field site had a range of variation, reflecting the heterogeneity of the soil and perhaps soil water hysteresis (Fig. A12). A set of parameters for the van Genuchten function was selected by inspection to represent the trend of the field moisture retention characteristic (Fig. A12), for which the values are shown on the graph.

The field results for seven tensiometers are presented for three depth intervals (Fig. A13). For those measured twice, in October 1994 and July 1995, the two measurements are connected by a solid line in the graph. The hydraulic conductivity generally decreased with soil matric potential, which was consistent with the prediction by the van Genuchten function shown as dashed curves. However, several tensiometers showed a slight increase in the hydraulic conductivity as matric potential decreased; in reverse to the prediction by the van Genuchten function. The moisture content corresponding to those tensiometers decreased with matric potential. Therefore, the reverse trend cannot be explained by soil water hysteresis. It is likely that freezing and thawing in winter had caused some change in the soil structure around porous cups, which resulted in the unpredictable trend in hydraulic conductivity.

CONCLUSIONS

The theoretical study of the tensiometer response test showed that the hydraulic conductivity of unsaturated soil can be determined easily by a curve fitting procedure. The laboratory study showed that the measurement error due to the disturbance of soil around the porous cup was in order of 50-100 % for a commonly used tensiometer. A single measurement typically took several minutes to hours. The method gives a reasonably good estimate of hydraulic conductivity in short time, and can be repeated in a field season to study the relationship between the conductivity and soil matric potential; therefore, it is attractive in clay-rich soil where existing methods are not applicable.

References

Buckingham, E., 1907. Studies on the movement of soil moisture. Bulletin 38. U. S. Department of Agriculture Bureau of Soils, Washington, DC.

Cassell, D.K. and Klute, A., 1986. Water potential: Tensiometry. In: Methods of soil analysis, Part I. Physical and mineralogical methods - Agronomy Monograph no.9., 2nd ed., Soil Sci. Soc. Am., 563-596.

Celia, M.A., Bouloutas, E.T. and Zarba, R.L., 1990. A general mass-conservative numerical solution for the unsaturated flow equation. Water Resour. Res., 26, 1483-1496.

Cooper, H.H., Jr., Bredehoeft, J.D. and Papadopulos, I.S., 1967. Response of a finite-diameter well to an instantaneous charge of water. Water Resour. Res., 3, 263-269.

d'Astous, A.Y., Ruland, W.W., Bruce, J.R.G., Cherry, J.A. and Gillham, R.W., 1989. Fracture effects in the shallow groundwater zone in weathered Sarnia-area clay. Can. Geotech. J., 26, 43-56.

Gardner, W.R., 1960. Measurement of capillary conductivity and diffusivity with a tensiometer. Trans. 7th Intern. Congr. Soil Sci., Madison, Wisconsin, 300-305.

Green, R.E., Ahuja, L.R. and Chong, S.K., 1986. Hydraulic conductivity, diffusivity, and sorptivity of unsaturated soils: Field methods. In: Methods of soil analysis, Part I. Physical and mineralogical methods - Agronomy Monograph no.9., 2nd ed., Soil Sci. Soc. Am., 771-798.

Gribb, M.M., 1996. Parameter estimation for determining hydraulic properties of a fine sand from transient flow measurements. Water Resour. Res., 32, 1965-1974.

Hvorslev, M.J., 1951. Time lag and soil permeability in ground-water observations. Corps of Engineers, U.S. Army, Waterways Experiment Station, Bull. No.36. 50pp

Hyder, Z. and Butler, Jr. J.J., 1995. Slug tests in unconfined formations: An assessment of the Bouwer and Rice technique. Ground Water, 33, 16-22.

Klute, A. and Gardner, W.R., 1962. Tensiometer response time. Soil Sci., 93, 204-207.

Maasland, M., 1957. Soil anisotropy and land drainage. In: Drainage of agricultural lands, Ed. Luthin, J.N., Agronomy Monograph, 7, Am. Soc. Agr., 216-285.

Marthaler, H.P., Vogelsanger, W., Richard, F. and Wierenga, P.J., 1983. A pressure transducer for field tensiometers. Soil Sci. Soc. Am. J., 47, 624-627.

Miller, J.J., Acton, D.F. and Arnaud, R.J.ST., 1985. The effect of groundwater on soil formation in a morainal landscape in Saskatchewan. Can. J. Soil Sci., 65, 293-307.

Narasimhan, T.N. and Dreiss, S.J., 1986. A numerical technique for modeling transient flow of water to a soil water sampler. Soil Sci., 141, 230-236.

Randolph, M.F. and Booker, J.R., 1982. Analysis of seepage into a cylindrical permeameter. Proc., 4th International Conference on Numerical Methods in Geomechanics, Edmondon, vol.1, 349-357.

Richards, L.A., Russell, M.B. and Neal, O.R., 1937. Further developments on apparatus for field moisture studies. Soil Sci. Soc. Am. Proc., 2, 55-64.

Rogers, J.S. and Klute, A., 1971. The hydraulic conductivity-water content relationship during nonsteady flow through a sand column. Soil Sci. Soc. Am. Proc., 35, 695-700.

Stratton, J.A., 1941. Electromagnetic theory. McGraw-Hill, New York, 615pp.

Sudicky, E.A., Unger, A.J.A. and Lacombe, S., 1995. A noniterative technique for the direct implementation of well bore boundary conditions in three-dimensional heterogeneous formations. Water Resour. Res., 31, 411-415.

Tokunaga, T., 1992. The pressure response of the soil water sampler and possibilities for simultaneous soil solution sampling and tensiometry. Soil Sci., 154, 171-183.

Topp, G.C., Davis, J.L. and Annan, A.P., 1980. Electromagnetic determination of soil water content: measurements in coaxial transmission lines. Water Resour. Res., 16, 574-582.

Towner, G.D., 1980. Theory of time response of tensiometers. J. Soil Sci., 31, 607-612.

van Genuchten, M.Th., 1980. A closed-form equation for predicting the hydraulic conductivity of unsaturated soils. Soil Sci. Soc. Am. J., 44, 892-898.

Table A1 Specification of porous cups.

	Stailness steel cup	Ceramic cup (A)	Ceramic cup (B)
Manufacturer	Mott Metallurigical	Soil Measurement Systems	Soilmoisture Equipment
Model	0.5 μ grade (1400-250-125-6-0.5)	1 bar standard (SP-031)	1 bar standard (655X01-B1M1)
Length	0.045 m	0.057 m	0.057 m
Inner diameter	0.00288 m	0.0164 m	0.0164 m
Outer diameter	0.00639 m	0.023 m	0.023 m
Saturated K	8.8×10^{-7} m s^{-1}	2.3×10^{-8} m s^{-1}	4.3×10^{-9} m s^{-1}
Bubbling pressure	29 kPa	100 kPa	100 kPa

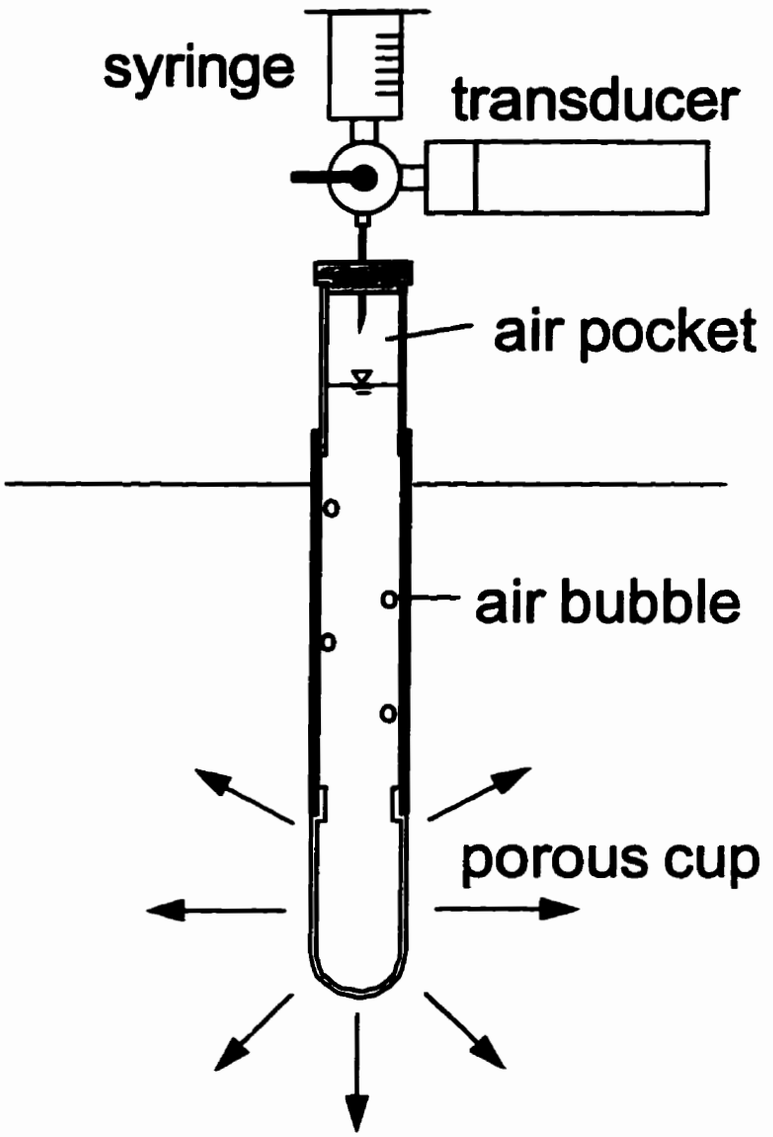

Fig. A1 Schematic diagram of the tensiometer response test apparatus.

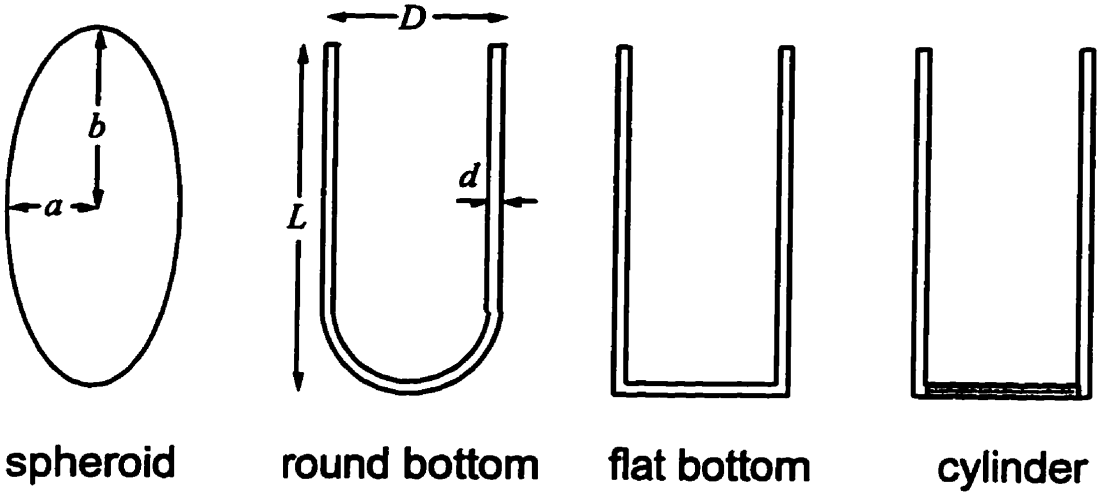

Fig. A2 Geometry of commonly used porous cups and the equivalent spheroid. The aspect ratio, $N = b/a$, of the spheroid is equal to L/D of the porous cup. The cylinder-type cup has a sealed bottom.

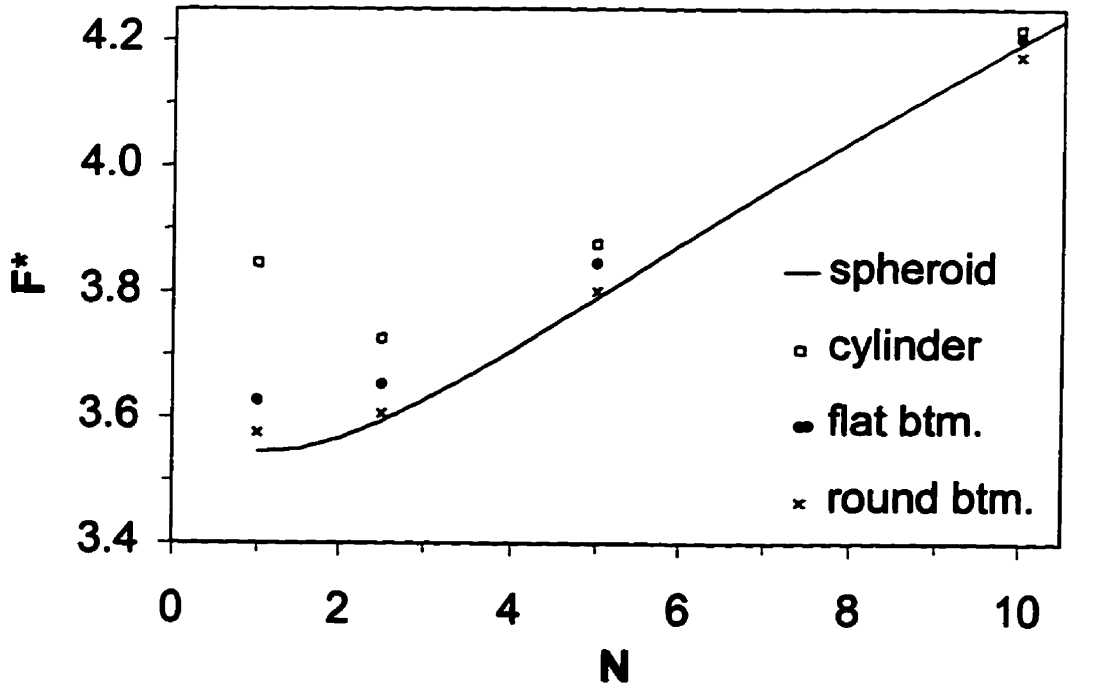

Fig. A3 Normalized shape factor versus aspect ratio for three types of porous cups.

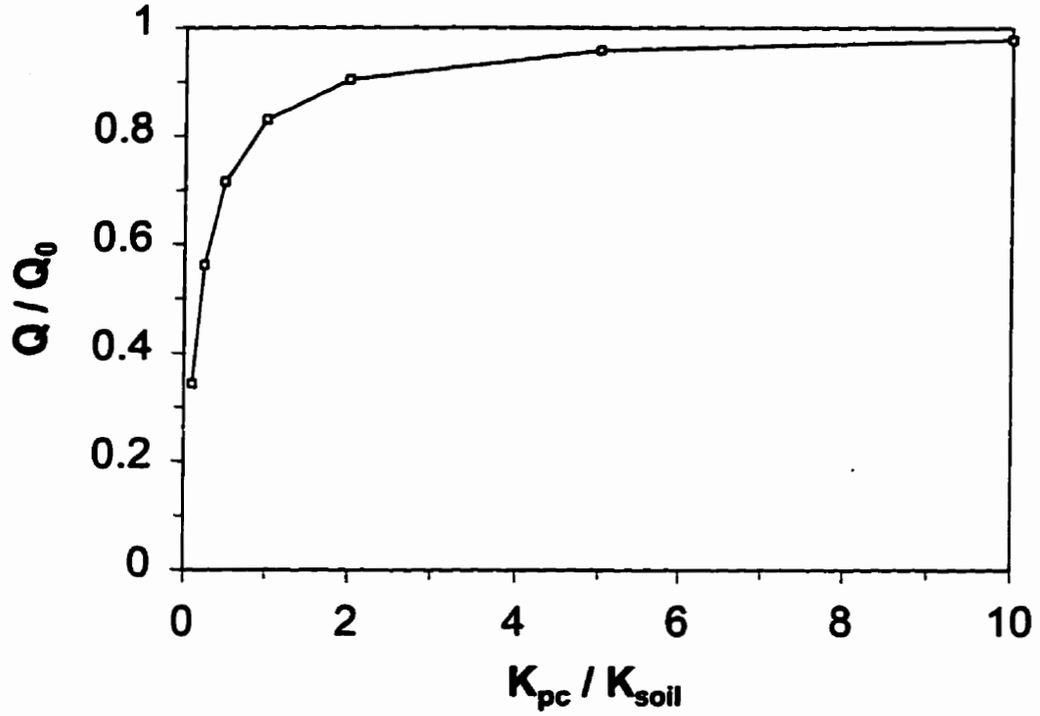

Fig. A4 Reduction in flow rate due to the head loss across the porous cup wall.

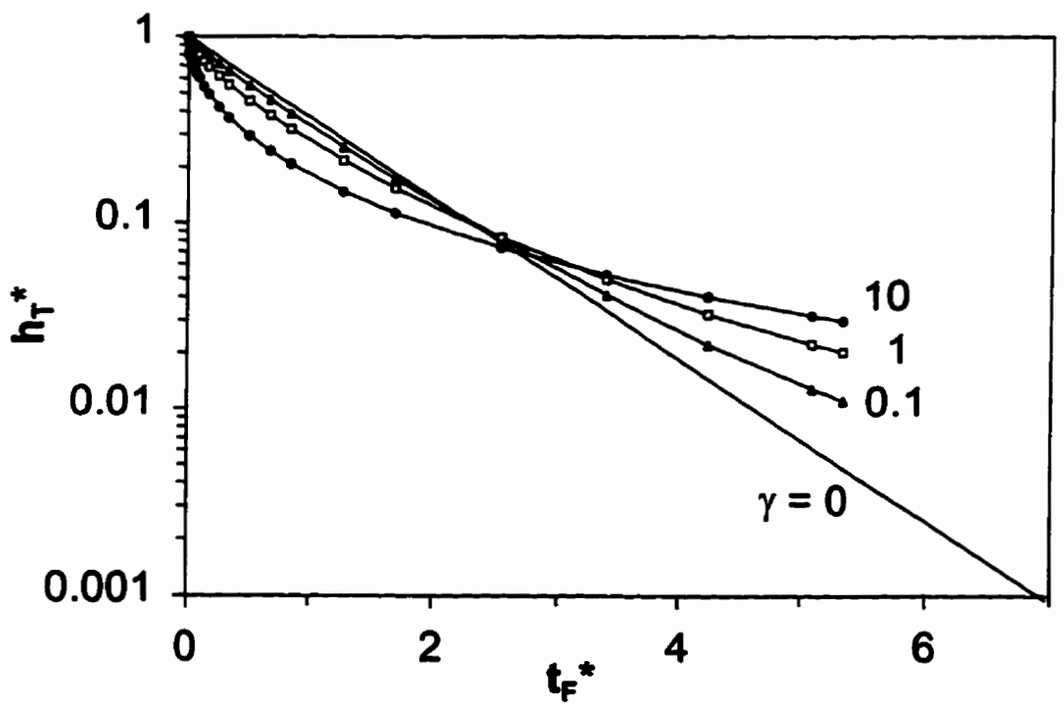

Fig. A5 Effects of soil moisture storage on head response during slug tests. The dimensionless time on the abscissa is defined by $t_F^* = tKF/S_s$.

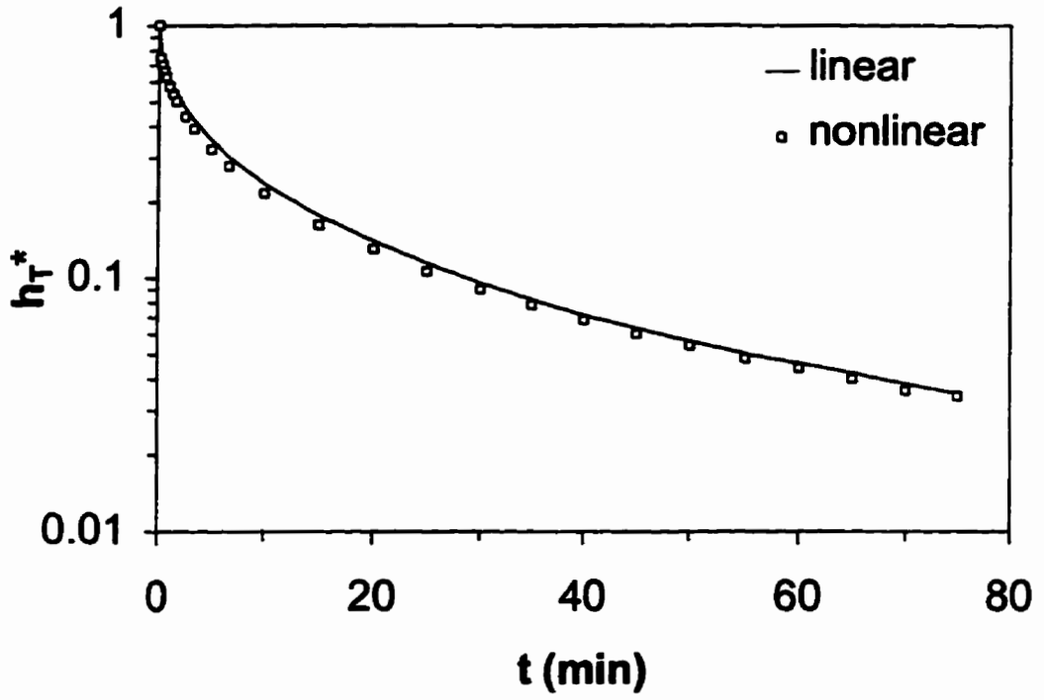

Fig. A6 Comparison of numerical solutions of linear and nonlinear flow equations. The matric potential head at the porous cup is -1.5 m, and the initial pressure change in head unit is 0.5 m.

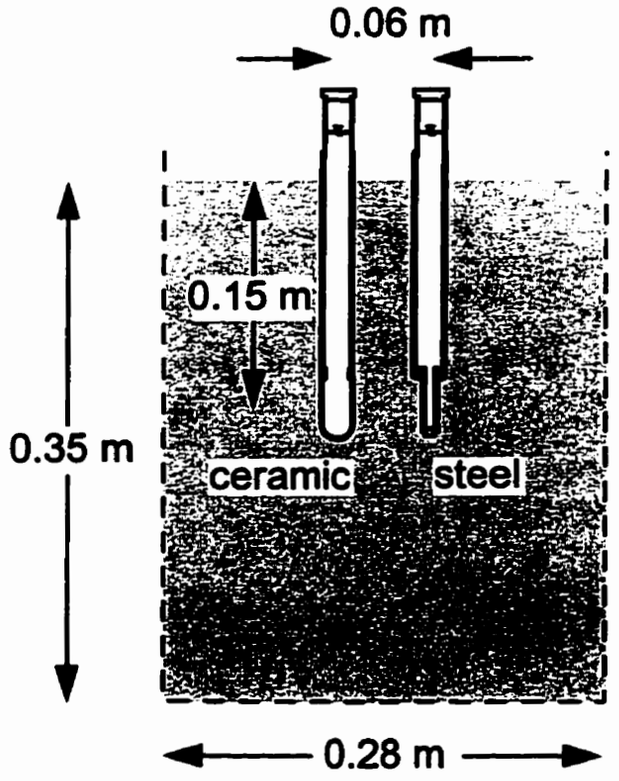

Fig. A7 Diagram of the laboratory experiments.

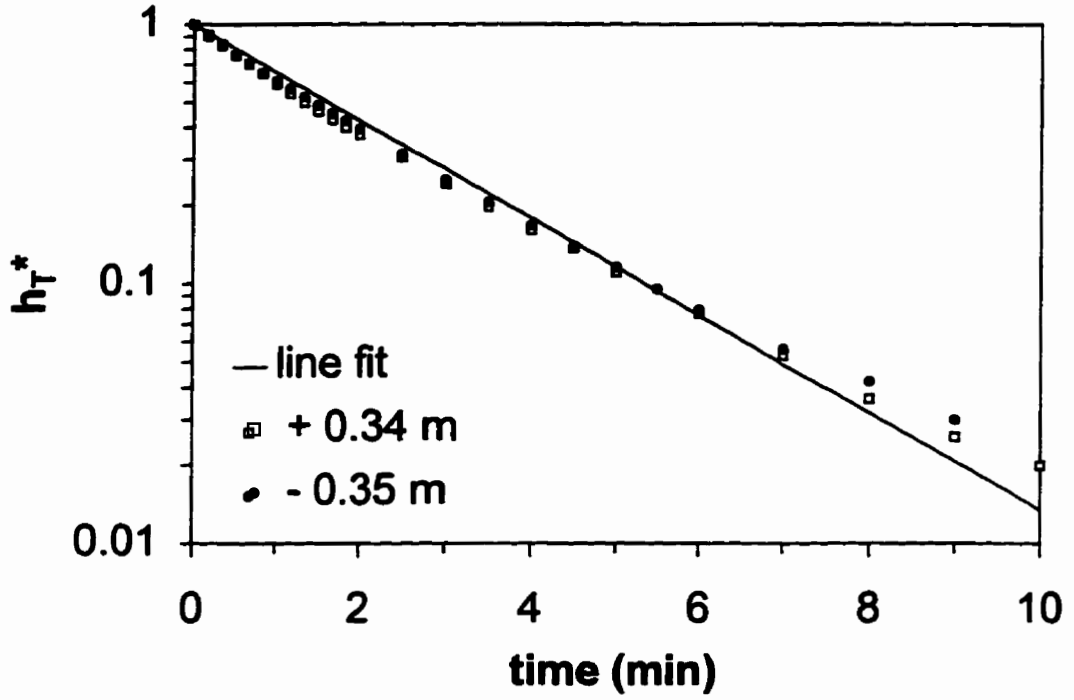

Fig. A8 Tensiometer response in two laboratory tests. Water flow direction was reversed between the two tests.

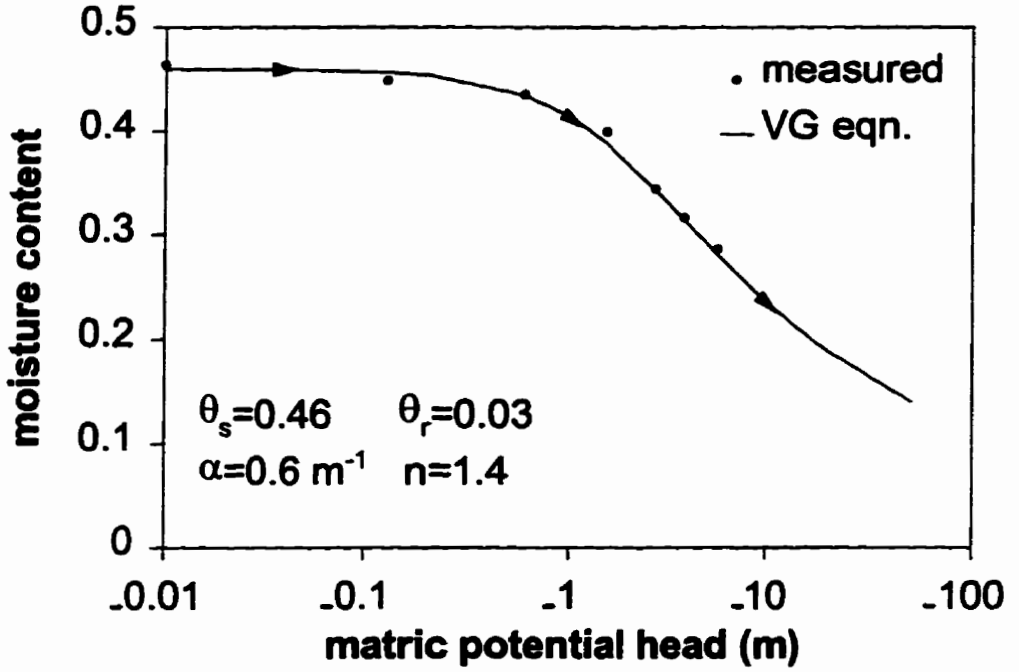

Fig. A9 Moisture retention curve for the soil used in the laboratory experiments. The values of the van Genuchten parameters are listed on the graph.

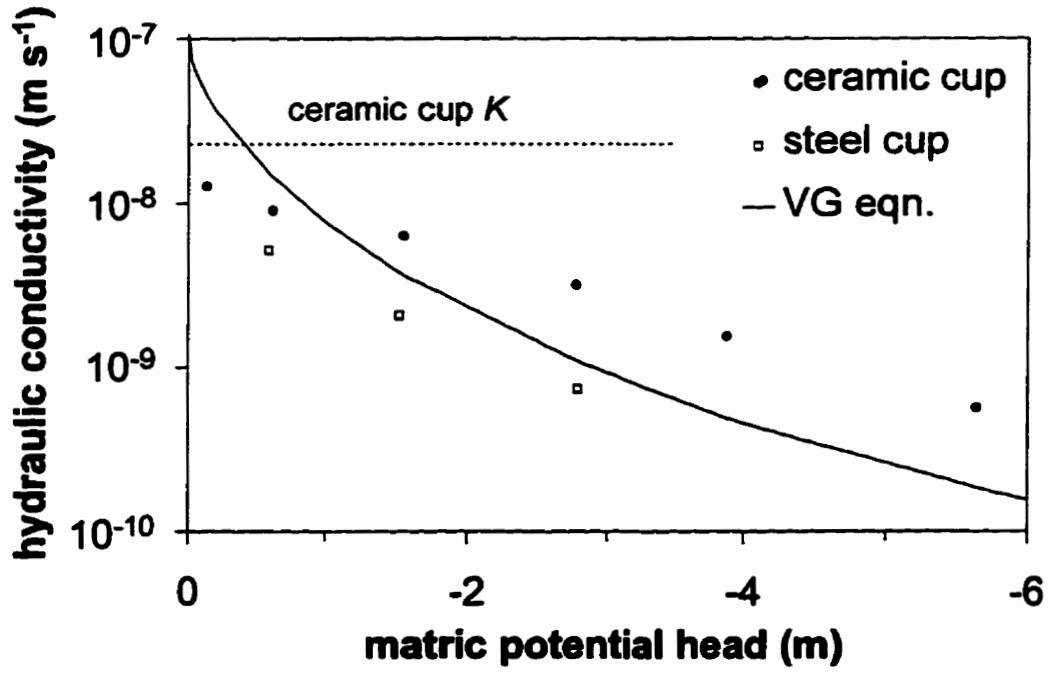

Fig. A10 Relationship between measured hydraulic conductivity and matric potential head. The solid curve shows the values predicted by the van Genuchten equation with the parameters listed in Fig. A9. The hydraulic conductivity of the steel cup is 10^{-6} m s^{-1} (not shown in the graph).

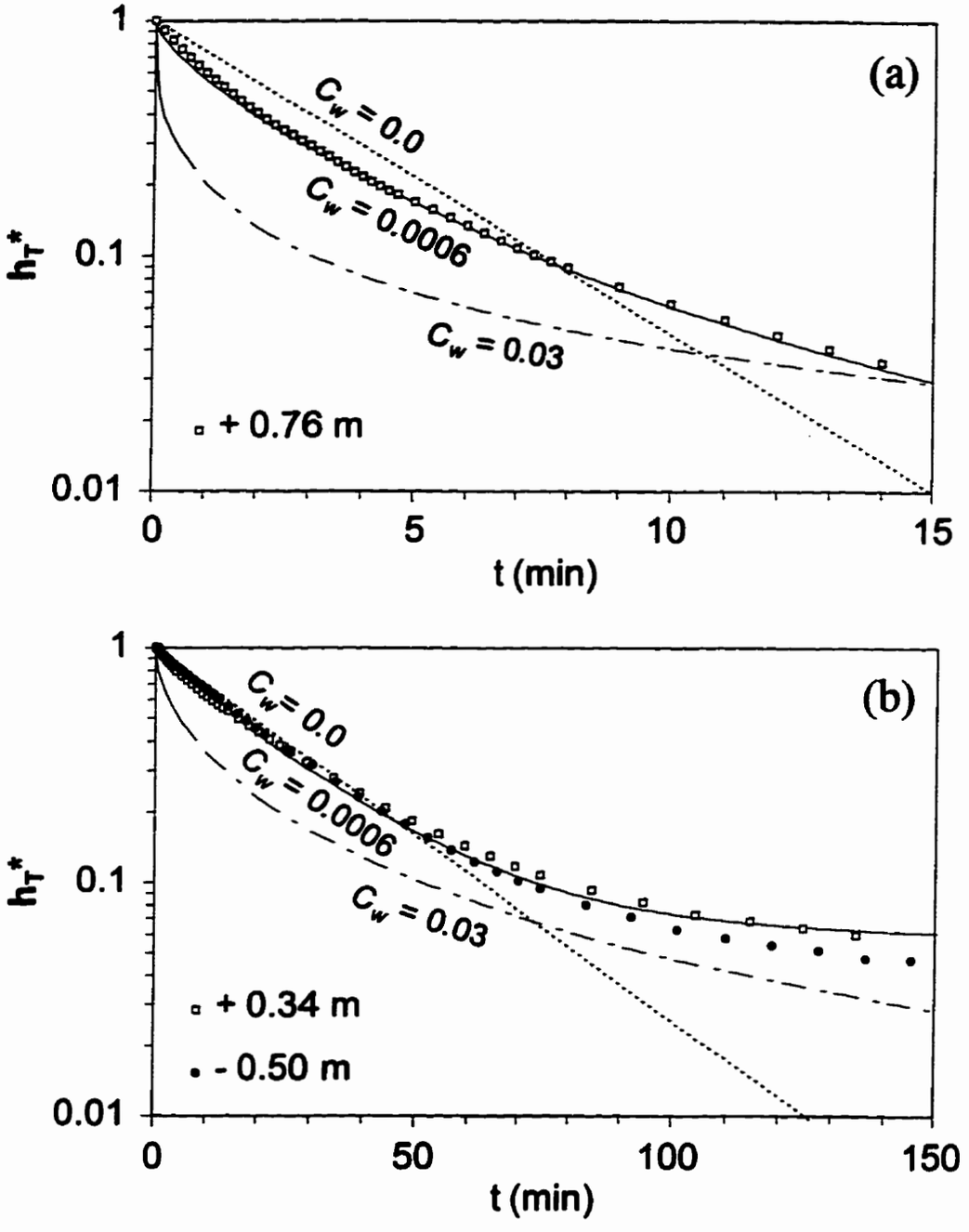

Fig. A11 Measured and simulated head response. (a) low gauge storage case using a positive pressure change. (b) high gauge storage case using both positive and negative pressure changes. The circles and squares show the measured response, while curves show the simulated response. The unit of the soil water capacity (C_w) is m^{-1}.

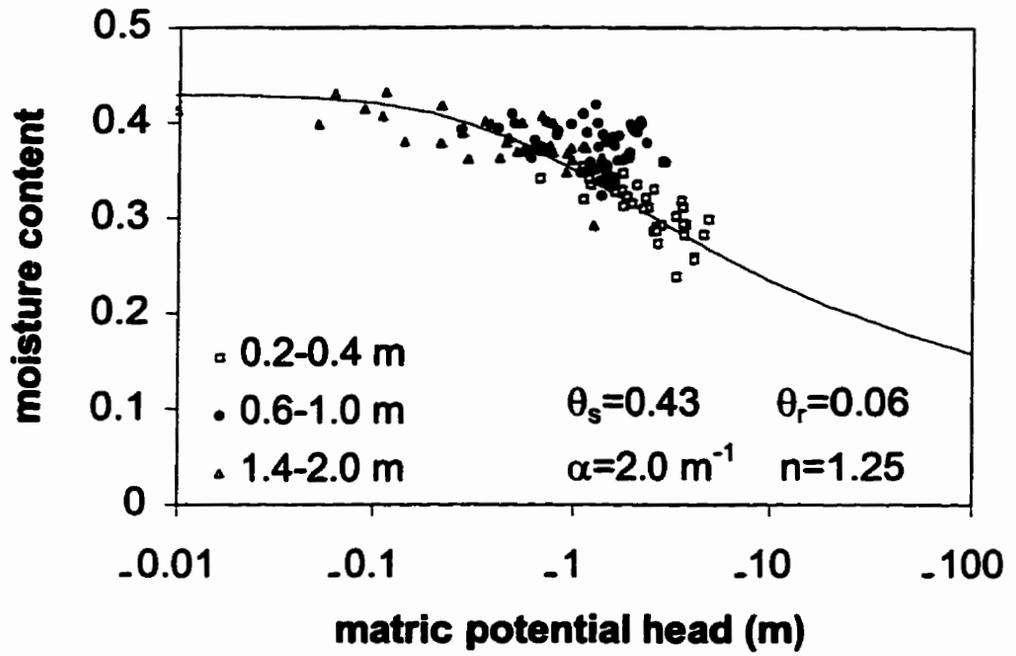

Fig. A12 The relationship between matric potential head and moisture content. The values of van Genuchten parameters are shown on the graph.

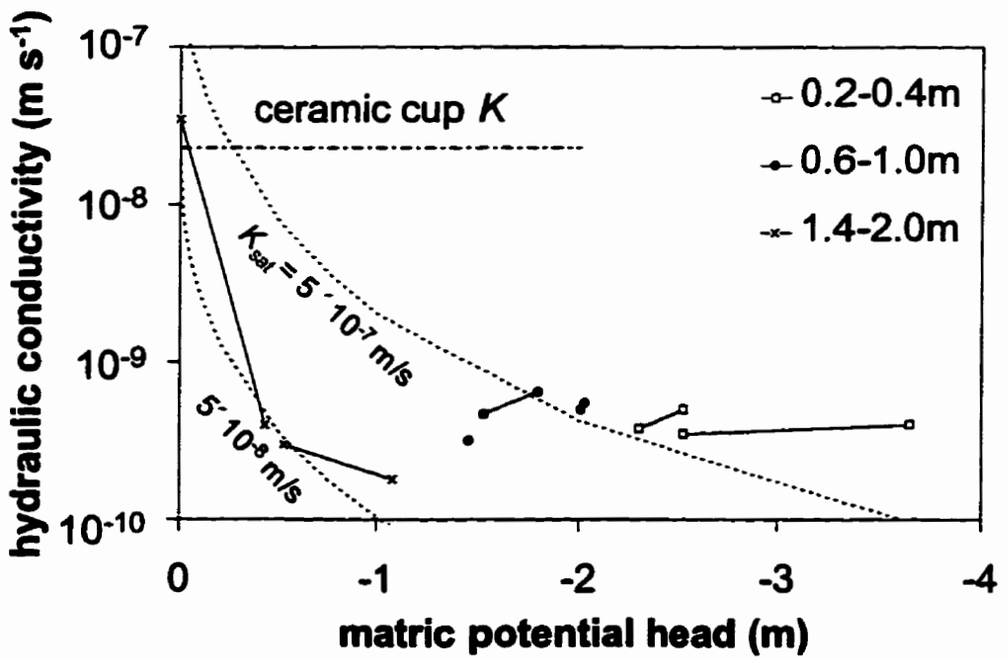

Fig. A13 Relationship between estimated hydraulic conductivity and matric potential head measured by field tensiometers. The dashed curves show the values predicted by the van Genuchten equation with the parameters listed in Fig. A12.

Appendix B

Detailed information on piezometers and wells

Locations and detailed information on piezometers and wells are listed in this appendix. The piezometer and well location are shown in Figures B1, B2, and B3, while the location numbers in those figures are referenced to the identification numbers in Table B1. The identification numbers are found in metal plates attached to each piezometer or well.

Table B1 contains; location number, identification number, depth from the ground surface to the centre of the sand pack, length of the casing, height of the casing above the ground surface, inside diameter of the casing, diameter of the bore hole, length of the screen, length of the sand pack, elevation (above mean sea level) of the top of the casing, saturated hydraulic conductivity estimated from the basic time lag, and basic time lag. The units of entries are in meters, unless otherwise stated.

Asterisks on the top-of-casing elevation indicate that the elevation changes due to freezing and thawing actions, and that the value was surveyed in the fall of 1994. Water table monitoring wells (wtmw) have sand packs extending from the bottom of the bore hole to the ground surface, and hence it is meaningless to assign specific values to mean depth, screen length, sand pack length, and basic time lag for the wells. The casing of stilling wells (sw) is sealed in the bottom, and perforated above the ground surface to allow hydraulic connection between the wells and the pond water.

The diameter of the bore holes listed here is equal to the diameter of augers used in the drilling. The effective diameter of the sand pack used in the calculation of the saturated hydraulic conductivity is slightly smaller than the listed values. For example, $d = 0.14$ m is used to represent the effective diameter of 0.15-m bore holes.

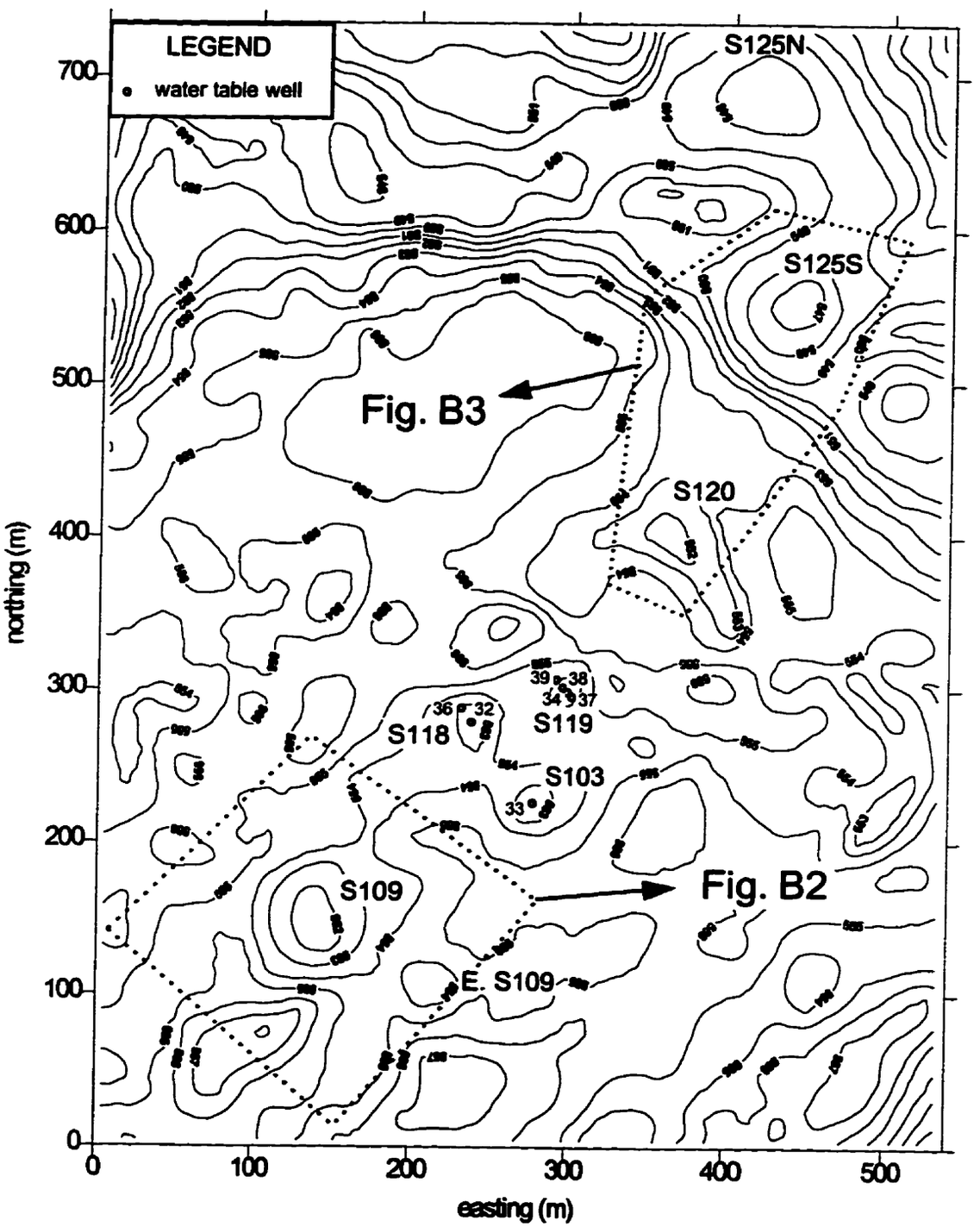

Fig. B1 Topographic map of the St. Denis site showing the location of wetlands. The water table monitoring wells that are shown in Figures B2 and B3 are indicated in this map.

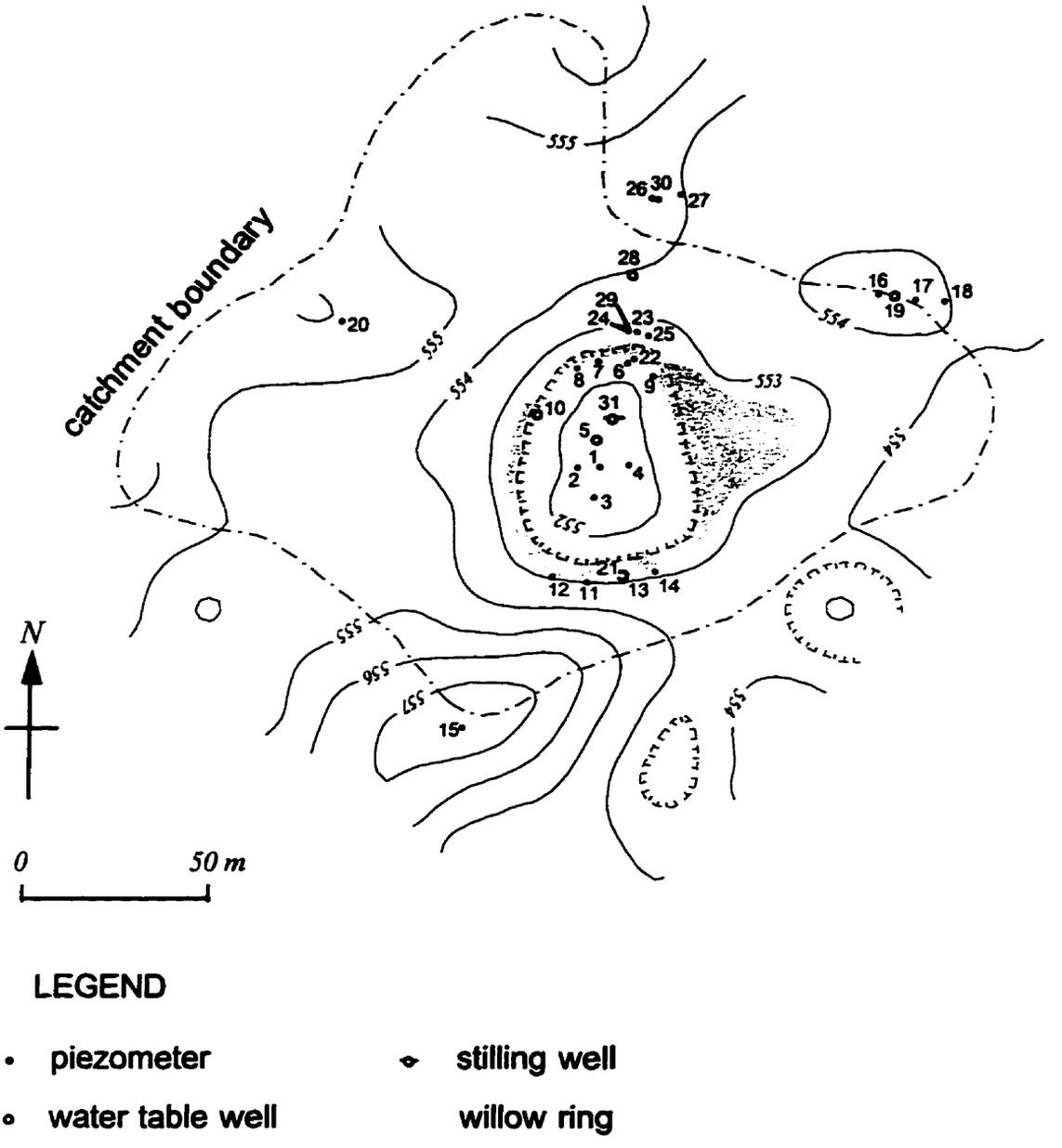

Fig. B2 Topographic map of S109 showing the location of piezometers and wells.

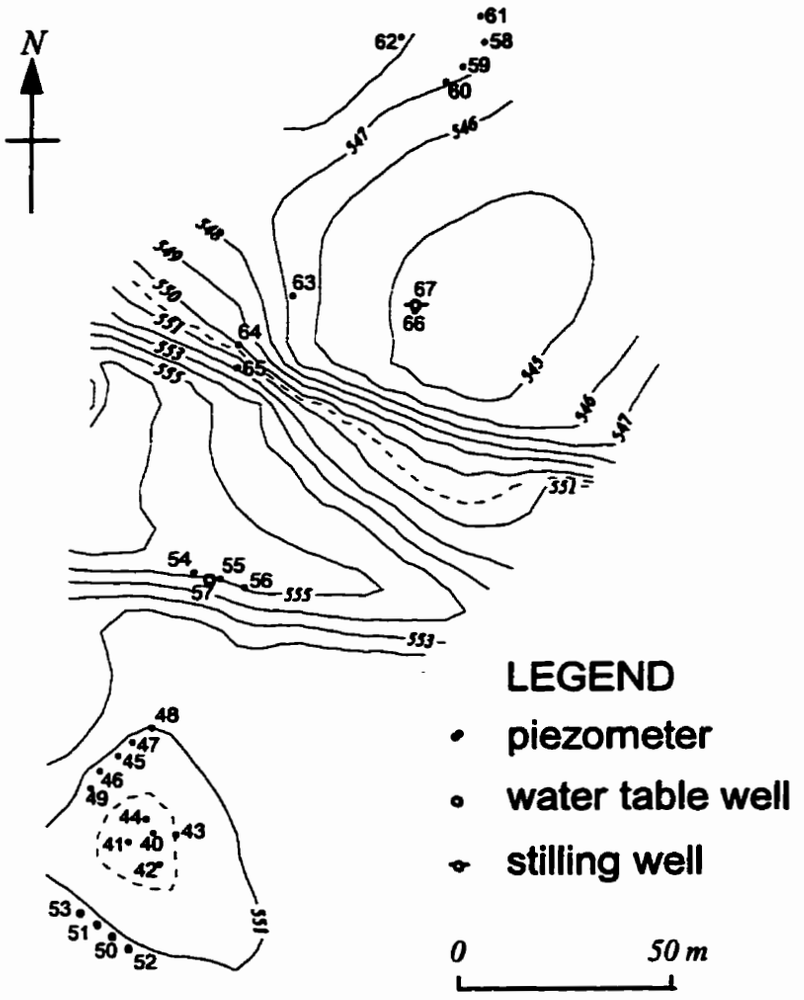

Fig. B3 Topographic map of S120 and S125S showing the location of piezometers and wells.

Table B1 Detailed information on piezometers and wells.

Loc.	ID	Mean depth	Casing length	Casing stick-up	Casing diam	Bore hole diameter	Screen length	Sand pack length	Top of casing elevation	K-sat (m/s)	Basic time lag (hr)
1	801P1	5.0	7.29	1.67	0.032	0.15	0.46	1.17	553.454	1.6e-06	0.05
2	801P2	3.1	5.20	1.65	0.032	0.15	0.40	0.96	553.366*	1.4e-08	6.01
3	801P3	2.4	4.31	1.59	0.032	0.15	0.38	0.69	553.445*	1.8e-07	0.57
4	801P4	1.7	3.42	1.33	0.032	0.15	0.43	0.73	553.277*	1.8e-07	0.55
6	802P1	6.7	8.67	1.06	0.032	0.15	0.40	1.86	553.300	2.7e-09	36
7	802P2	5.5	6.95	1.09	0.032	0.15	0.40	0.77	553.346	8.0e-11	1200
8	802P3	3.3	4.73	1.03	0.032	0.15	0.45	0.91	553.289	1.6e-07	0.54
9	802P4	1.4	2.89	1.08	0.032	0.15	0.35	0.73	553.290	9.0e-07	0.11
11	803P1	7.6	9.45	1.08	0.032	0.15	0.40	1.62	554.018	2.0e-09	30
12	803P2	5.2	6.61	1.07	0.032	0.15	0.40	0.70	553.981	1.3e-10	780
13	803P3	3.6	5.01	1.04	0.032	0.15	0.40	0.84	554.029	3.5e-07	0.26
14	803P4	1.4	2.88	1.03	0.032	0.15	0.40	0.85	553.974		
40	804P1	8.0	9.70	1.11	0.032	0.15	0.40	1.14	551.450		
41	804P2	5.2	6.64	1.03	0.032	0.15	0.40	0.81	551.421		
42	804P3	3.5	4.79	0.98	0.032	0.15	0.40	0.67	551.567*		
43	804P4	1.3	2.89	1.05	0.032	0.15	0.40	0.99	551.777*	4.8e-07	0.17
44	804P5	1.0	2.55	1.12	0.032	0.15	0.39	0.91	551.792*	1.5e-06	0.06
45	805P1	5.8	7.22	1.12	0.032	0.15	0.39	0.67	551.897		
46	805P2	4.8	6.23	1.04	0.032	0.15	0.40	0.78	551.823		
47	805P3	1.7	3.10	1.03	0.032	0.15	0.40	0.69	551.838	1.3e-06	0.08
48	805P4	3.5	4.92	1.04	0.032	0.15	0.40	0.79	551.960	2.6e-08	3.60
49	805P5	1.0	2.31	1.05	0.032	0.15	0.40	0.48	551.825		
50	806P1	6.9	8.36	0.86	0.032	0.15	0.40	1.19	553.022		
51	806P2	8.6	10.01	0.93	0.032	0.15	0.39	0.97	553.021		
52	806P3	5.4	6.67	0.90	0.032	0.15	0.40	0.81	553.129		
53	806P5	0.9	2.68	1.41	0.032	0.15	0.39	0.81	553.354		
58	807P1	5.3	6.66	1.06	0.032	0.15	0.40	0.70	548.304		
59	807P2	3.4	4.77	0.94	0.032	0.15	0.40	0.91	548.375		
60	807P3	2.5	3.91	0.98	0.032	0.15	0.39	0.89	548.300		
61	807P4	1.6	2.94	1.03	0.032	0.15	0.40	0.58	548.214		
62	808P1	4.8	6.13	0.89	0.032	0.15	0.40	0.80	549.100		
54	809P1	7.0	8.50	1.09	0.032	0.15	0.40	0.91	552.500		
55	809P2	4.8	6.64	1.43	0.032	0.15	0.40	0.90	552.432		
56	809P3	3.2	4.85	1.10	0.032	0.15	0.40	1.01	552.554		
15	8011P1	13.2	14.30	0.80	0.032	0.15	0.40	0.67	558.715	1.5e-11	6900
16	8012P1	7.4	9.06	1.14	0.032	0.15	0.87	1.13	555.412	2.0e-06	0.04
17	8012P2	5.5	6.67	0.85	0.032	0.15	0.40	0.64	555.277	6.0e-11	1770
18	8012P4	2.2	3.69	1.10	0.032	0.15	0.40	0.87	555.080		
20	8013P1	6.9	8.44	1.09	0.032	0.15	0.39	0.82	557.137	3.1e-08	3
10	80W1	wtmw	4.08	1.10	0.032	0.15			553.562		
5	80W2	wtmw	4.61	1.46	0.032	0.15			553.259*		
32	80W3	wtmw	3.89	1.10	0.032	0.15			553.398		
33	80W4	wtmw	3.90	1.19	0.032	0.15			553.450		
34	80W5	wtmw	3.90	1.20	0.032	0.15			554.059		
57	82W9	wtmw	7.18	1.10	0.035	0.15			552.468		
19	82W12	wtmw	5.62	1.10	0.035	0.15			555.366		

Table B1 Continued.

	ID	Mean depth	Casing length	Casing stick-up	Casing diam	Bore hole diameter	Screen length	Sand pack length	Top of casing elevation	K-sat (m/s)	Basic time lag (hr)
21	93W2	wtmw	2.98	0.85	0.032	0.06			553.747		
36	93W3	wtmw	1.57	0.29	0.032	0.06			553.445		
37	93W4	wtmw	1.50	0.18	0.032	0.06			553.224		
38	93W5	wtmw	1.50	0.22	0.032	0.06			553.171		
39	93W6	wtmw	2.85	0.69	0.032	0.06			554.301		
22	93UP2	11.0	12.77	1.09	0.013	0.15	0.60	1.40	553.437	1.2e-09	8.6
23	93UP3A	1.9	3.36	1.09	0.013	0.15	0.20	0.70	553.913	1.2e-06	0.01
23	93UP3B	6.8	8.38	1.09	0.013	0.15	0.20	1.05	553.913	7.0e-11	176
23	93UP3C	10.3	11.94	1.09	0.013	0.15	0.25	1.05	553.913	3.5e-10	35
24	93UP4	4.9	6.92	1.46	0.013	0.15	0.70	1.20	554.293	3.8e-09	11
25	93UP5A	14.6	16.15	0.99	0.013	0.15	0.20	1.10	553.814	4.5e-10	53
25	93UP5B	plugged	16.79	0.99	0.013	0.15	0.20		553.814		
25	93UP5C	21.8	24.57	0.99	0.013	0.15	0.25	3.60	553.814	1.0e-09	5.3
26	93UP6A	2.3	3.80	1.01	0.013	0.15	0.20	1.00	555.402		
26	93UP6B	4.7	6.24	1.01	0.013	0.15	0.20	1.05	555.402	2.0e-10	32
26	93UP6C	8.2	9.66	1.01	0.013	0.15	0.25	0.90	555.402	4.5e-10	30
27	93UP7A	13.2	14.72	1.02	0.013	0.15	0.20	1.05	555.160	6.0e-11	206
27	93UP7B	18.2	19.71	1.02	0.013	0.15	0.20	1.00	555.160	2.5e-10	51
27	93UP7C	21.9	24.60	1.02	0.013	0.15	0.25	3.30	555.160	1.3e-10	44
63	93LP1A	1.7	3.21	0.99	0.013	0.15	0.20	1.05	547.689		
63	93LP1B	3.7	5.18	0.99	0.013	0.15	0.20	1.00	547.689		
63	93LP1C	5.7	7.20	0.99	0.013	0.15	0.20	1.00	547.689		
63	93LP1D	9.3	10.80	0.99	0.013	0.15	0.25	1.00	547.689		
64	93LP2A	2.6	4.05	0.98	0.013	0.15	0.20	1.00	550.821		
64	93LP2B	4.6	6.08	0.98	0.013	0.15	0.20	1.00	550.821		
64	93LP2C	7.6	9.08	0.98	0.013	0.15	0.20	1.00	550.821		
64	93LP2D	11.3	12.82	0.98	0.013	0.15	0.25	1.00	550.821		
65	93LP3B	18.6	22.50	1.05	0.013	0.15	0.25	5.70	551.077		
28	94W7	3.2	6.10	0.80	0.041	0.05	2.00	4.30	554.737		
29	94UP8	2.0	3.05	0.65	0.027	0.05	0.30	0.90	553.552		
29	94UP9	1.9	3.15	0.75	0.027	0.10	0.30	1.00	553.612	2.8e-06	0.02
30	94UP10	4.0	5.45	0.85	0.021	0.10	0.30	1.30	555.230	1.0e-09	33
66	94LP4	3.0	4.35	1.10	0.027	0.06	0.30	0.55	545.862		
31	94SWL1	sw	3	1.20	0.041	0.06			553.017*		
67	94SWL2	sw	3	1.00	0.041	0.06			545.810*		

Appendix C

Chemical and isotopic analyses of pond water and groundwater

Results of chemical and isotopic analysis for pond water and groundwater are listed in Tables C1 and C2, respectively. Table C1 contains; wetland identification number, sampling date, temperature, electric conductivity, pH, major cations, major anions, alkalinity, $\delta^{18}O$, and $\delta^{2}H$. Temperature was measured at the field site. The reported values of electrical conductivity is the value standardized to 25 °C. The pH values in square bracket indicates that the measurement was made in the laboratory for samples collected from the field. The wetland E.S109 denotes a small depression east of S109 (Fig. B1) that is not identified by the Canadian Wildlife Service.

Table C2 contains; piezometer identification number, sampling date, temperature, electrical conductivity (standardized to 25 °C), field-measured pH, laboratory-measured pH, Eh (referenced to the standard hydrogen electrode), major cations, major anions, alkalinity, $\delta^{18}O$, $\delta^{2}H$, and saturation indices for mineral phases. The saturation indices for calcite, dolomite, and gypsum were calculated using PHRQPITZ (Plummer, L.N., Parkhurst, D.L., Fleming, G.W. and Dunkle, S.A., 1988. A computer program incorporating Pitzer's equations for calculation of geochemical reactions in brines. U. S. Geol. Surv. Water Resour. Inv. Rep. 88-4153):

$$SI = \log_{10}(IAP / K_{sp})$$

where SI is the saturation index, IAP is the ion activity product, and K_{sp} is the solubility constant.

Table C1 Results of chemical and isotopic analyes for pond water.

Wetland ID	Date	Temp (°C)	EC (µS/cm)	pH	Ca (mg/l)	Mg (mg/l)	Na (mg/l)	K (mg/l)	Cl (mg/l)	NO3 (mg/l)	SO4 (mg/l)	Alk (meq/l)	del18 (‰)	delD (‰)
S37	11-Jul-93	19	432	7.52	37.1	17.4	0.9	44.3	5.31	<.15	17.6	3.30		
S37	23-Jul-93	20.5	480	7.08	43.6	19.3	1.24	42.7	7.26	<.08	8.36	4.06		
S37	1-Aug-93	15	522	7.20	47.2	22.6	1.6	47.8	8.7	<.29	4.45	4.72		
S37	6-Aug-93	21	705	7.83	61.1	28.4	2.17	63	12.2	<.08	2.27	5.94		
S37	27-May-94	19	406	7.23	37.7	18.1	0.69	33.3	5.79	<0.03	3.07	3.70		
S37	23-Jun-94	23	441	7.72	43	22.5	0.81	36.3	5.65	0.06	1.04	4.53		
S37	30-Jun-94	17	464	7.28					5.92	<0.03	0.54	4.73		
S37	14-Jul-94	18		7.10	43.4	23.9	0.82	39.9	6.29	<0.03	0.53	4.85		
S37	28-Jul-94	25	494	7.33					6.59	0.08	1.35	4.83		
S37	17-Aug-94		486	7.15	37.3	25.5	0.65	40.1	5.32	<0.03	0.26	4.88		
S37	30-Aug-94		489	7.25					5.4	<0.03	0.33	4.88	-7.7	-94
S37	13-Sep-94	18	520	7.62	114	121	32.8	80.2	6.84	<.23	0.81	5.16		
S37	27-Sep-94	11	561	7.38					9.92	0.08	1.21	5.39		
S37	13-Oct-94	5	614	7.80					13.6	<0.22	<0.65	5.95	-6.3	-83
S50	1-Aug-93	15.5	4751	7.63	221	438	304	111	71	<1.7	2525	7.53		
S103	6-Jul-93	17	171	6.86	14.6	6.19	0.48	22.9	2.11	0.07	5.78	1.31		
S109	6-Jul-93	16	189	6.87	10.7	6.03	0.42	22.9	2.7	<.08	1.44	1.42	-14.9	-112
S109	23-Jul-93	17.5	233	6.79	15.3	8.89	0.29	27.3	4.04	<.03	0.23	1.90		
S109	1-Aug-93	15	257	6.68	15.4	9.17	0.33	31.9	3.96	<.08	0.84	2.08		
S109	12-Aug-93	23	293	6.50	19.7	9.81	0.6	32	4.72	<.16	<.16	2.29	-11.6	-106
S109	13-Sep-93	10	240	5.99	13.4	5.92	1.69	27	6.56	42.6	11.5	0.74		
S109	23-Sep-93	21	390	7.05	29.2	10.6	3.29	31.9	8.45	0.37	5.46	3.13		
S109	24-Mar-94	0	202	7.00					4.68	<0.03	4.30	1.61		
S109	12-Apr-94	6	196	6.99	15.6	6.42	0.5	26.2	3.96	<0.03	5.00	1.58	-21.8	-173
S109	28-Apr-94	10	252	7.07	80	10.6	0.64	26	3.6	0.03	4.19	2.16		
S109	11-May-94	14	305	7.19	28	11.3	0.6	29.8	4.54	<0.03	2.56	2.73		
S109	27-May-94	18	332	7.02	31.5	12.6	0.69	28.9	4.61	<0.03	1.12	3.05	-15.0	-137
S109	9-Jun-94			7.09					4.07	0.11	0.74	3.37		
S109	23-Jun-94		367	7.21	42	15.3	6.44	30.7	3.87	<0.03	0.38	3.64		
S109	30-Jun-94	19	385	6.91					4.24	<0.03	0.58	3.77		
S109	14-Jul-94	18		7.02	40.6	16.1	0.5	32.6	3.98	<0.03	0.17	3.87	-11.5	-113
S109	28-Jul-94	21	399	7.02					4.7	0.14	1.46	3.95		
S109	17-Aug-94		402	6.90	50.4	15.9	0.78	35.4	4.32	<0.03	0.17	3.89		
S109	30-Aug-94		398	7.08					4.24	<0.03	0.14	3.82	-9.3	-104
S109	13-Sep-94	15	410	7.18	40.1	16.7	0.91	37	4.76	<.03	0.08	3.89		
S109	27-Sep-94	11	439	7.21					5.45	<0.03	0.16	4.22		
S109	12-Oct-94	8	491	7.41					6.77	<0.13	<0.13	4.46	-7.5	-94
S109	15-Mar-95			[6.86]	7.00	3.12	0.37	29.1	3.87	4.17	3.45	1.02		
S109	30-Mar-95			[7.28]	15.7	8.55	0.94	30.5	6.54	<0.11	19.7	1.68		
S109	11-Apr-95			[7.90]	21.3	10.2	1.42	30.2	6.74	<0.18	30.7	1.84		
S109	21-Apr-95			[7.77]	24.1	11.4	1.53	29.4	6.58	<0.18	30.3	2.12		
S109	4-May-95			[7.87]	28	13.4	1.81	32.5	7.32	<0.2	35.9	2.34		-132
S109	1-Jun-95			[7.82]	28.4	16.2	1.65	42.3	8.58	<0.2	17	3.12		-115
S109	17-Jun-95			[7.89]	28.6	16.1	1.76	43.5	8.27	<0.2	3.88	3.30		-96
S109	1-Jul-95			[7.91]	29.9	14.9	2.3	37.1	8.21	<0.2	1.29	3.12		-89
S109	16-Jul-95				38.8	16.1	2.65	36.6	6.96	<0.14	0.88	3.74		-78
S109	6-Apr-96		381	[7.53]	12.2	6.09	0.61	24.1	2.88	6.72	7.78	1.28		
S109	8-Apr-96		360	[7.45]	13.1	5.97	0.59	17.9	2.29	4.02	10.9	1.21		
S109	17-Apr-96		205	[7.63]	18.4	7.77	0.72	17.9	2.19	0.39	14.8	1.55		
S109	26-Apr-96		236	[7.58]	20.9	9.19	0.8	18.4	2.56	<0.1	15.7	1.85		
S109	6-May-96		284	[7.52]	25.6	10.6	0.86	21.9	3.16	<0.1	15.2	2.16		
S109	16-May-96		287	[7.64]	28	12.2	0.88	21.1	3.46	<0.1	13.2	2.38		
S109	29-May-96		331	[7.68]	32.8	14.1	0.91	23.6	3.85	<0.1	13.3	2.80		

Table C1 Continued.

Wetland ID	Date	Temp (°C)	EC (µS/cm)	pH	Ca (mg/l)	Mg (mg/l)	Na (mg/l)	K (mg/l)	Cl (mg/l)	NO3 (mg/l)	SO4 (mg/l)	Alk (meq/l)	del18 (‰)	delD (‰)
S109	17-Jun-96		346	[7.72]	34.6	15.8	0.58	23.5	2.58	<0.09	7.62	3.14		
S109	2-Jul-96		345	[7.57]	34.9	15.6	0.61	21.6	2.09	<0.09	4.3	3.22		
S109	18-Jul-96		333	[7.88]	38.2	13.8	0.95	17.9	2.14	<0.09	6.84	3.06		
S109	6-Aug-96			[7.48]	42.4	14.6	1.12	20.2	2.61	<0.06	2.19	3.62		
S109	20-Aug-96			[7.53]	45.3	15.2	1.32	22.3	2.92	<0.06	2.92	3.70		
S109	11-Sep-96			[7.59]	42	15.3	1.44	23.6	3.69	<0.08	3.44	3.68		
S118	6-Jul-93	18	200	7.04	14.9	5.98	0.51	24.1	2.25	0.13	3.89	1.45		
S118	1-Aug-93	15	362	6.84	31.2	12.1	0.47	31.4	3.87	<.08	0.84	3.38		
S118	2-Jun-94	13	358	7.21	36.2	13.4	0.4	25	2.32	<0.18	0.2	3.28		
S120	1-Aug-93	15	276	6.96	26.6	10	0.73	19.5	2.2	<.14	<.14	2.55		
S120	13-Sep-93	10	223	6.35	29.4	8.23	1.34	17	2.42	0.12	0.88	2.93		
S120	23-Oct-93	5	454	7.06	59	15.8	2.57	21.8	2.31	<.03	4.44	4.74		
S120	6-Nov-93	4	533	7.22	82.4	20.4	3.15	28.4	6.08	<.03	6.84	6.51		
S120	2-Jun-94	13	316	7.19	34.8	10.5	0.84	24.4	4.38	<0.03	0.69	2.95		
S120	22-Jul-95				64.3	29.9	7.35	39.9	11.6	<0.14	3.73	6.28		
S120	7-Aug-95								15		1.86			
S124	23-Aug-93	22.5	1899	7.34	191	96.6	31.2	80.9	22	<.32	489	10.24		
S125N	23-Aug-93	23	1932	7.57	178	116	32.5	81.8	23.5	<.4	556	8.98		
S125N	6-Sep-93	15	2126	7.13	162	141	38.6	97.6	33.5	<.37	583	11.59		
S125N	13-Sep-93	11	1655	7.20	134	85.9	18.7	27	13.3		572	2.99		
S125S	6-Jul-93	19	1964	7.57	167	138	40.7	72.3	24.6	<.6	814	4.67	-12.9	-107
S125S	23-Jul-93	17.5	2323	7.35	226	168	44.6	87.9	25.5	<.67	1001	6.29		
S125S	1-Aug-93	15.5	2544	7.47	235	176	47.5	96.4	31.1	<.7	1025	7.50		
S125S	12-Aug-93	15	2738	7.42	256	205	58	103	31.7	<.8	1181	8.47	-11.8	-98
S125S	30-Aug-93	18.5	2479	7.20	222	192	55.4	101	35.2	<.75	1054	8.67		
S125S	6-Sep-93	13.0	2480	7.34	222	190	52.8	101	37.2	<.6	1084	8.35		
S125S	13-Sep-93	9.5	1885	6.75	166	142	40.2	83.6	30.9	<.5	840	5.63		
S125S	23-Oct-93	4.0	2398	7.33	253	209	57	107	39	<.75	1162	10.98	-12.6	-101.5
S125S	6-Nov-93	4.0	2714	7.85	316	265	72.8	127	48	<.93	1404	13.19		
S125S	24-Mar-94	0.0	1020	7.21					38.3	4.49	324	2.64		
S125S	12-Apr-94	7.0	913	7.25	74.5	44.7	10.4	60.7	26.8	<1.7	273	2.91	-18.9	-169
S125S	28-Apr-94	8.0	1330	7.45	120	73.6	19.8	67.9	31	<0.03	448	4.64		
S125S	11-May-94	12.0	1733	7.77	179	114	30.6	57.7	38.2	<0.26	625	6.10		
S125S	27-May-94	12.0	2300	7.64	203	177	51.1	95.2	37.3	<3.7	991	7.27	-11.0	-107
S125S	9-Jun-94	12.0		7.81					35.7	0.63	1136	7.64		
S125S	23-Jun-94		2510	7.66	249	235	67.7	104	38.4	<.63	1316	8.50		
S125S	30-Jun-94	16.0	2480	8.01					41.1	<.34	1291	9.38		
S125S	14-Jul-94	18.0		7.80	254	259	74.8	123	41.1	<.34	1284	9.74	-8.3	-91
S125S	28-Jul-94	24.0	2640	8.04					46.1	<.34	1380	10.83		
S125S	17-Aug-94		2850	7.93	261	278	78.3	119	48.5	<0.48	1293	12.05		
S125S	30-Aug-94		2950	7.92					50.5	<0.48	1354	12.03	-6.4	-88
S125S	13-Sep-94	19.0	3580	7.86	258	327	99.6	155	58.5	<1.4	1557	12.79		
S125S	27-Sep-94	10.0	3680	8.02					65.9	<0.89	1706	13.78		
S125S	12-Oct-94	4.0	3720	7.92					67.1	<0.13	1826	12.96	-5.2	-76
S125S	17-Jun-95			[7.92]	177	254	79.4	152	54.1	<1.1	1349	5.18		-71
S125S	16-Jul-95				214	314	114	200	70.4	<1.2	1899	5.50		-66
S133	27-May-94	14	230	6.92	19.2	5.58	0.29	21.4	1.52	<.03	0.32	1.62		
E.S109	6-Jul-93	21.5	295	7.18	28	6.72	0.32	19	0.4	<.04	0.82	2.30		
E.S109	12-Apr-96		334	[7.82]	36.6	11.6	0.97	18.8	3.38	20.6	25.1	2.24		
E.S109	16-May-96		457	[8.08]	60.9	17.6	1.28	23.8	8.04	0.48	27.6	4.24		

Table C2 Results of chemical and isotopic analyes for groundwater.

Piezo. ID	Date	Temp (°C)	EC (µS/cm)	pH	[pH]	Eh (mV)	Ca (mg/l)	Mg (mg/l)	Na (mg/l)	K (mg/l)	Si (mg/l)	Cl (mg/l)	NO3 (mg/l)	SO4 (mg/l)	Alk (meq/l)	del18 (‰)	delD (‰)	Saturation Indices Cal.	Dol.	Gyp.
801P1	4-Sep-93	9	1090	6.72		135	141	60.2	27.4	7.25		3.79		299	7.06	-18.2	-145	-0.39	-0.92	-0.95
801P1	10-Jun-94	11	850	6.89	7.19		143	56.9	20.2	6.94		4.19	<0.37	296	6.5419					
801P2	4-Sep-93	9	920	6.69		1	124	46.1	18.2	7.25		3.81		100	9.00	-18.6	-156	-0.32	-0.83	-1.41
801P2	10-Jun-94	14	890	6.98	7.19		130	47.1	35.5	7.45		5.58	1.5	232	7.3839					
801P3	4-Sep-93	9	1590	6.70		91	212	77.5	72.4	11.6		9.55		494	10.00			-0.15	-0.49	-0.67
801P3	10-Jun-94	12.3	1190	6.84	7.13		195	68.7	55.8	9.86		9.38	<0.30	386	9.9796					
801P4	4-Sep-93	10	2120	6.66		56	183	108	130	11.4		4.42		987	7.14	-18.9	-149	-0.47	-0.88	-0.53
801P4	19-Sep-93	12	2160	6.75		53	275	115	128	11.6		4.59		988	7.13			-0.18	-0.42	-0.39
801P4	9-Jun-94			6.94	7.17		250	101	130	10.2		5.85	4.13	914	7.0134					
801P4	10-Jun-94	14.6	1740	7.08	7.14		248	97.7	169	10.1		5.93	2.25	892	7.3241					
802P1	5-Sep-93	7	820	6.89		76	105	49.6	16.8	7.05	10.9	1.82		30.8	9.06	-16.3	-142	-0.20	-0.53	-1.95
802P2	5-Sep-93	8	1020	6.91		121	124	61.7	46.2	7.87	10.2	3.7		166	9.61	-16.6	-134	-0.11	-0.32	-1.23
802P3	4-Sep-93	7	870	6.70		59	108	50.5	39.4	8.45	10	3.13		102	9.05	-17.3	-141	-0.40	-0.93	-1.45
802P3	10-Jun-94	22.2	960	7.04	7.21		85.4	39.2	74.6	7.98		3.61	0.9	102	8.6918					
802P4	5-Sep-93	9	870	6.83		85	109	63.4	6.59	9.86	6.92	3.64		23	10.23	-20.0	-158	-0.16	-0.34	-2.09
802P4	5-Sep-93	9	820	6.75		169	87.5	62.5	17.8	10.4	6.35	3.44	1.25	22.6	9.61			-0.36	-0.64	-2.18
802P4	9-Jun-94			7.02	7.04		97.2	66.3	14.6	9.56		3.92	<0.15	20.3	10.681					
802P4	10-Jun-94	19.2	910	6.96	7.01		94.4	66.9	17.1	11.2		3.95	<0.15	22.1	10.634					
803P1	4-Sep-93	6	4350	6.98		141	346	547	150	14.8		18.3		2960	6.63	-15.9	-129	-0.19	0.05	-0.11
803P2	4-Sep-93	8	2300	6.80		272	585	169	68	11.3		12.2	16	1150	7.17	-16.6	-134	0.10	-0.10	-0.11
803P3	4-Sep-93	10	3550	6.92		118	318	407	77.2	20.5		5.73		2130	7.33	-17.2	-137	-0.11	0.18	-0.21
803P3	9-Jun-94			6.94	7.21		326	374	78.8	19		6.59	<1.3	2120	7.2332					
803P3	10-Jun-94	10.8	2600	6.96	7.25		312	383	82.4	18.7		6.99	1.2	2140	7.0486					
803P4	4-Sep-93	10	2850	6.81		127	285	348	55.2	17.6		2.29		1730	9.10	-21.4	-165	-0.13	0.11	-0.29
803P4	19-Sep-93	12	3670	6.66		101	345	414	60.2	19.9		2.22		2150	8.92			-0.22	-0.03	-0.19
803P4	10-Jun-94	10.8	1810	7.10	7.41		189	224	80.9	13.4		5.84	<0.71	1060	10.282					
804P1	7-Jul-94		940	7.24	7.35		120	51.1	36.5	7.74		3.99	<0.74	159	8.5542	-16.9	-140			
804P2	7-Jul-94		950	7.16	7.34		123	46.7	47.3	6.31		4.75	<0.74	170	8.5831	-17.9	-145			
804P3	7-Jul-94		810	7.16	7.32		117	40.9	19.7	4.82		5.46	<0.3	152	6.9624					
804P4	7-Jul-94		790	7.19	7.32		109	31.7	41.1	1.59		5.4	<0.30	172	6.0291					
804P5	7-Jul-94		1280	6.84	6.99		185	62.8	65.3	3		5.11	<0.99	314	10.667	-19.1	-152			
805P1	5-Sep-93	8	1160	6.76		158	123	49.5	112	6.62		3.18		160	9.95			-0.26	-0.69	-1.25
805P2	5-Sep-93	9	870	6.67		171	109	43	59.8	6.19		3.74		110	9.46			-0.37	-0.92	-1.42
805P3	5-Sep-93	10	700	6.30		261	83.3	44.1	21.1	11		1.78		12.2	8.13			-0.86	-1.76	-2.43
805P4	5-Sep-93	8	780	6.76		174	111	42.8	14.2	5.8		5.86		52.3	8.36			-0.32	-0.85	-1.70
805P5	5-Sep-93	8	870	6.72		232	39.4	21.5	172	4.09		8.17	0.3	48	9.88			-0.73	-1.52	-2.14

Table C2 Continued.

Piezo. ID	Date	Temp (°C)	EC (µS/cm)	pH	[pH]	Eh (mV)	Ca (mg/l)	Mg (mg/l)	Na (mg/l)	K (mg/l)	Si (mg/l)	Cl (mg/l)	NO3 (mg/l)	SO4 (mg/l)	Alk (meq/l)	del18 (‰)	delD (‰)	Saturation Indices Cal.	Dol.	Gyp.
806P1	5-Sep-93	8	990	6.90		163	114	74.1	33.3	8.3		2.99		150	9.97	-17.0	-136	-0.14	-0.26	-1.31
806P2	5-Sep-93	8	1090	6.90		150	120	71.7	49.3	7.93		3.25		196	9.55	-16.3	-150	-0.15	-0.31	-1.19
806P3	5-Sep-93	8	790	6.86		148	87.5	67.9	8.6	5.77		1.71		57.5	8.96	-17.3	-140	-0.30	-0.51	-1.78
806P5	7-Jul-94		1480	7.26	7.53		144	134	74.1	1.84		36.5	<1.24	421	11.031					
807P1	6-Sep-93	13	21400	7.09		144	388	4070	2080	51.9	9.62	184		19000	12.56	-13.6	-116	-0.14	1.15	0.03
807P2	6-Sep-93	13	14500	6.97		178	359	2700	1060	78.7	9.52	85.6		12800	8.39	-11.8	-107	-0.35	0.57	-0.06
807P3	6-Sep-93	13	7580	7.06		272	402	1140	366	74.2	10.6	29		5850	8.94	-11.8	-108	0.03	0.88	-0.03
807P4	19-Sep-93	10	20900	7.14		335	407	4890	1530	127		119		22700	6.61	-12.8	-110	-0.44	0.57	0.00
808P1	6-Sep-93	10	20100	7.06		180	395	4460	1890	51.2		140		21400	12.67			-0.23	0.95	-0.01
8011P1	27-Sep-94		2520		7.67		70	34.1	411	274		39.9	1.99	678	11.561	-16.7	-142			
8012P1	27-Sep-94		8450		7.18		411	1459	304	18.6		434.4	64.4	7200	8.678	-16.3	-138			
8012P2	27-Sep-94		7850		7.26		415	1260	493	18.4		44.2	3.58	6160	8.748	-15.7	-134			
8013P1	27-Sep-94		5050		7.29		500	507	317	17		128	3.58	3160	7.625	-15.5	-121			
80W1	4-Sep-93	8	680	6.68		31	91.7	34	2.75	13.6		3.66		17.6	7.34			-0.51	-1.25	-2.21
80W2	4-Sep-93	9	820	6.64		30	123	40.4	3.92	16.7		5.25		1.81	9.89			-0.30	-0.86	-3.12
80W3	5-Sep-93	13	600	6.39		129	77.2	29.4	1.27	23.1		1.87			6.67			-0.82	-1.76	
80W4	5-Sep-93	12	470	6.47		109	96.9	29.7	3.05	28.1		8.11			7.87			-0.60	-1.44	
80W5	5-Sep-93	9	510	6.77		122	71	24.2	1.81	12.4		1.2		4.85	5.73			-0.60	-1.43	-2.83
93W2	4-Sep-93	12	2850	7.06		343	379	344	116	22.8		3.51		2150	8.15			0.19	0.66	-0.14
93W2	10-Jun-94	14	2920	7.28	7.53		179	195	165	15.2		1.5	<0.45	968	12.781					
93W5	19-Sep-93	12	400	6.55		312	45	21.1	5.01	1.58		0.74	1.78	27.2	3.48	-20.2		-1.17	-2.37	-2.24
93W6	19-Sep-93	12	490	6.84		233	63.3	27.7	4.51	2.49		0.37	1.2	6.73	5.48	-20.9		-0.55	-1.17	-2.74
94W7	27-Sep-94		1400		7.28		183	96.3	13.9	8.43		5.34	20.5	504	6.397	-16.2	-155			
93UP2	11-Jun-94		950	7.70	7.69		86.8	58.1	35.3	13.3		4.84	<0.08	69.1	9.1917					
93UP2	26-Jul-95						84.8	53.4	72.1	9.55		4.07	<0.2	32.7						
93UP3A	11-Jun-94		1060	7.54	7.63		54.7	21.1	154	7.54		8.9	2.99	155	7.8782					
93UP3A	26-Jul-95						84.8	38.9	24	8.06		5.58	1.19	39.2						
93UP3B	11-Jun-94		2480	7.74	7.76		43.2	16.3	486	9.15		50.2	5.55	474	8.9182					
93UP3B	26-Jul-95						72.5	24.8	324	9.45		17.6	<0.43	479						
93UP3C	11-Jun-94		810	7.48	7.36		86.8	45.8	15.7	8.63		3.81	<0.36	61.5	7.6993					
93UP3C	26-Jul-95						92	52.1	17.5	7.46		2.46	<0.06	5.91						
93UP4	9-Jun-94			7.04	7.19		128	51.5	33.5	9.76		3.99	<0.15	139	8.3265					
93UP4	10-Jun-94	21.8	940	6.98	7.08		100	49.3	33.1	8.66		3.32	<0.15	125	8.0945	-18.0	-138			
93UP4	28-Jul-95						108	49.4	24.8	9.05		3.29	<0.06	104						

Table C2 Continued.

Piezo. ID	Date	Temp (°C)	EC (µS/cm)	pH	[pH]	Eh (mV)	Ca (mg/l)	Mg (mg/l)	Na (mg/l)	K (mg/l)	Si (mg/l)	Cl (mg/l)	NO3 (mg/l)	SO4 (mg/l)	Alk (meq/l)	del18 (‰)	delD (‰)	Saturation Indices Cal.	Dol.	Gyp.
93UP5A	11-Jun-94		1210	7.58	7.67		49.8	19.8	196	10.1		13.7	2.18	208	8.0448					
93UP5A	26-Jul-95						103	45.3	86.4	9.18		7.79	<1.1	229						
93UP5C	11-Jun-94		780	7.69	7.54		79.6	35.2	32.9	10.3		3.85	<0.25	46.6	7.581					
93UP5C	26-Jul-95						99.3	38.9	52.4	7.21		3.37	<0.25	73.7						
93UP6A	18-Jul-96		13100		7.90							105	77.8	12200	5.7					
93UP6B	11-Jun-94		4870	7.29	7.36		429	400	398	18.6		45.3	8.93	3140	6.3725					
93UP6B	28-Jul-95						440	420	404	16.5		42.7	9.36	3200						
93UP6C	11-Jun-94		2080	7.62	7.38		190	132	123	11.2		9.37	<0.59	924	6.9648					
93UP6C	28-Jul-95						190	130	279	12.8		13.3	<0.6	1150						
93UP7A	11-Jun-94		8150	7.40	7.55		448	951	725	33		71.1	14.3	6000	7.2942	-18.3	-147			
93UP7A	28-Jul-95						430	1160	549	25.4		53.7	<3.7	6400						
93UP7B	11-Jun-94		5060	7.07	7.17		474	286	522	19.3		64.7	10.7	3100	6.0437	-18.5	-149			
93UP7B	28-Jul-95						483	288	475	17.3		59.8	<0.9	3000						
93UP7C	11-Jun-94		4050	7.19	7.20		522	229	274	14.5		30.3	<1.8	2500	5.9875	-18.5	-151			
93UP7C	28-Jul-95						558	226	279	12.4		29.7	<1.4	2610						
94UP9	30-Aug-94				7.39							1.84	<0.12	16.2	9.644					
93LP1A	15-Oct-94		5360		7.08		513	668	233	62		78	<1.6	3770	9.301	-13.1	-122			
93LP1B	15-Oct-94		4750		7.02		486	529	221	49.7		55.6	<1.6	3040	4.806	-12.2	-114			
93LP1C	15-Oct-94		9990		7.26		257	176	2200	25.9		295	<1.6	5170	10.182	-12.2	-105			
93LP1D	15-Oct-94		4810		7.30		446	534	287	28.9		40.1	<1.6	3110	11.219	-13.4				
93LP2B	15-Oct-94				7.58		457	446	295	23		60.3	<1.6	2940	6.073					
93LP2C	15-Oct-94		4810		7.40		453	498	326	20.6		42.3	<1.6	3240	7.223	-13.3	-126			
93LP2D	15-Oct-94		4230		7.34		566	315	259	19.2		59.6	<1.6	2660	6.553	-15.7	-140			
93LP3B	15-Oct-94		2280		7.57		290	127	152	7.85		31.8	<1.3	974	9.543	-19.7	-162			
94LP4	2-Jul-95				7.67		560	976	169	106		41	<2	4380	27.42					
Meybm	19-Jul-95				7.44							4.93	<0.13	255	11.14					
Zebth-S	25-Jul-95				7.29							6.28	0.45	9.38	8.08					
Zebth-F	25-Jul-95				8.02							6.29	<0.08	61.4	7.82					

Appendix D

Water level records in piezometers and wells

The elevation of water level in piezometers, water table monitoring wells, and the ponds S109 and S125S are listed in Table D1. The datum of the elevation is set at 500 m above the mean sea level. Asterisks indicate the ice level in piezometers and wells.

Table D1 Elevation of water level in piezometers and wells.

Date	801P1	801P2	801P3	801P4	80W2	802P1	802P2	802P3	802P4	80W1	803P1	803P2	803P3	803P4
6-Jul-93						52.10	51.73	52.15	52.12		50.45	51.68	52.49	52.46
7-Jul-93						52.09	51.72	52.14	52.11		50.59	51.68	52.45	52.38
8-Jul-93						52.08	51.73	52.12	52.09		50.67	51.69	52.41	52.35
11-Jul-93						52.04	51.73	52.08	52.04	52.05	50.74	51.72	52.28	52.23
14-Jul-93						52.00	51.75	52.04	52.00	51.99	50.74	51.74	52.20	52.15
17-Jul-93	52.05	52.05	52.06	52.05	52.07	52.04	51.77	52.09	52.07	52.09	50.75	51.76	52.29	52.29
20-Jul-93	52.04	52.05	52.05	52.04	52.05	52.01	51.78	52.03	51.99	51.97	50.74	51.78	52.19	52.16
23-Jul-93				52.06		52.05	51.80	52.10	52.06	52.09	50.76	51.82	52.37	52.39
27-Jul-93				52.03		51.98	51.80	52.01	51.96	51.94	50.75	51.83	52.15	52.13
1-Aug-93	51.98	51.98	51.99	51.98	51.99	51.88	51.80	51.89	51.84	51.83	50.65	51.82	51.97	51.95
6-Aug-93				51.92		51.78	51.78	51.78	51.71	51.73	50.57	51.79	51.85	51.82
12-Aug-93	51.85	51.86	51.86	51.85	51.87	51.65	51.74	51.70	51.60	51.66	50.44	51.73	51.72	51.68
19-Aug-93	51.88			51.88		51.76	51.73	51.80	51.75	51.76	50.41	51.69	51.85	51.87
23-Aug-93	51.83	51.84	51.84	51.84	51.85	51.66	51.73	51.72	51.66	51.71	50.44	51.68	51.79	51.80
30-Aug-93	51.68	51.67	51.68	51.67	51.68	51.46	51.66	51.51	51.42	51.53	50.35	51.60	51.61	51.61
4-Sep-93	51.56	51.57	51.54	51.57	51.56			51.45			50.30	51.54	51.55	51.54
5-Sep-93	51.54	51.38	51.52	51.55	51.54	51.40	51.61	51.45	51.35	51.48	49.94	50.87	51.54	51.54
6-Sep-93	51.50	51.48	51.48	51.51	51.50	51.06	50.84	51.43	51.33	51.46	50.11	50.89	51.52	51.52
7-Sep-93	51.44	51.46	51.42	51.46	51.44	51.21	50.85	51.40	51.30	51.43	50.20	50.91	51.51	51.49
8-Sep-93	51.40	51.42	51.36	51.41	51.40	51.27	50.87	51.36	51.25	51.39	50.25	50.93	51.48	51.47
10-Sep-93	51.32	51.34	51.29	51.35	51.31	51.26	50.89	51.36	51.26	51.38	50.24	50.95	51.46	51.45
13-Sep-93	51.79	51.77	51.80	51.79	51.80	51.55	50.94	51.77	51.64	51.77	50.26	51.00	51.78	51.86
17-Sep-93	51.78	51.78	51.79	51.78	51.79	51.69	51.01	51.74	51.69	51.77	50.40	51.06	51.93	51.96
19-Sep-93	51.76	51.76	51.77	51.75	51.77	51.68	51.04	51.73	51.69	51.77	50.48	51.10	51.93	51.94
23-Sep-93	51.70	51.69	51.71	51.69	51.70	51.64	51.09	51.68	51.64	51.72	50.53	51.17	51.89	51.89
28-Sep-93	51.61	51.59	51.62	51.59	51.61	51.59	51.14	51.63	51.60	51.67	50.51	51.23	51.82	51.83
7-Oct-93	51.52	51.52	51.54	51.51	51.54	51.55	51.21	51.60	51.57	51.65	50.49	51.32	51.78	51.79
15-Oct-93	51.56	51.57	51.57	51.56	51.57	51.57	51.26	51.62	51.59	51.66	50.49	51.39	51.77	51.78
22-Oct-93	51.55	51.55	51.55	51.54	51.56	51.55	51.29	51.63	51.58	51.66	50.48	51.44		51.77
27-Oct-93	51.62	51.62	51.63	51.63	51.63	51.56	51.32	51.69	51.65	51.72	50.51	51.47	51.80	51.80
6-Nov-93	51.63	51.65	51.64	51.64	51.64	51.60	51.35	51.67	51.64	51.71	50.49	51.50	51.80	51.81
29-Nov-93	51.44	51.47	51.45	51.47	51.44	51.43	51.36	51.53	51.48	51.58	50.45	51.52	51.68	51.68
29-Dec-93	51.40	51.41	51.38	51.44	51.39	51.32	51.28	51.42	51.36	51.48	50.30	51.44	51.52	51.52
27-Jan-94	51.22	51.25	51.22	51.25	51.23	51.17	51.19	51.26	51.15	51.32	50.17	51.31	51.29	51.27
8-Mar-94	51.06	51.06	51.03	51.08	51.07									
17-Mar-94	51.55	51.50	51.26	51.81	51.51	51.51	51.00	51.55	51.76	51.98	49.97	51.08	51.12	51.21
24-Mar-94	52.22*	52.13*	52.12	52.14*	52.14*	52.04	51.12	52.12	51.99	52.05	50.09	51.15	51.84	51.94
29-Mar-94	52.14	52.13*	52.13	52.14*	52.12*	52.01	51.22	52.11	52.01	52.07	50.30	51.27	51.91	51.92
5-Apr-94	52.34	52.34	52.34	52.33	52.31*	52.27	51.37	52.35	52.30	52.34	50.56	51.46	52.39	52.42
8-Apr-94	52.33	52.33	52.33	52.33		52.28	51.43	52.36	52.32	52.36	50.65	51.54	52.45	52.52
12-Apr-94	52.50	52.49	52.50	52.49	52.53	52.37	51.50	52.53	52.50	52.52	50.77	51.65	52.62	52.67
16-Apr-94	52.58	52.57	52.58	52.57	52.61	52.50	51.58	52.58	52.57	52.58	50.85	51.74	52.55	52.57
21-Apr-94	52.59	52.58	52.58	52.58	52.62	52.53	51.67	52.59	52.58	52.58	50.92	51.86	52.57	52.57
28-Apr-94	52.58	52.58	52.58	52.57	52.61	52.53	51.79	52.59	52.58	52.58	50.97	51.99	52.58	52.58
4-May-94	52.56	52.55	52.56	52.56	52.59	52.51	51.88	52.56	52.55	52.56	50.99	52.08	52.56	52.55
11-May-94	52.53	52.52	52.53	52.52	52.55	52.48	51.95	52.53	52.53	52.53	50.99	52.14	52.51	52.51
19-May-94	52.55	52.54	52.54	52.55	52.58	52.49	52.03	52.55	52.55	52.54	51.02	52.22	52.61	52.60
27-May-94	52.55	52.56	52.55	52.55	52.58	52.51	52.12	52.56	52.56	52.55	51.14	52.29	52.59	52.58
2-Jun-94	52.56	52.56	52.56	52.56	52.59	52.52	52.13	52.57	52.57	52.56	51.15	52.32	52.61	52.60
9-Jun-94	52.58	52.57	52.57	52.57	52.60	52.53	52.21	52.58	52.58	52.58	51.17	52.37	52.66	52.66
16-Jun-94	52.57	52.58	52.58	52.57	52.61	52.53	52.25	52.59	52.58	52.57	51.17	52.40	52.66	52.66
23-Jun-94	52.54	52.54	52.54	52.53	52.57	52.50	52.27	52.54	52.51	52.52	51.16	52.41	52.49	52.46
30-Jun-94	52.50	52.50	52.50	52.49	52.53	52.45	52.28	52.50	52.49	52.50	51.08	52.39	52.48	52.49

Table D1 Continued.

Date	801P1	801P2	801P3	801P4	80W2	802P1	802P2	802P3	802P4	80W1	803P1	803P2	803P3	803P4
7-Jul-94	52.48	52.48	52.48	52.47	52.50	52.43	52.28	52.48	52.47	52.47	51.01	52.36	52.43	52.42
15-Jul-94	52.43	52.42	52.42	52.42	52.45	52.37	52.27	52.42	52.39	52.40	50.95	52.33	52.31	52.29
21-Jul-94	52.43	52.43	52.43	52.43	52.46	52.38	52.29	52.43	52.40	52.42	50.97	52.33	52.37	52.35
28-Jul-94	52.37	52.36	52.36	52.36	52.39	52.30	52.27	52.35	52.30	52.30	50.91	52.28	52.21	52.19
4-Aug-94	52.31	52.31	52.31	52.30	52.34	52.22	52.24	52.29	52.23	52.20	50.81	52.17	52.20	52.17
7-Aug-94	52.31	52.31	52.31	52.31	52.34	52.23	52.25	52.31	52.27	52.25	50.79	52.19	52.22	52.22
11-Aug-94	52.27	52.29	52.26	52.28	52.32	52.22	52.24	52.29	52.25	52.23	50.81	52.18	52.18	52.17
17-Aug-94	52.24	52.25	52.25	52.24	52.30	52.16	52.21	52.24	52.17	52.15	50.80	52.17	52.17	52.16
24-Aug-94	52.19	52.12	52.18	52.19	52.22	52.07	52.17	52.13	52.05	51.99	50.72	52.07	51.93	51.90
30-Aug-94	52.16	52.16	52.15	52.15	52.19	52.04	52.14	52.11	52.05	52.01	50.67	52.01	51.93	51.90
13-Sep-94	52.04	52.04	52.03	52.03	52.07	51.91	52.06	51.95	51.91	51.84	50.62	51.90	51.77	51.73
20-Sep-94	51.95	51.97	51.95	51.95	52.00	51.81	52.00	51.85	51.82	51.78	50.55	51.83	51.69	51.65
28-Sep-94	51.88	51.87	51.87	51.87	51.91	51.66	51.92	51.69	51.67	51.67	50.50	51.76	51.60	51.56
4-Oct-94	51.86	51.86	51.83	51.86	51.88	51.67	51.87	51.74	51.69	51.73	50.47	51.72	51.65	51.60
12-Oct-94	51.77	51.77	51.77	51.76	51.81	51.55	51.79	51.59	51.57	51.61	50.45	51.67	51.58	51.54
19-Oct-94	51.73	51.72	51.72	51.72	51.76	51.54	51.73	51.60	51.57	51.64	50.46	51.65	51.61	51.56
26-Oct-94	51.70	51.70	51.69	51.69	51.71	51.51	51.69	51.61	51.58	51.65	50.41	51.63	51.63	51.60
3-Nov-94	51.62	51.61	51.60	51.62	51.64	51.48	51.62	51.55	51.50	51.59	50.43	51.60	51.58	51.54
15-Nov-94	51.46	51.51	51.45	51.46	51.47	51.42	51.54	51.47	51.42	51.52	50.39	51.55	51.53	51.49
29-Nov-94	51.23	51.28	51.20	51.24	51.22	51.23	51.19	51.31	51.23	51.37	50.33	51.48	51.40	51.36
13-Dec-94	51.06	51.11	51.03	51.07	51.06	51.07	51.14	51.15	51.05	51.21	50.20	51.36	51.21	dry
31-Jan-95	50.84	50.87	50.80	50.85	50.85	50.72	50.84	50.83	50.70	50.90	49.82	50.97	50.79	dry
25-Feb-95	50.70	50.73	50.64	50.70	50.70	50.56	50.68	50.67	50.54	50.76	49.67	50.80	50.64	dry
15-Mar-95	50.88	51.24	50.71	50.91	50.70	50.31	50.57	50.59	dry	50.68	49.58	50.65	50.60	dry
24-Mar-95	51.94	52.06	51.84	51.87	52.24	50.71	50.54	50.85	50.69	50.98	49.81	50.81	51.00	dry
11-Apr-95	52.25	52.28	52.18	52.26	52.31	51.62	50.77	51.68	51.63	51.63	50.21	51.18	51.54	51.34
21-Apr-95						51.84			51.83					
4-May-95	52.29	52.30	52.28	52.26	52.33	51.88*	51.22	52.08	51.98	52.11	50.52	51.58	52.01	51.98
23-May-95	52.25	52.25	52.24	52.22	52.28	52.18	51.54	52.25	52.24	52.24	50.76	51.87	52.31	52.28
1-Jun-95	52.20	52.20	52.19	52.16	52.22	52.11	51.64	52.18	52.12	52.11	50.76	51.93	52.16	52.12
17-Jun-95	52.06	52.07	52.05	52.03	52.10	51.93	51.73	51.97	51.90	51.86	50.59	51.90	51.83	51.78
25-Jun-95	52.00	52.00	51.98	51.96	52.03	51.83	51.73	51.83	51.76	51.77	50.51	51.84	51.76	51.72
1-Jul-95	51.97	51.97	51.95	51.93	52.00	51.81	51.74	51.79	51.73	51.77	50.51	51.81	51.80	51.79
9-Jul-95	51.87	51.88	51.86	51.84	51.91	51.64	51.71	51.62	51.54	51.64	50.48	51.76	51.65	51.61
16-Jul-95	51.78	51.78	51.76	51.74	51.83	51.48	51.67	51.49	51.40	51.56	50.44	51.70	51.58	51.55
22-Jul-95	51.74	51.74	51.70	51.69	51.79	51.48	51.64	51.50	51.41	51.58	50.45	51.67	51.65	51.65
11-Aug-95	51.63	51.61	51.58	51.58	51.67	51.30	51.47	51.41	51.34	51.57	50.27	51.46	51.54	51.68
18-Sep-95	50.74	50.79	50.69	50.74	50.78	50.99	51.28	51.05	50.94	51.19	50.29	51.35	51.35	51.45
10-Oct-95	51.46	51.47	51.42	51.44	51.48	51.35	51.15	51.38	51.42	51.53	50.37	51.26	51.72	51.84
1-Dec-95	51.57	51.59	51.55	51.54	51.58	51.53	51.30	51.60	51.55	51.67	50.56	51.54	51.80	51.83
10-Jan-96	51.31	51.33	51.28	51.30	51.32	51.27	51.26	51.35	51.24	51.43	50.34	51.41	51.44	51.45
8-Feb-96	51.03	51.05	50.99	51.00	51.05	51.00	51.13	51.11	50.97	51.19	50.18	51.12	51.27	51.07
8-Apr-96	51.94*	52.17	51.75*	52.00*	51.85*	52.09	51.13	52.33	52.10	52.39	50.19	51.17	51.66	52.09
12-Apr-96	51.86*	52.41	51.76*	52.14*	51.86*	52.30	51.23	52.43	52.34	52.42	50.30	51.26	52.14	52.33
17-Apr-96	52.13	52.46	52.45			52.38	51.36	52.48	52.43	52.48	50.52	51.42	52.27	52.40
25-Apr-96						52.45	51.56	52.52		52.52	50.75	51.66	52.51	52.52
6-May-96	52.51	52.62	52.50	52.46	52.44	52.47	51.73	52.53	52.52	52.52	50.90	51.86	52.53	52.48
16-May-96						52.49	51.91	52.55	52.55	52.54	51.00	52.04	52.63	52.61
29-May-96						52.49	52.04	52.54	52.55	52.53	51.05	52.20	52.56	52.52
17-Jun-96	52.43	52.44	52.41	52.38	52.46	52.39	52.15	52.44	52.44	52.43	51.03	52.29	52.44	52.42
2-Jul-96	52.42	52.43	52.41	52.36	52.45	52.38	52.21	52.42	52.40	52.42	51.06	52.34	52.39	52.34
18-Jul-96						52.55	52.31	52.60	52.60	52.60	51.11	52.41	52.60	52.60
6-Aug-96						52.42	52.33	52.47	52.45	52.46	50.98	52.38	52.36	52.34

Table D1 Continued.

Date	80W3	80W4	80W5	804P1	804P2	804P3	804P4	804P5	805P1	805P2	805P3	805P4	805P5
6-Jul-93	52.42	52.25	52.67						50.40	50.86	50.88	50.95	
7-Jul-93	52.42	52.24	52.61						50.40	50.86	50.87	50.90	
8-Jul-93	52.42	52.23	52.60										
11-Jul-93	52.38	52.15	52.49						50.41	50.84	50.84	50.83	
14-Jul-93	52.36	52.07	52.39						50.42	50.82	50.82	50.80	
17-Jul-93	52.39	52.19	52.51	47.28	50.77		50.85	50.85	50.44	50.85	50.85	50.85	
20-Jul-93	52.36	52.10	52.35	47.27	50.77		50.84	50.84	50.45	50.83	50.82	50.81	
23-Jul-93	52.39	52.20	52.47						50.46	50.85	50.85	50.85	
27-Jul-93	52.34	52.02	52.27						50.47	50.82	50.81	50.79	
1-Aug-93	52.23	51.81	52.12	47.24	50.77		50.80	50.79	50.47	50.78	50.75	50.70	
6-Aug-93	51.96	51.61	52.01						50.46	50.74	50.69	50.63	
12-Aug-93	51.74	51.48	51.82	47.20	50.75		50.71	50.71	50.44	50.69	50.64	50.57	
19-Aug-93	51.90	51.64	51.74						50.45	50.69	50.68	50.64	50.70
23-Aug-93	51.73	51.48	51.80	47.26	50.74		50.69	50.69	50.44	50.68	50.63	50.59	50.67
30-Aug-93	51.51	51.30	51.66	51.45	50.71		50.64	50.63	50.41	50.62	50.53	50.46	50.60
5-Sep-93	51.47	51.24	51.60						50.38	50.58	50.47	50.42	50.56
6-Sep-93	51.46	51.23	51.59	47.22	50.67	50.59	50.59	50.59	49.95	50.58	50.48	50.40	50.56
7-Sep-93	51.44	51.19	51.59						49.96	50.56	50.44	50.39	50.54
8-Sep-93	51.39	51.15	51.57						49.97	50.55	50.40	50.35	50.52
10-Sep-93	51.42	51.17	51.58						49.98	50.53	50.39	50.33	50.50
13-Sep-93	52.02	51.56	51.58	47.31	50.66	50.65	50.65	50.64	50.03	50.65	50.70	50.67	50.66
17-Sep-93	51.92	51.52	51.90						50.07	50.63	50.63	50.63	50.62
19-Sep-93	51.88	51.50	51.97						50.09	50.62	50.61	50.60	50.61
23-Sep-93	51.83	51.47	52.00	47.34	50.64	50.62	50.62	50.62	50.12	50.61	50.58	50.56	50.59
28-Sep-93	51.77	51.44	51.96	47.33	50.62	50.59	50.59	50.59	50.15	50.58	50.54	50.51	50.57
7-Oct-93	51.75	51.46	51.91	47.33	50.59	50.56	50.56	50.56	50.18	50.55	50.52		50.55
15-Oct-93	51.78	51.51	51.88	47.35	50.57	50.55	50.55	50.55	50.19	50.54	50.51	50.49	50.54
22-Oct-93	51.77	51.53	51.89	47.36	50.54	50.54	50.54	50.54	50.19	50.52		50.48	50.55
27-Oct-93	51.83	51.59	51.94	47.38	50.54	50.54	50.55	50.54	50.20	50.54	50.54	50.52	50.54
6-Nov-93	51.79	51.57	51.85	47.40	50.52	50.62*	50.80*	50.62*	50.20	50.53	50.51	50.50	50.52
29-Nov-93	51.65	51.52	51.73		50.48*	50.53*	50.54*	50.54*			50.36	50.33	50.39
29-Dec-93		51.38		47.37					50.03	50.21	50.22	50.18	50.23
27-Jan-94				47.32					49.85	49.94	49.96	49.94	49.98
17-Mar-94				47.28					49.51	50.12	50.24	49.91	50.43
24-Mar-94	52.26	52.27	51.85	47.21	50.46*	50.55*	50.54*	50.55*	49.65	50.96	50.94	50.82	51.03*
29-Mar-94	52.22	52.14	51.38	47.30					49.79	50.99	50.95	50.83	51.01*
5-Apr-94	52.68	52.58*	52.89	47.41				50.41*	49.96	51.09*	51.09	51.04	51.11*
8-Apr-94	52.69	52.58	52.79	47.42	50.44*	50.45*	50.55	50.38*	50.02	51.18*	51.16*	51.04	51.08
12-Apr-94	52.87	52.72	53.04	47.51	50.43*	50.56	50.57	50.55	50.11	51.21	51.21		51.20
16-Apr-94	52.90	52.80	53.10	47.53	50.47	50.54	50.56	50.55	50.19	51.22	51.23	51.22	51.23
21-Apr-94	52.89	52.81	53.06	47.54	50.47	50.54	50.56	51.23	50.28	51.22	51.23	51.23	51.23
28-Apr-94	52.86	52.78	52.86	47.57	50.52	50.54	51.23	51.22	50.40	51.21	51.22	51.22	51.21
4-May-94	52.83	52.75	52.66	47.58	50.56	50.27	51.21	51.18	50.46	51.17	51.19	51.18	51.17
11-May-94	52.75	52.69	52.58	47.57	50.78	50.23	51.17	51.15	50.52	51.14	51.14	51.13	51.14
19-May-94	52.79	52.72	52.81	47.63	50.88	51.18	51.19	51.17	50.61	51.17	51.18	51.18	51.17
27-May-94	52.80	52.74	52.88	47.67	50.96	51.18	51.19	51.17	50.68	51.18	51.18	51.18	51.18
2-Jun-94	52.82	52.76	52.97	47.68	50.97	51.19	51.20	51.19	50.69	51.19	51.22	51.20	51.19
9-Jun-94	52.85	52.79	53.00	47.71	51.05	51.19	51.19	51.20	50.76	51.21	51.21	51.21	51.21
16-Jun-94	52.85	52.79	53.01	47.78	51.08	51.21	51.23	51.21	50.79	51.21	51.21	51.21	51.21
23-Jun-94	52.80	52.75	52.90	47.69	51.10	51.17	51.18	51.16	50.80	51.16	51.16	51.15	51.16
30-Jun-94	52.75	52.69	52.71	47.65	51.10	51.13	51.15	51.13	50.80	51.13	51.13	51.12	51.13

Table D1 Continued.

Date	80W3	80W4	80W5	804P1	804P2	804P3	804P4	804P5	805P1	805P2	805P3	805P4	805P5
7-Jul-94	52.71	52.65	52.52	47.65	51.09	51.11	51.12	51.10	50.80	51.10	51.10	51.09	51.10
15-Jul-94	52.63	52.57	52.28	47.60	50.81	51.06	51.07	51.05	50.77	51.05	51.04	51.02	51.05
21-Jul-94	52.64	52.58	52.34	47.66	50.87	51.06	51.07	51.06	50.78	51.05	51.05	51.14	51.05
28-Jul-94	52.54	52.48	52.12	47.58	50.89	51.00	51.01	51.00	50.75	50.99	50.98	50.95	50.99
4-Aug-94	52.45	52.38	51.95	47.55	50.90	50.97	50.99	50.95	50.69	50.93	50.92	50.85	50.92
11-Aug-94	52.40	52.33	51.95	47.58	50.91	50.94	50.95	50.94	50.70	50.93	50.93	50.90	50.94
17-Aug-94	52.32	52.21	51.83	47.57	50.90	50.91	50.92	50.90	50.67	50.90	50.88	50.85	50.90
24-Aug-94	52.05	51.87	51.72	47.56	50.88	50.86	50.87	50.85	50.64	50.84	50.80	50.75	50.84
30-Aug-94	51.91	51.75	51.64	47.56	50.87	50.83	50.84	50.82	50.61	50.81	50.79	50.72	50.81
13-Sep-94	51.50	51.35	51.59	47.54	50.81	50.73	50.74	50.72	50.53	50.71	50.64	50.56	50.70
28-Sep-94	51.26	51.05	51.42	47.50	50.72	50.58	50.60	50.58	50.41	50.56	50.39	50.30	50.54
12-Oct-94	51.26	51.01	51.33	47.49	50.64	50.49	50.50	50.49	50.30	50.44	50.29	50.22	50.42
26-Oct-94	51.34	51.10	51.35	47.52	50.56	50.40	50.41	50.40	50.21	50.35	50.27	50.25	50.35
29-Nov-94	51.18	51.02	51.19	47.43	50.59*	49.83	49.83	49.80	49.92	49.83	49.87	49.88	49.85
17-Jun-95	51.93	51.90	51.92	47.41	50.84	50.84	50.84	50.84	50.35	50.82	50.78	50.75	50.80
16-Jul-95	51.38	51.32	51.96	47.41	50.76	50.69	50.68	50.68	50.36	50.66	50.54	50.49	50.62
22-Jul-95				47.44	50.75	50.67	50.67	50.67	50.36	50.64	50.53	50.50	50.60
28-Jul-95				47.40	50.70	50.61	50.61	50.61	50.34	50.56	50.37	50.32	50.50
4-Aug-95				47.38	50.67	50.55	50.55	50.56	50.29	50.49	50.26	50.24	50.42
11-Aug-95	51.46	51.30	52.11	47.47	50.72	50.61	50.61	50.61	50.33	50.59	50.56	50.56	50.56

Table D1 Continued.

Date	806P1	806P2	806P3	806P5	807P1	807P2	807P3	807P4	808P1	809P1	809P2	809P3	82W9	S125S
6-Jul-93	50.13	47.97	51.29	51.18	45.19	45.53	46.35	46.48	46.21					45.075
7-Jul-93	50.15	47.97	51.24	51.12	45.19	45.74	46.35	46.39	46.22					45.068
8-Jul-93					45.19	45.85	46.31	46.34	46.23					45.068
11-Jul-93	50.17	47.98	51.09	50.97	45.18	46.05	46.17	46.15	46.28					45.054
14-Jul-93	50.18	47.99	51.00	50.90	45.21	46.09	46.07	46.04	46.34					45.046
17-Jul-93	50.22	48.03	51.01	50.91	45.28	46.13	46.16	46.21	46.39					45.07
20-Jul-93	50.23	48.04	50.97	50.86	45.33	46.16	46.12	46.09	46.45					45.06
23-Jul-93	50.26	48.06	51.04	50.93	45.42	46.19	46.21	46.23	46.51					45.09
27-Jul-93	50.27	48.07	50.93	50.83	45.48	46.19	46.05	45.99	46.55					45.06
1-Aug-93	50.27	48.09	50.79	dry	45.55	46.10	45.87	45.79	46.59					45.03
6-Aug-93	50.26	48.10	50.69	dry	45.62	46.00	45.76	45.67	46.61					44.99
12-Aug-93	50.24	48.10	50.56		45.68	45.86	45.58	45.50	46.60					44.96
19-Aug-93	50.23	48.11	50.60		45.75	45.72	45.47	45.40	46.60					44.97
23-Aug-93	50.23	48.13	50.62		45.79	45.70	45.50	45.46	46.59					44.95
30-Aug-93	50.18	48.11	50.49		45.75	45.59	45.40	dry	46.53					44.91
5-Sep-93	50.15	48.10	50.43											
6-Sep-93	49.71	47.61	50.42		45.75	45.53	45.32	dry	46.52					44.89
7-Sep-93	49.73	47.63	50.43		45.38	45.24	45.33	dry	46.14					
8-Sep-93	49.74	47.65	50.39		45.44	45.28	45.32	dry	46.15					
10-Sep-93	49.75	47.66	50.39		45.50	45.30	45.32	dry	46.15					
13-Sep-93	49.80	47.70	50.59		45.62	45.34	45.26	dry	46.21					44.95
17-Sep-93	49.84	47.74	50.79		45.66	45.43	45.61	45.72	46.22					44.95
19-Sep-93	49.87	47.77	50.79		45.68	45.54	45.68	45.76	46.23					44.95
23-Sep-93	49.90	47.80	50.75		45.69	45.64	45.68	45.70	46.26					44.93
28-Sep-93	49.92	47.83	50.67		45.69	45.66	45.59	45.59	46.29					44.92
7-Oct-93	49.96	47.90	50.61		45.71	45.63	45.48	45.47	46.31					44.89
15-Oct-93	50.00	47.96	50.59		45.72	45.58	45.42	45.40	46.31					44.88
22-Oct-93	50.00	47.99	50.59		45.69	45.53	45.41	45.35	46.28					
27-Oct-93	50.03	48.03	50.62		45.68	45.52	45.43	dry	46.28					44.87
6-Nov-93	50.04	48.07	50.59		45.60	45.43	45.35	dry	46.22					44.88
29-Nov-93	50.00	48.13	50.46		45.39	45.35	45.28		46.10	49.13	49.73	49.54	49.78	
29-Dec-93	49.89	48.13	50.25		45.08	45.35	45.14		45.91	49.02	49.42	49.09	49.46	
27-Jan-94	49.72	48.08	49.90		44.81	44.96	44.95		45.72	48.83	48.90	48.58	48.98	
17-Mar-94	48.75	47.90	49.65		44.38	44.57	44.58		45.32	51.46	48.48	48.01	49.96	
24-Mar-94	49.35	47.85	50.21	dry	44.29	44.47	44.59		45.25	54.46*	51.41*	47.83	51.34	45.15
29-Mar-94	49.41	47.86	50.38	dry	44.24	44.43	44.70		45.22	51.35*	51.42*	47.81	48.36	45.15
5-Apr-94	49.53	47.89	50.64	50.84	44.20	44.47	44.91		45.20	51.39*		47.90	51.34	45.23
8-Apr-94	49.58	47.92	50.70	50.92	44.20	44.50	45.02		45.21	51.04*		47.96	51.18	45.22
12-Apr-94	49.65	47.95	50.82	50.95	44.20	44.55	45.13		45.21	51.24		48.01	51.11	45.23
16-Apr-94	49.70	47.96	50.87	51.02	44.18	44.56	45.19		45.21	51.24		47.98	51.11	45.22
21-Apr-94	49.78	47.99	50.99	51.09	44.18	44.63	45.32		45.23	51.10		48.06	50.97*	45.21
28-Apr-94	49.91	48.04	51.14	51.19	44.18	44.77	45.52		45.31	50.53		48.17	50.97*	45.21
4-May-94	49.84	48.09	51.15	51.16	44.21	45.04	45.62		45.41	50.26		48.36	50.72*	45.19
11-May-94	50.08	48.14	51.11	51.11	44.23	45.30	45.60		45.57	50.01		48.71	49.60	45.16
19-May-94	50.20	48.22	51.25	51.20	44.32	45.40	45.62	dry	45.77	49.83		49.56	50.11	45.20
27-May-94	50.33	48.31	51.25	51.18	44.48	45.71	45.95	dry	46.00	49.41		50.06	50.36	45.23
2-Jun-94	50.42	48.33	51.27	51.19	44.57	45.86	46.01	45.97	46.15	49.76		50.22	50.47	45.26
9-Jun-94	50.47	48.43	51.28	51.22	44.75	45.97	46.04	46.07	46.32	49.75		50.35	50.61	45.30
16-Jun-94	50.51	48.48	51.29	51.23	44.98	46.04	46.10	46.12	46.48	49.76		50.43	50.67	45.32
23-Jun-94	50.55	48.51	51.15	51.10	45.14	46.08	45.94	45.83	46.57	49.78		50.21	50.44	45.28
30-Jun-94	50.55	48.52	51.05	51.05	45.30	45.95	45.73	45.61	46.62	49.75		49.94	50.24	45.26

Table D1 Continued.

Date	806P1	806P2	806P3	806P5	807P1	807P2	807P3	807P4	808P1	809P1	809P2	809P3	82W9	S12[illegible]
7-Jul-94	50.54	48.52	51.01	51.02	45.43	45.79	45.60	45.49	46.61	49.70		49.85	50.15	45.26
15-Jul-94	50.52	48.52	50.91	50.93	45.51	45.65	45.48	45.37	46.58	49.65		49.63	49.97	45.22
21-Jul-94	50.54	48.55	50.98	50.97	45.61	45.59	45.46	dry	46.58	49.63		49.74	50.07	45.23
28-Jul-94	50.49	48.52	50.88	50.95	45.60	45.52	45.38	dry	46.52	49.57		49.48	49.82	45.18
4-Aug-94	50.47	48.52	50.73	50.78	45.57	45.47	45.29		46.50	49.54		49.26	49.61	45.14
11-Aug-94	50.47	48.53	50.77	50.81	45.65	45.35	45.18		46.40	49.43		49.19	49.55	45.15
17-Aug-94	50.40	48.52	50.70	dry	45.64	45.29	45.14		46.33	49.36		49.07	49.44	45.12
24-Aug-94	50.39	48.50	50.59	dry	45.62	45.22	45.07		46.23	49.28		48.95	49.32	45.08
30-Aug-94	50.36	48.48	50.55		45.59	45.13	45.01		46.16	49.21		48.83	49.22	45.07
13-Sep-94	50.28	48.45	50.43		45.55	45.03	44.88		45.98	49.08		48.78	49.19	45.00
28-Sep-94	50.14	48.39	50.19		45.40	44.87	44.74		45.77	48.97	49.06	48.62	49.08	44.91
12-Oct-94	50.03	48.34	50.14		45.25	44.72	44.64		45.59	48.87	48.98	48.50	48.99	44.86
26-Oct-94	49.98	48.33	50.20		45.17	44.68	44.58		45.47	48.80	49.07	48.59	49.07	44.85
29-Nov-94	49.76	48.22	49.90		44.70	44.42	44.48		45.13	48.66	48.96	48.45	48.96	
17-Jun-95	49.96	48.08	50.63		44.31	45.36	45.23	dry	45.27	48.56	49.39	49.08	49.43	44.99
16-Jul-95	50.05	48.17	50.51		44.77	45.08	44.96	dry	45.49	48.69	49.53	49.00	49.51	44.91
22-Jul-95	50.07	48.20	50.52							48.75	49.63	49.09	49.61	
28-Jul-95	50.05	48.19	50.39							48.77	49.61	49.08	49.59	
4-Aug-95	50.03	48.21	50.29							48.82	49.65	49.15	49.64	
11-Aug-95	50.06	48.29	50.53		45.04	44.87	44.71	dry	45.51	48.90	49.90	49.22	49.80	44.88

Table D1 Continued.

Date	8011P1	8012P1	8012P2	8012P4	82W12	8013P1	93W2	93W3	93W4	93W5	93W6	S109
7-Jul-93								52.48	52.61	52.59		
8-Jul-93								52.48	52.64	52.59	52.93	
11-Jul-93								52.42	52.52	52.48	52.50	
14-Jul-93								52.37	52.44	52.39	52.42	
17-Jul-93							52.25	52.39	52.51	52.50	52.44	52.05
20-Jul-93							52.15	52.36	52.39	52.36	52.37	52.04
23-Jul-93							52.32	52.43	52.48	52.48	52.45	
27-Jul-93							52.11	52.34	52.31	52.28	52.32	
1-Aug-93							51.94	52.22	52.15	52.11	52.14	51.98
6-Aug-93							51.83	52.09	52.03	52.00	52.01	
12-Aug-93							51.70	52.00	51.84	51.82	51.83	51.86
19-Aug-93							51.84	dry	dry	dry	51.75	51.88
23-Aug-93							51.76	dry	dry	51.80	51.81	51.83
30-Aug-93							51.59			dry	51.68	51.70
4-Sep-93							51.53					
5-Sep-93							51.52			dry	51.61	
6-Sep-93							51.50				51.60	
7-Sep-93							51.48				51.60	
8-Sep-93							51.45				51.61	
10-Sep-93							51.43				51.57	
13-Sep-93							51.76	dry	dry	dry	51.59	51.79
17-Sep-93							51.88	dry	51.91	51.87	51.95	51.78
19-Sep-93							51.88	52.02	51.98	51.96	52.01	51.76
23-Sep-93							51.83	52.03	52.01	51.99	52.03	51.68
28-Sep-93							51.78	dry	51.97	51.94	51.98	
7-Oct-93							51.75	dry	51.93	51.89	51.92	
15-Oct-93							51.75		51.90	51.88	51.89	
22-Oct-93									51.89	51.88	51.88	
27-Oct-93							51.78		51.93	51.95	51.92	
6-Nov-93							51.78		51.85	51.85	51.84	
29-Nov-93	46.70	51.63	51.66	51.57	51.57	52.98	51.67				51.73	
29-Dec-93	46.70	51.27	51.51	dry	51.20	52.61	51.56				dry	
27-Jan-94	46.69	50.88	51.30	dry	50.90	52.29	51.28					
17-Mar-94	46.74	50.43	50.87		50.43	51.81	51.12					
24-Mar-94	46.71	50.22	50.75			51.53	51.87				dry	
29-Mar-94	46.71	50.23	50.70		50.29	51.45	51.92				dry	52.14
5-Apr-94	46.72	50.37	50.66		50.35	51.49	52.41				52.79	52.34
8-Apr-94	46.73	50.46	50.65		50.41	51.57	53.74				52.55	52.35
12-Apr-94	46.74	50.58	53.90*	dry	50.47	51.55	52.72	52.86			52.95	52.50
16-Apr-94	46.72	50.50	53.89*	dry	50.51	51.46	52.57					52.57
21-Apr-94	46.72	50.63	53.92*	53.71*	53.86*	51.40	52.58	52.87			52.88	52.58
28-Apr-94	57.12*	50.77	53.81*	53.77*	53.92*	51.35	52.57	52.85	52.85	52.86	52.70	52.57
4-May-94	46.74	50.93	53.66*	53.57*	53.62*	51.43	52.55	52.81	52.66	52.67	52.59	52.55
11-May-94	56.56*	51.18	50.76	51.40*	53.59*	51.46	52.51	52.74	52.58	52.57	52.54	52.52
19-May-94	46.76	51.50	50.94	51.50	53.06*	51.42	52.58	52.78	52.83	52.53	52.78	52.54
27-May-94	46.92	52.14	51.10	52.42	52.06	51.57	52.55	52.80	52.88	52.89	52.87	52.55
2-Jun-94	46.91	52.36	51.23	52.60	52.29	51.53	52.58	52.83	52.94	52.95	52.90	52.55
9-Jun-94	46.92	52.51	51.39	52.72	52.45	51.76	52.62	52.84	53.00	53.00	53.00	52.57
16-Jun-94	46.92	52.60	51.55	52.78	52.54	52.16	52.62	52.86	53.02	53.02	53.02	52.57
23-Jun-94	46.94	52.61	51.72	52.68	52.58	52.82	52.47	52.79	52.89	52.90	52.84	52.54
30-Jun-94	46.93	52.32	51.83	52.39	52.35	53.06	52.48	52.73	52.71	52.71	52.65	52.50

Table D1 Continued.

Date	8011P1	8012P1	8012P2	8012P4	82W12	8013P1	93W2	93W3	93W4	93W5	93W6	S109
7-Jul-94	46.93	52.18	51.89	52.21	52.18	53.02	53.74	52.69	52.53	52.52	52.52	52.47
15-Jul-94	46.91	52.00	51.93	52.03	52.02	53.01	52.31	52.60	52.30	52.29	52.32	52.42
21-Jul-94	46.94	52.01	51.97	52.04	51.96	52.96	52.36	52.62	52.37	52.36	52.38	52.43
28-Jul-94	46.93	51.89	51.98	51.93	51.90	52.92	52.21	52.47	52.14	52.13	52.14	52.36
4-Aug-94	46.91	51.68	51.96	51.77	51.89	52.82	52.12	52.33	51.97	51.96	51.96	52.31
7-Aug-94	46.92	51.60	51.95	51.72	51.62	52.72	52.22					52.31
11-Aug-94	46.93	51.63	51.93	51.67	51.61	52.73	52.19	52.29	51.95	51.95	51.94	52.29
17-Aug-94	46.93	51.54	51.90	51.63	51.54	52.73	52.18	52.19	51.84	51.84	51.83	52.25
24-Aug-94	46.92	51.45	51.86	51.57	51.45	52.59	51.93	52.03	dry	dry	51.72	52.18
30-Aug-94	46.91	51.43	51.85	51.56	51.37	52.43	51.94	dry	dry	dry	51.65	52.16
13-Sep-94	46.93	51.37	51.73	dry	51.33	52.46	51.77	dry			dry	52.04
20-Sep-94	46.91	51.28	51.67	dry	51.27	52.33	51.69				dry	51.97
28-Sep-94	45.15	51.23	51.44		51.23	52.30	51.61					51.88
4-Oct-94	45.22	51.21	51.42		51.15	52.16	51.66					51.85
12-Oct-94	45.27	51.09	51.38		51.10	52.09	51.59					51.79
19-Oct-94	45.37	51.14	51.38		51.12	52.18	51.62					
26-Oct-94	45.44	51.19	50.79		51.12	52.18	51.64					
3-Nov-94	45.47	51.06	50.84		51.04	52.01	51.58					
15-Nov-94	45.54	51.07	50.90		51.02	51.94	51.53					
29-Nov-94	45.61	51.00	50.93		50.98	51.88	51.40					
13-Dec-94	45.66	50.85	50.92		50.84	51.73	51.20					
31-Jan-95	45.88	50.44	50.70		50.43	51.51	dry					
25-Feb-95	45.95	50.25	50.54		50.25	51.27	dry					
15-Mar-95	46.01	50.12	50.42		50.24	51.18	dry					52.12
24-Mar-95	46.06	50.07	50.38		50.16	51.21	51.02					
11-Apr-95	46.11	50.18	50.33	dry	50.09	51.13	51.55					
4-May-95	46.16	50.55	50.26	dry	50.51	51.03	52.01					
23-May-95	46.24	51.60	50.57	51.46	51.56	51.07	52.29					52.25
1-Jun-95	46.27	51.68	50.77	51.72	51.65	51.19	52.12					52.20
17-Jun-95	46.33	51.55	51.04	51.67	51.54	51.54	51.81	dry			52.16	52.07
25-Jun-95	46.34	51.52	51.11	51.57	51.47	51.61	51.73					51.99
1-Jul-95	46.36	51.56	51.17	51.54	51.50	51.78	51.75					51.97
9-Jul-95	46.38	51.60	51.23	51.56	51.55	51.92	51.60					51.88
16-Jul-95	46.39	51.62	51.28	51.56	51.57	52.01	51.52	dry			51.98	51.79
22-Jul-95	46.43	51.72	51.36	51.59	51.65	52.21	51.58					
11-Aug-95	46.55	51.78	51.56	dry	51.68	52.34	51.45	dry			52.14	
18-Sep-95	46.61	52.27	52.01	52.20	52.25	53.29	51.26					
10-Oct-95	46.70	52.46	52.18	52.41	52.40	53.21	51.65					
1-Dec-95	46.77	52.00	52.24	51.94	51.99	53.26	51.75					
10-Jan-96	46.80	51.09	51.78	dry	51.18	52.64	51.41					
8-Feb-96	46.84	50.64	51.38	dry	50.73	52.22	51.11					
8-Apr-96	46.90	50.18	50.60		50.20	51.42	51.59					52.21
12-Apr-96	46.90	50.18	50.57		50.16	51.39	52.16					52.41
17-Apr-96	46.94					51.53	52.28					52.47
25-Apr-96	46.94	50.30	50.50	dry	50.26	51.37	52.50					
6-May-96	46.92					51.26	52.51					52.52
16-May-96	46.95	50.90	50.56	dry	50.82	51.35	52.58					52.54
29-May-96	46.95	51.46	50.75	52.04	51.41	51.27	52.52					
17-Jun-96	46.98	52.25	51.15	52.34	52.19	51.38	52.40					52.43
2-Jul-96	47.06	52.49	51.53	52.54	52.47	52.12	52.34					52.42
18-Jul-96	47.08	52.39	51.87	52.51	52.37	53.36	52.57					52.59
6-Aug-96	47.09	51.93	52.03	52.00	51.98	53.27	52.35					52.46

Table D1 Continued.

Date	93UP2	93UP3 A	93UP3 B	93UP3 C	93UP4	93UP5 A	93UP5 C	93UP6 A	93UP6 B	93UP6 C	93UP7 A	93UP7 B	93UP7 C
3-Oct-93	47.19	51.68	48.05	46.04	48.01					48.11			
10-Oct-93	47.49	51.68	49.72	47.22	51.49					48.36			
15-Oct-93	47.46	51.64	50.38	47.35	52.00					48.41			
22-Oct-93	47.54	51.57	50.86	47.43	51.58					48.45			
27-Oct-93	47.52	51.66	51.05	47.50	51.61	47.51	45.83			48.53			
6-Nov-93	47.62	51.64	51.16	47.56	51.61	47.80	46.16		49.99	48.44		45.56	45.47
29-Nov-93	47.71	51.50	51.18	47.65	51.52	48.03	46.26		51.34	48.56	46.51	47.39	46.43
29-Dec-93	47.74	51.34	51.01	47.67	51.35	47.78	46.31		51.55	48.56	47.65	47.41	46.50
27-Jan-94	47.72	51.14	50.84	47.66	51.19	47.58	46.28		51.13	48.57	48.21	47.43	46.54
17-Mar-94	47.50	51.67	50.61	47.51	51.17	47.42	46.20		50.75	48.54	48.09	47.47	46.52
24-Mar-94	47.56	51.76	50.95	47.48	51.79	47.15	46.15		50.54	48.38	47.86	47.40	46.42
29-Mar-94	47.58	51.76	51.10	47.51	51.80	47.32			50.44	48.35	47.82	47.40	46.41
5-Apr-94	47.62	52.10	51.33	47.53	52.11	47.33			50.44	48.38	47.84	47.39	46.43
8-Apr-94	47.65	52.15	51.42	47.56	52.13	47.36			50.51	48.43	47.89	47.44	46.46
12-Apr-94	47.68	52.33	51.51	47.58		47.38			50.56	48.43	47.92	47.46	46.51
16-Apr-94	47.67	53.91	51.58		52.36	47.35			50.51	48.38	47.82	47.37	46.38
21-Apr-94	47.71	52.50	51.72	47.59	52.48	47.40	46.23		50.55	48.36	47.81	47.37	46.43
28-Apr-94	47.75	52.54	51.86	47.64	52.53	47.44	46.20		50.62	48.34	47.77	47.35	46.39
4-May-94		52.51	52.01	47.67	52.41	47.44	46.21		50.76	48.41	47.55	47.32	46.37
11-May-94	47.83	52.47	51.96	47.72	52.49	47.49	46.23		50.94	48.42	47.66	47.32	46.34
19-May-94	47.86	52.53	51.97	47.71	52.52	47.50	46.29		51.06	48.39	47.69	47.32	46.35
27-May-94	47.94	52.52	52.06	47.84	52.56	47.68	46.33		51.37	48.52	47.81	47.40	46.48
2-Jun-94	48.03	52.55	52.06	47.81	52.57	47.69	46.33		51.61	48.49	47.74	47.35	46.41
9-Jun-94	47.91	52.56	52.08	47.85	52.60	47.65	46.32		52.02	48.54	47.76	47.38	46.44
11-Jun-94	46.34	52.49	45.99	46.26		46.20	45.27	dry	50.69	46.34	46.93	46.00	45.88
16-Jun-94	48.02	52.59	49.20	47.85	52.45	47.46	46.39	dry	52.21	48.70	47.81	47.51	46.49
23-Jun-94	47.99	52.45	50.95	47.90	52.50	47.77	46.41	51.89	52.52	48.66	47.58	47.45	46.53
30-Jun-94	47.96	52.42	51.54	47.88	52.43	47.75	46.40	52.11	52.50	48.69	47.72	47.47	46.51
7-Jul-94	47.88	52.36	51.73	47.84	52.40	47.69	46.39	52.18	52.36	48.62	47.74	47.44	46.47
15-Jul-94	47.92	52.25	51.80	47.85	52.30	47.72	46.39	52.23	52.27	48.68	47.83	47.50	46.53
21-Jul-94	47.95	52.33	51.84	47.87	52.37	47.73	46.41	52.14	52.19	48.70	47.89	47.53	46.57
28-Jul-94	47.89	52.12	51.80	47.85	52.22	47.74	46.39	52.15	52.13	48.70	47.94	47.53	46.52
4-Aug-94	47.90	52.03	51.71	47.82	52.10	47.66	46.38	52.11	51.95	48.65	47.87	47.49	46.53
7-Aug-94	47.92	52.14	51.67	47.83	52.09	47.61	46.38	52.00	51.93	48.68	47.88	47.50	46.59
11-Aug-94	47.92	52.10	51.68	47.84	52.07	47.65	46.41	51.97	51.89	48.70	47.93	47.55	46.59
17-Aug-94	47.93	51.96	51.76	47.86		47.66	46.41	52.02	51.81	48.71	47.94	47.53	46.55
24-Aug-94	47.93	51.79	51.54	47.88		47.65	46.40	51.86	51.72	48.72	47.94	47.52	46.55
30-Aug-94	47.91	51.79	51.48	47.85		47.61	46.38	51.83	51.58	48.65	47.91	47.52	46.52
13-Sep-94	47.94	51.70	51.45	47.88		47.66	46.42	51.71	51.56	48.74	47.99	47.56	46.59
20-Sep-94	47.92	51.61	51.38	47.87		47.63	46.41	51.65	51.46	48.71	47.96	47.55	46.58
28-Sep-94	47.93	51.55	51.32	47.88		47.68	46.42	dry	51.46	48.74	47.98	47.56	46.59
4-Oct-94	47.91	51.53	51.26	47.87		47.63	46.41	dry	51.35	48.67	47.94	47.55	46.58
12-Oct-94	47.91	51.47	51.20	47.85		47.62	46.38		51.32	48.70	47.94	47.53	46.53
19-Oct-94	47.94	51.49	51.20	47.88		47.66	46.43		51.38	48.80	48.03	47.60	46.62
26-Oct-94	47.95	51.51	50.34	47.78		47.40	46.46		51.25	48.81	47.66	47.42	46.63
3-Nov-94	47.94	51.46	50.88	47.87		47.64	46.44		51.29	48.80	47.83	47.60	46.60
15-Nov-94	47.93	51.42	51.10	47.89		47.69	46.46		51.25	48.80	47.97	47.62	46.63
29-Nov-94	47.93	51.27	51.02	47.88		47.70	46.45		51.21	48.82		47.60	46.64
13-Dec-94	47.89	51.06	50.86	47.85		47.67	46.43		51.09	48.76	47.90	47.62	46.63
31-Jan-95	47.69	50.62	50.37	47.66		47.51	46.32		50.77	48.68	48.00	47.56	46.59
25-Feb-95	47.57	dry	50.18	47.50		47.33	46.23		50.56	48.50	47.88	47.48	46.51
15-Mar-95	47.52	dry	50.01	47.43		47.26	46.17		50.48	48.41	47.81	47.39	46.45
24-Mar-95	47.48	dry	50.02	47.45		47.25	46.14		50.46	48.41	47.80	47.37	46.43
11-Apr-95	47.45	51.10	50.44	47.39		47.21	46.12		50.44	48.35	47.79	47.37	46.46

Table D1 Continued.

Date	93UP2	93UP3 A	93UP3 B	93UP3 C	93UP4	93UP5 A	93UP5 C	93UP6 A	93UP6 B	93UP6 C	93UP7 A	93UP7 B	93UP7 C
21-Apr-95	47.51	51.34	50.67	47.43	51.71	47.18	46.08		50.40	48.39	47.68	47.30	46.36
4-May-95	47.57	51.63	50.97	47.49	51.70	47.23	46.12		50.57	48.30	47.64	47.27	46.34
23-May-95	47.66	52.16	51.50	47.57	52.15	47.31	46.15		51.05	48.35	47.62	47.25	46.32
1-Jun-95	47.70	51.96	51.57	47.62	52.04	47.39	46.19		51.47	48.41	47.64	47.24	46.32
17-Jun-95	47.70	51.71	51.40	47.64	51.81	47.45	46.21		51.77	48.48	47.66	47.25	46.33
25-Jun-95	47.69	51.63	51.30	47.61	51.73	47.42	46.21		51.68	48.42	47.63	47.27	46.37
1-Jul-95	47.70	51.67	51.26	47.62	51.69	47.43	46.22		51.71	48.46	47.66	47.29	46.39
9-Jul-95	47.71	51.52	51.22	47.62	51.64	47.43	46.22		51.73	48.48	47.65	47.29	46.36
16-Jul-95	47.70	51.44	51.15	47.62	51.58	47.41	46.21		51.70	48.48	47.64	47.28	46.35
22-Jul-95	47.72	51.46	51.12	47.63	51.54	47.46	46.23	dry	51.79	48.57	47.72	47.33	46.41
11-Aug-95	47.70	51.36	50.71	47.65	51.17	47.40	46.25	dry	51.77	48.62	47.54	47.35	46.40
18-Sep-95	47.73	51.19	51.01	47.70	51.18	47.47	46.31	52.39	52.46	48.79	47.82	47.45	46.46
10-Oct-95	47.85	51.50	50.99	47.76	51.39	47.48	46.35	52.48	52.50	49.00	48.00	47.62	46.57
1-Dec-95	47.94	51.64	51.28	47.92	51.60	47.72	46.52	52.57	52.59	49.23	48.30	47.83	46.79
10-Jan-96	48.02	51.28	51.02	47.99	51.30	47.75	46.57	52.03	52.02	49.21	48.35	47.86	46.81
8-Feb-96	48.06	50.97	50.79	48.06	51.01	47.75	46.60	51.78	51.67	49.18	48.36	47.82	46.77
8-Apr-96	47.68	52.02	51.01	47.64	51.76	47.45	46.29	dry	50.82	48.73	48.05	47.57	46.60
12-Apr-96	47.69	52.12	51.19	47.63	52.00	47.42	46.27	dry	50.79	48.66	48.02	47.57	46.59
17-Apr-96	47.72	52.27	51.40	47.65	52.17	47.46	46.28		50.85	48.74	48.07	47.59	46.62
25-Apr-96	47.77								50.71	48.61	47.98	47.56	46.58
6-May-96	47.77	52.50	51.87	47.72	52.48	47.47	46.30	dry	50.65	48.52	47.91	47.51	46.55
16-May-96					52.51								
29-May-96	47.87	52.50	52.00	47.82	52.49	47.59	46.35	dry	51.64	48.47	47.79	47.38	46.48
17-Jun-96	47.93	52.37	51.95	47.87	52.36	47.66	46.39	52.21	52.24	48.55	47.76	47.37	46.48
2-Jul-96	47.96	52.34	51.96	47.92	52.39	47.70	46.41	52.64	52.62	48.66	47.81	47.46	46.53
18-Jul-96	48.03	52.56	52.04	47.96	52.54	47.71	46.46	52.59	52.67	48.76	47.86	47.52	46.57
6-Aug-96	47.99	52.32	51.96	47.95	52.35	47.70	46.46	52.28	52.45	48.85	47.96	47.54	46.58

Table D1 Continued.

Date	93LP1 A	93LP1 B	93LP1 C	93LP1 D	93LP2 A	93LP2 B	93LP2 C	93LP2 D	93LP3 B	94W7	94UP9	94UP10	94LP4
10-Oct-93		45.15	46.04										
15-Oct-93		45.35	46.10	37.11									
22-Oct-93		45.57	46.12	37.99									
27-Oct-93		45.61	46.11	38.84				38.18	45.09				
6-Nov-93		45.59	46.12	40.19				42.54	45.07				
29-Nov-93	44.66	45.56	46.11	42.71				45.93	45.22				
29-Dec-93	44.95	45.39	46.03	44.24		44.97	41.86	46.43	45.32				
27-Jan-94	44.99	45.17	45.73	44.76		45.26	44.66	46.31	45.40				
17-Mar-94	45.08	45.07	45.39	45.05		46.05	45.23	46.22	45.45				
24-Mar-94	44.84	44.89	45.30	44.95		45.83	44.96	46.06	45.45				
29-Mar-94	44.87	44.92	45.30	44.96		45.79	45.17	46.01	45.45				
5-Apr-94	45.03	45.05	45.31	45.00	dry	45.91	45.43	46.02	45.45				
8-Apr-94	45.12	45.13	45.32	45.03	dry	45.95	45.55	46.03	45.45				
12-Apr-94	45.27	45.26	45.33	45.03	46.74	46.04			45.39				
16-Apr-94	45.34		45.37	44.97	dry	45.92	45.66	46.01	45.41				
21-Apr-94	45.69	45.72	45.45	44.96	dry	45.99	45.71	45.97	45.41				
28-Apr-94	45.82	45.83	45.53	44.97		46.13	45.79	45.97	45.36				
4-May-94	45.78	45.79	45.61	45.05		46.18	45.88	45.98	45.38				
11-May-94	45.70	45.72	45.64	45.11		46.24	45.93	45.99	45.39				
19-May-94	45.77	45.79	45.72	45.14		46.24	45.97	46.02	45.41				
27-May-94	45.99	46.00	45.86	45.23	dry	46.37	46.11	46.09	45.41				
2-Jun-94	45.96	45.99	46.00	45.28	dry	46.39	46.09	46.07	45.42				
9-Jun-94	45.97	46.01	46.19	45.35	46.77	46.58	46.18	46.06	45.43				
11-Jun-94													
16-Jun-94	45.96	46.02	46.41	45.43	dry	46.79	46.31	46.06	45.46				
23-Jun-94	45.89	45.97	46.57	45.54	47.01	47.02	46.49	46.10	45.45				
30-Jun-94	45.71	45.80	46.60	45.61	46.91	47.04	46.58	46.10	45.46				
7-Jul-94	45.70	45.78	46.59	45.60	46.80	47.00	46.53	46.06	45.40				
15-Jul-94	45.56	45.67	46.54	45.69	dry	46.90	46.63	46.20	45.48	50.34			
21-Jul-94	45.64	45.73	46.50	45.72	dry	46.86	46.65	46.24	45.48	52.09			
28-Jul-94	45.59	45.66	46.48	45.67		46.77	46.62	46.28	45.47	51.99			
4-Aug-94	45.36	45.46	46.35	45.73		46.61	46.56	46.27	45.48	51.82			
7-Aug-94										51.72			
11-Aug-94	45.33	45.44	46.31	45.71		46.59	46.54	46.26	45.47	51.78			
17-Aug-94	45.33	45.43	46.20	45.75		46.48	46.52	46.31	45.49	51.71	51.14		
24-Aug-94	45.24	45.32	46.11	45.73		46.41	46.49	46.32	45.51	51.67	51.90	49.51	
30-Aug-94	45.14	45.24	46.03	45.68		46.30	46.41	46.27	45.50	51.59	51.86	49.50	
13-Sep-94	45.12	45.19	45.88	45.68		46.26	46.42	46.35	45.51	51.57	51.72	49.51	
20-Sep-94										51.50	51.64	49.43	
28-Sep-94	44.97	45.05	45.73	45.55		46.12	46.32	46.31	45.52	51.38	51.55	49.44	
4-Oct-94										51.36	51.55	49.32	
12-Oct-94	44.86	44.96	45.60	45.42		45.93	46.18	46.30	45.52	51.32	51.48	49.30	
19-Oct-94										51.36	51.50	49.36	
26-Oct-94	45.02	45.02	45.31	44.79		45.94	45.95	46.22	45.52	51.36	51.51	49.30	
3-Nov-94										51.32	51.46	49.28	
15-Nov-94										51.29	51.42	49.23	
29-Nov-94	44.89	44.95	45.35	45.18		45.81	46.01	46.31	45.59	51.21	51.27	49.21	
13-Dec-94										51.01	51.06	49.09	
31-Jan-95										50.54	50.87	48.72	
25-Feb-95										50.36	50.87	48.52	
15-Mar-95										50.19	50.83	48.42	
24-Mar-95										50.18	50.83	48.39	
11-Apr-95										50.56	51.04	48.41	
21-Apr-95													

Table D1 Continued.

Date	93LP1 A	93LP1 B	93LP1 C	93LP1 D	93LP2 A	93LP2 B	93LP2 C	93LP2 D	93LP3 B	94W7	94UP9	94UP10	94LP4
4-May-95													
23-May-95													
1-Jun-95													
17-Jun-95	45.31	45.28	45.33	44.94		46.37	46.14	45.92	45.47	51.67	51.69	49.84	44.96
25-Jun-95										51.63	51.61	49.71	
1-Jul-95										51.62	51.64	49.71	
9-Jul-95										51.54	51.49	49.68	
16-Jul-95	45.06	45.11	47.69	45.06		46.22	46.16	46.00	45.45	51.46	51.41	49.63	44.88
22-Jul-95										51.46	51.43	49.68	
11-Aug-95	44.86	44.97	45.51	45.18		46.20	46.21	46.05	45.45	51.25	51.34	49.66	
18-Sep-95										51.65	51.16	50.44	
10-Oct-95										51.82	51.46	50.51	
1-Dec-95										51.81	51.59	50.55	
10-Jan-96										51.26	51.25	49.98	
8-Feb-96										50.90	50.94	49.61	
8-Apr-96										51.08	51.87	48.84	
12-Apr-96										51.22	52.01	48.78	
17-Apr-96										51.41	52.17	48.85	
25-Apr-96										51.78		48.75	
6-May-96										52.17	52.45	48.89	
16-May-96										52.40			
29-May-96										52.50	52.44	50.14	
17-Jun-96										52.40	52.30	50.41	
2-Jul-96										52.46	52.27	50.64	
18-Jul-96										52.48	52.50	50.63	
6-Aug-96										52.10	52.24	50.34	